Report No. BDK84-977-23

Final Report

Quantification of the Physical Properties Required of Raised Pavement Markers and Accelerated Laboratory Testing

Qing Lu, Ph.D., P.E.
Principal Investigator
University of South Florida

Manjriker Gunaratne, Ph.D., P.E.
Co-Principal Investigator
University of South Florida

Yunlong Zhang, Ph.D.
Associate Professor
Texas Transportation Institute

and

Lukai Guo
Bin Yu
Graduate Assistants
University of South Florida

Submitted to

Florida Department of Transportation
605 Suwannee Street, MS 30, Tallahassee, FL 32399-0450

By the

Department of Civil and Environmental Engineering
College of Engineering
University of South Florida
Tampa, FL 33620
Ph. (813) 974-7971
Fax (813) 974-4962

April 30, 2014

DISCLAIMER

The opinions, findings, and conclusions expressed in this publication are those of the authors and not necessarily those of the State of Florida Department of Transportation.

This document is disseminated under the sponsorship of the U.S. Department of Transportation in the interest of information exchange. The United States Government assumes no liability for the contents or use thereof.

SI (MODERN METRIC) CONVERSION FACTORS

Approximate Conversions to SI Units				
Symbol	**When You Know**	**Multiply By**	**To Find**	**Symbol**
		Length		
in	inches	25.4	millimeters	mm
ft	feet	0.305	meters	m
yd	yards	0.914	meters	m
mi	miles	1.61	kilometers	km
		Area		
in²	square inches	645.2	square millimeters	mm^2
ft²	square feet	0.093	square meters	m^2
yd²	square yard	0.836	square meters	m^2
ac	acres	0.405	hectares	ha
mi²	square miles	2.59	square kilometers	km^2
		Volume		
fl oz	fluid ounces	29.57	milliliters	mL
gal	gallons	3.785	liters	L
ft³	cubic feet	0.028	cubic meters	m^3
yd³	cubic yards	0.765	cubic meters	m^3
	NOTE: volumes greater than 1000 L shall be shown in m^3			
		Mass		
oz	ounces	28.35	grams	g
lb	pounds	0.454	kilograms	kg
T	short tons (2000 lb)	0.907	megagrams (or "metric ton")	Mg (or "t")
		Temperature (exact degrees)		
°F	Fahrenheit	5 (F-32)/9 or (F-32)/1.8	Celsius	°C
		Illumination		
fc	foot-candles	10.76	lux	lx
fl	foot-Lamberts	3.426	candela/m^2	cd/m^2
		Force and Pressure or Stress		
lbf	poundforce	4.45	newtons	N
lbf/in²	poundforce per square inch	6.89	kilopascals	kPa

Approximate Conversions from SI Units				
Symbol	**When You Know**	**Multiply By**	**To Find**	**Symbol**
		Length		
mm	millimeters	0.039	inches	in
m	meters	3.28	feet	ft
m	meters	1.09	yards	yd
km	kilometers	0.621	miles	mi
		Area		
mm²	square millimeters	0.0016	square inches	in^2
m²	square meters	10.764	square feet	ft^2
m²	square meters	1.195	square yards	yd^2
ha	hectares	2.47	acres	ac
km²	square kilometers	0.386	square miles	mi^2
		Volume		
mL	milliliters	0.034	fluid ounces	fl oz
L	liters	0.264	gallons	gal
m³	cubic meters	35.314	cubic feet	ft^3
m³	cubic meters	1.307	cubic yards	yd^3
		Mass		
g	grams	0.035	ounces	oz
kg	kilograms	2.202	pounds	lb
Mg (or "t")	megagrams (or "metric ton")	1.103	short tons (2000 lb)	T
		Temperature (exact degrees)		
°C	Celsius	1.8C+32	Fahrenheit	°F
		Illumination		
lx	lux	0.0929	foot-candles	fc
cd/m²	candela/m^2	0.2919	foot-Lamberts	fl
		Force and Pressure or Stress		
N	newtons	2.225	poundforce	lbf
kPa	kilopascals	0.145	poundforce per square inch	lbf/in^2

* SI is the symbol for the International System of Units. Appropriate rounding should be made to comply with Section 4 of ASTM E380. (Revised March 2003)

TECHNICAL REPORT DOCUMENTATION PAGE

1. Report No.	2. Government Accession No.	3. Recipient's Catalog No.
4. Title and Subtitle Quantification of the Physical Properties Required of Raised Pavement Markers and Accelerated Laboratory Testing		5. Report Date April 30, 2014 6. Performing Organization Code
7. Author(s) Qing Lu, Manjriker Gunaratne, Yunlong Zhang, Lukai Guo, and Bin Yu		8. Performing Organization Report No.
9. Performing Organization Name and Address Department of Civil and Environmental Engineering College of Engineering University of South Florida, Tampa, FL 33620		10. Work Unit No. (TRAIS) 11. Contract or Grant No. BDK84-977-23
12. Sponsoring Agency Name and Address Florida Department of Transportation 605 Suwannee Street, MS 30, Tallahassee, FL 32399		13. Type of Report and Period Covered Final Report March 2012 – March 2014 14. Sponsoring Agency Code
15. Supplementary Notes		

16. Abstract

Retroreflective raised pavement markers (RRPMs) can provide lane and directional information at night, particularly during wet weather conditions. In recent years, the RRPM service life in Florida has been generally shorter than expected. Moreover, the accuracy of current RRPM laboratory testing methods and procedures have been challenged.

This report presents the research conducted over a two-year period to improve current RRPM designs and to develop new laboratory tests that can predict marker field performance. Current RRPM performance with typical failure modes and contributing factors were identified through literature review, nationwide questionnaire survey, and field survey. Finite element models (FEMs) of the tire/RRPM/pavement system were built to analyze the critical stress fields in RRPMs, for both field use scenarios and laboratory testing conditions, to explore the effects of various geometric features and material properties on critical stresses, and therefore to propose improved RRPM designs and laboratory test procedures. Strains in field RRPMs were measured with strain gauges to verify FEM results. Two new laboratory tests that better simulate field loading conditions were proposed, and a revised pendulum impact test was developed. New RRPM designs that may have an average service life longer than that of current RRPMs were recommended.

17. Key Word	18. Distribution Statement
Raised Retroreflective Pavement Marker, Finite Element Model, Laboratory Test, Revised Pendulum Impact Test	No restrictions.

19. Security Classif. (of this report)	20. Security Classif. (of this page)	21. No. of Pages	22. Price
Unclassified.	Unclassified.	184	

Form DOT F 1700.7 (8-72) Reproduction of completed page authorized

ACKNOWLEDGMENTS

The authors are indebted to Mr. Paul Vinik, State Structural Material Systems Engineer, Florida Department of Transportation (FDOT), Gainesville, Florida, for his project management efforts. The authors also much appreciate all participants of questionnaire surveys from Materials Office and Pavement Maintenance Office of each state Department of Transportation. Finally, the financial support from FDOT is gratefully acknowledged.

EXECUTIVE SUMMARY

Retroreflective raised pavement markers (RRPMs) are used on roadways as a supplement of pavement markings to provide lane and directional information at night. Their use can greatly improve drivers' safety in a dark environment, particularly under wet pavement conditions.

In recent years, RRPMs in Florida have demonstrated increasingly poor performance, and there have been cases of premature failures, which led to frequent replacement of newly installed RRPMs. Due to the vast number of markers required on Florida highways, the total cost due to such increased maintenance effort is large. Therefore it is necessary to investigate the causes of early failures of RRPMs and to propose alternatives or improvements to the current RRPM designs and to develop more effective laboratory testing and evaluation procedures.

This report presents the research conducted over a two-year period to quantify critical physical responses of RRPMs to traffic loading and corresponding required RRPM properties for longer service life and to propose and develop proper laboratory tests that can predict marker field performance.

The research started with a literature review of current use of RRPMs on U.S. highways among all the states. It showed that the main RRPM brands approved on the U.S. highways include 3M, Rayolite, Ennis, and Apex, with different types of products. A map of the RRPM use in the U.S. was developed, which shows that most permanent nonsnowplowable RRPMs are installed in southern regions and that some states have replaced nonsnowplowable RRPMs with snowplowable RRPMs in recent years.

A nationwide questionnaire survey was conducted to collect information on RRPM usage and performance of each state Department of Transportation (DOT) and their efforts to increase RRPM durability. A one-year repeated field condition survey was also conducted on Florida highways to document major failure modes and corresponding developing trends of RRPMs. The typical failure modes captured included lens cracking and loss, body cracking and breakage, detachment, sinking, and contamination. The surveys suggest that heavy traffic significantly contributes to RRPM damages. The survey also shows that RRPMs on rigid pavements have higher risk of detachment failure, and high precipitation and high temperature may accelerate RRPM deterioration.

A tire/RRPM/pavement system was modeled using the finite element analysis software *ANSYS 12.0* to analyze the critical stresses induced in RRPMs under dynamic loading. Four RRPM structures characterized from 3M 290, Ennis C80, Ennis C88, and Rayolite RS markers and two pavement types (rigid and flexible) were included in the model analysis, along with varying loading and impact conditions. The analysis shows that maximum von Mises stress, compressive maximum principal stress, and shear stress all concentrate on the corner and edges of RRPM's top shell, while tensile stress is scattered on the top shell and the bottom edges of a RRPM. RRPMs suffer from a high compressive stress and relatively smaller shear and tensile stresses, which indicates that RRPMs are more prone to be damaged by compression or shear rather than tension. Moreover, RRPMs on rigid pavements suffer more compressive and shear impacts than on flexible pavements.

FEM analysis with changes of RRPM design features was also performed. The results suggest that for RRPMs with larger height, the strength of RRPM body should be improved to sustain higher internal stresses, while for RRPMs with lower height, the bond strength of adhesive at the interface of RRPM and pavement deserves more attention. Besides height, a larger difference between top width and bottom width can mitigate potential failures at RRPM bottom. RRPMs with curved bottom edges generally experience lower stresses than the ones with straight bottom edges. Moreover, the use of hollow internal structure may accelerate RRPM body failure. Considering the materials of RRPMs, the material in Ennis C80 is better than that in 3M 290 in terms of producing lower stresses under the same structure and loading conditions.

Strains in four RRPM models (3M 290, Ennis 980, Rayolite RS, and Apex 921AR) were measured with strain gauges in the field under various wheel loads, tire types, and speeds. Results showed a trend of strain increase with wheel load, but no clear relationship between strain and vehicle speed. Marker materials showed slight viscoelastic behavior but no discernible plastic behavior. Under the same loading conditions, the highest tensile strain was measured on 3M 290 and the highest compressive strain was measured on Apex 921AR. Strains calculated from FEMs are in general consistent with the field measured strains, with a few exceptions.

FEMs of RRPMs in laboratory test setups were built and analyzed. For current RRPM laboratory tests, based on FEM analysis of stress distribution in RRPMs in both the laboratory and field conditions, it is indicated that the ASTM D 4280 compressive test can better simulate the tensile and compressive damage in critical parts of RRPMs than the ASTM flexural test. Moreover, elastomeric pads are necessary in the longitudinal flexural test, but not necessary for the compressive test. Through FEM analysis, it was determined that the pendulum impact test, originally developed by Texas Transportation Institute (TTI), can generate proper stresses on "fragile" RRPM points (i.e., the corner and the middle of non-lens edge of RRPM top shell) to test RRPM qualities. The critical stresses generated by impact on these locations can be adjusted by changing the weight of the impact steel rod. FEM analysis also suggested two new laboratory tests to be further evaluated: a revised reversed latitude flexural test (RRLFT), and an offset latitude flexural test (OLFT). These two new laboratory tests can better simulate the real tire-marker condition in terms of critical stress distribution match.

To verify the stress conditions in different RRPM types, the compressive and flexural tests specified in ASTM standards D 4280 and three new tests (the revised pendulum impact test, the RRLFT, and the OLFT) were conducted on six types of RRPM (3M 290, 3M 290 PSA, Ennis 980, Ennis C80, Rayolite RS, and Apex 921AR). The rank of marker performance based on the ASTM compressive or flexural test results is generally consistent with FEM results and observed marker field performance. The marker performance ranking from the RRLFT is the same as that from the ASTM standard flexural test. However, the typical marker failure modes generated in the RRLFT are more diversified and closer to the failure modes observed in the field. The OLFT provides no significant advantage over the RRLFT. The pendulum impact test was revised from its original design by incorporating a repetitive impact load whose magnitude and speed can be adjusted. Results of this test are consistent with the FEM results and observed field performance. The revised pendulum impact test, however, is portable, versatile, and easy to operate. It is

recommended that the revised pendulum impact test should be further evaluated and potentially implemented.

Based on the effects of geometric and material factors on stress magnitudes, the potential areas of improvement to extend the service life of RRPMs were analyzed and identified. Specifically, one new RRPM was suggested, based on the original 3M 290 design, through decreasing its height to 12 mm, replacing the original materials with those of Ennis C80, and filling the 3M 290 hollows. With these proposed design improvements, the critical von Mises stress in the new RRPM drops from 173 MPa to 108 MPa. Based on the assumption that the service life of an RRPM can be defined by its structural integrity and based on a preliminary relationship between stress, rating change, and life cycle cost, it was roughly estimated that this proposed new RRPM design can extend the average RRPM service life from 3 years to 5 years, and save 44% cost in an analysis period of 15 years.

TABLE OF CONTENTS

LIST OF FIGURES

LIST OF TABLES

CHAPTER 1 INTRODUCTION

1.1 Background

Retroreflective raised pavement markers (RRPMs) are routinely used in Florida to supplement highway pavement markings. RRPMs are very effective in providing lane and directional information at night, particularly during wet weather conditions when other pavement markings have reduced retroreflective properties.

To be effective, an RRPM must be retained in place and possess sufficient retroreflectivity. Accordingly, the service life of RRPM is defined by measures of effectiveness (MOEs), termed as "rating" suggested in the National Transportation Product Evaluation Program (NTPEP). Durability is the ability of an RRPM to stay in place, maintain its function at reasonable levels with respect to its color and retroreflectivity, and withstand damage. Color relates to the daytime color of the shell and the nighttime retroreflected color of the lens. Retroreflectivity is essentially a ratio of the amount of light reaching the RRPM to the amount of light reflected by the RRPM.

In recent years, RRPMs in Florida have demonstrated increasingly poor performance, particularly in terms of durability, and there have been cases of massive failure of RRPMs shortly after installation. These failures have been attributed to poor manufacturing of RRPMs as the result of increased level of competition and reduction in RRPM prices, issues related to installation procedure and quality, and extreme traffic or environmental conditions.

The RRPM models used on Florida roadways must all have passed Florida Department of Transportation (FDOT) laboratory test specifications. Their performance in the field, however, varies significantly. RRPM models from different manufacturers also have different structural designs of body and lenses, which invariably affect structural durability and retroreflectivity. In addition, the service life of RRPMs on Florida roadways, particularly on the roadways with high traffic volumes, is generally shorter than expected. This is to say, the current laboratory testing methods and procedures may not adequately predict the RRPM performance in the field and so not ensure sufficient durability of RRPMs. On the other hand, field testing needs a prolonged period of time and a significant level of resources, such as lane closure and other types of traffic control measures. In situ evaluation also puts evaluators at high risk. With new RRPM models becoming available on the market at a rather fast pace, comprehensive field testing on all RRPM models is often infeasible.

Considering the amount of funds spent each year on RRPMs in Florida, it would be cost effective to have markers with long lives. With long-life markers, not only the total cost of markers used may be reduced, the disturbance to traffic during marker maintenance and replacement would also be reduced. In addition, the safety benefits from RRPMs that maintain their effectiveness cannot be overestimated.

Therefore, it is necessary to investigate how the structural and optical design features of RRPMs affect durability and retroreflectivity. It is also essential to re-evaluate the currently used laboratory testing procedures and potentially develop new test procedures that can better correlate laboratory test results with field performance. An appropriate laboratory test procedure may be used for sampling and qualifying RRPM products, and along with a better understanding

of the effects of marker structures and designs, it will facilitate development by manufacturers of high quality markers and help FDOT to identify RRPMs that meet the structural and optical requirements for five years of service life on Florida roadways.

1.2 Objectives

Based on the background information introduced above, the research objectives of this study include:

a. Conduct a literature review on the experience and/or research findings of US states and overseas agencies with regard to RRPM performance;
b. Determine the current performance levels and predominant failure modes of RRPMs on Florida's roadways through field surveys and interviews with FDOT staff;
c. Develop a finite element model (FEM) of the tire/RRPM/pavement system to gain insight into critical stresses induced by live traffic in RRPMs, and to provide recommendations on design of RRPMs with adequate structural integrity to resist the stresses;
d. Develop laboratory tests to properly evaluate and rank RRPMs;
e. Identify areas of improvement in design criteria and manufacturing methods to extend the service life of RRPMs.

1.3 Scope

A literature survey is performed to evaluate the status of the current practice and recent research on RRPM performance and potential approaches to improve durability. The literature survey also covers types of RRPMs, laboratory test methods, and installation techniques.

A questionnaire survey form is designed and distributed to other states to collect information on their experience on current RRPM conditions and their efforts to increase RRPM durability.

A field condition survey is conducted to document and collect the details of various failure modes under different traffic and climate conditions. The survey areas are recommended by FDOT RRPM maintenance crew around the City of Tampa area, which are intended to include roadways with a multitude of geometries, and varying brands of RRPMs, traffic volumes, and service ages. The observed failure modes are to be associated with the critical stresses in RRPMs identified in subsequent FEM analysis.

A tire/RRPM/pavement system is modeled using the finite element analysis software *ANSYS 12.0* to analyze the critical stresses induced in RRPMs under dynamic loading, so as to help determine appropriate laboratory testing procedures for RRPMs. The FEM analysis includes scenarios of Ennis C80 as a sample with varying levels of tire load, tire velocity, angle of impact, and location of impact on the RRPM.

FEM analysis of RRPMs with changes of design features is also performed. Based on the obtained relationship between critical stress reduction and adjustments to RRPM designs, recommendations are provided on changes to the design of RRPMs to achieve lower critical stresses, thus potentially improved RRPM durability.

Finite element models of RRPMs in laboratory test setups are also built and used to help determine appropriate laboratory test methods. Due to the fact that RRPMs may fail in different modes under various combinations of external factors, multiple laboratory tests are used to evaluate RRPMs, with each test procedure identifying one type of failure potential. Variables that are considered in this task include: test setup (compression, flexural tension, and shear), loading location, load magnitude, and loading rate.

Based on the findings in this research, the potential areas of improvements to extend the service life of RRPMs beyond five years are analyzed and identified. The expected service life extension from the improvement of RRPMs is estimated based on stress analysis and comparison of RRPMs with current designs and with proposed improvements. Once the new performance life is estimated, a life cycle cost analysis is performed to evaluate the economic benefit from these improvements in terms of reduced costs.

CHAPTER 2 LITERATURE REVIEW

This chapter mainly introduces current RRPM categories and typical laboratory tests for RRPM mechanistic properties. Because the main purposes of this study are not concentrated on optical and chemical aspects, the other relevant laboratory tests (optical tests) and the information collected for RRPM installation techniques are summarized in Appendices A and B.

2.1 Types of RRPM

According to *FDOT 2010 Standard Specifications for Road and Bridge Construction, Section 970*, RRPMs are mainly categorized into two classes in Florida: Class A for temporary and Class B for permanent. Class B permanent RRPMs are further divided into two categories in some other states: snowplowable RRPM and nonsnowplowable RRPM. The components of snowplowable RRPMs typically include cast iron housing and reflective lens. This special structure of snowplowable RRPM is suited in snowplow regions. On the contrary, nonsnowplowable RRPMs are commonly installed on roadways that do not experience snow plowing. In this study, the use of snowplowable or nonsnowplowable RRPMs in the US are summarized in Figure 2-1, based on one comprehensive review of DOT specifications and qualified or approved product lists (QPLs/APLs) of RRPMs in each state.

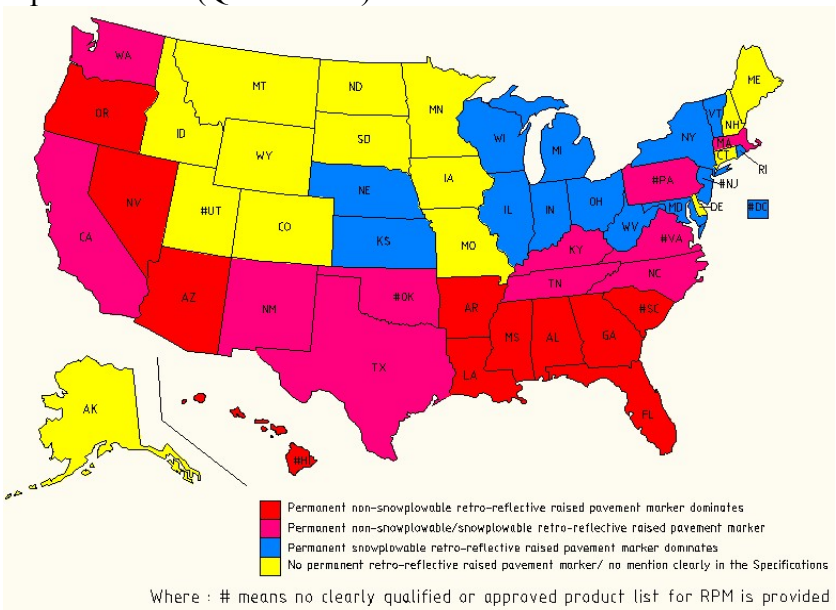

Figure 2-1 Use of Snowplowable or Nonsnowplowable RRPMs in the U.S.

In Figure 2-1, the yellow areas represent states that do not use permanent retro-reflective RRPMs. These areas, however, may still use temporary RRPMs. The red areas are the states where the permanent nonsnowplowable RRPMs dominates. The blue areas mark the snowplowable RRPMs' spread. The pink areas mean the states without preference of using snowplowable or nonsnowplowable RRPMs. Since all the information in this map was derived from DOT specifications and QPLs/APLs, the map only describes the current use of RRPMs on U.S. Route highways, U.S. Interstate highways, and State Route highways. The use of RRPMs on local roads and streets is not considered in this map. During the questionnaire survey in this study, it was discovered that a few states had recently stopped using nonsnowplowable RRPMs and begun to use snowplowable ones instead.

Figure 2-1 is mainly intended to exhibit how widely these types of RRPMs are used: the states using permanent nonsnowplowable RRPMs are concentrated in the southern areas where ambient temperature is perennially warm; while, instead of permanent RRPMs, northern states prefer temporary or snowplowable ones.

Thus, based on this map and FDOT specifications, only permanent nonsnowplowable RRPMs are of interest in this study. Through searching the state DOT QPLs/APLs, four companies are mainly approved for manufacturing nonsnowplowable RRPMs:

- 3M,
- Ennis/Stimsonite,
- Rayolite, and
- Apex.

For 3M, the major product is 3M 290, including PSA series (PSA stands for pressure sensitive adhesive, which means a simple pressure can activate the adhesive function); For Ennis/Stimsonite, six RRPM products are provided: C80, C88, Model 911, Model 980, Model 948, and Model 953; For Apex, 921AR is the only product, but widely appearing, on the state DOT QPLs/APLs; For Rayolite, the main products include AA (All Acrylic), RS (Round Shoulder), SS (Squared Shoulder), and Model 2002. Specifically, these types also contain ARC (abrasion resistant coats) and FH category difference. The use of these RRPMs in various states is summarized in Table 2-1, and plotted in Figure 2-2.

Table 2-1 Current Types of RRPMs in the U.S. States

	3M	Ennis/ Stimsonite						Rayolite				Apex
	290	C80	C88	911	980	948	953	AA	RS	SS	2002	921AR
Alabama	✓		✓			✓		✓	✓		✓	✓
Arizona	✓	✓	✓	✓	✓		✓	✓			✓	
Arkansas	✓			✓		✓						✓
California	✓		✓	✓		✓	✓	✓	✓	✓	✓	✓
Florida	✓	✓			✓				✓			✓
Georgia	yellow	✓		✓		✓			✓		✓	✓
Louisiana	yellow /blue	✓		✓		✓		✓	✓		✓	✓
Mississippi			✓	✓						✓	✓	
New Mexico	✓											
North Carolina		✓	✓					✓		✓	✓	
Tennessee	✓		✓	✓		✓		✓			✓	✓
Texas	✓	✓	✓	✓				✓	✓		✓	✓
Nevada	✓	✓	✓	✓			✓	✓	✓			✓
Oregon			✓	✓		✓		✓				
Washington	✓	✓	✓	✓		✓	✓	✓	✓		✓	✓
Massachusetts	✓	✓										
Kentucky						✓					✓	

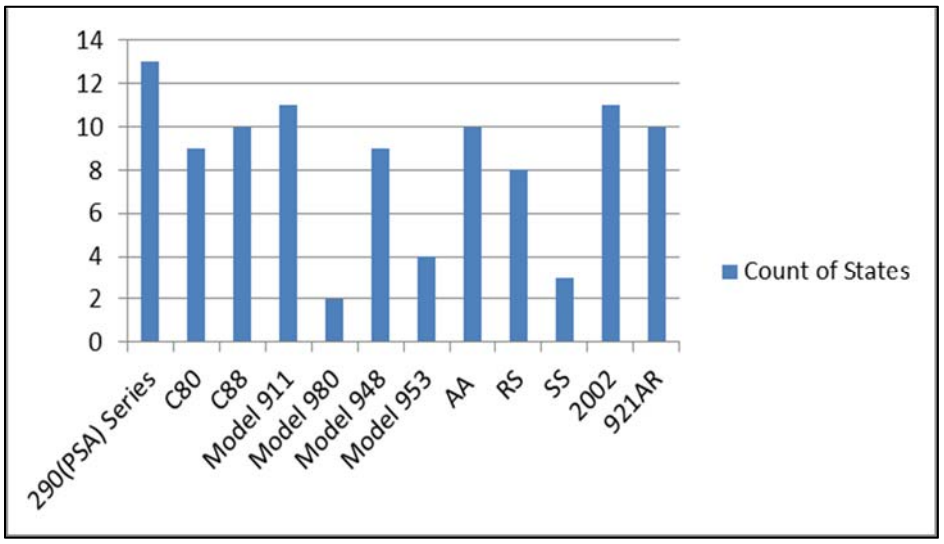

Figure 2-2 Number of States Using Various Models of RRPMs

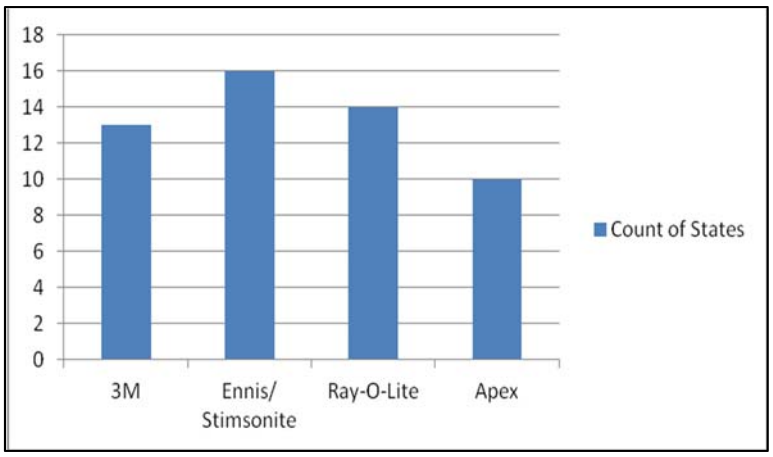

Figure 2-3 Number of States Using Various Brands of Nonsnowplowable RRPMs

Figure 2-2 illustrates that the 3M 290 (PSA) series is one of the most widely used RRPMs in the US. On the contrary, less than four states select Model 980, 953, and SS. Moreover, based on Figure 2-3, it is safe to say that the Ennis/Stimsonite products also have a large RRPM market share relying on its various advanced products.

For more concise and confirmed descriptions, the current ID numbers of QPLs/APLs for permanent nonsnowplowable RRPMs are listed in Table 2-2, along with short descriptions of each RRPM product.

Based on the information provided by manufacturers, the materials and structures of the RRPMs are listed as follows:

- 3M 290 and 290 PSA RRPMs have a polycarbonate lens with built-in micro cube corners and body with internal ribs. The retroreflective lens is coated with a protective

material that combines ceramic and polymeric elements. Compared with 290, 290 PSA is pressure sensitive adhesive for ease in application.

- Apex Model 921AR markers consist of an acrylonitrile butadiene styrene (ABS) plastic shell filled with a tightly adherent potting compound. The shell is molded of methyl methacrylate conforming to ASTM D788 Grade 8, and contains one or two thin-untempered-glass covered prismatic retro-reflective faces. The base of the marker is free from gloss and substances.
- Rayolite Round Shoulder ARC FH markers use an ABS shell to house the reflective lens that is molded of optic grade methyl methacrylate (plastic). The fill material consists of inert thermosetting compound with filler designed for impact and wear resistance. The Round Shoulder ARC has an improved smooth-edge.
- Ennis Paint Model 980 markers are newly developed to provide high performance by using long-life and high level of the patented prismatic glass lens, durable injection mold polymers, and a patented sure grip grooved base.
- Ennis Paint Model C80-FH markers (formerly under the name of Avery Dennison Corporation) using air gap technology are injection-molded by high-impact polymers which can obtain extra endurance. Its no-metallized cellular lens design can provide double ASTM standard initial brightness, and even allows lens to keep working after damage. It also has a patented sure grip grooved base.
- Ennis Paint Model C88 markers that set the industry standards worldwide more than 40 years ago have a lens coating to protect against abrasion.
- Ennis Paint Model 948 and 953 markers have the glass protected lens against abrasion. Ennis Paint Model 911 markers are the first ones which have the glass protected lens.
- Rayolite AA markers consist of all acrylic (AA), having rib and fish hook designs to create maximum adherence between the shells and fill materials. A protective brow protects the top area of the lens from deterioration. The ARC II markers have the abrasion resistant coats which are chemically bonded to the lens surface to protect it from the grinding action of dirt, sand and contact from traffic volume. The AA ARC II FH markers additionally have interior coatings which further protect the markers from UV rays and moisture penetrations.
- Rayolite Model 2002 markers are superior, compared with the AA ARC II FH markers, due to their reduced and smoothed-edge shapes that minimize the tire impact.

Table 2-2 DOT QPL/APL for Permanent Nonsnowplowable RRPMs

Product ID	Sample Picture	Note	DOT-QPL/APL No.
3M 290 Series		Thermoplastic markers, may maintain high retroreflectivity values even after damage; relative good performance in terms of retroreflectivity and structural damage in the TTI study (Zhang, et al. 2009)	ALDOT,V-2; AZDOT,V-23; AKDOT, 721.02; Caltrans,06-446504; FDOT,S706-0207; GDOT,76; TxDOT,DMS-4200; LADOT,09; NMDOT; TNDOT,9829; NVDOT,0255; WSDOT; MassDOT
3M 290 PSA Series		Thermoplastic markers with pressure sensitive adhesive	ALDOT,V-2; AZDOT,V-23; FDOT,S706-0209; GDOT,76

Table 2-2 DOT QPL/APL for Permanent Nonsnowplowable RRPMs (Continued)

Product ID	Sample Picture	Note	DOT-QPL/APL No.
Ennis Paint (Avery Dennison) Model C80-FH Marker		Injection molded marker with better durability than older models such as Avery Dennison C-88	AZDOT,V-23; FDOT,S706-0212; GDOT,76; NCDOT-NP11-5558; TxDOT,DMS-4200; NVDOT,0182; WSDOT; MassDOT
Ennis Paint (Avery Dennison) Model C88 Marker		The first and original "Stimsonite" model	ALDOT,V-2; AZDOT,V-23; Caltrans,06-446504; MIDOT; NCDOT-NP11-5555; TNDOT,05077; TxDOT,DMS-4200; NVDOT,0183; ORDOT,693; WSDOT
Ennis Paint Model 911 Marker		Model 911 is the first glass protected lens marker. Model 948 has low-profile design, the existing small layer of glass attached over the acrylic lens to improve the durability of the reflective face (Ullman, 1994). Stimsonite models 911, 948, or 953 Markers can keep working on 10000 vpd/lane AADT up to and beyond one year. These acrylic based corner-cube lens reflectors have an additional glass layer to protect the reflector from damage. Of the high-performance models at the highest volume site, the Stimsonite 911, 948, and 953 had the lowest percent of damage and number of missing markers (FHWA-RD-97-152).	AZDOT,V-23; AKDOT, 721.02; Caltrans,06 446504; MIDOT; TxDOT,DMS-4200; NVDOT,0180; WSDOT; GDOT,76; LADOT,09; TNDOT,9311; ORDOT,629
Ennis Paint Model 948 Marker			ALDOT,V-2; AKDOT, 721.02; Caltrans,06-446504; GDOT,76; WSDOT;LADOT,09; TNDOT,9312; ORDOT,148; KYDOT
Ennis Paint Model 953 Marker			AZDOT,V-23;Caltrans,06-446504;NVDOT,0181;WSDOT
Ennis Paint Model 980 Marker		Glass face in Model 980 improves reflectivity; special bottom of Model 980 provides more retention on roadway surface; Model 980 is "recommended for high AADT and high intensity traffic condition". (Ennis, 2014).	AZDOT,V-23;FDOT,S706-0211
Apex Model 921AR		Prismatic, may have serious retroreflectivity performance issues; average retroreflectivity values dropped below 50 after 12 months, even on low traffic locations; mid-bottom up cracking on flexible pavements (Zhang, et al. 2009)	ALDOT,V-2; AKDOT, 721.02; GDOT,76; Caltrans,06-446504; FDOT,S706-0208; NVDOT,0172; WSDOT; LADOT,09; TNDOT,11008; TxDOT,DMS-4200
Rayolite Round Shoulder		It has brightly colored house obtaining high visibility for daytime delineation. The Round Shoulder has an enhanced round shape that reduces tire impact and increases its lifetime.	Caltrans,06-446504; TxDOT,DMS-4200

Table 2-2 DOT QPL/APL for Permanent Nonsnowplowable RRPMs (Continued)

Product ID	Sample Picture	Note	DOT-QPL/APL No.
Rayolite Round Shoulder (ARC)		The abrasion resistant coats protect the lens.	ALDOT,V-2;LADOT,09; NVDOT,0177; WSDOT
Rayolite Round Shoulder (ARC FH)		Round Shoulder FH has an interior coating that protects marker from UV rays and moisture. Showed relative good performance in terms of retroreflectivity and structural damage in the TTI study (Zhang, et al. 2009)	FDOT,S706-0210
Rayolite AA		Rayolite AA markers consist of all acrylic having rib and fish hook designs and a protective brow.	ALDOT,V-2; Caltrans,06-446504; NCDOT-NP11 5580-5588; NVDOT,0175; ORDOT,529; WSDOT
Rayolite AA (ARC II)		The abrasion resistant coats protect the lens.	ALDOT,V-2; AZDOT,V-23; Caltrans,06-446504; GDOT,76; TxDOT,DMS-4200; LADOT,09; TNDOT,02090; NVDOT,0176; ORDOT,529; WSDOT
Rayolite AA (ARC II FH)		The AA ARC II FH markers additionally have interior coatings which further protect the markers from UV rays and moisture penetrations.	AZDOT,V-23
Rayolite Model 2002 (ARC II FH)		The structure of Rayolite Model 2002 is similar to AA, but obtains reduced and smoothed-edge shapes that minimize the tire impact and increase the useful. An abrasion resistant coating is chemically bonded to the lens surface to protect it from the grinding action of dirt, sand and contact from traffic volume.	ALDOT,V-2; AZDOT,V-23; Caltrans,06-446504; GDOT,76; TxDOT,DMS-4200; LADOT,09; MIDOT; NCDOT-NP11 5567-5569; TNDOT,02064; WSDOT; KYDOT

According to the above information about materials and structures, in summary, RRPMs can be categorized by different materials and structures.

2.1.1 With or Without Fill Material

Considering the properties and prices of RRPM materials, manufacturers design RRPM inside in two ways: with or without fill materials. On one hand, if the RRPM body material is acrylic, manufacturers do not fill other materials in these RRPMs, and the body structure is hollow, such as 3M 290 series and Ennis C80as shown in Figure 2-4. On the other hand, for saving cost, manufacturers fill some RRPMs with inert thermosetting compound, instead of acrylic. These RRPMs, such as Rayolite RS and Ennis C88, are fully solid as shown in Figure 2-5.

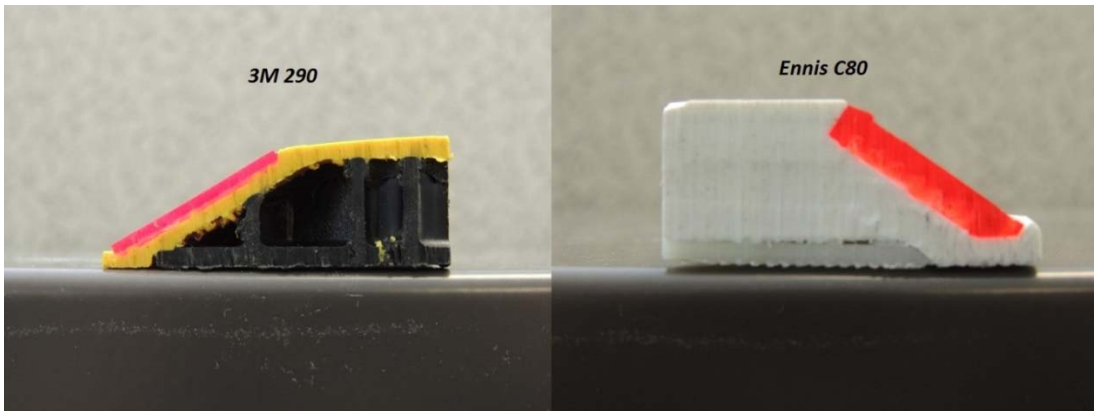

Figure 2-4 Cross-sections of 3M 290 and Ennis C80

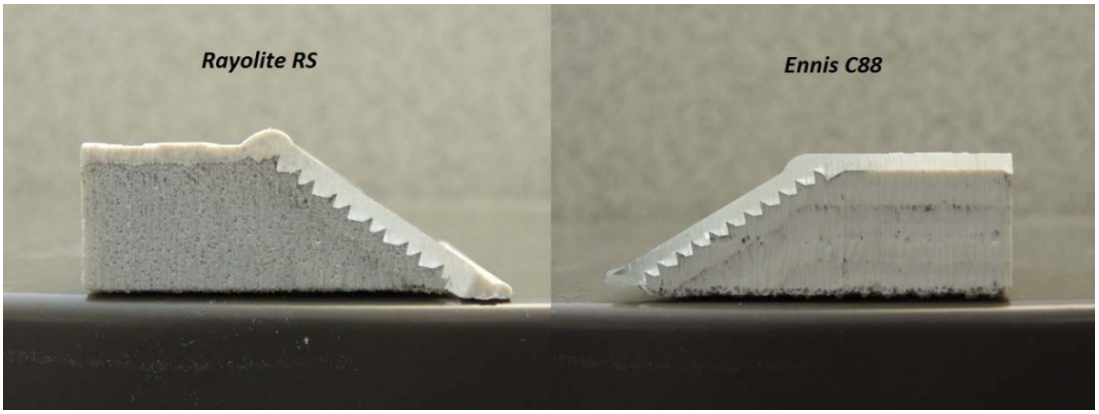

Figure 2-5 Cross-sections of Ennis C88 and Rayolite RS

2.1.2 Rigid or Flexible Bottom

Different materials also make RRPM bottoms rigid or flexible. Some RRPMs have flexible bottoms as shown in Figure 2-6, such as 3M 290 series and Ennis C80.Some RRPMs have rigid bottoms, as shown in Figure 2-7, such as Rayolite RS and Ennis C88. Similar to the analysis of rigid and flexible plates on pavement design, this categorization method is also necessary for further stress analysis.

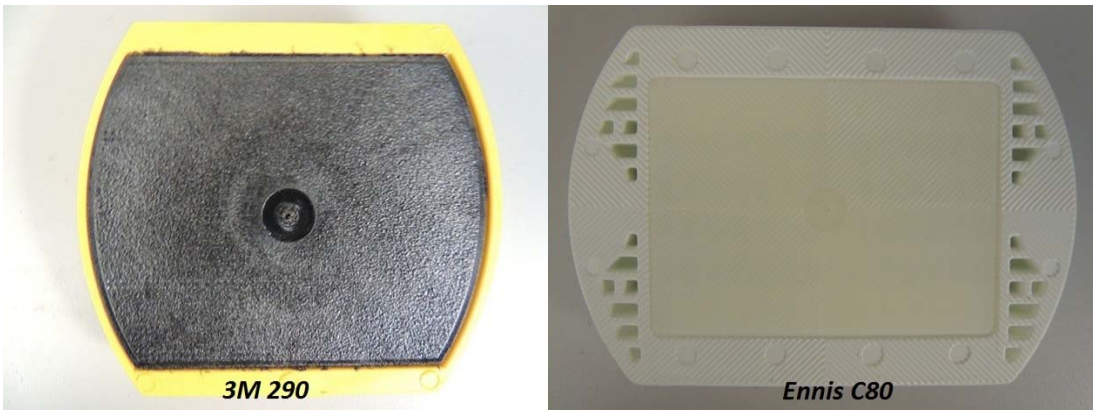

Figure 2-6 Bottoms of 3M 290 and Ennis C80

Figure 2-7 Bottoms of Rayolite RS and Ennis C88

2.1.3 Squared Bottom or Bottom With Curve

Geometrically, all RRPMs can be depicted by five variables (bottom length, bottom width, top length, top width, and height). The main RRPM visual differences are caused by RRPM bottom shape changes. Thus, from the geometric perspective, all RRPM can be divided into two categories: type I with squared bottom, such as Ennis C88, and type II with bottom with curve, such as Ennis C80. Because the radius of bottom curve in type I can be determined from bottom width and length shown in Figure 2-8, this category makes both RRPM types to transform to each other very conveniently, especially when building finite element models of RRPMs.

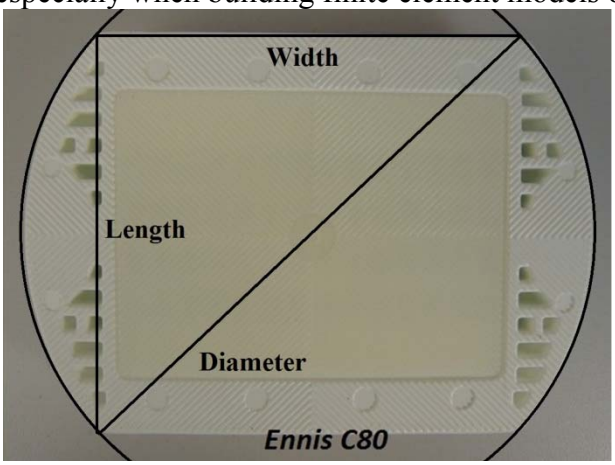

Figure 2-8 Geometric Relations on Bottom of Ennis C80

2.2 Laboratory Tests

Currently, although the RRPM models used on Florida roadways all meet the FDOT's laboratory test specifications, the service life of RRPMs on Florida roadways, particularly on those heavy-traffic roadways, are generally shorter than expected. So, one of the objectives of this project is to seek ameliorated laboratory test procedures to evaluate the qualities of RRPMs and to predict their field performance. This section provides the details of current laboratory tests.

Current specifications on laboratory tests can be mainly divided into three categories: American Society of Testing and Materials (ASTM) standards D 4280, National Transportation Product

Evaluation Program (NTPEP) procedures, and State DOT specifications, such as DMS-4200 from Texas Department of Transportation (TxDOT). Among these categories, the ASTM one is most widely adopted.

These specifications mainly contain twelve tests:

- compressive test,
- flexural test,
- lens impact test,
- lens color test,
- resistance to temperature cycling test,
- abrasion resistance for lens surface test,
- retro-reflectivity/coefficient of luminous intensity for new RRPMs test,
- retro-reflectivity/coefficient of luminous intensity for aged RRPMs test,
- water soak resistance test, and
- adhesive bond test.

Because this study focuses on the mechanical properties of RRPMs, the first three above mechanical tests are mainly discussed in this section. Following are the descriptions of these various tests and comparisons of different test specifications. All states' selections of these current tests with various test parameters are listed in Table 2-3.

2.2.1 Compressive Test

The compressive test, as described in ASTM D 4280, measures the failure potential of RRPM under a compressive load. In this test, markers should be first conditioned at 23.0±2.0°C (73.4±3.6°F) for four hours prior to testing, and then loaded between two steel plates, as illustrated in Figure 2-9. The load is applied at a rate of 2.5 mm (0.1 in.)/min. Under a load of 2,727 kg (6,000 lb), the deformation of marker shall be less than 3.3 mm (0.13 in.), and without breakage. Three specimens are tested, and more than one failure of them will cause rejection of the entire lot (ASTM, 2008).

The compressive tests in NTPEP, Florida, Alabama, North Carolina, Arkansas, Kentucky, Louisiana, and Tennessee are all in accordance with ASTM D 4280.

However, there are some variations in the details of the test procedures among various other states. These variations are mainly in three aspects: tolerated load, number of test and retest, and test method.

Table 2-3 RRPM Laboratory Tests

		National Standards		Other State Standards												
	FDOT	ASTM D4280 (LADOT, MSDOT, ALDOT, SCDOT)	NTPEP (KYDOT, NCDOT)	Caltrans	TxDOT	NCDOT	WSDOT	ORDOT	NVDOT	AZDOT	NMDOT	OKDOT	ARDOT	GDOT	TNDOT	VADOT	HIDOT
Compressive Test (lb)	✓ 6,000	✓ 6,000	✓ 6,000.	✓ 2,000	✓ 2,000	✓ 4,000	✓ 2,000	✓ 1,500 4,000	✓ 2,000	✓ 2,000	✓ 2,000	✓ 9,000.	✓ 6,000	✓ 2,000 4,000	✓ 6,000	crushing 44,000	✓ 22,000
Tensile Test (lb)	✓ 2,000	✓ 2,000	✓	✓	✓ 2,000	✓	✓ 2,000	✓	✓ 2,000		✓ 2,000	✓		✓ 2,000	✓ 2,000	✓ 55,000	□
Flexural Test	✓	✓											✓	✓		✓	
Lens Impact Test	✓	✓	✓			✓	✓							✓	✓	✓	
Lens Color Test	✓	✓	✓	✓		✓	✓	✓	✓	✓	✓		✓	✓	✓	✓	✓
Resistance to Temperature Cycling Test	✓	✓	✓		✓	✓						✓	✓	✓	✓		
Abrasion Resistance for Lens Surface Test	✓	✓		✓						✓				✓	✓	✓	
Retroreflectivity / Coefficient of Luminous Intensity for New RRPMs Test	✓	✓	✓	✓	✓	✓	✓	✓	✓	✓	✓	✓	✓	✓	✓	✓	✓
Retroreflectivity / Coefficient of Luminous Intensity for Aged RRPMs Test			✓		✓	✓							✓				✓
Water Soak Resistance Test				✓					✓								
On-Road Test	✓ 2 Years for Class B	1-year test Recommended, not required	✓ 2 Years		✓ 1 Year	✓								1-year test Recommended, not required	1-year test Recommended, not required	□	□
Adhesive Bond Test								✓	✓				✓		✓		✓

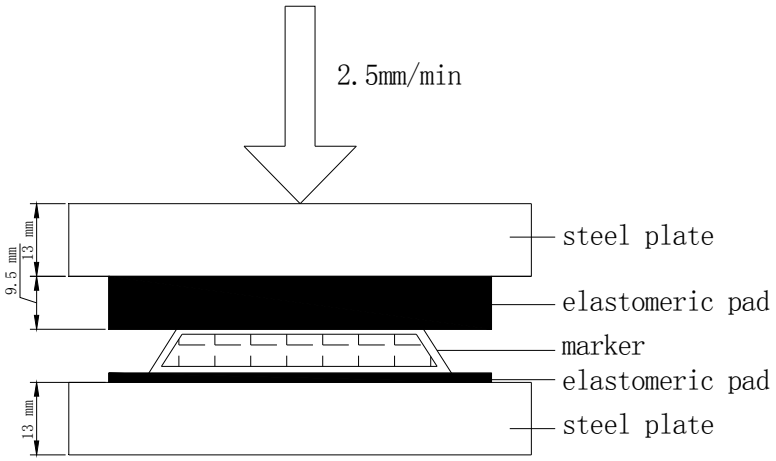

Figure 2-9 Compressive Test

2.2.1.1 Tolerated Load

For the tolerated load, Arizona, Texas, Hawaii, Nevada, California, South Carolina, Mississippi, and Washington only apply the compressive load up to 907 kg (2,000 lb.).

In Georgia Department of Transportation (GDOT) specifications, the load is based on the dimensions of markers. For standard raised markers of 4×4 inches (100×100 mm), it is no less than 907 kg (2,000 lb.) at the rate of 0.2 inch per minute. For low-profile markers of 4×2 inches (100×50 mm), it is no less than 1,814 kg (4,000 lb.) at the rate of 0.03 inch per minute (GDOT, 2012). Similar standards exist in Oregon which allows 680 kg (1,500 lb.) load for standard raised markers of 4×4 inches (100×100 mm) and 1,814 kg (4,000 lb.) load for low-profile markers of 4×2 inches (100×50 mm) (ORDOT, 2000).

Oklahoma does not follow ASTM D 4280, but ASTM D 788 instead, which is about the filled materials in the marker. The state specifications only mention that the potting compound filler shall be capable of withstanding a 4,082 kg (9,000 lb.) load (ODOT, 2009). Virginia and New Mexico do not mention compressive test specifically. Instead, Virginia requires a crushing strength that is no less than 1,814 kg (4,000 lb), in accordance with VTM-71 (VDOT 2007).

These various tolerated loads are expressed more clearly in Table 2-4 and Figure 2-10.

Table 2-4 Number of States Using Various Tolerated Loads

	6000 lb	2000 lb	Based on Dimensions	N/A
No. of States	7	8	2	3

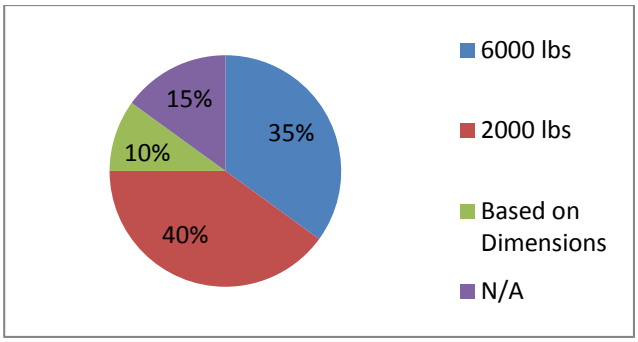

Figure 2-10 Various Loads' Proportions in States

2.2.1.2 Number of Tests and Retests

The number of specimens and definitions of failure also vary with states. For states that apply the 907 kg (2,000 lb.) load, the deformation of the marker or the delamination between the shell and the filler of the marker shall normally not exceed 3 mm, while ASTM D 4280 requires that only the deformation of the marker not to exceed 3.3 mm. Moreover, Hawaii, Georgia, and Oregon allow retest: if any one of three markers fails to satisfy the compressive strength requirements, six additional specimens can be tested. Failure of any one of these six specimens will cause the rejection of the entire lot or shipment represented by this sample (ORDOT, 2000).

Texas requests five random samples. One quality index value is used to analyze the compression result:

$$Q_L = (X - LSL)/s$$

where,

Q_L = quality index value,
X = average result from test,
LSL = lower specification limit,
s = standard deviation from test.

This quality index value shall be equal to or greater than 1.23.

2.2.1.3 Test Methods

Hawaii, Washington, California, South Carolina and Mississippi conduct another compressive test which is totally different from the ASTM procedure. In their tests, marker base is centered down and over open end of vertically positioned hollow metal cylinder, one inch high, with internal diameter of three inches, and wall thickness of l/4 inch. Then, at a rate of 0.2 inch per minute, a compressive load is applied to the top of a one inch diameter solid metal plug placed on top of the marker, as necessary to break the marker (WSDOT, 2012a). California and Mississippi also request to use protective eye glasses or shield (Caltrans, 2006).

In Georgia and Oregon, the test method is dependent on RRPM dimensions. For standard raised markers of 4×4 inches (100×100 mm), the vertically positioned hollow metal cylinder is used, as the above-mentioned method. For low-profile markers of 4×2 inches (100×50 mm), it is directly placed on a 12 mm thick flat steel plate (ORDOT, 2000), which is similar to the ASTM test method.

2.2.2 Flexural Test

In ASTM D 4280, markers are first conditioned at 23.0±2.0°C (73.4±3.6°F) for four hours prior to the flexural test. The test set-up is shown in Figure 2-11. A compressive load is applied through a top steel bar at a rate of 5.0 mm (0.2 inch) per minute until the marker breaks. The load at breakage should be higher than 8,914 N (2,000 lbf). Three replicates are tested, and more than one failure will cause rejection of the entire lot (ASTM, 2008).

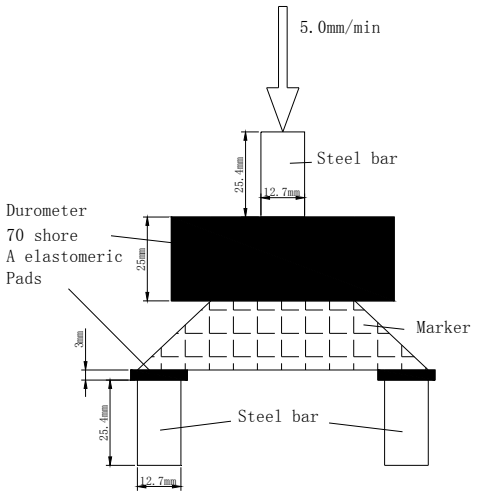

Figure 2-11 Flexural Test

The flexural tests in NTPEP, Florida, Alabama, North Carolina, Arkansas, Kentucky, and Louisiana are all in accordance with ASTM D 4280. The other states that install RRPMs do not conduct this test.

2.2.3 Lens Impact Test

The lens impact test measures the resistance of retroreflective lens to an impact load. In ASTM D 4280, a marker specimen is first placed in a convection oven at 55°C (130°F) for one hour. Then, while at the elevated temperature, the reflective face of the marker is impacted by a dart fitted with a semi-spherical head dropping vertically onto the approximate center of the reflective surface. The general set-up of this test is shown in Figure 2-12. The marker specimen is set on a steel fixture to keep the reflective face horizontal, and the fixture is placed on a solid surface. Test results are based on inspection for cracking and delamination. For acceptable markers, the face of the lens shall show no more than two radial cracks longer than 6.4 mm (0.25 in.), and there shall be no radial cracks extending to the edge of the abrasion resistant area and no delamination.

Ten specimens are tested for each requirement. Failure of more than one of the specimens will cause rejection of the entire lot.

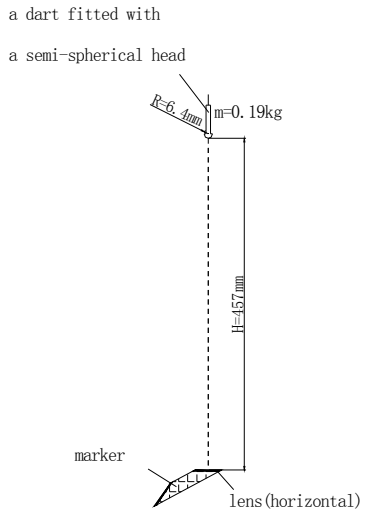

Figure 2-12 Lens Impact Test

The lens impact tests in NTPEP, Florida, Alabama, North Carolina, South Carolina, Kentucky, Louisiana, and Tennessee are all in accordance with ASTM D 4280. Additionally, Florida, South Carolina, and Mississippi approve concentric crack appearance after impact. Mississippi also notes that on two color units, the red lens may not be glass covered and if so the marker should not be subjected to the impact test.

Texas conducts the impact test during the pre-qualification process. The principles are similar to those in ASTM D 4280. However, Texas uses a solid right-circular cylinder (20-lb weight and 2-inch diameter) with a flat impact face having rounded edges, instead of dart. Moreover, the solid, flat, steel plate which fixes RRPM is at least 0.5 inch thick. The height of the cylinder is variable, and the RRPMs are tested at increasing heights until failure occurs. When the lens or body cracks, the height of the cylinder is recorded. This recorded height shall be larger than 6 inch; otherwise the products will be rejected.

CHAPTER 3 QUESTIONNAIRE SURVEY

3.1 Introduction to Questionnaire Survey

To gather up-to-date RRPM information from experienced engineers and specialists, a questionnaire survey was administered and distributed electronically across the nation. The respondents involved contract managers, maintenance engineers, and other personnel in various state DOTs. Considering the purpose of the study and the selections of the field survey locations discussed in Chapter 5, the respondents were separated into three groups: Group A from FDOT District 7 (Tampa area), Group B from other FDOT Districts, and Group C from other states (mainly DOT personnel with a few from the industry). The information on respondents is summarized in Table 3-1.

Table 3-1 Information on Respondents and Survey Participation

Questionnaire Range	Target Respondents	Number of Respondents Contacted	Number of Total Responses Received	Number of Complete Answers Received
FDOT District 7 (Tampa area)	Maintenance Engineer, Contracts Project Manager, Inspector, Maintenance Technical Coordinator	7	5	4
Other FDOT Districts	District Maintenance Administrator, Maintenance Engineer, Contract Manager,	11	4	4
Other States	State Maintenance Engineer, Director of Maintenance, State Traffic Operations Engineer, Roadway Maintenance Management Engineer, Traffic Control Devices Engineering Manager, Pavement Marking Supervisors, Traffic Control Specialist Manager.	45	28	12
Total Number of Responses				20

3.2 Survey Design

Since this questionnaire survey concentrated on the physical properties required of RRPMs, following questions were designed to elicit the information related to current RRPM performance, potential failure reasons, and suggestions of RRPM service life extension:

- At which locations may RRPMs experience more damage and replacement?
- Do trucks cause more RRPM damage than cars? /Are RRPMs installed between outside lanes replaced more frequently than RRPMs installed between inside lanes?
- What types of RRPMs (based on FDOT qualified product list if in Florida) are most commonly used? Why? Are there any RRPMs seen as good markers and any seen as bad markers in terms of field performance?

- What failure modes are often observed (e.g., lens cracking, RRPM body cracking, and loss of RRPMs [adhesive failure]) on asphalt pavements/ concrete pavements?
- What is the general frequency of replacement of RRPMs?
- Can you recommend some roadway sites in Hillsborough county for us to conduct field condition survey, including sites where RRPMs are frequently replaced and where RRPMs last for long periods?
- Have you observed more RRPMs damages on concrete pavements than on asphalt pavements?
- Are glass lenses better than acrylic lenses, considering the total price, their performance, and their service life?
- Do you have any thought on what can be done to extend RRPMs service life?
- Does your state use non-snowplowable RRPMs?

Since respondents' experiences were various in different areas and the purpose of this study focused on improvement of RRPM performance in Florida, the questions in the questionnaire survey were slightly different among these three groups. For more clearly stating the questions' purposes and their corresponding answer groups, one flowchart on this questionnaire survey is shown in Figure 3-1.

Then, based on this flowchart, the targeted questions and corresponding responses are summarized in the following sections, with subtle nuances among different respondents.

3.3 Questionnaire Survey Results

3.3.1 RRPM Types and Performance Comparison

Responses from Group A showed that 3M and Stimsonite were more commonly used because they were cheaper. 3M was deemed to be a good marker which had a longer service life on the road and Stimsonite as not so good in the field performance. The markers should meet the ASTM D 4280 specifications.

Responses from Group B showed that Type B markers which were listed on the FDOT QPL were the only RRPMs installed on the road. Before beginning work, the certification of materials was checked. No significant different performances existed between manufacturers.

Responses from Group C were various in different states. Georgia used 2×4 inches or 4×4 inches size RRPMs. Their color and installation were based on the line pattern: Type 1 was a two-way yellow installed on double yellow, two way left turn lanes, single yellow skips and the skip line on a no passing zone. Type 2 was one-way yellow installed on the solid line on a no passing zone. Type 3 was two-way red and white installed on white skip lines, turn lanes, gore lines and islands on interstates and multi-lane routes. All approved markers had similar service lives.

In South Carolina, plastic makers with reflective surfaces, such as 3M 290, became more widely used in recent years. As for performance, the interstate routes provided the toughest environment and the potted style markers had traditionally performed best. On these styles of markers, the use of acrylic lenses with scratch resistant coatings was permitted. However, years ago South Carolina required glass lenses which seemed to provide better performance, but was also more expensive. Practically, Rayolite, Ennis (Stimsonite) and 3M markers which complied with the requirements of specifications were installed on contracts.

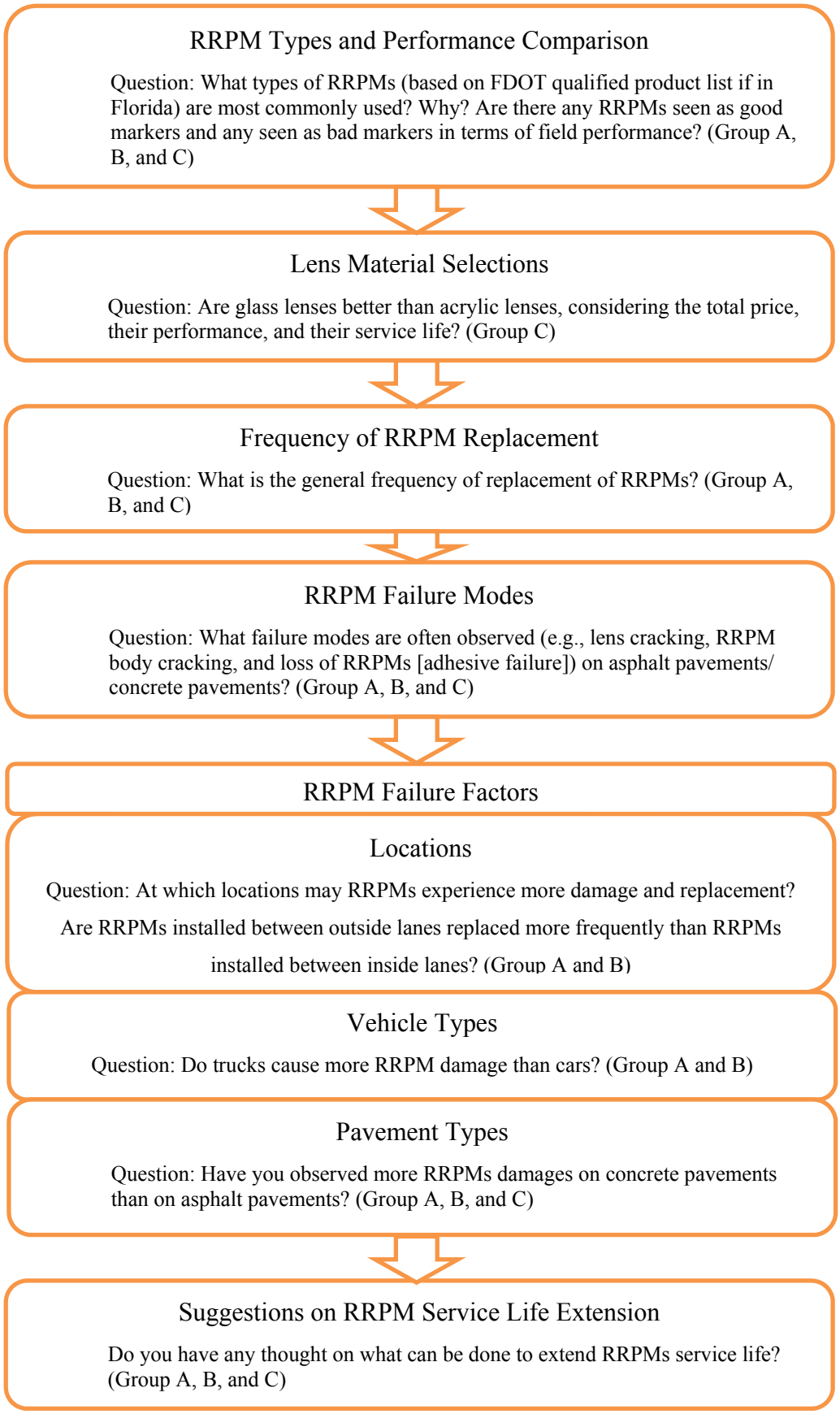

Figure 3-1 Flowcharts of Questionnaire Survey Design

Louisiana preferred 3M because of low bids. Contractors also seemed to select more of the Ennis and Rayolite markers. The Ennis markers seemed to hold up better. Arkansas installed 3M, Ennis, and Rayolite markers based on supply contract specifications, without significant different performance between manufacturers. In Arizona, 3M 290 markers occupied the most of the RRPM market for a while. Although Ennis 88, 911 and 980, Apex 920 or 921, Rayolite round shoulder, ARC II markers had been approved, they were not often used. Washington selected the Stimsonite model 88 RRPMs to install in the Olympic Region because they withstood the plow abuse and normal highway use. Other RRPMs similar to the Stimsonite 948 ones were also installed in Washington but they did not hold up well. Respondents from Nevada and North Carolina only mentioned that the 3M markers had no significant difference in performance from other types of markers.

One respondent from California thought that 3M was the best type: they seem to outlast all others by far, where reflectivity was concerned. He also mentioned that the worst type was Rayolite: they did not seem to last longer than a year or so regardless of traffic.

In summary, 3M, Ennis, and Rayolite were the most popular RRPMs' manufacturers in these states. 3M had dominated for quite a while because of its cheaper price and good field performance. Although the type of RRPM used varies among states, it shows that all these seven states used 3M 290. Oppositely, Apex was not so popular.

Considering field performance, Group A generally preferred 3M and regarded Stimsonite as not so good. Group B claimed that there was no significant difference in performance between manufacturers. In Group C, three respondents made the same comment as Group B. One respondent from Louisiana replied that Ennis seemed better, and another respondent from Arizona felt that 3M dominated. Figure 3-3 illustrates that most of the respondents felt no significant difference in field performance of these approved RRPMs.

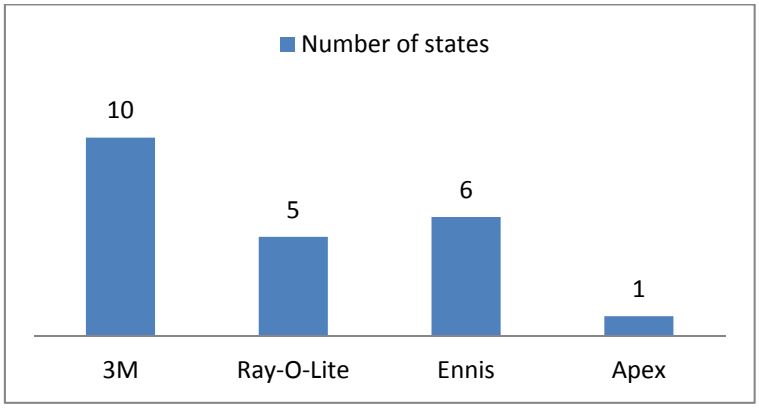

Figure 3-2 Numbers of States Using Various RRPMs

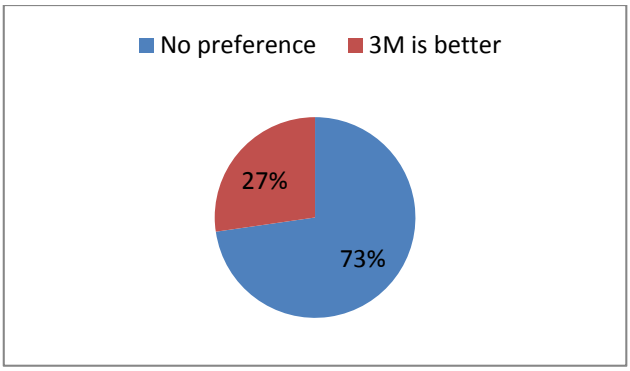

Figure 3-3 Comments on RRPM Selections and Their Percentages

3.3.2 Lens Material Selection

Several respondents from Group C stated that glass lenses performed better than acrylic for durability, but when they cracked, moisture got in the lens and deteriorated the prisms. One respondent believed that glass lenses retained better retroreflectivity than acrylic. Moreover, the cost for manufacturing glass lens was higher than acrylic. Therefore, companies might not produce them if the competition was producing acrylic lenses. On the contrary, one respondent believed that since most of the cost was in the installation, the longest lasting lens, not the cheapest, should be considered.

3.3.3 Frequency of RRPM Replacement

The results from three groups are summarized in Table 3-2 and plotted in Figure 3-4.

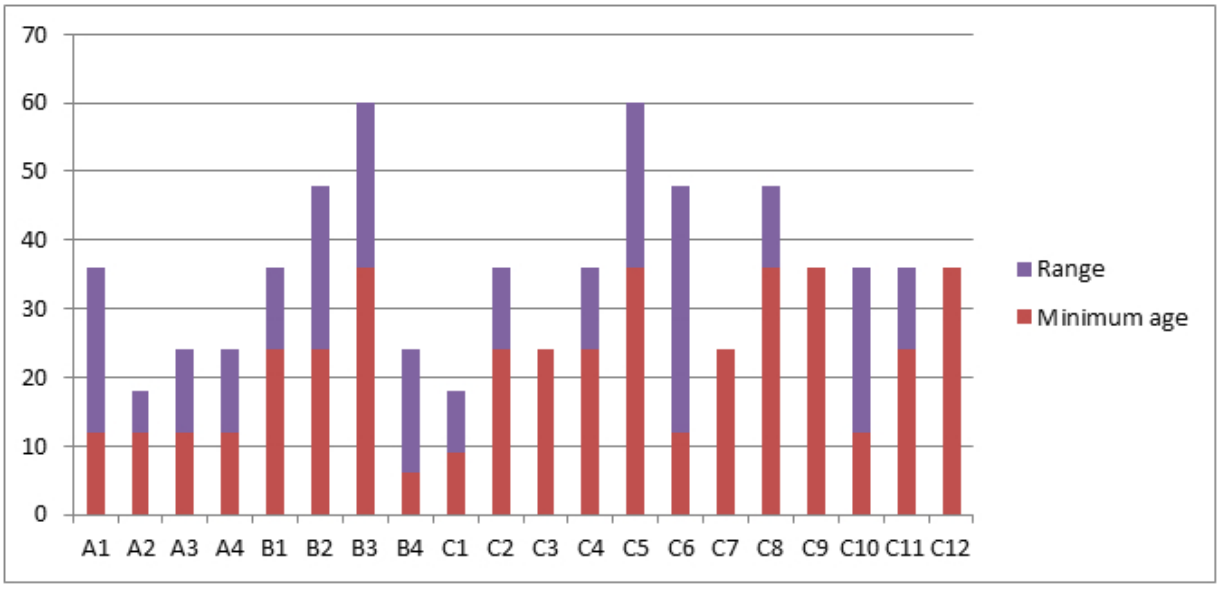

Figure 3-4 Replacement Intervals of RRPMs (month)

Table 3-2 Interval of Replacement of RRPMs (month)

	Answer No.	Max. age	Min. age	Ave. age
Group A	A1	36	12	24
	A2	18	12	15
	A3	24	12	18
	A4	24	12	18
Group B	B1	36	24	30
	B2	48	24	36
	B3	60	36	48
	B4	24	6	15
Group C	C1	18	9	13.5
	C2	36	24	30
	C3	24	24	24
	C4	36	24	30
	C5	60	36	48
	C6	48	12	30
	C7	24	24	24
	C8	48	36	42
	C9	36	36	42
	C10	36	12	24
	C11	36	24	30
	C12	36	36	30
Average		35.4	21.8	28.6

Based on Figure 3-4, the estimated intervals of RRPM replacements varied with respondents. Figure 3-5 and Figure 3-6 illustrate that most respondents estimated the minimum age of RRPMs to be between 12 and 24 months and the maximum age to be approximately between 24 and 36 months, depending on traffic volume, truck traffic percentage, and locations of RRPMs on the road.

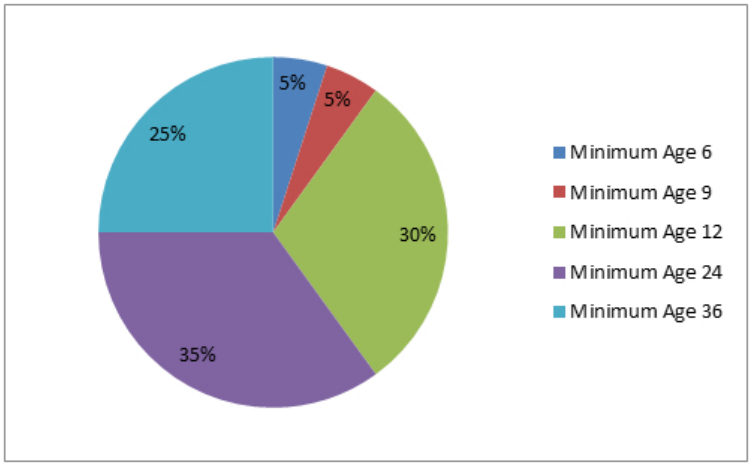

Figure 3-5 Percentage of Respondents With Various Estimated Minimum Ages of RRPMs

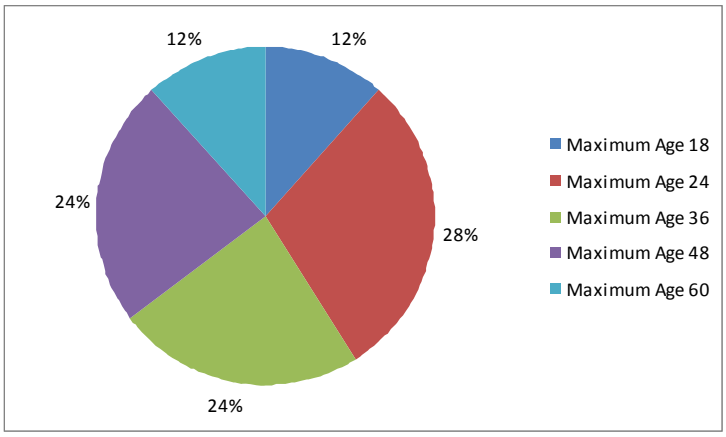

Figure 3-6 Percentage of Respondents With Various Estimated Maximum Ages of RRPMs

3.3.4 RRPM Failure Modes

Responses from Group A showed that according to current observation, it was true that most of the suffered damages were lens and body cracking, and scuffing of the lens surface. Moreover, there was one more item of failure mode: sinking into the pavement surface, which typically occurred on new asphalt pavements. The adhesion tracking onto lens caused by sun heating, rain and dirt were also deemed as failure.

Response from Group B showed that the respondents' answers for the failure modes on asphalt pavements were different, as listed in Table 3-3 and plotted in Figure 3-7. As can be seen, lens and body cracking, sinking and loss were the three main observed failure modes of RRPMs on asphalt pavements in Florida. Additionally, two respondents emphasized that the loss of RRPMs should be the most failure mode. For the failure modes on concrete pavements, their answers were the same: adhesive failure.

Table 3-3 Main Failure Modes and Number of Respondents in Group B

	Failure Modes		
	Loss	Crack	Sink
Number of Respondents	3	3	1

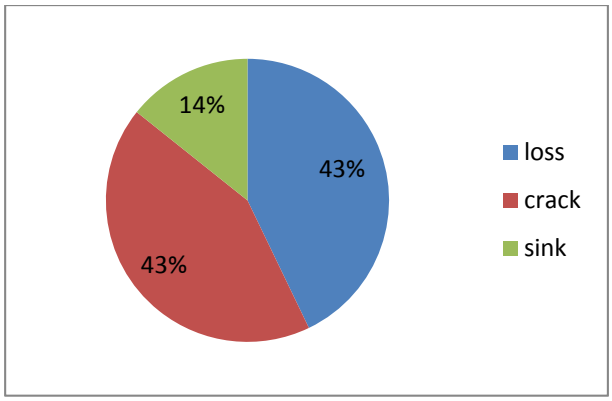

Figure 3-7 Main Failure Modes and Percentage of Respondents in Group B

The answers from group C were similar to those from Group B. The specific results are shown in Table 3-4 and Figure 3-8.

Table 3-4 Main Failure Modes and Number of Respondents in Group C

	Failure Modes		
	Loss	Crack	Sink
Number of Respondents	7	7	3

In conclusion, the respondents' answers showed that lens and body crack and loss of RRPMs were the main failure modes, and their proportions were almost equal. Sinking was another common failure mode on flexible pavements.

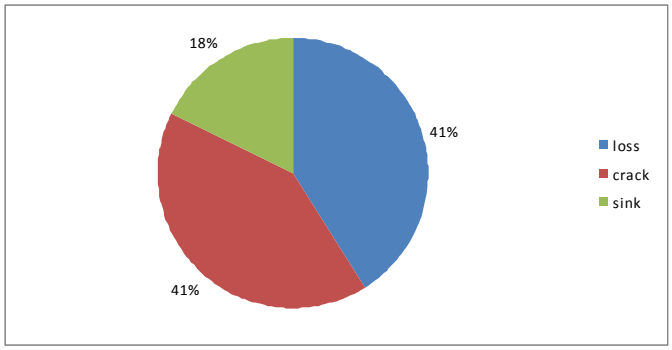

Figure 3-8 Main Failure Modes and Percentage of Respondents in Group C

3.3.5 Failure Factors: Locations

Group A respondents listed following more frequent damage locations: areas where highly frequent vehicle movements (weaving, turning and stopping) occur, such as high volume traffic areas, multilane, gore areas (U-turns and sharp turns), nearby bus or shipping terminals. Moreover, the heavy traffic volume could cause more damage and replacement. Group A also stated that RRPMs were replaced more often on the outside lanes than on inside lanes.

Group B respondents listed following more frequent damage locations: most damage is done by vehicle contact in curves, intersections (particularly on turn lane lines) and multilane (between the outside and middle lane on 6-lane Interstate highways). Truck stop entrances and high speed highways also provided the majority areas for damage.

In summary, the responses to this question are summarized in Table 3-5 and Figure 3-9. As can be seen, RRPM damages were mainly contributed by the vehicle's high probability of contacting RRPMs and its high impact to RRPMs. High traffic volume, multilane for lanes changing, and existing curves for lanes turning were all the factors that caused higher probability of contacting RRPMs. Meanwhile, heavy traffic volume and high traffic speed were the factors that caused higher traffic impact to RRPMs. Moreover, RRPMs on outside lanes were replaced more frequently than those on inside lanes.

Table 3-5 Locations of Damaged RRPMs and Number of Respondents

Location	Main reason	Number of respondents from Group A	Number of respondents from Group B	Total number of respondents
High volume traffic areas	High probability	2	0	2
Multilane for lanes changing	High probability	1	2	3
Gore area (U-turns and sharp turns)/Intersection/ Curve for lanes turning	High probability	1	3	4
Heavy volume on area roads/ Bus or shipping terminals, or nearby landfill/Truck Stop Entrances	High impact	2	1	3
High speed roadways	High impact	0	1	1

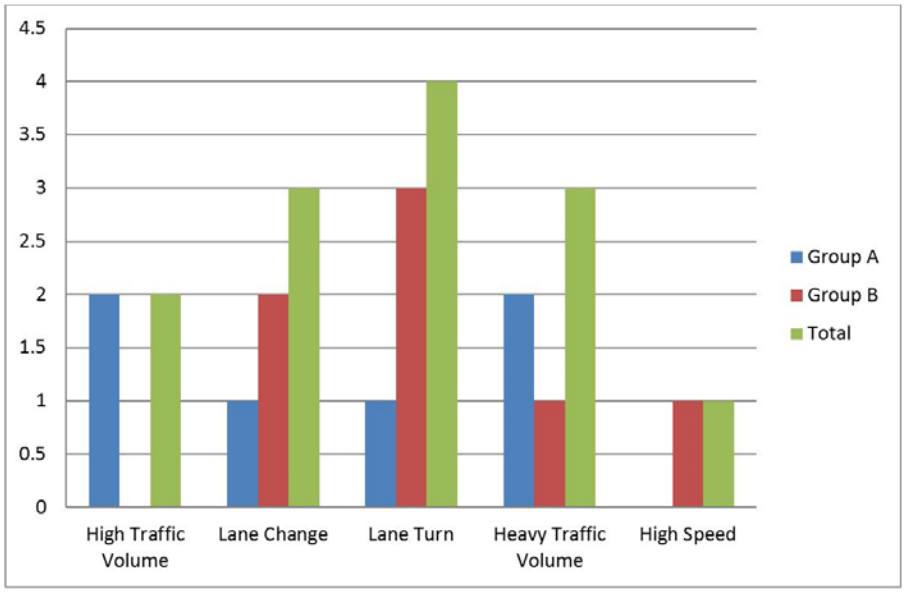

Figure 3-9 Location of Damaged RRPMs and Number of Respondents

Figure 3-9 shows that most respondents regarded that more damage and replacement of RRPMs occur in the existing curves, such as gore area and intersection. Fewest respondents thought the high speed could cause more damage and replacement of RRPMs.

3.3.6 Failure Factors: Vehicle Type

Responses from Groups A and B were the same: trucks did cause more RRPMs damage. On the Interstate highways, the truck lanes showed more wear and loss than the non-truck lanes (replacement is needed about twice as much.).

3.3.7 Failure Factors: Pavement Type

Respondents from Group A agreed that more RRPMs damages occurred on concrete pavements than on asphalt pavements, simply due to the harder concrete surface (only one respondent answered this). Respondents from Group A also stated that adhesion failure occurred more

frequently on concrete or old asphalt pavements, and more frequently when using epoxy adhesive instead of bituminous adhesive.

Three respondents from Group B believed that loss on concrete was more than loss on asphalt because of the poor adhesive issue. One respondent claimed that the answer could not be conclusive.

The respondents from Group C had different opinions on this question, and the answers were divided into three types, which are shown in Table 3-6 and Figure 3-10. Table 3-6 shows that most respondents agreed that RRPM damages on concrete pavements were more than those on asphalt pavements.

For this question, one state traffic operations engineer in South Carolina pointed out that only about 1% of roads on the state system were concrete surface and most of those were on the interstate system where annual daily traffic (ADT), vehicle speeds and percentage of trucks were all high. That was one potential reason why RRPMs were more damaged on concrete pavements than on asphalt pavements, which was related to the pavement type itself.

One respondent stated that he did not have any documented proof which was worse. However, he found a lot more missing RRPMs on concrete pavements because these locations usually had a concentration of RRPMs and were a lot more noticeable.

Table 3-6 Answers and Number of Respondents on Pavement Type Effects

Answer	Number of Respondents
No answer	2
Directly answer yes	3
Directly answer no	3

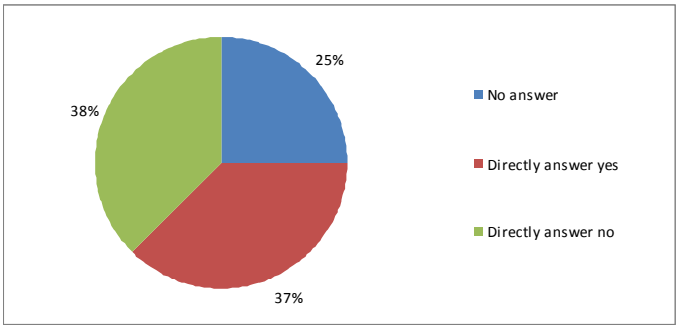

Figure 3-10 Answers and Number of Respondents on Pavement Type Effects

3.3.8 Suggestions of Field Survey Site Selection

For preparing further field survey, this questionnaire survey also asked respondents from Group A to recommend some field survey sites, based on their own experience in this particular area. In conclusion, they listed following sites that were valuable to field survey, which are shown in Figure 3-11:

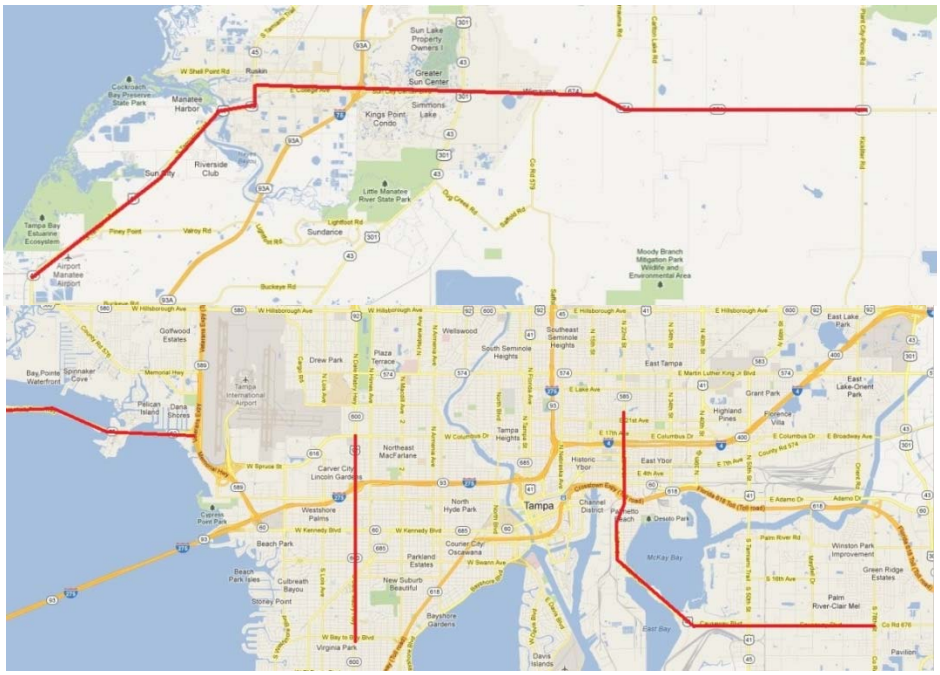

Figure 3-11 Roadways Recommended for Field RRPM Survey

- Dale Mabry Highway (in front of Tampa Stadium) for frequent replacement and US41 South of Ruskin where field life is longer.
- SR 60 and Dale Mabry that are high traffic areas. SR 674 has less traffic crossing East and West of I-75, but heavy truck volume towards Polk County.
- 22nd St. with heavy truck traffic.

3.3.9 Suggestions on RRPM Service Life Extension

The methods recommended by the respondents for extending RRPM service life are listed as following:

- Improvements in adhesion,
- Profile height decrease,
- A stronger piece shell and going back to fill the shell with epoxy.

Other experiences and suggestions shared by specialists include:

- The placement of markers was normally following the painted lines which were usually in the joint of the roadway. Moving this joint and/or paint from each other and RRPMs would last longer. The specification stated that RRPMs would not be placed within this joint, but it was not adhered to.
- The greater surface area (4”×4”) marker, as opposed to 5”×2” marker, reduced sinking on asphalt pavements and provided better bonding.
- Adhesive failure was almost always contributed to the issue of improper installation.
- RRPMs with sheeting under the lenses worked the best due to the fact if moisture got under the lens the sheeting was designed to withstand rain, UV exposure, etc.
- The embedded reflector into asphalt also presented a problem if removal was ever required, as damage to the asphalt occurred when digging the old reflectors out. Considering this situation, when replacing old reflectors, crews should generally put a new reflector in front of the old one, leaving the old reflector in place.

It is worth pointing out that some states, such as Washington and California, preferred to install recessed RRPMs. Since they had started recessing, all the RRPMs had switched to a 5-6 years life cycle. However, one problem they were experiencing was the bottom of the recess cuts was failing and if they could resolve that problem the recess cut kept a visible RRPM in place for several years. The one negative issue with the recessed RRPM verse the surface mounted RRPM was that the surface mounted RRPM was a lot more visible at long distances.

3.3.10 Update of RRPM Map

Four respondents who respectively worked in Virginia, Pennsylvania, Tennessee, New Mexico, Oklahoma, and Kentucky replied that their states did not use RRPMs anymore, although their DOT specifications did mention RRPMs. Considering the weather conditions, these DOTs all used snowplowable RRPMs and temporary RRPMs, instead. Based on these answers, the map plotted in Figure 2-1 was modified as shown in Figure 3-12.

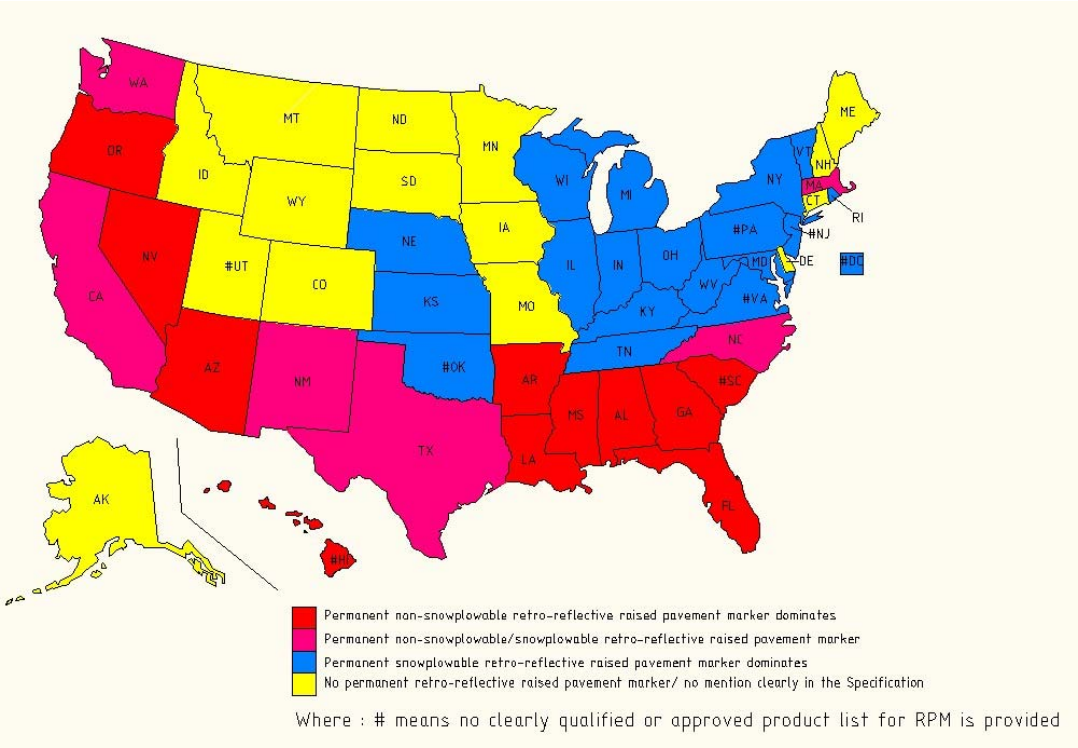

Figure 3-12 Use of Snowplowable or Nonsnowplowable RRPMs in the U.S. (modified after questionnaire survey)

3.4 Findings from Questionnaire Survey

In summary, 3M, Ennis, and Rayolite were the most popular RRPMs manufacturers in these states. Most of the respondents felt no significant difference in field performance of these approved RRPMs, with the maximum age approximately between 24 and 36 months. For the lens material selection, the glass lenses performed really better for durability and retroreflectivity, but more expensive. Moreover, the cracked glass lens would let moisture in and deteriorate the prisms. Therefore, companies might not produce them if the competition was producing acrylic lenses.

For the RRPM failure modes, the lens and body crack and loss of RRPMs were the most typical failure modes mentioned by respondents. Sinking was another common failure mode on flexible pavement.

For the reasons of RRPM failure, RRPM damages were mainly contributed by vehicle's high probability of contacting RRPMs and its high impact to RRPMs. High traffic volume, multilane for lanes changing, and existing curves for lanes turning (gore area and intersection) were all the factors that caused higher probability of contacting RRPMs. Meanwhile, heavy traffic volume and high traffic speed were the factors that caused higher traffic impact to RRPMs. Moreover, RRPMs on outside lanes were replaced more frequently than those on inside lanes. Most respondents also agreed that the various pavement types lead different probabilities of RRPM failure modes: more RRPMs damages occurred on concrete pavements than on asphalt pavements, simply due to the harder concrete surface (only one respondent answered this).

This questionnaire survey also provided sites for further field survey, suggested potential methods to extend RRPM service life and updated the map of current use of RRPMs in the U.S.

CHAPTER 4 FIELD EVALUATION AND RRPM PERFORMANCE

The RRPM models used on Florida roadways all pass FDOT's laboratory test specifications; however, their performance in the field varies significantly. A series of field surveys, during May 2012 through June 2013, was conducted to document and collect the details of various failure modes under different traffic and climate conditions.

This survey was conducted through visual observation backed up by digital photography. The geometric characteristics and the conditions of the roadways were determined from the geographic information system (GIS) data and straight line diagrams (SLDs), which were both available on FDOT website. All climate information, including monthly precipitation and monthly temperature, were collected from National Climatic Data Center.

4.1 Field Survey Introduction

4.1.1 Objectives of Field Survey

A series of field surveys were conducted over a period of approximately one year; observations from one survey suggested changes in the objectives for the following survey.

During the first field survey, the following questions were answered:

1) Which types of RRPMs are widely used on FDOT roadways and how do they perform?
2) Which major failure modes do the RRPMs exhibit in the field?

Because of lack of RRPM age information, evaluation and comparison of the RRPM performances could not be based on only a single field survey. Considering the issue of censoring data, a repeated-measurement field survey was indispensable to further analysis. Based on the time series surveys, the following questions were answered:

1) Which factors may potentially affect RRPMs field performance, including roadway geometric characteristics, traffic and weather conditions?
2) How did the specific failure mechanisms develop in the long run?
3) Which types of RRPMs have better durability?

4.1.2 Site Selection

Generally, the first step of field evaluation was selection of field survey sites. For this purpose, many elements were considered: area type (urban or rural), pavement type (concrete, asphalt, or seal coat), traffic condition (average daily traffic [ADT] and truck percentage), environmental conditions, multiple lanes, and geometric characters (Zhang, 2009). Specifically, the geometric features also included tangent, horizontal curve, vertical curve, width, and position (entry and departure approaches at intersections).

Based on consulting with FDOT personnel, three main routes, as shown in Figure 4-1, were selected in this research. One route was from 10 miles south of Ruskin, along US 41, then turned to SR 674, and ended at the intersection with Plant City-Picnic Rd. The second route was on Dale Mabry Hwy and 22 St, which were connected by SR 60. The third route was along 22 St, then crossed SR 60 to Causeway Blvd, and ended at the intersection with Maydell Dr..

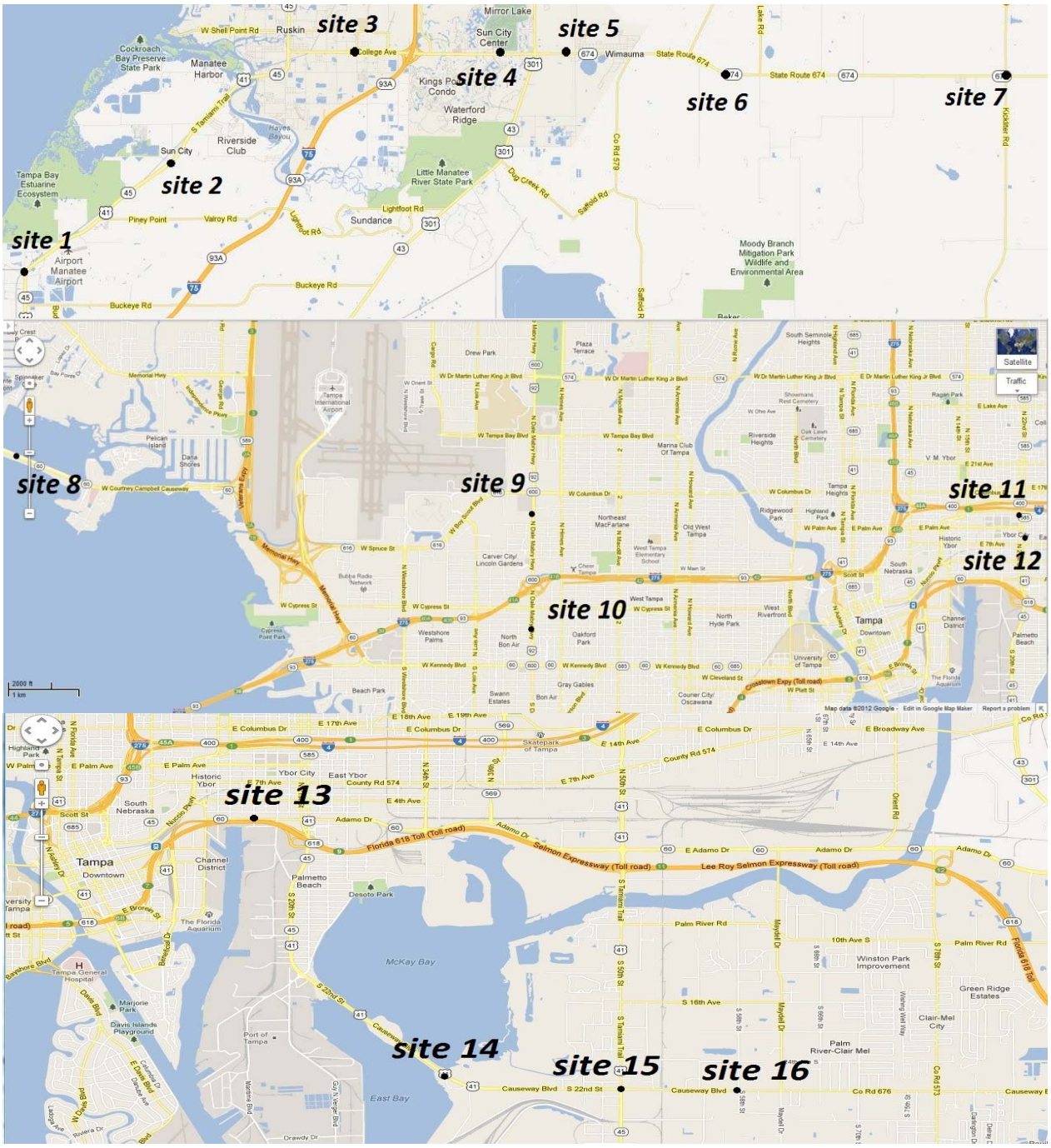

Figure 4-1 Locations of Roadway Sections Surveyed

4.1.3 Visual Observation and Performance Measurement Method

Visual observation was rated on three dimensions: marker case, lens surface, and lens interior. Their conditions were expressed as the method to measure the performance of RRPMs, in accordance with NTPEP:

$$R = \sum_{i=0}^{5} \beta_i R(i)$$

where,

R = Total rating

R (i) = Rating defined by NTPEP:
R (5) = 5-Excellent; Completely Intact, “Like New” Condition
R (4) = 4-Good; Minor Scrapes and Scratches
R (3) = 3-Fair; Obvious Damage but still Functional
R (2) = 2-Poor; Major Damage, Marginally Functional
R (1) = 1-Very Poor; Non-functional
R (0) = 0-Missing
β_i = Estimated proportion

4.2 Field Survey Results

4.2.1 RRPM Types and Road Condition in Field Survey

On these three routes, there were four types of RRPMs observed: 3M 290, AA ARC II, C80, and Round Shoulder. In accordance with literature review, 3M 290 was also the most widely used RRPM on these routes. The proportions of their observed installation sites are expressed in Figure 4-2.

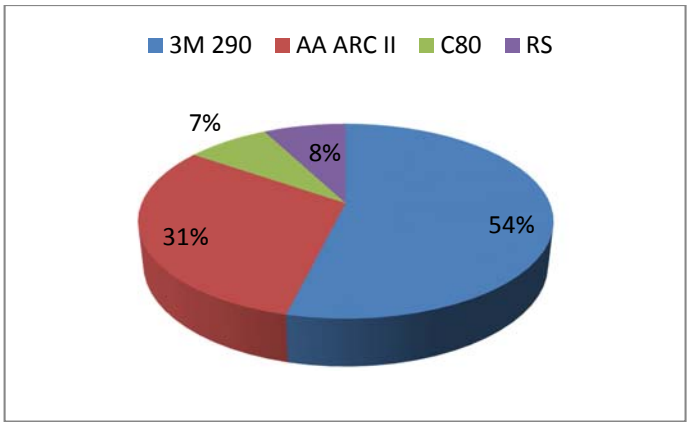

Figure 4-2 Proportions of RRPM Installation Sites

For the road condition, nine sites were paved by asphalt concrete (AC), two sites were paved by cement concrete (CC), and two sites were paved by the combination of AC and CC. The proportions of pavement types are shown in Figure 4-3.

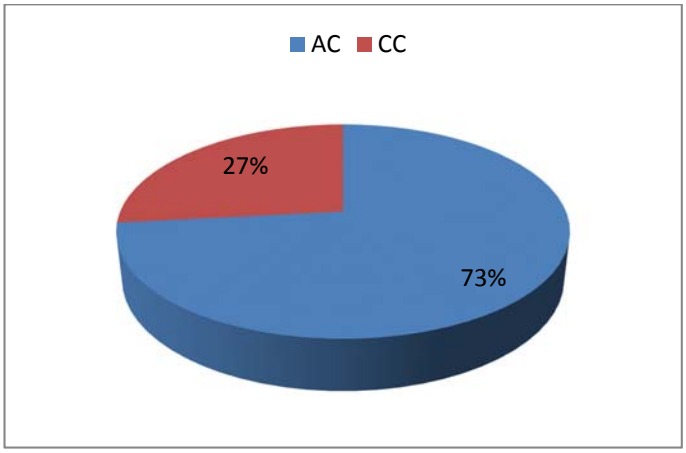

Figure 4-3 Proportions of Pavement Types

It is worth pointing out that, unfortunately, in ensuing field surveys, some sites (sites 6, 7 and 8) experienced resurfacing and those old RRPMs were replaced. Thus, the observation results at these sites from first survey could not be used for a time series comparison. However, the failure process of new RRPMs at these sites, starting from second field survey, could be captured through ensuing field surveys.

4.2.2 Observed Failure Modes

Generally, the RRPMs failure modes could be categorized into four types: lens breakage and loss; cracking of the RRPM body; complete loss of RRPM from pavement surface; and severe abrasion or contamination of the retro-reflective faces (Zhang et al., 2009). For more specific description, this study further divided the above four modes into seven categories, as follows:

- LC: lens cracking
- LL: lens loss
- BC: body cracking
- BB: body breakage
- LR: complete loss of RRPMs from pavement surface with only adhesive remaining
- AC: severe abrasion or contamination of the retroreflective faces
- S: sinking of RRPMs into asphalt concrete

Based on the first field survey on the selected FDOT roadways, the counts of sites with different observed failure modes are listed in Table 4-1.

Table 4-1 Counts of Sites with Different Failure Modes of Four RRPM Brands

	LC	LL	BC	BB	LR	AC	S	No. of Sites Surveyed
3M 290	1	0	2	2	3	10	6	11
AA ARC II	3	2	3	1	2	3	1	5
C80	0	0	0	0	0	1	0	1
Round Shoulder	0	0	0	0	0	1	0	1

It can be seen from Table 4-1 that:

- 3M 290 was most widely installed at these field survey sites, followed by AA ARC II.
- For 3M 290 markers, because no lens loss (LL) was observed at these sites, their lenses appeared relatively sturdy. However, there were frequent abrasion or contamination of the lens surface (AC) and marker sinking (S).
- All distress modes were found on AA ARC II.
- Both marker bodies of AA ARC II and 3M 290 seemed weak in the middle. AA ARC II had an abrasion resistant coating which had two bond parts. The bond boundary in the middle body of the RRPMs seemed weak to resist cracking.
- C80 and Round Shoulder (RS) markers only showed abrasion or contamination of the retroreflective faces. At these survey sites, C80 and RS were only observed on portland cement concrete pavements (PCC). Compared with 3M 290, C80 might protect the lens more effectively since its lens was slightly dented.

However, many RRPMs' failure extents, in the first field survey, were not commensurate with the roads' condition, such as those at sites 1, 2, 4, 5, 8, 9, 10, 13, 14, and 15. These sites sustained heavy truck traffic and showed pavement distresses such as cracking, but the markers looked fine. This situation inspired to consider the issue of markers' replacement frequency, and encouraged

to necessarily make a time series of repeated surveys. Taking site 13 (on SR 60) for instance, the remaining adhesives on the pavement indicated that the markers had been replaced for at least four times in the last few years. The age information of the markers, however, could not be obtained from FDOT, which limited the extent of analysis of the field data. As a solution, the marker conditions at these sites were further surveyed to provide longitudinal performance data profiles, as described in the next section.

4.2.3 Comparison of RRPM Durability

The RRPM conditions, at this series of field surveys, were measured and shown in Table 4-2. The trends of their ratings are plotted in Figure 4-4 through Figure 4-6. However, for consistent analysis of RRPM performances, the ratings at repaved sites (6, 7, 8, 13 sites) are not considered in this section.

Table 4-2 Rating Results from 1st, 2nd, 3rd and 4th Field Surveys

Site ID (RRPM type)	Truck AADT	Lane	AADT	Rating			
				May, 2012	September, 2012	January, 2013	June, 2013
Site 4 (3M 290)	1152	2	33500	4.05	3.95	3.9	3.85
Site 5 (Rayolite AA)	1384	2	12700	4.05	3.65	3.65	3.55
Site 9 (Rayolite RS)	1513	3	60500	4.1	4.1	3.7	3.4
Site 10 (C80)	1338	3	53500	3.3	3.3	3.25	3.25
Site 11 (Rayolite AA)	1120	2	16000	3.3	3.3	3.15	2.95
Site 12 (3M 290)	1632	3	17000	2.7	2.7	2.65	2.55
Site 15 (3M 290)	1694	2	19700	2.6	1.2	1.2	1.05
Site 16 (3M 290)	1694	2	19700	3.5	2.2	2.2	2.2

Figure 4-4 Ratings of 3M 290 from 1st, 2nd, 3rd, and 4th Field Surveys

Figure 4-5 Ratings of Rayolite RS and Ennis C80 from 1st, 2nd, 3rd, and 4th Field Surveys

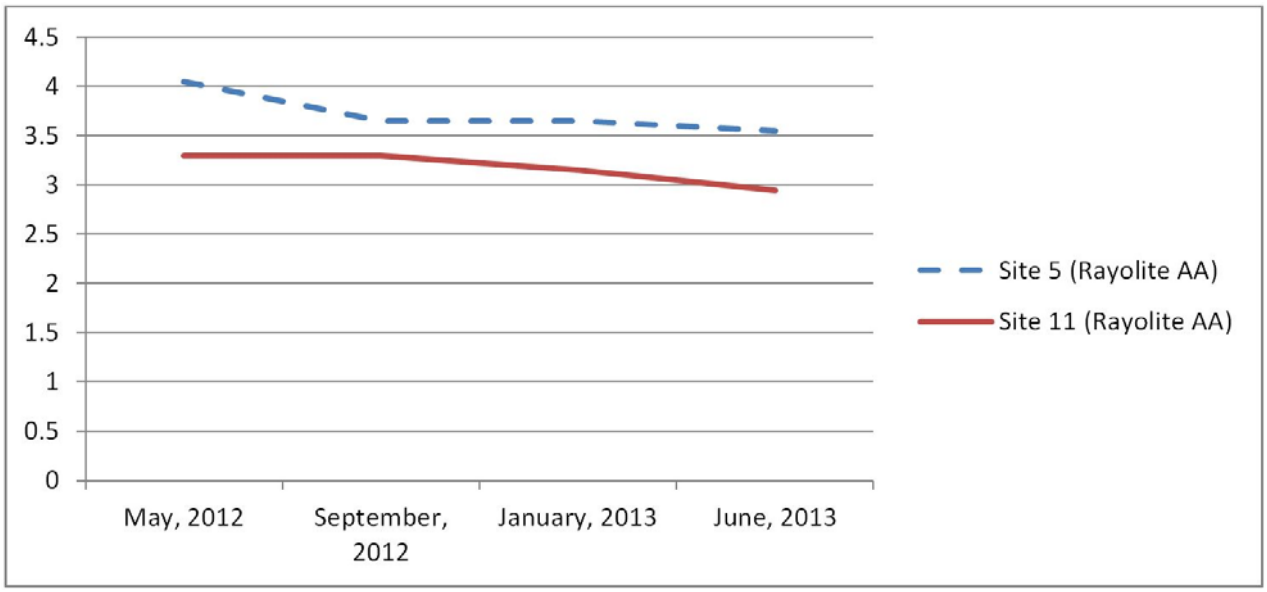

Figure 4-6 Ratings of Rayolite AA from 1st, 2nd, 3rd, and 4th Field Surveys

Table 4-3 explains the main reason of dramatically decreased RRPM ratings during May to September in 2012 at sites 15, 16, and 5 was RRPM detachment from pavement. For 3M 290, Figure 4-4 shows that, although its ratings were decreased from May to September in 2012, it retained performance from September in 2012 to June in next year. In other words, the detachment failure ceased and the rest of the maintained RRPMs kept their performance after September in 2012. The latest ratings at site 15 and 16 strongly requested that these RRPMs with unreliable ratings should be replaced.

Figure 4-5 shows that the Rayolite at site 9 suffered severe deterioration during September, 2012 through June, 2013. Figure 4-5 also illustrates that the Ennis C80 steadily retained "good" rating at site 10, although detachment failures occurred at that site. For Rayolite AA, the enormous detachments of RRPM contributed to the dramatic decrease of RRPM performance at site 5. At site 11, the rating of Rayolite AA slightly dropped from 3.3 to 2.95, after September, 2012.

Table 4-3 Rating Details of 1st, 2nd, 3rd, and 4th Field Surveys

Site ID	Marker Type	Survey 1								Survey 2								Survey 3								Survey 4							
			Performance (%)						Rating		Performance (%)						Rating		Performance (%)						Rating		Performance (%)						Rating
		Date	1	2	3	4	5	0	Total	Date	1	2	3	4	5	0	Total	Date	1	2	3	4	5	0	Total	Date	1	2	3	4	5	0	Total
4	3M 290	5/10 2012				95	5		4.05	9/11 2012			5	95			3.95	2/4 2013			10	90			3.9	6/19 2013			15	85			3.85
5	Rayolite AA ARC II					95	5		4.05					85	5	10	3.65					85	5	10	3.65				10	75	5	10	3.55
6	3M 290			10	80	10			3					20	80		4.8				15	20	50	15	3.75				15	40	30	15	3.55
7	Rayolite AA ARC II				15	65		20	3.05					10	70	20	3.9					20	80		4.8				10	50	40		4.3
8	3M 290	5/11 2012				90	10		4.1	9/12 2012				5	95		4.95	1/30 2013				5	95		4.95	6/20 2013				20	80		4.8
9	Rayolite RS					90	10		4.1					90	10		4.1			5	20	75			3.7			15	30	55			3.4
10	Ennis Paint Model C80					70	10	20	3.3					70	10	20	3.3					75	5	20	3.25					75	5	20	3.25
11	Rayolite AA ARC II				70	30			3.3				70	30			3.3			5	75	20			3.15			25	55	20			2.95
12	3M 290				50	30		20	2.7				50	30		20	2.7			5	45	30		20	2.65			15	35	30		20	2.55
13	3M 290; Rayolite AA ARC II	5/21 2012				20	80		4.8					20	80		4.8					20	80		4.8					5	75		3.95
15	3M 290				60	20		20	2.6				40			60	1.2				40			60	1.2			15	25			60	1.05
16	3M 290					50	30	20	3.5				20	40		40	2.2				20	40		40	2.2				20	40		40	2.2

Based on the RRPM ratings from this series of field survey, for clear analysis of performance and durability of different RRPMs, several rating indicators were calculated, as listed in Table 4-4. In the table, "Overall Average Rating" is the average of ratings from the four surveys from all sites with the same RRPM type; "Average Rating Drop After One Year" is the difference in average ratings from the 1st survey and from the 4th survey; and "Average Latest Rating" is the average rating from the 4th survey.

Table 4-4 Different Rating Types of RRPMs

	Overall Average Rating	Average Rating Drop After One Year	Average Latest Rating
	All Sites		
3M 290	2.66	0.80	2.41
Rayolite AA	3.45	0.43	3.25
Rayolite RS	3.83	0.70	3.40
C80	3.28	0.05	3.25
	Overall Average Rating	Average Rating Drop After One Year	Average Latest Rating
	Sites with Lowest Truck AADT		
3M 290 at Site 4 (Truck AADT = 1152)	3.94	0.20	3.85
Rayolite AA at Site 11 (Truck AADT = 1120)	3.18	0.35	2.95
Rayolite RS at Site 9 (Truck AADT = 1513)	3.83	0.70	3.40
C80 at Site 10 (Truck AADTT = 1338)	3.28	0.05	3.25

The upper portion of Table 4-4 illustrates that generally Rayolite RS had the best overall rating and best latest rating at these sites. However, because for 3M 290 several sites (i.e., sites 12, 15, and 16) with truck traffic volumes significantly higher than other sites were included in the average, 3M 290 was at an unfavorable position during the comparison. To correct for this bias, the ratings from sites with the lowest truck AADT were listed in the lower portion of Table 4-4 for comparison. Considering that Rayolite RS experienced more truck AADTT than 3M 290 (1513 versus 1152), it is safe to say that both 3M 290 and Rayolite RS had good performance at low truck AADT sites. From the perspective of durability or performance drop over time, 3M 290 performed better than Rayolite RS (0.20 vs. 0.70). Moreover, although C80 had a relatively low average rating (3.28), its performance did not deteriorate much over a year.

4.2.4 Pavement Type Effect on RRPM Retention Loss

Both questionnaire survey and field survey showed that RRPMs had a high risk of retention loss. From the perspective of RRPM's mechanical failure, retention loss was often triggered by adhesive failure and generated large amount of censoring data, which interrupted observation on the failure process of RRPM itself. Intuitively, RRPM detachment was more frequently observed on cement concrete (CC) pavements than on asphalt concrete (AC) pavements. Thus, the detachment proportions versus pavement types are plotted in Figure 4-7, which excludes repaved sites. Because the detachment proportion did not develop obviously after the second field survey,

Figure 4-7 only records the first two field survey results. Figure 4-7 verifies observers' intuitions: RRPMs on CC pavements had a higher risk of retention loss than those on AC pavements.

It is worth pointing out that the rainy season between May and September might also elevate the detachment chance. In other words, precipitation had potential interaction with pavement surface type on RRPM detachment probability. This hypothesis should be tested with more data.

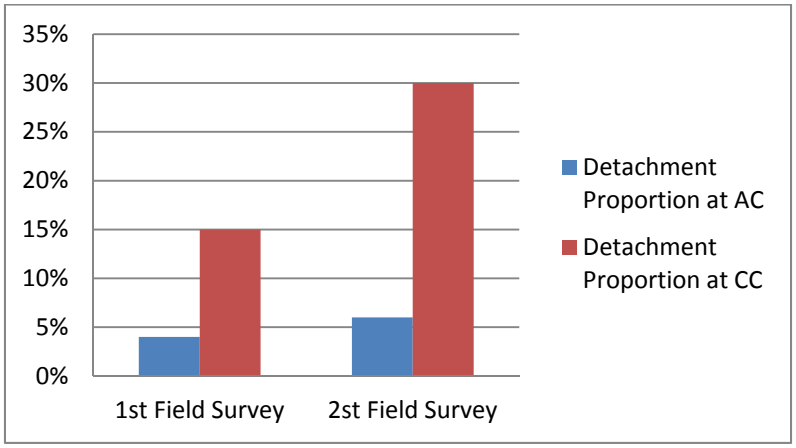

Figure 4-7 Detachment Proportion on AC and CC Pavements

4.2.5 AADT Effect on RRPM Rating

For more clearly comparing the effects of AADT and heavy truck AADT on RRPM ratings, Figure 4-8 and Figure 4-9 show that truck AADT had significant negative effect on RRPM ratings, but AADT did not. In other words, more trucks could damage RRPMs more severely. This result was in accordance with the questionnaire survey result. Moreover, based on the trends in Figure 4-8 and Figure 4-9, the effects of truck AADT on RRPM ratings were nonlinear. Increasing truck AADT may significantly reduce the RRPM ratings.

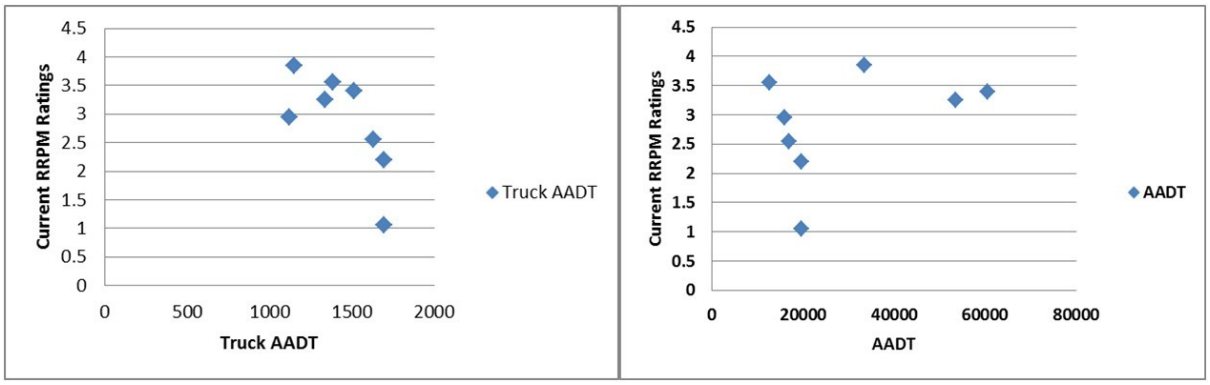

Figure 4-8 Current RRPM Ratings vs. Truck AADT and AADT

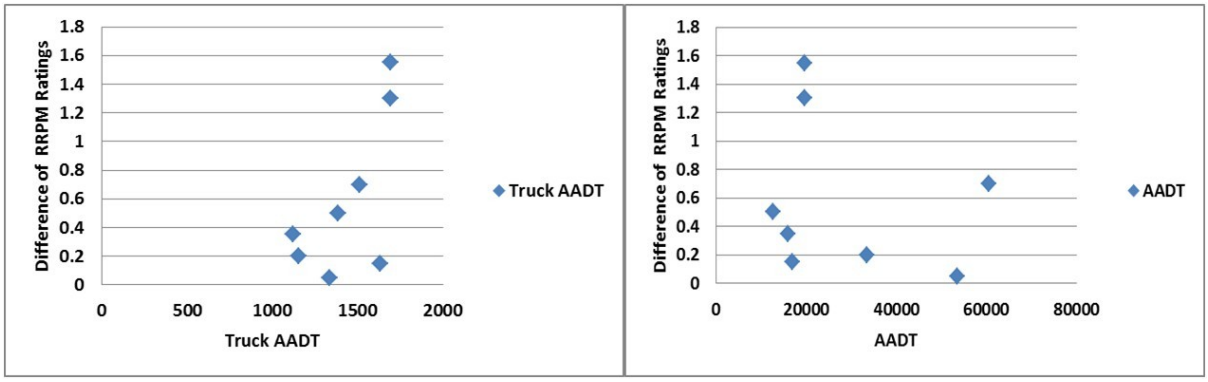

Figure 4-9 Differences of RRPM Ratings vs. Truck AADT and AADT

Based on the data of truck AADT and difference of RRPM ratings, several curve fitting functions were tried in regression analysis to obtain the best fit curve for these two variables. A linear model, a quadratic model, a cubic model, and an exponential model were checked, with relevant R-squares shown in Table 4-5 and fitted functions shown in Figure 4-10. It could be seen that the cubic model was the best for Truck AADT and RRPM rating difference.

Table 4-5 R-Squared Values on Curve Estimation of Truck AADT and RRPM Rating

Model Summary and Parameter Estimates	
Dependent Variable: Rating Difference	
Equation	Model Summary
	R Square
Linear	.450
Quadratic	.601
Cubic	.609
Exponential	.255
The independent variable is Truck AADT.	

4.2.6 Climate Effect on RRPM Rating

The level of average precipitation in Florida was one of the highest in U.S. The temperature in Florida was also relatively higher than those in most other states in U.S. Thus, testing climate effect on RRPM performance was necessary. The RRPM rating changes, with corresponding temperature and precipitation, are listed in Table 4-6.

Table 4-6 Rating and Climate Information

	May to September,2012	September, 2012 to January, 2013	January to June, 2013
Overall Rating Drop	0.36	0.08	0.19
Precipitation	41.57	7.33	10.33
Average Temperature	80.02	65.48	60.40

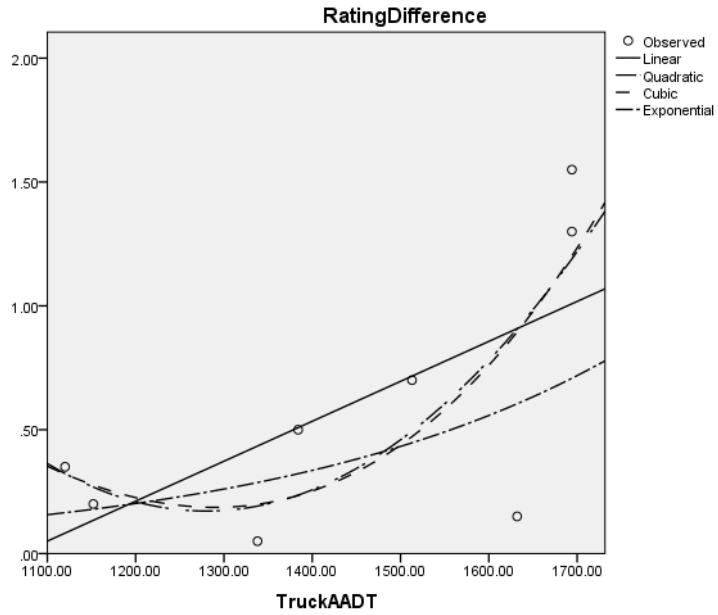

Figure 4-10 Curve Estimation of Truck AADT and RRPM Rating in SPSS

Table 4-6 illustrates that the overall RRPM rating decreased more significantly in the summer season than in other seasons. The table also shows that in the summer season both precipitation level and air temperature are higher than those in the other seasons. This consistent trend indicates that a high precipitation level combined with a high temperature may accelerate the deterioration of RRPMs.

4.3 Specific Failure Process Captured in Field Survey

Although the individual RRPM could not be easily identified from these three field surveys, the structural damage processes of some RRPMs, as shown in Figure 4-11 through Figure 4-15, were coincidently captured.

Figure 4-11 One 3M 290 Marker at Site 15 (on Causeway Blvd & S 50th St.)

Figure 4-11 successfully captures the whole cracking extension process from May, 2012, to January, 2013. It shows that, on May, 2012, the crack already existed between lens and slope. It extended along the edge of RRPM top to the finger grip (the middle of RRPM shell), during May to September, 2012. The crack kept extending along the edge of RRPM finger grip till January,

2013. This captured process hinted that the finger grip might protect the RRPM's main body by controlling the direction of cracking extension in this specific case.

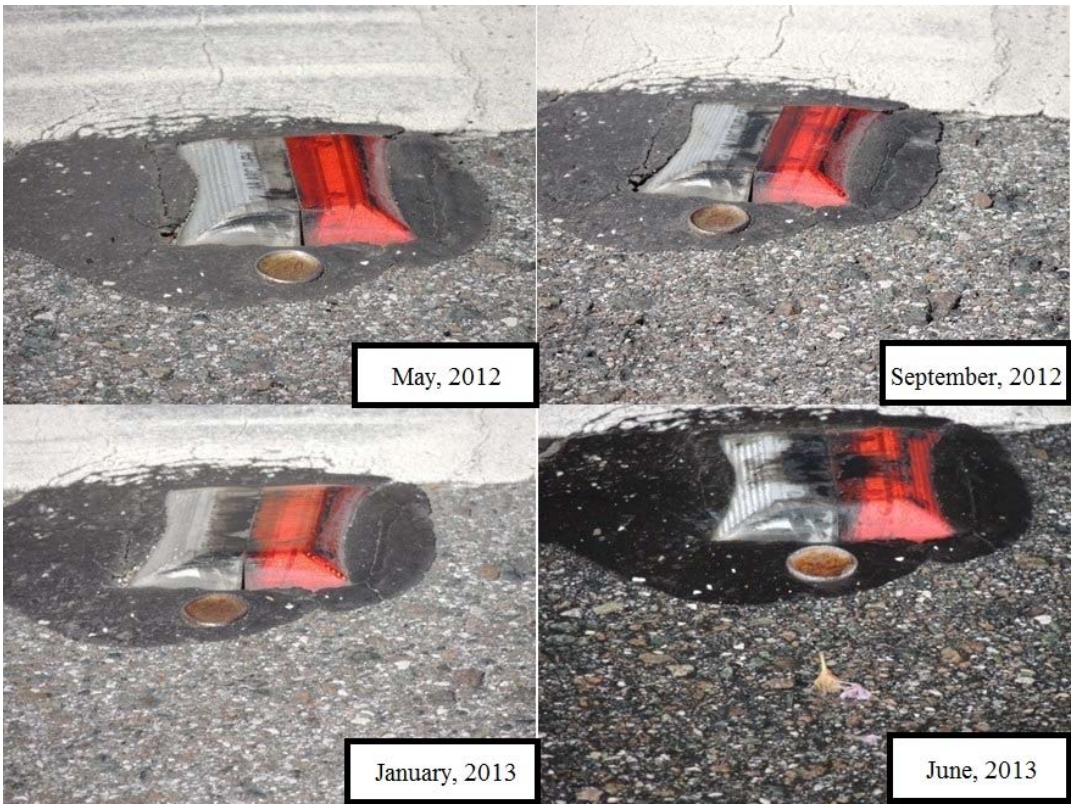

Figure 4-12 One Rayolite AA ARC II FH Marker at Site 11 (on 21st St., Under I-4)

Figure 4-12 shows that, although Rayolite AA had cracked in the middle of shell before May 2012, the crack did not develop in the next 13 months. These captured images show the good durability of AA ARC II marker.

Figure 4-13 shows that the top corners of lens of Rayolite RS started to be severely abraded, after September, 2012. The abrasion area was enlarged and extended to main body, till June, 2013. Figure 4-13 also verifies the decreased ratings of Rayolite RS shown on Figure 4-5. Compared with the crack extension on 3M 290 captured in Figure 4-11, this whole abrasion process exhibited Rayolite RS's worse durability. In other words, although Rayolite RS itself had strong structure features, if some abrasions occurred on its top corners, Rayolite RS would be destroyed very soon.

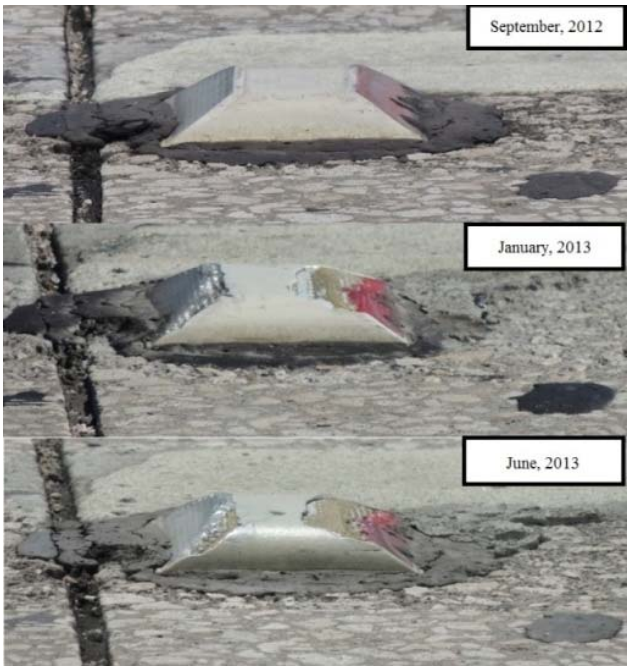

Figure 4-13 One Rayolite RS Marker at Site 9 (North of I-275 on N Dale Mabry Hwy)

Figure 4-14 3M Marker No.1 at Site 15 (Causeway Blvd & S 50th St.)

Figure 4-14 captures another crack extension process on 3M 290. This crack was generated on the lens' top corner before September 2012. After around one year, this crack extended along top shell to the red lens. Furthermore, severe contamination occurred after September, 2012. The bituminous adhesive even covered finger grips. However, without considering the bituminous contamination, this case demonstrated that 3M 290 still kept functional after suffering severe damage.

Figure 4-15 3M Marker No.2 at Site 15 (Causeway Blvd & S 50th St.)

Figure 4-15 also captures the severe contamination process occurred on 3M 290 at site 15. Moreover, although the corner of white side lens was damaged one year ago, the crack did not develop tremendously in the next 13 months. This slight crack development on 3M 290 in one year also showed its high durability.

In conclusion, based on the comparison between Figure 4-11, Figure 4-13, Figure 4-14 and Figure 4-15, the damage on Rayolite RS developed faster and more dramatically than that on 3M 290. In other words, 3M 290 had better durability than Rayolite RS. This conclusion was also verified by Table 4-4, at lowest truck AADT condition column.

CHAPTER 5 METHODOLOGY

5.1 Finite Element Model

In this research, finite element model (FEM) is implemented not only to emulate the real field condition of a tire/marker/pavement system in different scenarios, but also to simulate the RRPM laboratory tests with different testing parameters.

Specifically, for studying the tire/marker/pavement system, it is very easy to change values of various factors (e.g., tire loading, tire speed, contact angle, and contact location) and observe their effects through FEM analysis. Similarly, the geometric features of RRPMs may also be easily changed and studied in FEM. It would otherwise take much longer time and cost much more to achieve these tasks through field or laboratory testing.

From the perspective of laboratory tests, FEM can also exhibit stress distributions in an RRPM under the impacts of different laboratory apparatus. The laboratory test parameters can also be changed in FEM, such as impact location and speed, to modify current standard laboratory tests to meet real field conditions. Moreover, new laboratory tests can be designed before being operated under real equipment.

An FEM can bridge the stress distributions produced in laboratory tests and those under real tire impact. In other words, an FEM can be implemented to efficiently seek better laboratory tests, which can produce similar kinds of critical stresses in the markers as produced during the tire/marker impact.

5.1.1 Finite Element Model of Tire/Marker/Pavement System

In real scenarios, RRPMs are installed on rigid or flexible pavements and bear the impact from tires with random directions, velocities, and impact locations. This whole contacting process is not static, but dynamic. Moreover, RRPMs and tires both have complex components which cannot be regarded as simple geometric objects. Thus, building FEM can efficiently simulate this whole system and analyze the real stress-strain condition. This system consists of three components: a pavement model, an RRPM model, and a tire model, as shown in Figure 5-1.

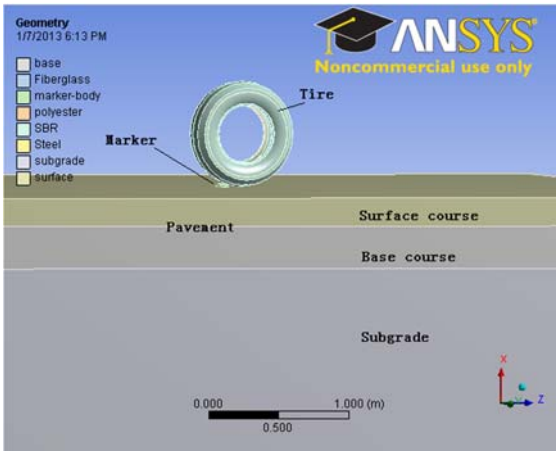

Figure 5-1 Tire/Marker/Pavement System

5.1.1.1 Pavement Model

Normally, pavement has two basic types: flexible and rigid. For a flexible pavement, it typically has three layers: surface of asphalt, base and subgrade courses of aggregates and soil. For a rigid one, the surface is paved with portland cement concrete instead and probably without base course. After pavement parameters such as layer thickness, density, Poisson's ratio, and Young's modulus are loaded into FEM software (i.e., ANSYS 12.0 in this study), an FEM of pavement can be easily generated.

5.1.1.2 Tire Model

The tire model used in this research was previously developed by a University of South Florida (USF) investigation team for a Locked Wheel Skid Tester (LWST) study (Kosgolla, 2012). The cross sectional profile of this tire model is captured through slicing a spent standard ASTM E524-08 tire. This tire model is composed of two polymer biased plies, two fiberglass belted plies, steel beads and tire rubber. As the main tire components contributing to friction, a styrene butadiene rubber (SBR) tire rubber reveals both hyperelastic and viscoelastic properties. In ANSYS 12.0, Mooney-Revlin model can be applied for hyperelastic property, and Prony series model can represent viscoelastic property. These relevant material properties and empirical data are derived from previous ASTM studies (ASTM 2001; ASTM 2006). Based on the above information, a three-dimension tire model is generated with SolidWorks 2010 software, and then imported into the ANSYS platform as the dynamic impact source.

5.1.1.2.1 Tire Validation

The tire is a significant factor that influences the reliability of the FEM results. A validation process was performed before using the tire to carry out any further FEM simulations. The tire/pavement contact pressure distributions of the built model were verified using the real data measured from a program named 'three-dimensional tire/pavement contact stresses under slow moving wheel loads', which was undertake in South Africa, as the reference (De Beer et al. 1997). The FEM simulations reproduced various field test scenarios, studying the tire/pavement contact stress at different combinations of load and inflation pressure of a pneumatic tire. Three inflation pressure levels, 0.42 MPa, 0.62 MPa, and 0.72 MPa, and three levels of load, 20kN, 40kN, and 50kN, were factored. The simulation results and the field data were then compared.

As can be found in Figure 5-2, Figure 5-3, and Figure 5-4, the peak values and the contact pressure distributions of the FEM simulations are approximate to the observations of field data. At a constant low tire inflation pressure, the tire/pavement contact pressure of the field data tends to act as a saddle curve with the increase of load, which can also be found in the contact pressure patterns of the FEM simulations. In general, the FEM simulations reproduced the phenomena observed in the field test: tire inflation pressure predominantly controls the vertical contact pressures on the pavement at the tire center while tire load controls those at the edges. Through the comparisons, the built tire is validated about the reliability and can be used for further analysis.

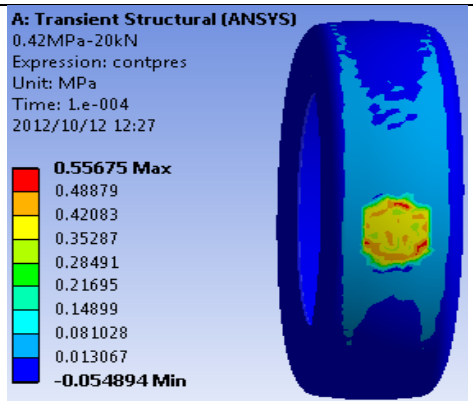

Simulation distribution of the contact pressure (0.42 MPa, 20 kN)

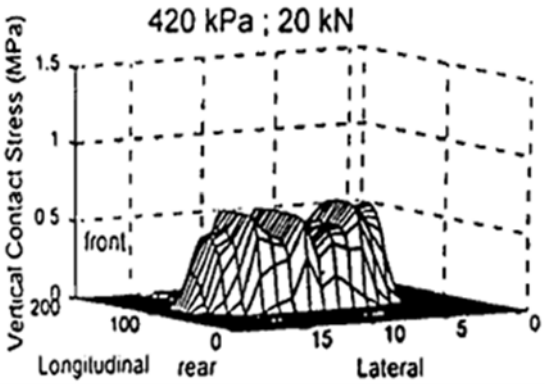

Field data plot (0.42 MPa, 20 kN)

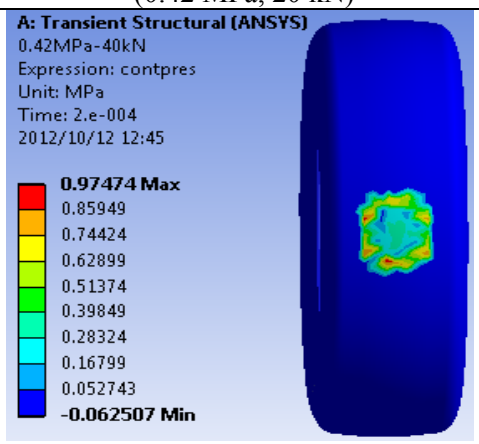

Simulation distribution of the contact pressure (0.42 MPa, 40 kN)

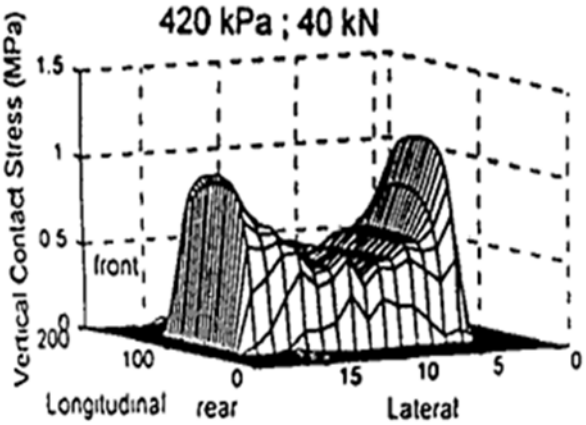

Field data plot (0.42 MPa, 40 kN)

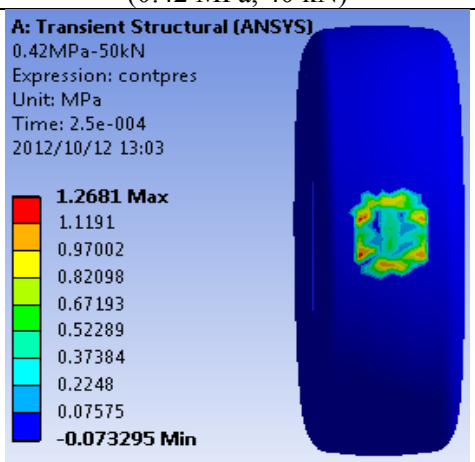

Simulation distribution of the contact pressure (0.42 MPa, 50 kN)

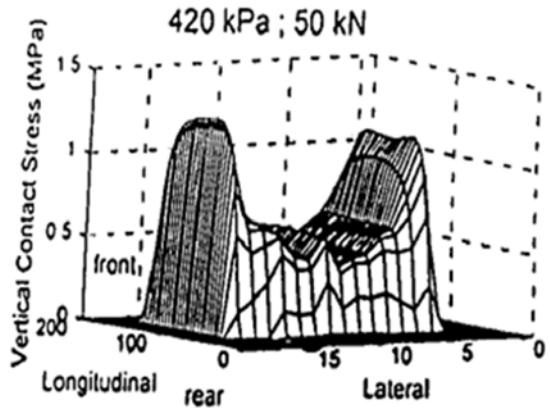

Field data plot (0.42 MPa, 50 kN)

Figure 5-2 Comparisons of Simulation Contact Pressures and Field Data (Inflation Pressure 0.42 MPa)

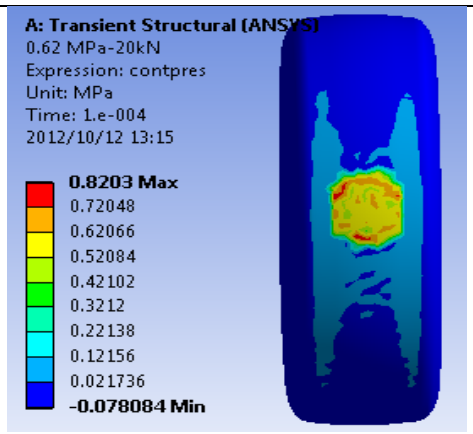

Simulation distribution of the contact pressure
(0.62 MPa, 20 kN)

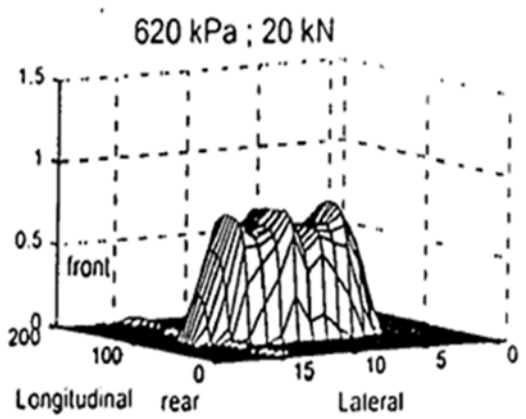

Field data plot (0.62 MPa, 20 kN)

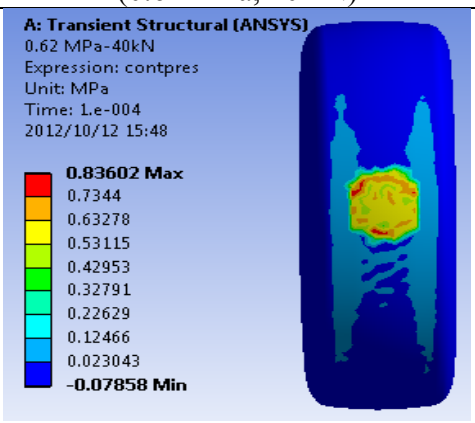

Simulation distribution of the contact pressure
(0.62 MPa, 40 kN)

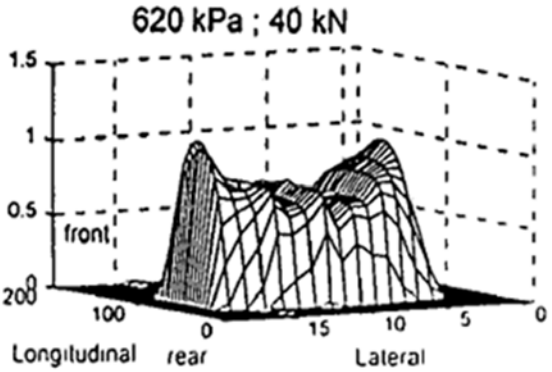

Field data plot (0.62 MPa, 40 kN)

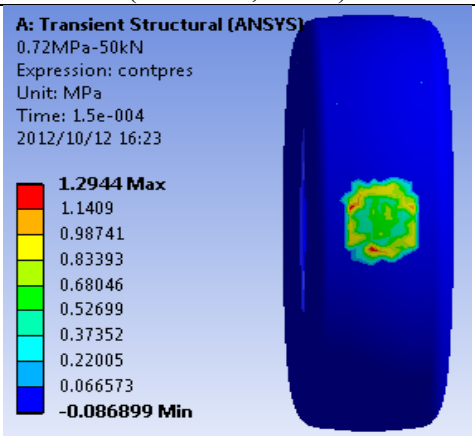

Simulation distribution of the contact pressure
(0.62 MPa, 50 kN)

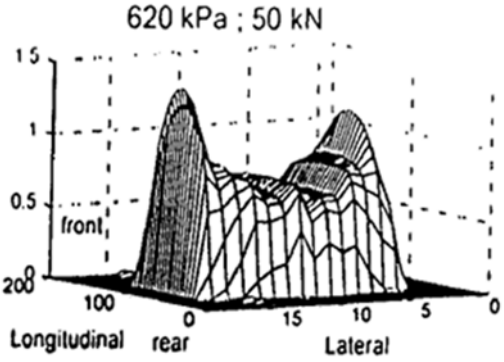

Field data plot (0.62 MPa, 50 kN)

Figure 5-3 Comparisons of Simulation Contact Pressures and Field Data (Inflation Pressure 0.62 MPa)

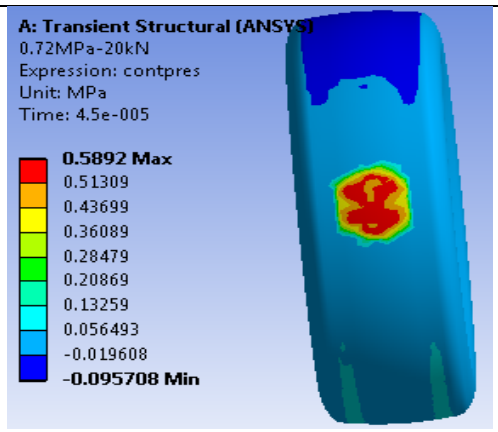

Simulation distribution of the contact pressure
(0.72 MPa, 20 kN)

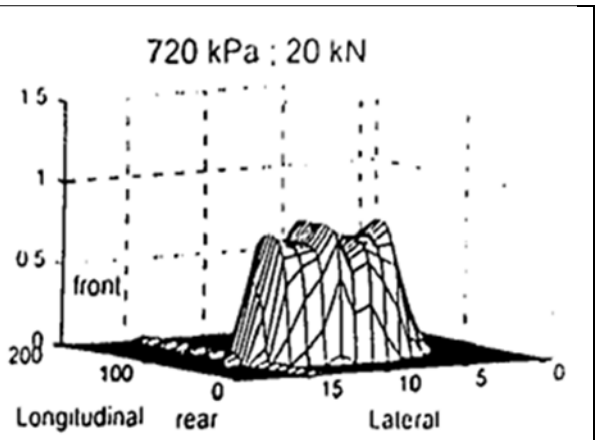

Field data plot (0.72 MPa, 20 kN)

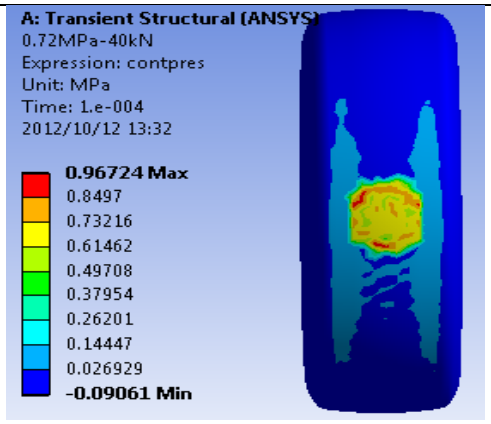

Simulation distribution of the contact pressure
(0.72 MPa, 40 kN)

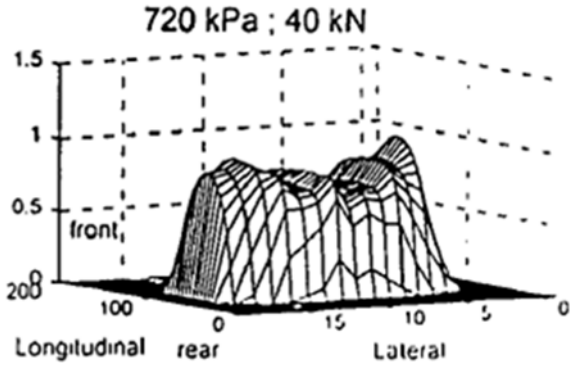

Field data plot (0.72 MPa, 40 kN)

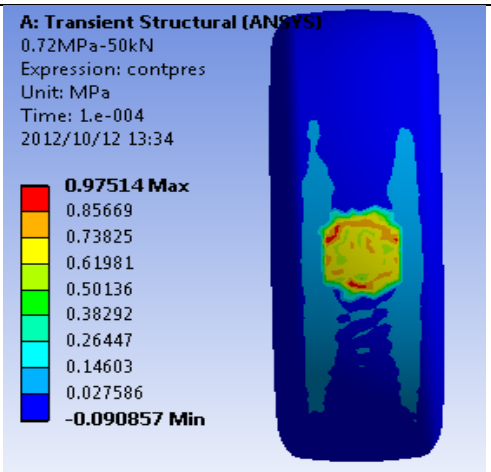

Simulation distribution of the contact pressure
(0.72 MPa, 50 kN)

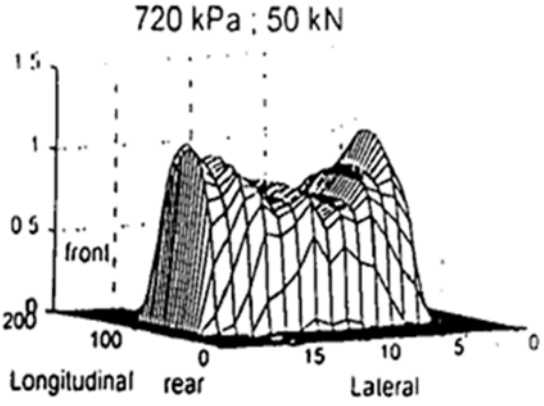

Field data plot (0.72 MPa, 50 kN)

Figure 5-4 Comparisons of Simulation Contact Pressure and Field Data (Inflation Pressure 0.72 MPa)

For further verification, the simulation results are also compared with the tire-pavement contact stress distributions produced in an earlier study by TTI (Zhang et al., 2009), as shown in Figure 5-5 and Figure 5-6, with 0.69 MPa tire pressure and 24 kN load.

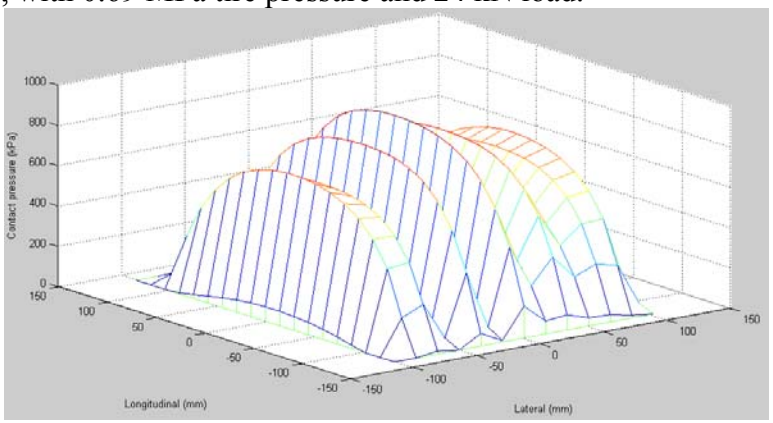

Figure 5-5 Tire-pavement Contact Stress Distribution Based on TTI Data (Zhang et al., 2009)

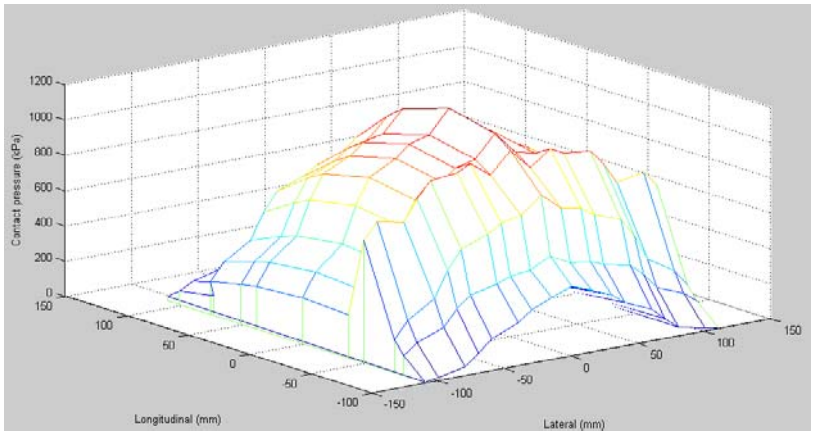

Figure 5-6 Tire-pavement Contact Stress Distribution Based on Simulation Results

As we can find that, the tire-pavement contact stress distribution of the simulation results is slightly different from that produced in the TTI study. This is due to the differences in the tire models used. In the TTI study, a grooved tire model was used, while in this study a smooth tire model is selected. Due to the existence of grooves on the TTI tire, the contact stress increases at the ridge parts and decreases at the interval between the ridges. The smooth tire used in the simulation is free of any grooves, which makes the contact stress to decrease monotonically with the increase of distance from the tire-pavement contact area center. Despite this, the peak values of the two tires are not unacceptably different, 899 kPa for the TTI tire and 1118 kPa for the FEM tire; moreover, after calculating the ratio of encapsulated volume divided by the shadow area (equivalent tire-pavement contact pressure), the results are approximating, 874 kPa for the TTI data and 957 kPa. Based on the above calculation, the tire adopted in this study is deemed as valid for the subsequent FEM analysis.

5.1.1.3 RRPM Model

5.1.1.3.1 Details of RRPM Geometric Characteristics

As mentioned in the literature review, RRPMs can be categorized into two types: one with squared bottom, such as Ennis C88, and the other with curved bottom, such as Ennis C80. Moreover, geometrically, the profiles of all RRPM types can be described by six basic factors: bottom length (BL), bottom width (BW), height (H), ratio of top width and bottom width (TOB), bottom shape (BS), and slope of lens. Moreover, in this study, for better analysis of the stress distribution in the RRPM body, less significant geometric features, such as finger-grip, fillet, and chamfer, are also used to develop the more precise RRPM FEM.

It is worth pointing out that, because a complicated RRPM structure will significantly extend the ANSYS running time and occupy much more computer memory, in some cases, a simpler RRPM structure is preferred, rather than a complicated one. The accuracy of RRPM model is determined by the specific study purpose.

5.1.1.3.2 Measurements of RRPMs and Material Properties

Precise geometric information about each RRPM was gathered by measuring the substructure of bisected RRPMs using a vernier caliper (Figure 5-7). The major geometry information of four RRPMs, including 3M 290, Ennis C80, Ennis C88, and Rayolite RS, is listed in Table 5-1.

For collecting the information of material properties, an extensive literature review was performed from multiple sources, such as manufacturer specifications, published studies, and Google searching. These obtained material properties are summarized in Table 5-2 through Table 5-4. Because both Rayolite RS and Ennis C88 use inert thermosetting compound materials, the material properties of Rayolite RS are very close to those of Ennis C88.

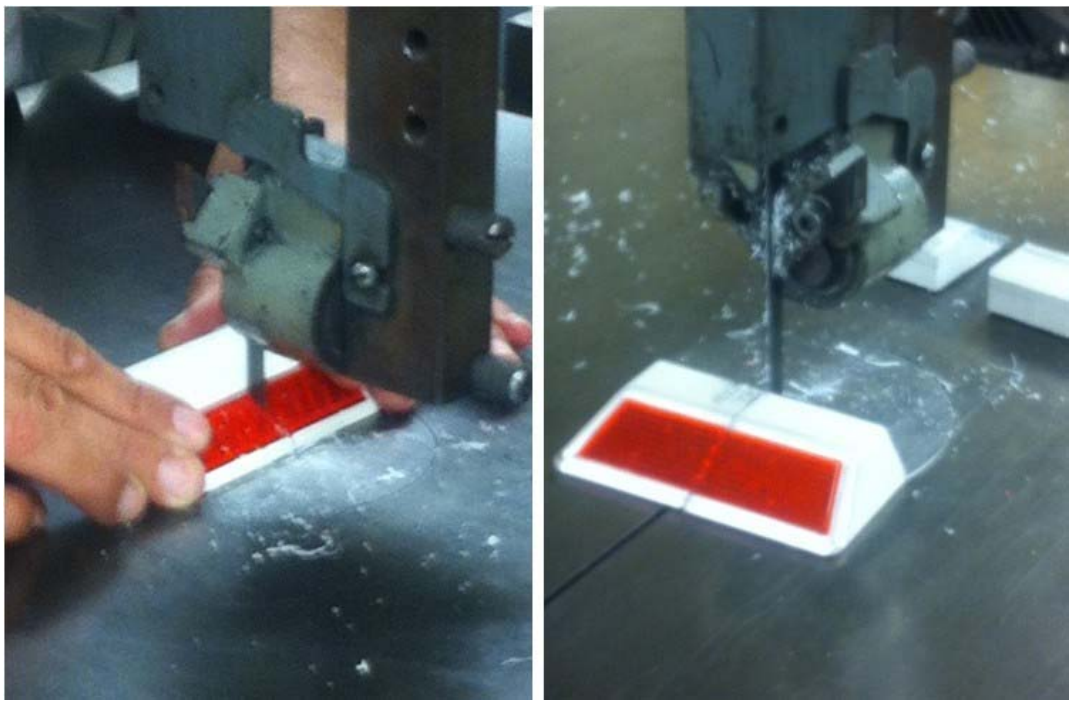

Figure 5-7 Cutting the RRPMs to Measure the Geometric Information

Table 5-1 Profiles of RRPMs (mm)

Type	Thickness	Length	Width	Top Length	Top Width
3M 290	15.7	88.9	72.3	44.9	69.8
Ennis C80	17.5	80.8	86.3	39.2	78.0
Ennis C88	18.1	101.0	101.0	40.1	85.8
Rayolite RS	17.3	99.3	100.2	48.8	57.5

Table 5-2 Material Properties of 3M 290

Body and Lens (Acrylic)		
Density	1350	kg/m^3
Young's modulus	5800	MPa
Poisson ratio	0.35	-
Yield strength	80	MPa

Table 5-3 Material Properties of Ennis C80

Body (Acrylic)		
Density	1040	kg/m^3
Young's modulus	2100	MPa
Poisson ratio	0.35	-
Yield strength	44	MPa
Lens (Acrylic)		
Density	1190	kg/m^3
Young's modulus	3103	MPa
Poisson ratio	0.11	-
Yield strength	70	MPa

Table 5-4 Material Properties of Rayolite RS

Filler (Inert Thermosetting Compound)		
Density		kg/m^3
Young's modulus	2600	MPa
Poisson ratio	0.44	-
Yield strength		MPa
Housing (Acrylonitrile Butadiene Styrene)		
Density		kg/m^3
Young's modulus	2300	MPa
Poisson ratio	0.37	-
Yield strength		MPa
Lens (Methyl Methacrylate)		
Density		kg/m^3
Young's modulus	2450	MPa
Poisson ratio	0.37	-
Yield strength		MPa

5.1.1.3.3 Building RRPM Models in ANSYS

All four types of RRPMs (3M 290, Ennis C80, Ennis C88, and Rayolite RS) were built in ANSYS based on the dimensions of RRPMs. And the material properties of each RRPM component are inputted into "Engineering Data" section in ANSYS.

In the stress distribution analysis section, all these four RRPM models were implemented, although 3M 290 and Ennis C80 are geometrically the same. Moreover, hollow-3M 290 was built to observe the stress distribution on the hollow surface. For Rayolite RS and Ennis C88, extra filler and housing parts were also built with different materials.

In the RRPM profile study section, as mentioned in section 5.1.3.2, only two geometric types of RRPM were built and analyzed: one with curve-edge bottom shape (Ennis C80 and 3M 290), and the other one with squared bottom shape (Ennis C88 and Rayolite RS).

In the external factor analysis section, since the developing trends of RRPMs are the same, this study only selected Ennis C80 to carry on the sensitivity analysis related to tire loading, tire speed, contact angle, and contact location.

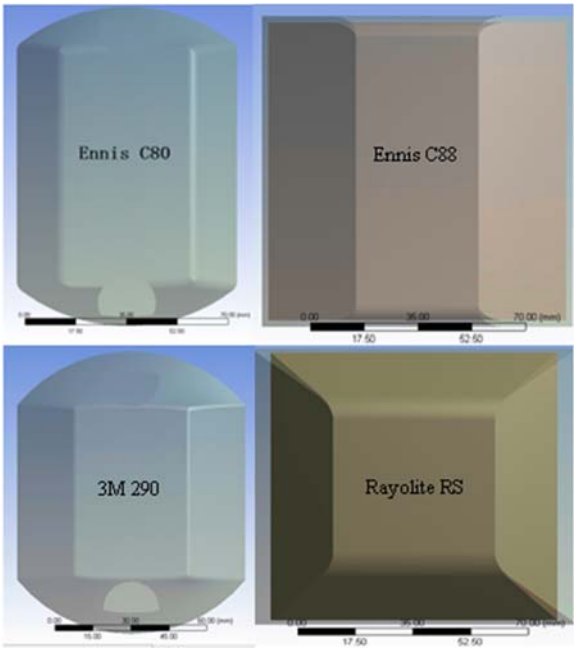

Figure 5-8 FEMs of RRPMs in ANSYS

5.1.1.4 Contact Model

Because contact process is highly nonlinear, special skills are required to assure the accuracy of FEM simulation. A powerful analysis tool in ANSYS can execute the contact command. In this study, surface to surface contact elements were selected since the gap between the two contact interfaces is suitably captured. Because pavement and maker are relatively stiffer than the tire, the pavement surface elements and the RRPM surface elements were treated as target elements (blue part in Figure 5-9) and the bottom surface elements of the rubber block were treated as contact elements (red part in Figure 5-9).

The CONTA 174 element was selected as contact element in this study since it is capable of changing the coefficient of friction with "temperature, time, normal pressure, sliding distance, or sliding relative velocity" (ANSYS, 2012). TARGE 170 was also selected as the target elements. Because Augmented-Lagrangian algorithm can prevent element penetration effectively, this algorithm was picked as the contact algorithm (ANSYS, 2012). To obtain more accurate simulations at the expense of additional running time, the stiffness matrix was updated for each iteration. The coefficient of friction (μ) was defined using the Coulomb friction model with field surveyed value (ANSYS, 2012).

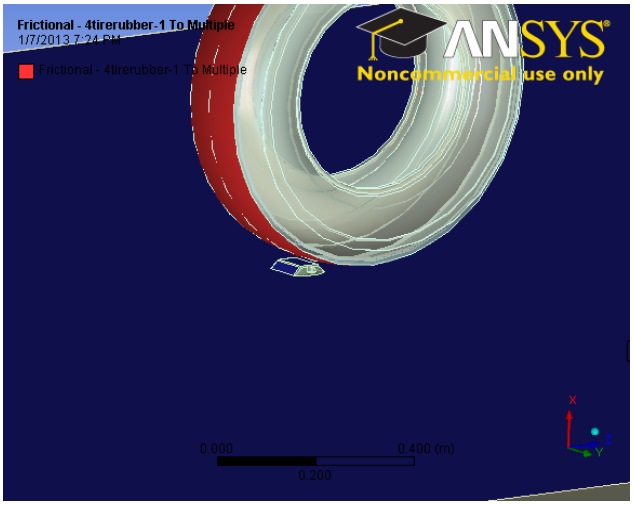

Figure 5-9 Tire-Marker Contact System

5.1.1.5 Mesh Generation

After building the tire-marker-pavement FEM system and setting the contact model, this system was directly meshed by the "mesh" tool in ANSYS, as illustrated in Figure 5-10. The specific mesh generate function was decided by the extent of RRPM geometric feature complication. This powerful mesh generation function in ANSYS prevents the time-consuming issue from traditional mesh generation methods.

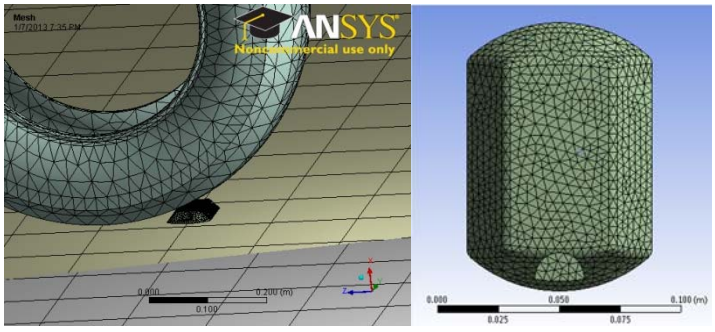

Figure 5-10 Mesh Generation

With different sizes of tire, marker, and pavement, their corresponding finite element sizes also vary. Element sizes of tire, marker, and pavement are 4 mm, 40 mm, and 150 mm, respectively.

5.1.2 Finite Element Model of Laboratory Tests

Compared to the FEM of pavement/marker/tire system, FEM of laboratory tests is relatively simpler. Instead of tire and pavement, RRPMs are fixed on laboratory apparatus, impacted by steel bar, elastomeric pad, steel plate, steel rod, and so on. The specific FEMs of various laboratory tests are described in the next chapter.

5.2 Experimental Design

In this research, the experimental designs mainly contain two parts: fractional factorial design and full factorial design. In many study cases, the entire model program would involve almost one hundred combinations of various factors and their corresponding levels. Considering the time consuming operation of ANSYS, to reduce the simulation work and meanwhile maintaining the reliability of conclusions, a fractional factorial design was preferred. However, compared to the fractional factorial design, because full factorial design can provide much more information on variables' interactions, a full factorial design is preferred to explain more complicated relationships. Thus, proper experimental designs were picked based on specific situations.

5.2.1 Orthogonal Design

5.2.1.1 Basic Concept of Orthogonal Design

Orthogonal design is a highly fractionated factorial design. Some representative points from full-scale test are selected in this multi-factor multi-level experimental design to efficiently observe relationships between factors and effects. If these representative points are evenly dispersed and neatly comparable, the main effects can be easily captured, since all interactions between the controls can be negligible.

Specifically, one typical example of fractional factorial design with four factors at three levels is introduced as follows. If one experimental design has 4 factors at 3 levels, a full factorial design includes $3^4 = 81$ cases, as shown in Figure 5-11. Compared to the full factorial design, a fractional factorial design only requests $3^{4-2} = 9$ tests, as shown in Figure 5-12. Although the fractional factorial design neglects most cases, it still can exhibit the integral situation by highly representative cases without any redundancy. The prerequisite of this orthogonal design is that the cases shall be evenly distributed.

Because of uniform appearance of other control factors which can be offset by each other, every factor in fractional factorial design can be viewed as independent (Hedayat et al., 1999). Take factor A for instance. As the level of factor A increases, all other factors (B, C, D) on corresponding levels appear only once on "horizontal face" in Figure 5-12. Thus, orthogonal design has two properties: 1) no factor is redundant and unimportant; 2) the main effect of every factor can be captured efficiently. However, this property also leads lack of interaction information and threatens the accuracy of observed main effects on orthogonal design.

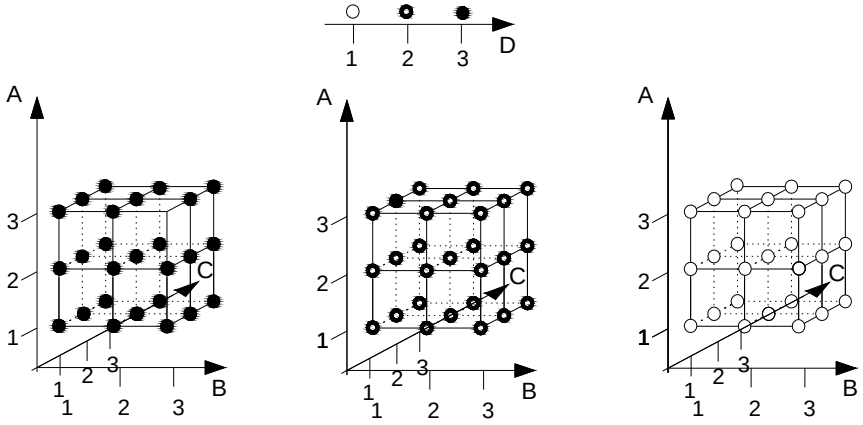

Figure 5-11 3^4 Full Factorial Design

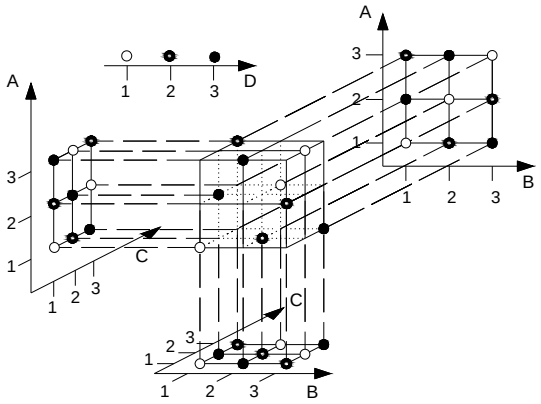

Figure 5-12 3^{4-2} Fractional Factorial Design

The test arrangement in Figure 5-12 can be transferred into Table 5-5:

Table 5-5 Orthogonal Table of $L_9(3^{4-2})$

Factor / Level / Test	A	B	C	D
1	1	1	1	1
2	1	2	2	2
3	1	3	3	3
4	2	1	2	3
5	2	2	3	1
6	2	3	1	2
7	3	1	3	2
8	3	2	1	3
9	3	3	2	1

5.2.1.1 Orthogonal Design Application

The application of orthogonal design in this study was to analyze the effects of external factors on RRPM stress magnitudes. Four external factors were selected, including tire load, tire rolling speed, tire and RRPM contact angle, and contact point offset. Each external factor has three levels. It demands 81 combinations by full factorial design. Thus, the $L_9(3^{4-2})$ table, as shown in Table 5-5 was selected.

5.2.2 Full Factorial Design

5.2.2.1 Simple Regression Model on Full Factorial Design

Since the orthogonal design only captures the main effect of each factor, the interactive effects within factors cannot be observed. However, it is possible that the interactive effects exist within factors. Thus, full factorial designs were also developed to seek potential interactions. Compared to the fractionated factorial design, a full factorial design is more comprehensive: it can simultaneously test the main effects and multi-way interactive effects in linear regression models. Take the most simple 2-factor model for instance:

$$Y = \beta_0 + \beta_1 X_1 + \beta_2 X_2 + \beta_{12} X_1 X_2 + \varepsilon$$

In this simple regression model, β_{12} is the interactive effect; β_1 and β_2 respectively represent the main effect of X_1 and X_2 (Hill and Lewicki, 2006). ANOVA is obtained from statistical software, such as SPSS, to analyze the main effects and interaction effects of these factors. Statistically, all "beta" coefficients, R-squared, t value can be calculated and then used to test hypothesis. For example, if t value of X_1 X_2 is larger than critical value, β_{12} means both variables significantly change their effects on response Y each other (Hill and Lewicki, 2006).

5.2.2.2 Full Factorial Design Analysis on RRPM Geometric Optimization

Considering the important effects of RRPM geometric factors on RRPM stress magnitudes, one 3×3×3×3×2 full factorial design was used with a regression model. Basic geometric factors (BL, BW, H, and TOB) are treated as quantitative independent variables in this regression model; BS is treated as a dummy variable, which is used to observe the effects of bottom shape conversion between squared bottom and bottom with curve edges; The stress magnitude is the dependent variable in this model. Because of all possible combinations between these factors, this regression model not only tests the main effect of each geometric factor, but also checks all 2-way interactions, 3-way interactions and 4-way interactions between these geometric factors.

$$\begin{aligned}
stress = {} & \beta_0 + \beta_1 \times BL + \beta_2 \times BW + \beta_3 \times H + \beta_4 \times TOB + \beta_5 \times BS + \beta_6 \times BL \times BW \\
& + \beta_7 \times BL \times H + \beta_8 \times BL \times TOB + \beta_9 \times BL \times BS + \beta_{10} \times BW \times H + \beta_{11} \times BW \times TOB \\
& + \beta_{12} \times BW \times BS + \beta_{13} \times H \times TOB + \beta_{14} \times H \times BS + \beta_{15} \times TOB \times BS + \beta_{16} \times BL \times BW \times H \\
& + \beta_{17} \times BL \times BW \times TOB + \beta_{18} \times BL \times BW \times BS + \beta_{19} \times BL \times H \times TOB + \beta_{20} \times BL \times H \times BS \\
& + \beta_{21} \times BL \times TOB \times BS + \beta_{22} \times BW \times H \times TOB + \beta_{23} \times BW \times H \times BS + \beta_{24} \times BW \times TOB \times BS \\
& + \beta_{25} \times H \times TOB \times BS + \beta_{26} \times BL \times BW \times H \times TOB + \beta_{27} \times BW \times H \times TOB \times BS \\
& + \beta_{28} \times BL \times H \times TOB \times BS + \beta_{29} \times BL \times BW \times TOB \times BS + \beta_{30} \times BL \times BW \times H \times BS \\
& + \beta_{31} \times BL \times BW \times TOB \times H \times BS + \varepsilon
\end{aligned}$$

in which BL is bottom length of RRPM; BW is bottom width of RRPM; H is height of RRPM; TOB is ratio of top width and bottom width; and β's are parameters to be estimated and ε is a random error term.

However, since it excludes 5-way interactions, this regression model is not a saturated model. Because the result of stress magnitude is accurately calculated by ANSYS, the stress magnitude is fixed in each case. All degrees of freedom will be consumed by a saturated regression model. Thus, for statistical inference, it is necessary to exclude the 5-way interaction terms to release some degrees of freedom.

5.3 Stress Indicator Determination

Considering the observed RRPM failure modes and RPMM material properties, four types of stresses were selected as indicators in this study: von Mises stress, principal stress, shear stress on bottom, and normal stress on bottom. Based on the various locations of RRPM failure modes and different stress distributions on RRPMs, these stresses can be connected to specific failure modes.

5.3.1 Von Mises Stress

Von Mises stress, which is also termed as equivalent tensile stress, is the most commonly used stress indicator for plastic deformation. The magnitude of Von Mises stress is determined by principal stresses in three directions, as shown in the following equation:

$$2\sigma_v^2 = (\sigma_1 - \sigma_2)^2 + (\sigma_2 - \sigma_3)^2 + (\sigma_3 - \sigma_1)^2$$

where $\sigma_1, \sigma_2, \sigma_3$ are principal stresses. It can also be expressed by normal stresses and shear stresses:

$$2\sigma_v^2 = (\sigma_{11} - \sigma_{22})^2 + (\sigma_{22} - \sigma_{33})^2 + (\sigma_{33} - \sigma_{11})^2 + 6(\sigma_{23}^2 + \sigma_{31}^2 + \sigma_{12}^2)$$

where $\sigma_{11}, \sigma_{22}, \sigma_{33}$ are normal stresses and $\sigma_{12}, \sigma_{23}, \sigma_{13}$ are shear stresses. The above equations illustrate that the von Mises stress is treated as a scalar, which can be used to formulate the von Mises yield criterion. Because the von Mises yield criterion is independent of the first stress invariant, it is "applicable for the analysis of plastic deformation for ductile materials" (Wikipedia, 2013).

5.3.2 Principal Stress

To capture the specific magnitudes and distributions of compressive stress and tensile stress, the principal stresses in three directions were calculated sequentially: maximum principal stress, middle principal stress and minimum principal stress. The sign of principal stress can identify the stress is compression or tension.

One previous study showed that the compressive stress mainly causes the damage occurring on top edges and non-lens sides of marker, while the tensile stress causes the mid-bottom fracture and body bending of markers more frequently (Zhang et al., 2009).

5.3.3 Shear Stress at RRPM Bottom

Besides the abrasion and cracks on RRPM body and lens, literature and field surveys also illustrate that the retention failure is another major RRPM failure mode. Normally, the poor retention performance is probably caused by shear stress, which is generated by impact from

high speed vehicles. Since the shear stress occurs on the interface of marker and adhesive, the shear stress at the RRPM bottom face was calculated in this study.

5.3.4 Normal Stress at RRPM Bottom

The damage caused by normal stress at RRPM bottom also may cripple the RRPM service life significantly. This normal stress damage is especially manifested as sinking of RRPM into flexible surface of asphalt concrete pavement. Moreover, normal stress at RRPM bottom may also generate tensile failure. Thus, analysis of normal stress at RRPM bottom is necessary, not only to prevent sinking, but also to avoid detachment.

CHAPTER 6 STRESS ANALYSIS OF FIELD RRPMS

In this chapter, stress conditions of the four RRPMs in real traffic scenarios were investigated. Eight types of FEMs, consisting of pavement (both flexible and rigid ones), tire, and each of the four RRPMs, including 3M 290, Ennis C80, Ennis C88, and Rayolite RS, were built. The finite element analysis was performed in three main steps, with the first one evaluating the stress response of each RRPM under the same traffic scenario and the second one testing other stress indicators to analyze potential RRPM failure mechanisms. The third one tested the impacts of different external variables, hollows, and various RRPM profiles on the stresses of RRPMs. The final section presents studies of the retention loss failure, based on force condition on the various RRPM bottoms.

The FEM simulated the process of a tire rolling over the RRPM, which, as an initial assumption, can be divided into three stages: the approach of the tire to the retroreflective lens of the RRPM, the instantaneous stay of the tire on top of the RRPM, and the movement of the tire over the other retroreflective lens of the RRPM. However, during the FEM simulation process in this study, the third stage was not found because the tire detached from the RRPMs at the top, rotated in the air for a distance, and then contacted with pavement again, avoiding contact with the lens on the other side. Thus the stress responses of the RRPMs of the former two stages were discussed. In the baseline case, the external variables, including tire load of 5000 lb, tire velocity of 70 mph, 0 degree contact angle, and 0 inch contact offset, were used. The contour plots of von Mises stress of each RRPM were also presented to exhibit general stress distributions.

6.1 Von Mises Stress Analysis

6.1.1 Stress Analysis of RRPM on Flexible Pavements

6.1.1.1 Von Mises Stress on 3M 290

Figure 6-1 and Figure 6-2 illustrate the stress trend with offset distance and the contour plots of a 3M 290 model on a flexible pavement. The offset distance of zero in Figure 6-1 is defined as the point that a tire sits at the center of the RRPM. Thus, a negative x-value means approaching the RRPM, and a positive x-value means leaving the RRPM.

As can be found in Figure 6-1, the maximum Von Mises stress in 3M 290 is around 140 MPa. The stress first increases as the tire begins to contact with 3M 290 until the maximal value and then decreases as the tire detaches from 3M 290. Revealed in Figure 6-2, despite the offset distance, the maximum stress occurs on the two tips of the RRPM due to stress concentration, especially significant when the tire is on top of the 3M 290.

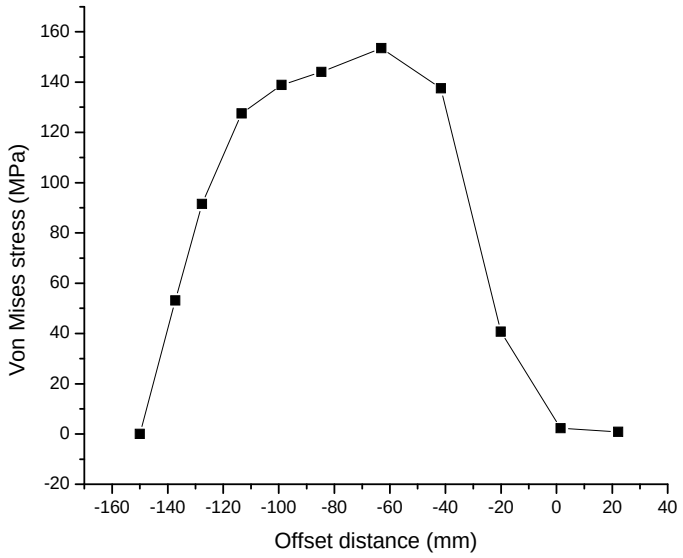

Figure 6-1 Maximal Von Mises Stress Trend with Offset Distance of 3M 290 Model

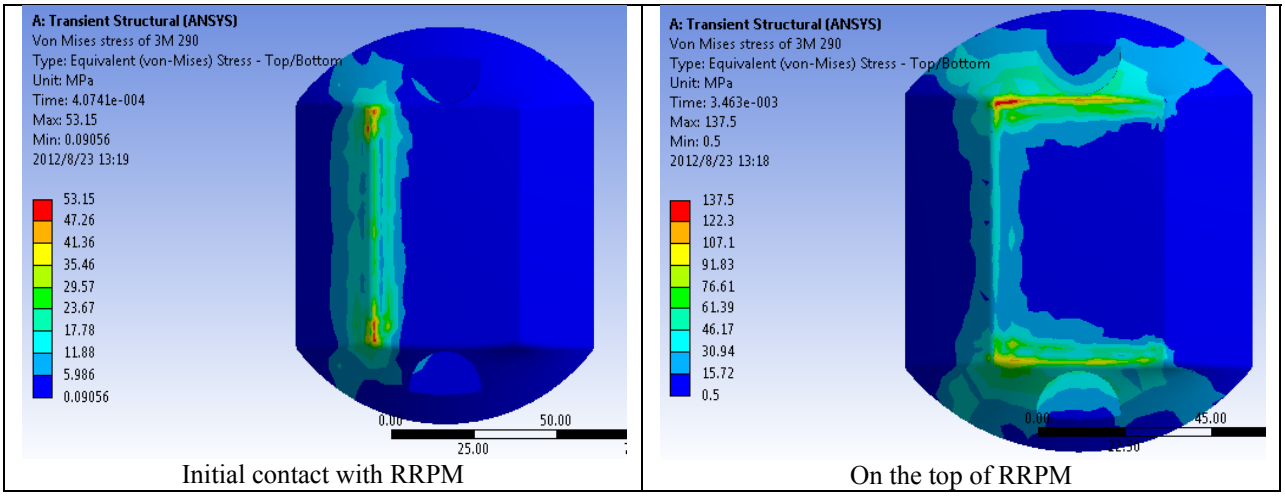

Initial contact with RRPM | On the top of RRPM

Figure 6-2 Von Mises Stress Contour Plots of 3M 290 Model

6.1.1.2 Von Mises Stress on Ennis C80

In a similar fashion, Figure 6-3 and Figure 6-4 are the stress trend with offset distance and the contour plot of Ennis C80 model. As can be found in Figure 6-3, the stress trend with offset distance of Ennis C80 model is similar to that of 3M 290 model, with the maximum von Mises stress around 130 MPa. As found in Figure 6-4, the maximum stress occurs in the rim of the RRPM as the tire begins to contact and then shifts to the two tips as the tire sits on the top of the RRPM, which is not fully similar to the case of Ennis C80 model.

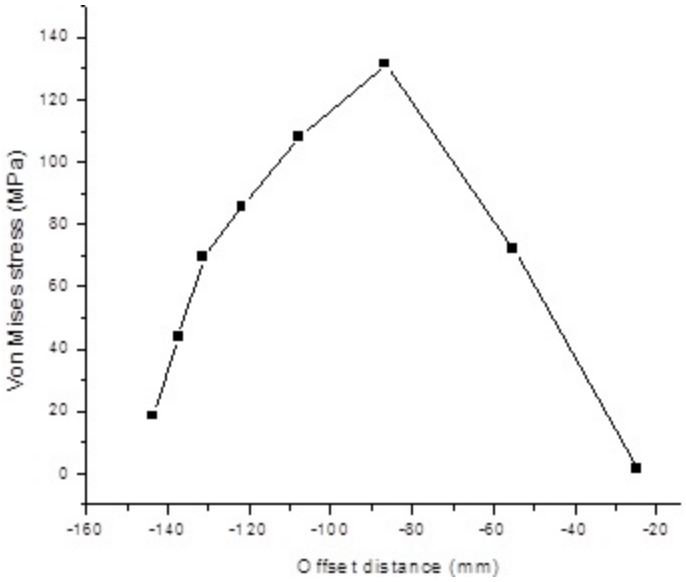

Figure 6-3 Maximal Von Mises Stress Trend with Offset Distance of Ennis C80 Model

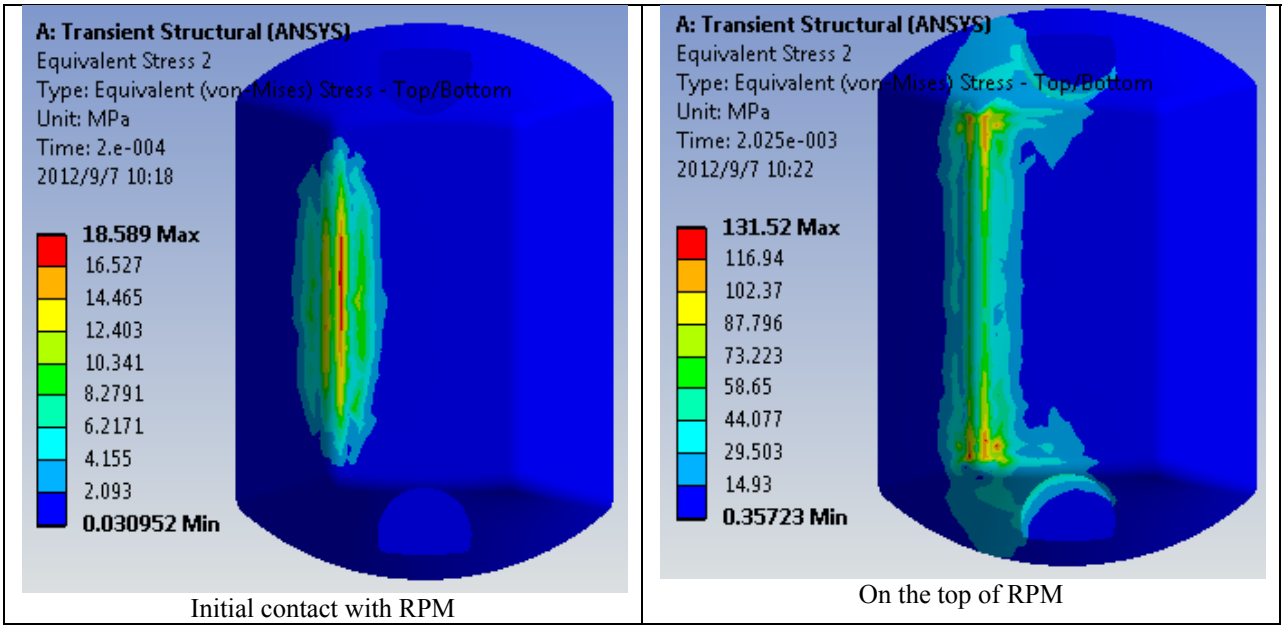

Initial contact with RPM

On the top of RPM

Figure 6-4 Von Mises Stress Contour Plots of Ennis C80 Model

6.1.1.3 Von Mises Stress on Ennis C88

Similarly, Figure 6-5 and Figure 6-6 are the stress trend with offset distance and the contour plots of Ennis C88 model. Unlike the former two RRPMs, structurally, the Ennis C88 marker consists of two parts: filler and housing (lens is considered as functional part, not structural part). The contour plots of both parts are presented to be compared.

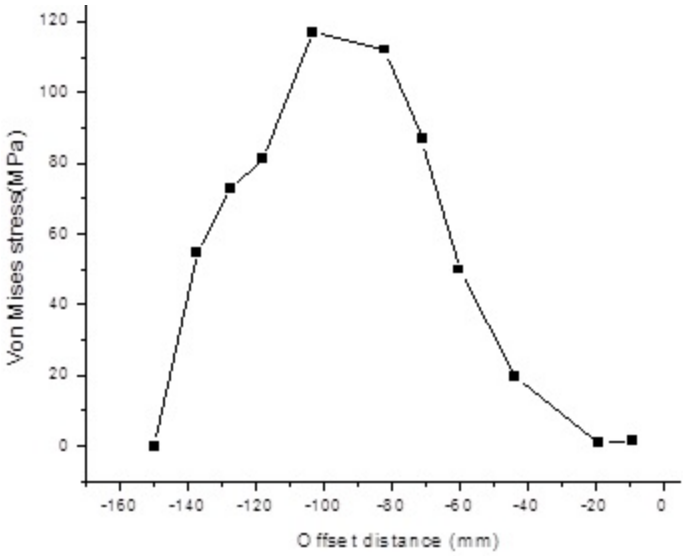

Figure 6-5 Maximal Von Mises Stress Trend with Offset Distance of Ennis C88 Model

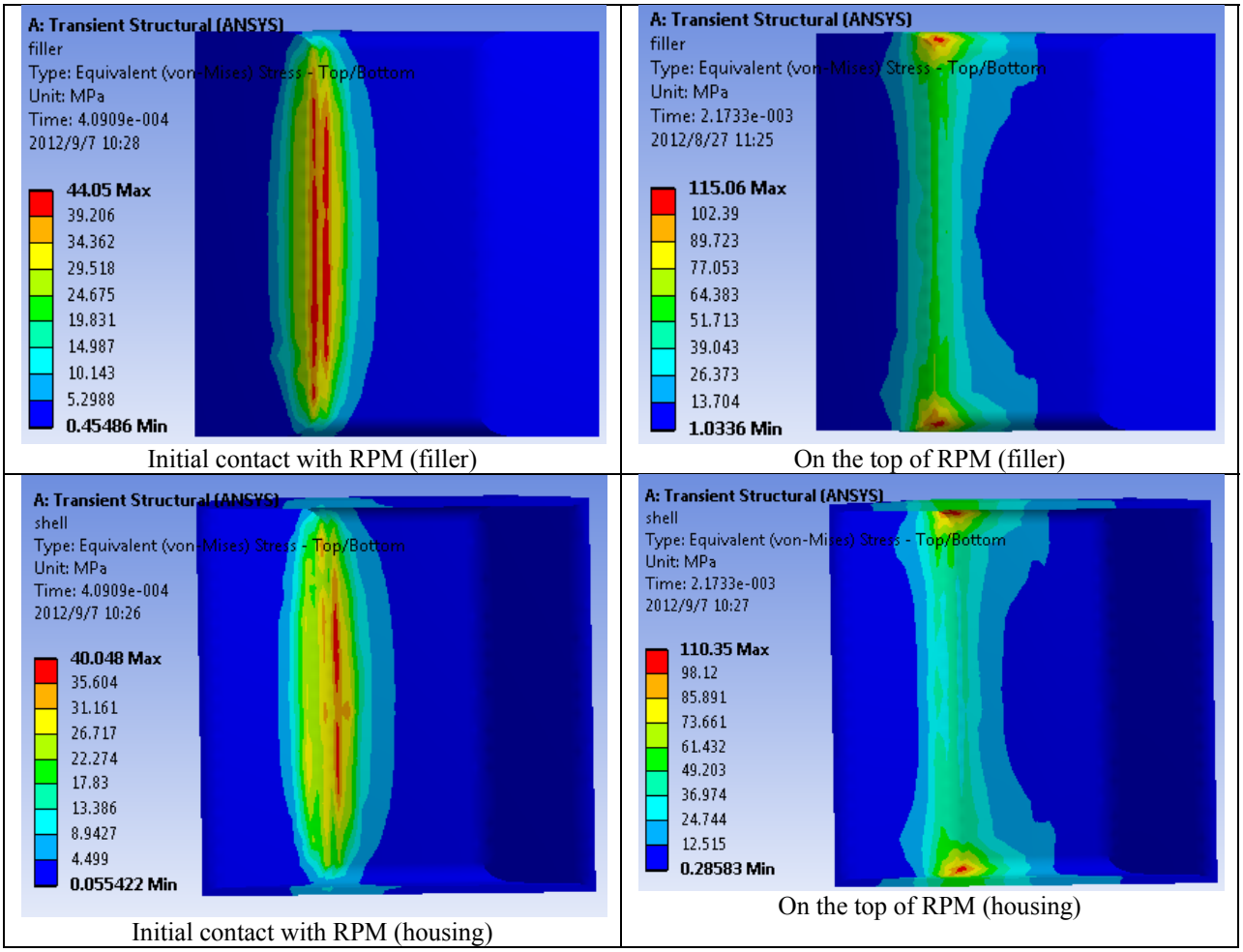

Initial contact with RPM (filler)

On the top of RPM (filler)

Initial contact with RPM (housing)

On the top of RPM (housing)

Figure 6-6 Von Mises Stress Contour Plots of Ennis C88 Model

The developing trend of Ennis C88 is similar to those of the former two, with the maximum von Mises stress around 110 MPa. Unlike the former two RRPMs, the maximal values of the stress do not appear on the skin layer but on the interface between the housing and filler, which may be attributed to the two different material properties of the two substructures. The maximal von Mises stress of Ennis C88 RPM is around 115 MPa.

6.1.1.4 Von Mises Stress on Rayolite RS

Figure 6-7 and Figure 6-8 are the stress trend with offset distance and the contour plot of Rayolite RS model. The Rayolite RS marker also consists of two structures (lens is the functional part): filler and housing. The contour plots of both parts are presented to be compared.

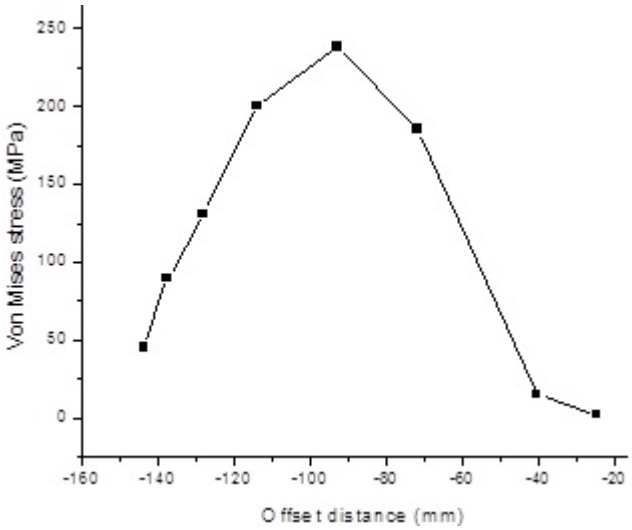

Figure 6-7 Maximal Von Mises Stress Trend with Offset Distance of Rayolite RS Model

The stress response of Rayolite RS is similar to that of Ennis C88 due to the similar structure. The maximum von Mises stress of Rayolite RS is around 240 MPa. The great stress difference of Rayolite RS and C88 may be due to the different geometric design since the top surface of Rayolite RS is very small compared to the other RRPM but needs further verification.

The filler is made of thermosetting compound, a brittle material. Thus, aside from von Mises stress, the tensile stress along the vehicular moving direction within the filler is investigated to evaluate the potential of brittle crack, as shown in Figure 6-9 and Figure 6-10.

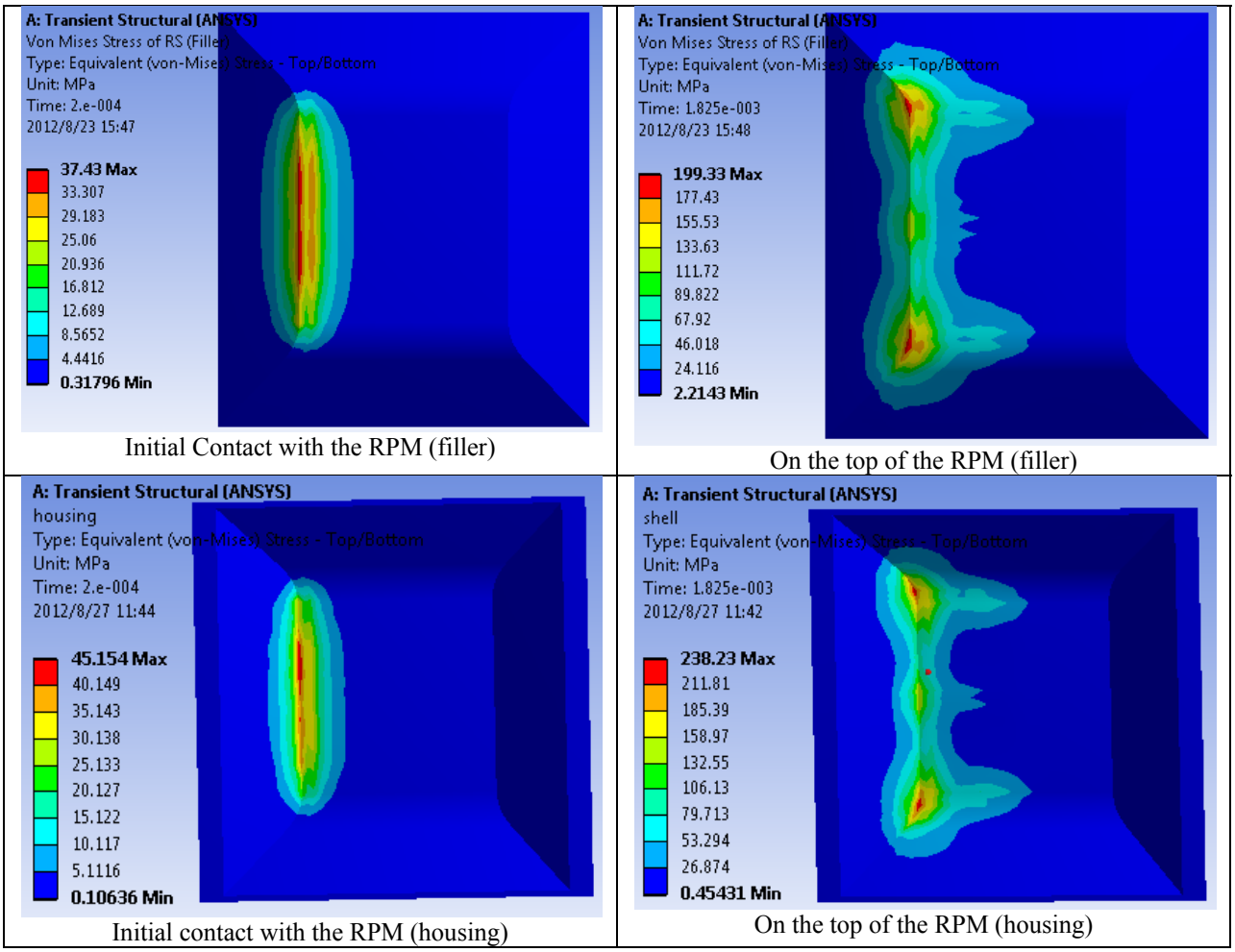

Figure 6-8 Von Mises Stress Plots of Rayolite RS Model

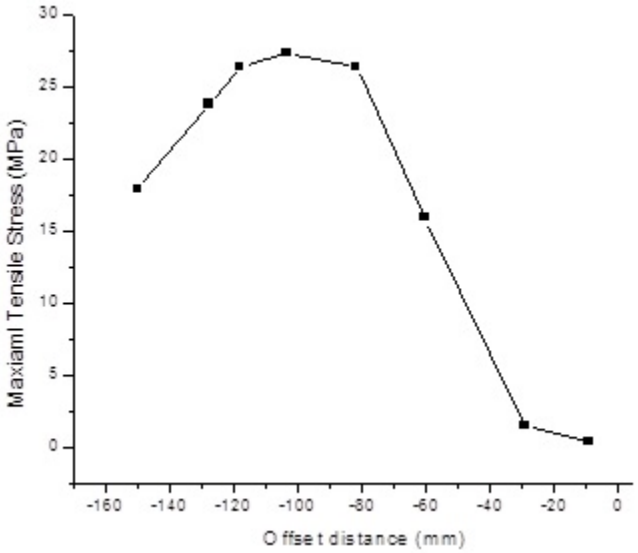

Figure 6-9 Maximal Tensile Stress Trend with Offset Distance of Rayolite RS Model

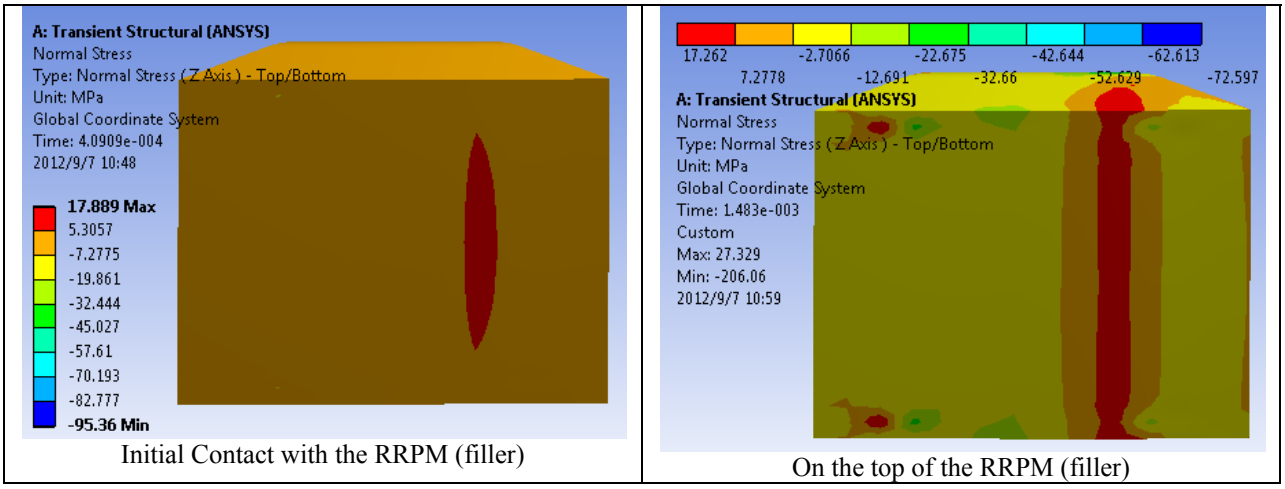

Initial Contact with the RRPM (filler)

On the top of the RRPM (filler)

Figure 6-10 Tensile Stress Plots of Rayolite RS Model

As reflected in Figure 6-9 and Figure 6-10, substantial tensile stresses do exist within the RRPM, with the maximal value of 27 MPa. Considering this, it is quite possible to witness bottom-up crack for Rayolite RS.

6.1.2 Stress Analysis of RRPMs on Rigid Pavements

Following the methods above, the stress responses of various RRPMs on rigid pavements were analyzed, but only performing step one's work. Figure 6-11 and Figure 6-12 are the stress trends with offset distance and the contour plots of 3M 290 model on rigid pavement.

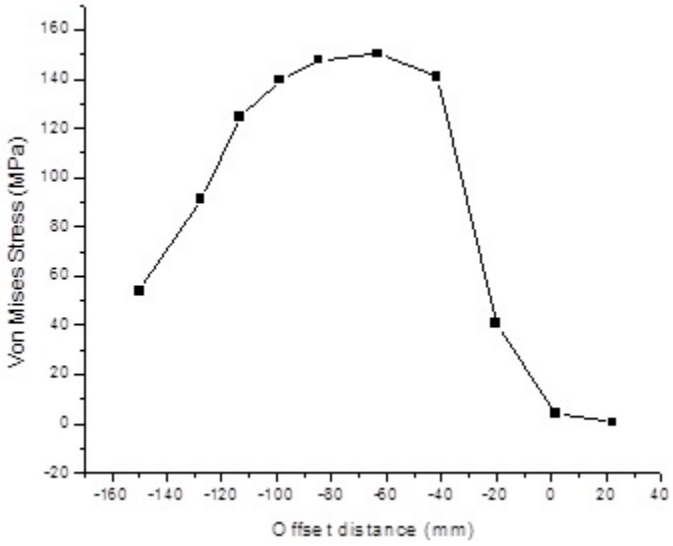

Figure 6-11 Maximal Von Mises Stress Trend with Offset Distance of 3M 290 Models on Rigid Pavement

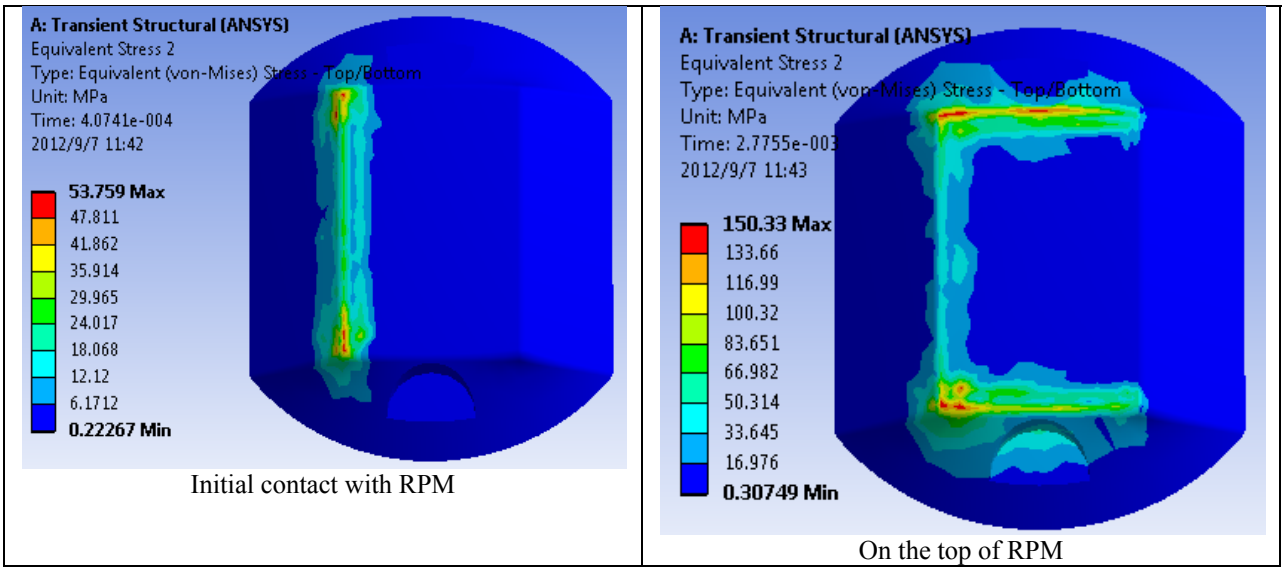

Figure 6-12 Von Mises Stress Contour Plots of 3M 290 Model on Rigid Pavement

As can be seen from Figure 6-1 and Figure 6-2, and Figure 6-11 and Figure 6-12, the maximal von Mises stress trend with offset distance and the stress distribution pattern of the RRPM on a rigid pavement are very much similar to those on a flexible pavement. And these similarities are true for the other three RRPMs. In this sense, only comparisons of extreme stress values on the two pavements for each RRPM are provided, as plotted in Figure 6-13.

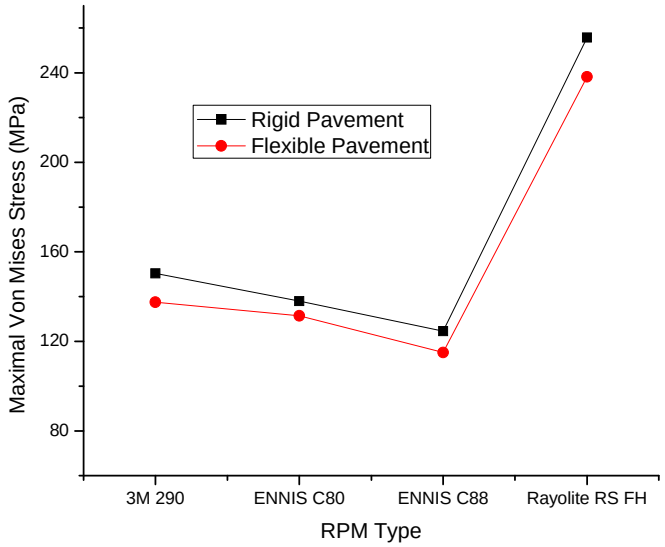

Figure 6-13 Maximal Von Mises Stress Comparisons of Various RRPMs on Rigid and Flexible Pavements

It is found that the maximal von Mises stresses of each RRPM on flexible pavements are smaller than those on rigid pavements.

6.1.3 Summary of Step One's Work

According to the previous FEM analysis, the maximal von Mises stresses are 137.5 MPa, 131.5 MPa, 115.1 MPa, and 238.2 MPa for 3M 290, Ennis C80, Ennis C88, and Rayolite RS, respectively. Thus the Ennis C88 shall have the superior structural damage resistance, followed by Ennis C80 and 3M 290, with Rayolite RS being the worst. Through comparing the von Mises stresses on RRPMs with different pavement surfaces, it is found that flexible pavements can "protect" RRPMs better than rigid pavements.

However, field failures of RRPMs include lens breakage and loss, cracking of the RPM body, retention loss of RRPMs, severe lens abrasion or contamination. Considering this, more indices are needed to evaluate the four RRPMs.

6.2 Other Stress Indicator Analysis

6.2.1 Stress Conditions and Damage Incentives of Various RRPMs on Flexible Pavements

Failure modes of plastic materials vary tremendously depending on the loading conditions and can be classified into the following categories: mechanical mode, thermal mode, chemical mode, radiation mode, electrical mode, and synergistic mode (Smithers Rapra, 2012). The mechanical damage is one of the frequently observed modes of RRPMs on field pavements. Typical plastic materials that are used to fabricate the RRPM include: polycarbonate, acrylic, polymethyl methacrylate (PMMA), acrylonitrile butadiene styrene (ABS), inert thermosetting compound, and others. Although with different material properties, all the materials are prone to yield under certain levels of compressive, tensile, or shear stresses. In other words, an RRPM on a pavement could be compressed, tensed, and sheared to damage. Table 6-1 lists the ranges of the mechanical properties of relevant materials. Considering this, three indicators, maximal principal stress (positive meaning tension and negative meaning compression) and maximal shear stress, from FEM analysis are selected to represent the stress conditions occurred within the RRPM structure and to account for the mechanical damage.

Table 6-1 Mechanical Property of Some RRPM Materials

Material	Young's modulus (MPa)	Shear modulus (MPa)	Tensile strength (MPa)	Elongation (%)	Compression strength (MPa)	Shear strength (MPa)	Reference
ABS-general purpose	2275-2900	700-1050	41-60	5-25	60-86	-	(Matbase, 2012)
PMMA	1800-3100	1700	48-76	2-10	83-124	-	
Acrylic	3000	-	70 (maximum)	5.1 (maximum)	-	-	(Plastics International, 2012)
Polycarbonate	2380	780	62 (yield)	110	85	40 (yield)	
Polycarbonate 10% GF	3100	-	55 (break)	15 (break)	96	-	
Polycarbonate 20% GF	5900	-	110 (break)	5 (break)	110	-	

6.2.2 Principal Stresses and Shear Stresses on 3M 290

Figure 6-14 and Figure 6-15 show the stress trends with offset distance and the contour plots of 3M 290 model. One point to clarify is that the negative maximum principal stress uses the absolute value so that all the three stress indicators are located in the same quadrant.

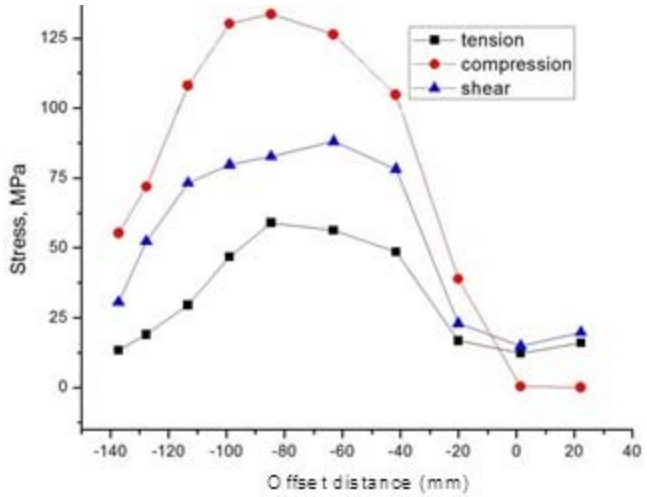

Figure 6-14 Stress Trends with Offset Distance of 3M 290 Model on Flexible Pavements

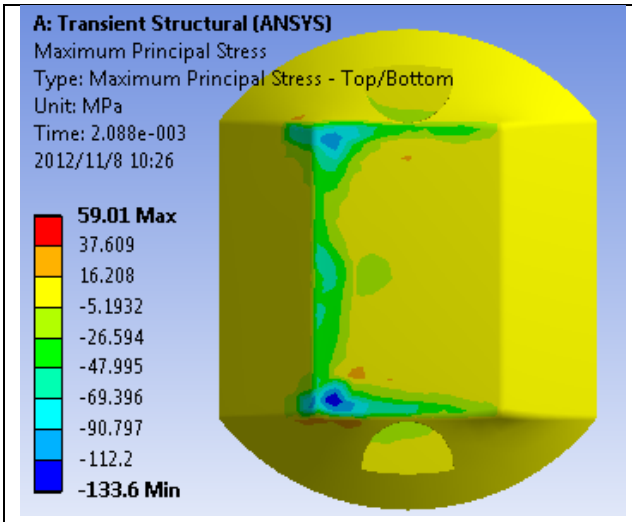

Contour plot of the maximum principal stress

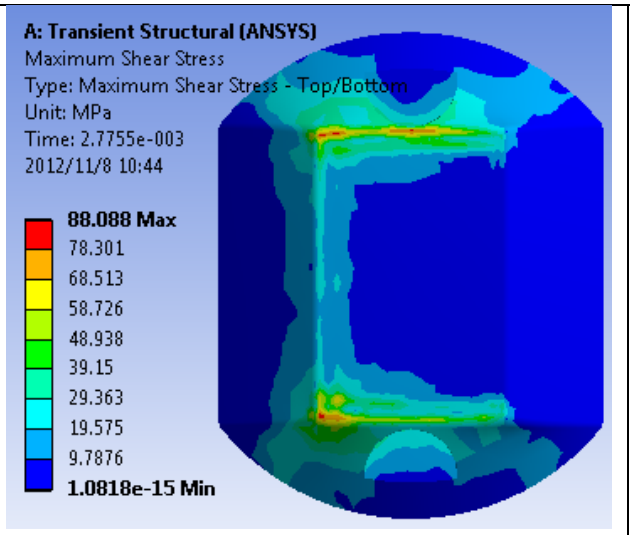

Contour plot of the maximum shear stress

Figure 6-15 Contour Plots of 3M 290 Model on Flexible Pavements

As can found in Figure 6-14, the maximum principal stresses (positive and negative) and maximum shear stress in the RRPMs are around 59 MPa, 134 MPa, and 88 MPa, respectively. The compression and shear mainly locate on the tips and rims of the surface while the tension scatters within the RRPM. And the compressive stress is much larger than the tensile stress. Referring to the values in Figure 6-14, the RRPM is more prone to be compressed and sheared to damage than stretched. For the developing trends of the three indicators, they first increase as the tire begins to contact with the RRPM until the maximum value and then decrease as the tire detaches from the RRPM.

6.2.3 Principal Stresses and Shear Stresses on Ennis C80

In a similar fashion, Figure 6-16 is the stress trends with offset distance of Ennis C80 model. The contour plots of the three stresses of the model are very much similar to those of 3M 290, so they are not presented.

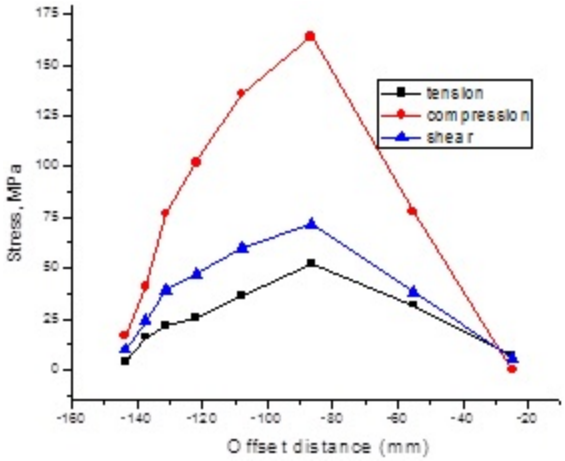

Figure 6-16 Stress Trends with Offset Distance of Ennis C80 Model on Flexible Pavements

As can found in Figure 6-16, the maximum principal stresses (positive and negative) and maximum shear stress in the RRPM are around 51 MPa, 163 MPa, and 72 MPa, respectively. Based on the critical stress, the same damage scenarios of the RRPM can be inferred.

6.2.4 Principal Stresses and Shear Stresses on Ennis C88

Similarly, Figure 6-17 is the stress trends with offset distance of Ennis C88 model. Unlike the former two RRPMs, structurally, the Ennis C88 marker consists of two parts: filler and housing (lens is considered as functional part, not structural part).

As shown in Figure 6-17, the maximum principal stresses (positive and negative) and maximum shear stresses in the RRPM are around 55 MPa, 146 MPa, and 66 MPa, respectively. Based on the critical stresses, a similar mechanical damage infer of the model can be made to previous two models.

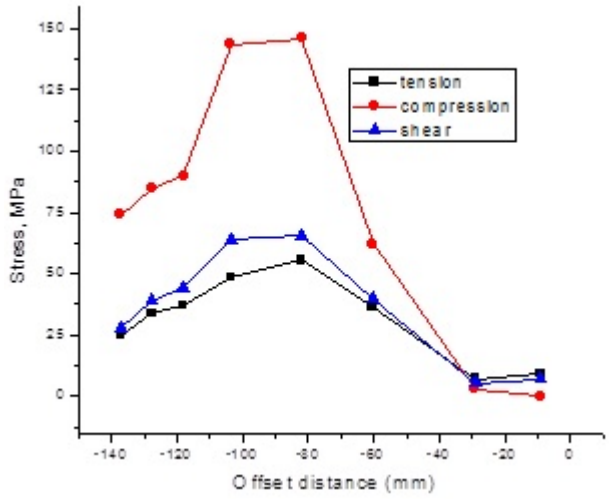

Figure 6-17 Stress Trends with Offset Distance of Ennis C88 Model on Flexible Pavements

6.2.5 Principal Stresses and Shear Stresses on Rayolite RS

Figure 6-18 plots the stress trends with offset distance of Rayolite RS model.

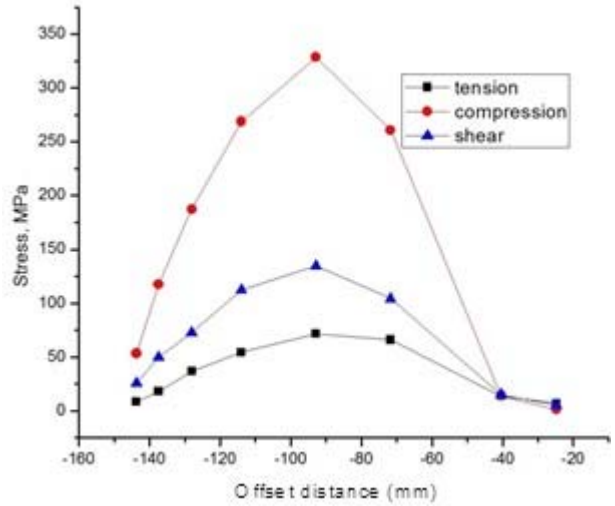

Figure 6-18 Stress Trends with Offset Distance of Rayolite RS Model on Flexible Pavements

The maximum principal stresses (positive and negative) and maximum shear stress in the RRPM are around 72 MPa, 324 MPa, and 134 MPa, respectively. Based on these values, the Rayolite RS is very possible to be compressed or sheared other than tensioned.

6.2.6 Stress Conditions and Damage Incentives of Various RRPMs on Rigid Pavements

Following the methods above, the stress responses of various RRPMS on rigid pavements were analyzed. Figure 6-19 and Figure 6-20 are the stress trends with offset distance and the contour plots of 3M 290 model on rigid pavements, respectively.

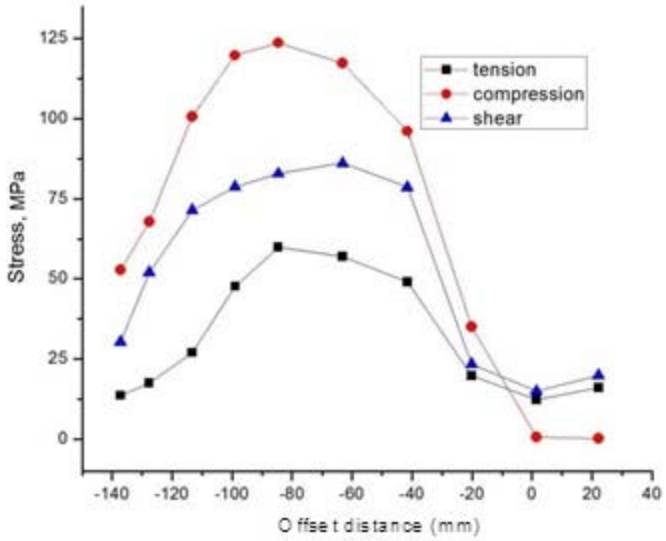

Figure 6-19 Stress Trends with Offset Distance of 3M 290 Model on Rigid Pavements

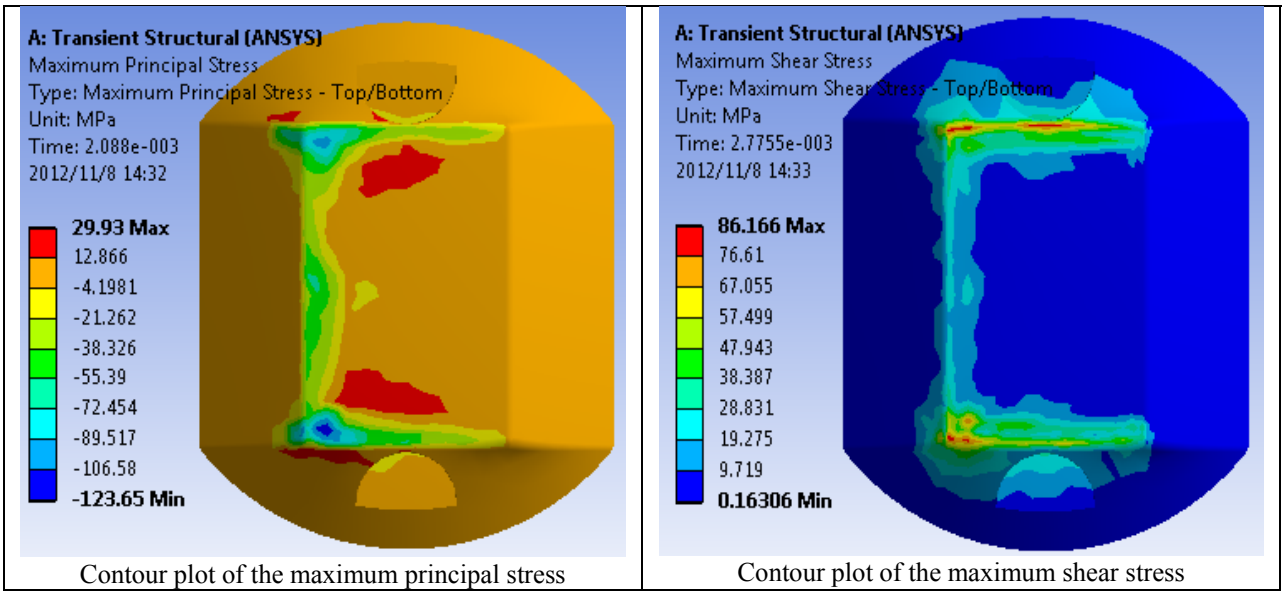

Contour plot of the maximum principal stress

Contour plot of the maximum shear stress

Figure 6-20 Contour Plots of 3M 290 Model on Rigid Pavements

The stress patterns of the RRPM on rigid pavements are quite similar to those on flexible pavements. The peak values of the principal stresses (positive, negative) and shear stress are around 30 MPa, 124 MPa, and 86 MPa, respectively. Still, the compressive and shear strength are the dominating factors that may lead to mechanical damage of the RRPM.

The stress patterns and developing trends for the other three RRPMs resemble the situations of 3M 290 model and so are not discussed in detail here. The peak values of the tensile and compressive principal stresses and shear stress are 51 MPa, 163 MPa and 72 MPa, respectively for the Ennis C80 model; 55 MPa, 146 MPa and 66 MPa, respectively for the Ennis C88 model; and 72 MPa, 324 MPa, and 134 MPa, respectively for the Rayolite RS model. Comparisons of the stress magnitudes of RRPMs on rigid pavements to those on flexible pavements suggest that RRPMs suffer more compressive and shear impacts than tensile impact on rigid pavements. In

other words, RRPMs are more easily damaged by compression and shear on rigid pavements than on flexible pavements. Thus, compressive maximum principal stress and maximum shear stress were selected as evaluation indicators for a more thorough and comprehensive FEM analysis of the RRPMs, including external factors analysis, geometric and material design optimizations, and laboratory test simulations.

6.2.7 Summary of Step Two's Work

The above preliminary analysis gives some clues of the stress responses as well as damage incentives of the four RRPMs on both types of pavements, which are summarized as follows:

- The stress trends with offset distance of the three indicators are the same: increasing as the tire begins to contact with the RRPM until the maximum value and then decreasing as the tire leaves the RRPM;
- The compressive maximum principal stress and shear stress concentrate on the two tips and rims of the RRPM structure while tensile maximum principle stress scatters;
- 3M 290, Ennis C80, and Ennis C88 RRPMs exhibit similar stress responses while the Rayolite RS has much higher ones;
- The four RRPMs suffer from a large compressive stress and relatively smaller shear and tensile stresses, and the RRPMs are more prone to be damaged by compression and shear, rather than tension.
- RRPMs on rigid pavements suffer more compressive and shear impacts than on flexible pavements.

6.3 Analysis of Effects of External Parameters

After the completion of the first two steps' work, this section examines the effects of external factors—tire loading, tire speed, contact angle, and contact location—on the critical von Mises stress inside the markers on flexible pavements. Since the developing trends of each RRPM are the same, Ennis C80 RRPM that was reported to have good field performance was selected to carry on the sensitivity analysis. The levels of involved factors are listed in Table 6-2.

Table 6-2 Matrix of Test Scenarios of External Parameters

	Trial 1	Trial 2	Trial 3
Tire inflation pressure (psi)	100	100	100
Tire load (lb)	3000	5000	7000
Tire rolling speed (mph)	60	70	50
Tire/RPM contact angle (degrees, from vertical)	0	5	10
Contact point offset (inches from RPM center)	0	1	2

As above mentioned, it was realized that the entire modeling program would involve 81 combinations of influencing factors for a full factorial design, as expected from Table 6-2. To reduce the simulation work while maintaining the reliability of conclusions, an orthogonal design was used. In this study, the orthogonal $L_9(3^{4-2})$ table orthogonal table can be converted into Table 6-3, with the elements in Table 5-5 substituted by the involved parameters in Table 6-2.

Here, it is worth pointing out that, only the individual effects of each parameter were considered while the interactive effects were ignored.

Nine sets of FEM simulation were performed. The simulation results in terms of the maximal von Mises stress and the range analysis of the results are listed in Table 6-4. From the range value, it can be concluded that tire load and tire/RRPM contact angle are the most dominating factors that influence the critical stress in the RRPMs, followed by tire rolling speed, and with the contact point offset having the least impacts.

Table 6-3 Orthogonal Table of FEM Parameters

factor / level / number	Tire load (lb)	Tire rolling speed (mph)	Tire/RPM contact angle (degree)	Contact point offset (inch)
1	3000	60	0	0
2	3000	70	5	1
3	3000	50	10	2
4	5000	60	5	2
5	5000	70	10	0
6	5000	50	0	1
7	7000	60	10	1
8	7000	70	0	2
9	7000	50	5	0

Table 6-4 Maximum Von Mises Stress of Each Simulation

Factor / Number	Tire load (lb)	Tire rolling speed (mph)	Tire/RPM contact angle (degree)	Contact point offset (inch)	Maximal Von Mises Stress (MPa)
1	3000	60	0	0	129.0
2	3000	70	5	1	227.7
3	3000	50	10	2	200.2
4	5000	60	5	2	224.8
5	5000	70	10	0	276.6
6	5000	50	0	1	232.8
7	7000	60	10	1	266.1
8	7000	70	0	2	221.0
9	7000	50	5	0	255.7
Avg.1	185.6	206.6	194.3	220.4	
Avg.2	244.7	241.7	236.1	242.2	
Avg.3	247.6	223.0	247.6	215.3	
Range	62.0	35.1	53.4	26.9	

As reflected in Figure 6-21, tire load and contact angle have consistent impacts on the maximal von Mises stress in the RRPMs, namely, increasing maximal stress with the increase of tire load and contact angle, while the other two factors, tire speed and offset distance, have no consistent effects. And a closer look at the data in the tire speed effect and offset distance effects subfigures suggests that the numbers are close. Thus it is acceptable to conclude that tire speed and offset distance have minor effects on the stress response of the RRPMs.

Aside, some snapshots of contour plots are presented to give a general concept of the impacts of the involved parameters. As revealed in Figure 6-22, the stress concentration location shifts as the contact angle and the offset distance vary.

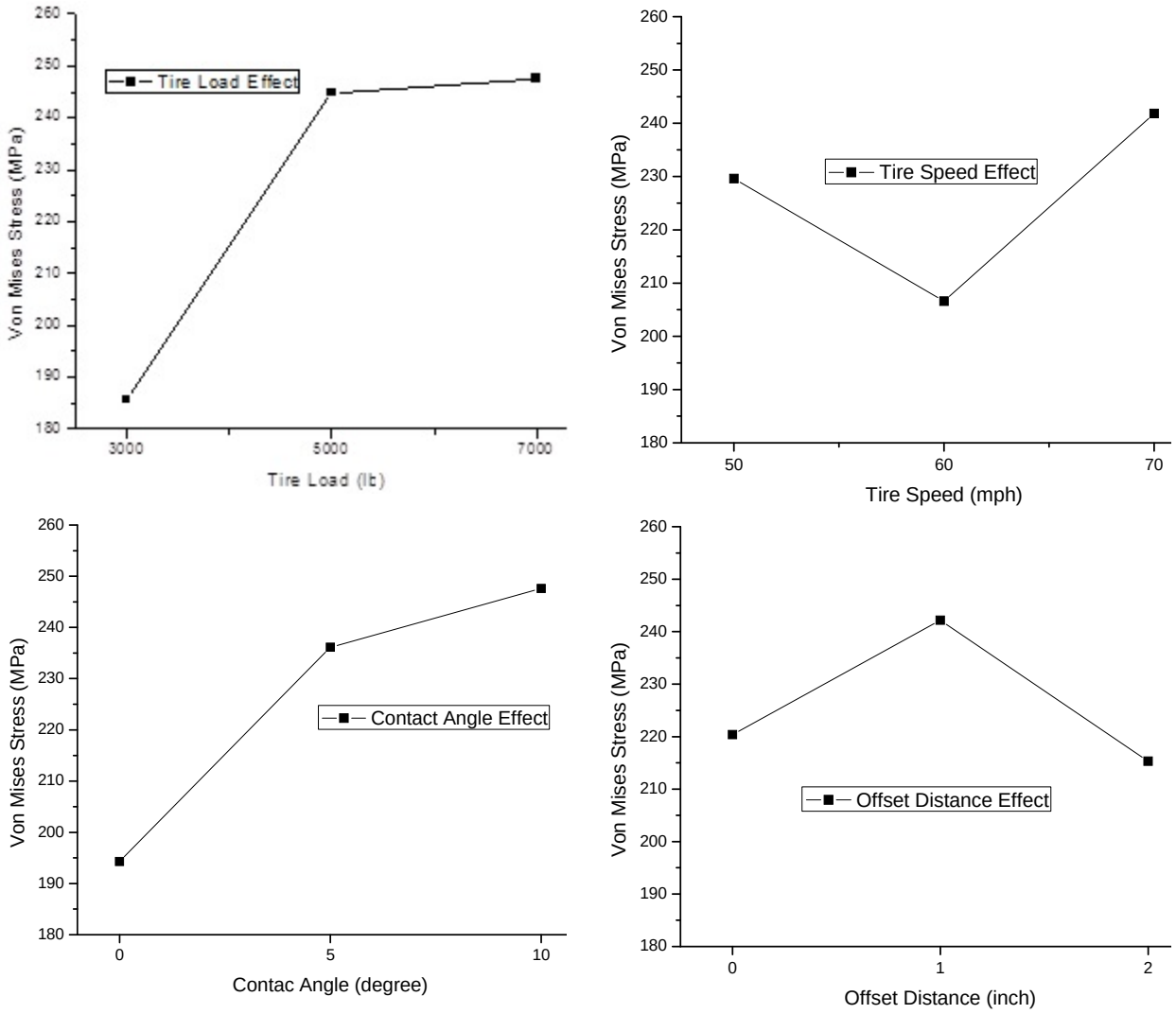

Figure 6-21 Effect Trends of Various Variables

6.4 Analysis of Effects of Hollow in 3M 290

After cutting the 3M-290 model into quadrant pieces, it was found that there exist hollow cylinder and rectangles within the marker structure. This research strived to model the 3M model as precisely as possible by excavating the hollow parts from the built FEM. After performing the simulation, the results are listed and plotted.

As can be found in Figure 6-23 and Figure 6-24, the maximum von Mises stress in the RRPM is around 170 MPa. The stress trend with offset distance is disparate from that of the model of solid structure, and the maximal von Mises stress increases from 140 MPa (solid model) to 170 MPa (hollow model). The solid model witnesses stress concentration around the tips and rims of markers while the hollowed model witness stress concentration around the excavated part of the model. Since the RRPM structure is hollow, it is expected that the surface experiences bending

and the bottom of the hollowed structure suffers from tensile stress. The RRPM mode is sliced to observe the inside structured, as shown in Figure 6-25.

The simulation results clearly indicate that there are tensile stresses occurring at the bottom of the hollowed structure, which agrees with the prior expectation. The existing tensile stress explains the occurrence of the surface damage occurred in the 3M RPM in heavy truck lanes.

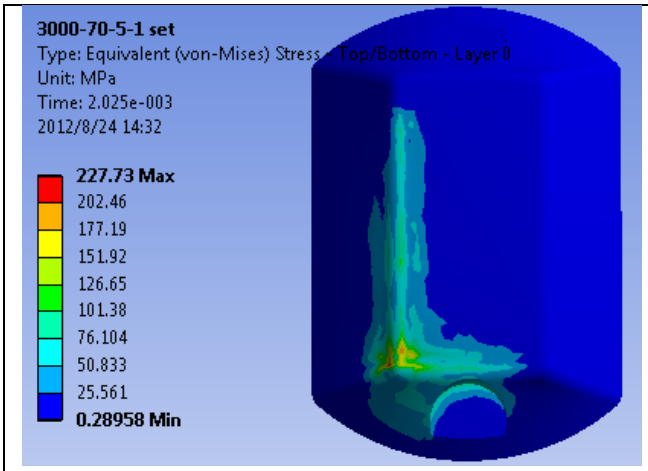

Number 2-the maximal von Mises stress scenario

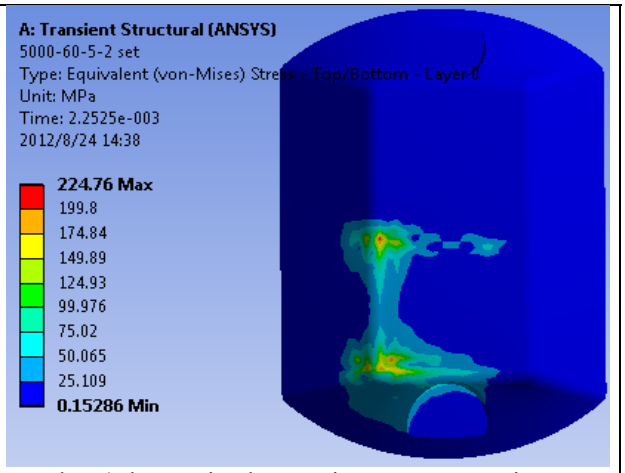

Number 4-the maximal von Mises stress scenario

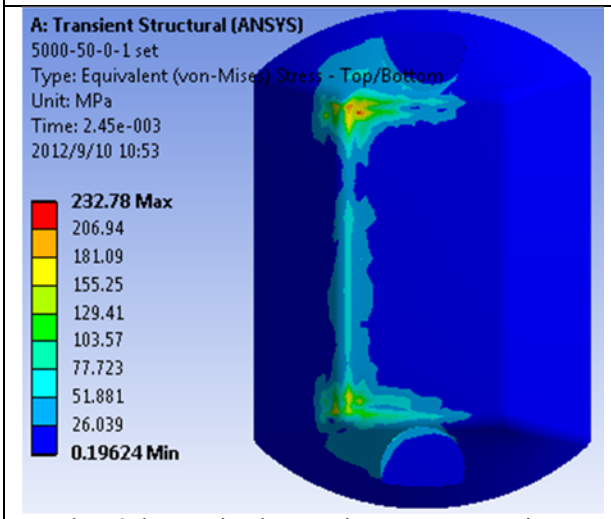

Number 6-the maximal von Mises stress scenario

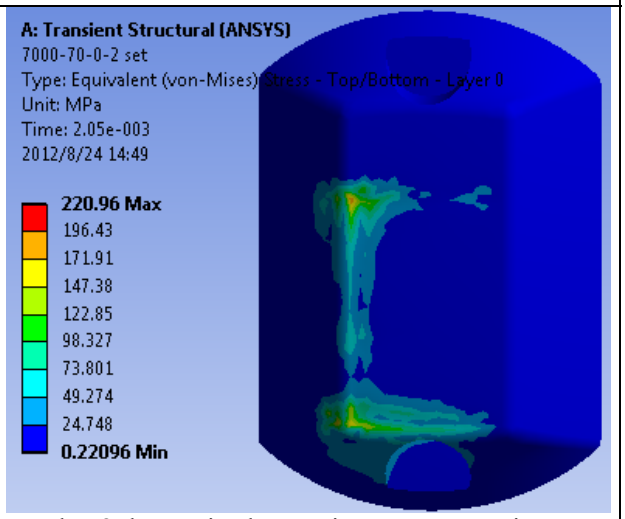

Number 8-the maximal von Mises stress scenario

Figure 6-22 Snapshots of Example Simulation Contours

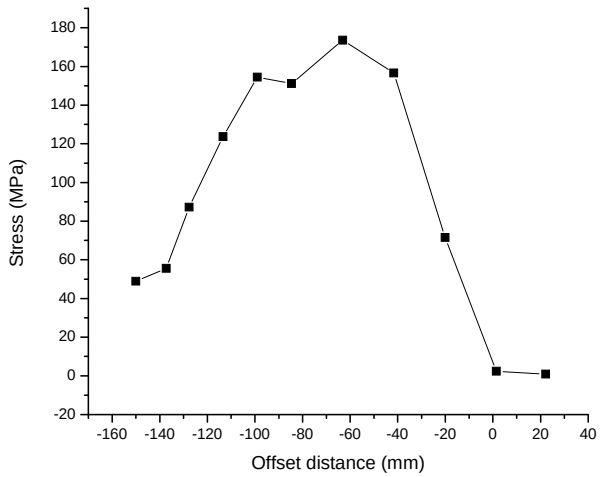

Figure 6-23 Stress Trend with Offset Distance of 3M 290 Model (Hollow)

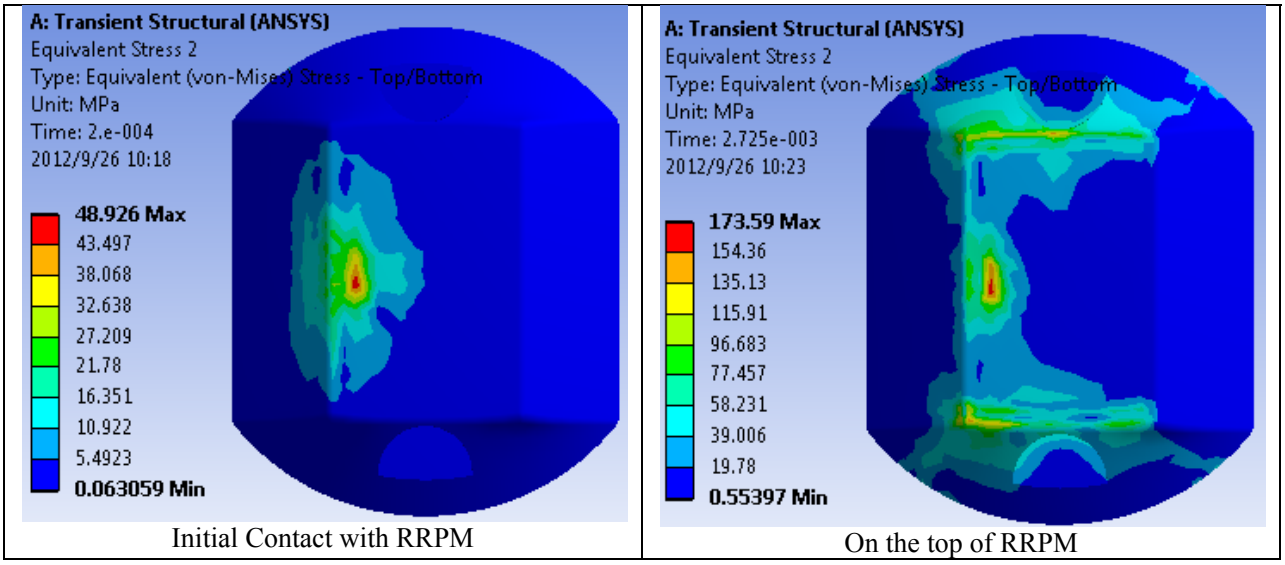

Initial Contact with RRPM | On the top of RRPM

Figure 6-24 Von Mises Stress Plot of 3M 290 Model

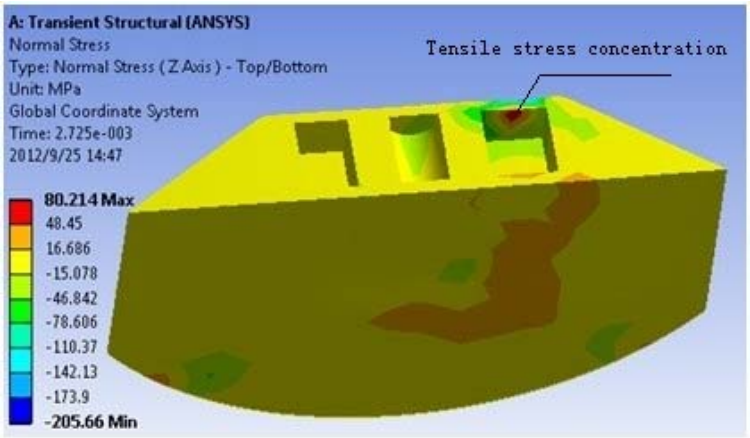

Figure 6-25 Tensile Stress along the Tire Moving Direction within the RRPM Structure

6.5 Analysis of Effects of Geometric Factors

As mentioned in Section 5.1.1.3.1, the basic frame of RRPM can be specified by six basic geometric factors: BL, BW, H, TOB, BS and slope of lens. In this section, one full factorial design with these factors except slope of lens is conducted to test stress states with all possible geometric dimension combinations. The test scenarios are listed in Table 6-5. For more clearly observing these geometric factors' effects, BL, BW, H, and TOB are analyzed under different RRPM types (different BS) individually in the first two subsections. Then, the effects of BS are captured in the third subsection.

Table 6-5 Matrix of Test Scenarios of Geometric Factors

Factor	Level	Abbreviation	Value
Bottom Length (BL) (mm)	1	BL1	64.5
	2	BL2	75.9
	3	BL3	87.3
Bottom Width (BW) (mm)	1	BW1	70.2
	2	BW2	75.2
	3	BW3	80.2
Height (H) (mm)	1	H1	13.5
	2	H2	15.5
	3	H3	17.5
Top Width over Bottom Width (TOB)	1	TOB1	0.8
	2	TOB2	0.9
	3	TOB3	1.0
Bottom Shape (BS) (RRPM Type)	1	BS1	1 (Bottom with Curve Edges)
	2	BS2	0 (Squared Bottom)

The results were statistically analyzed in software SPSS. It is worth pointing out that, on full factorial analysis, SPSS treats each level of factors and their interactions as dummy variable in the process of parameter estimation. SPSS also treats the highest level as base. Thus, the parameter estimation is individually specified on each level, which is not exhibited as a simple constant coefficient of one variable. In other words, the results can reflect statistically significant effects, and these effects might be not "consistent" for all levels.

6.5.1 Analysis Results for Type 1 RRPMs

Without considering the bottom shape difference, the regression model for full factorial analysis for RRPMs with curved bottom edges can be simplified as following:

$$\begin{aligned} stress = {} & \beta_0 + \beta_1 \times BL + \beta_2 \times BW + \beta_3 \times H + \beta_4 \times TOB + \beta_5 \times BL \times BW \\ & + \beta_6 \times BL \times H + \beta_7 \times BL \times TOB + \beta_8 \times BW \times H + \beta_9 \times BW \times TOB \\ & + \beta_{10} \times H \times TOB + \beta_{11} \times BL \times BW \times H + \beta_{12} \times BL \times BW \times TOB \\ & + \beta_{13} \times BL \times H \times TOB + \beta_{14} \times BW \times H \times TOB + \varepsilon \end{aligned}$$

All main effects, two-way and three-way interactions were tested for statistical significance in SPSS based on F values. The specific statistic results obtained in SPSS are listed in Appendix C. Generally, the following results are observed for Type 1 RRPMs:

- From the perspective of main effects, the stresses in RRPM body, except the minimum principal stress, are only significantly affected by bottom width (BW) and height (H). However, for the stresses at RRPM bottom, almost all geometric factors have significant effects, except the RRPM height and shear stress.
- For two-way interactions, there are four impressive findings. First, although both bottom length (BL) and ratio of top and bottom widths (TOB) have no significant influence on equivalent stress, their combination can significantly affect equivalent stress; Second, bottom width (BW) with ratio of top and bottom widths (TOB), and bottom length (BL) with ratio of top and bottom widths (TOB) have significant interactions on the minimum principal stress in RRPM body; Third, bottom length (BL) with bottom width (BW) have high interactions on maximum normal stress and shear stress at the RRPM bottom, but not on minimum normal stress; Fourth, there are most geometric factor interactions on minimum normal stress at RRPM bottom.
- Bottom width (BW), bottom length (BL), and ratio of top and bottom widths (TOB) have significant three-way interactions on minimum normal stress, minimum principal stress, and average shear stress at RRPM bottom.

Since each specific tendency of these effects is recorded by the estimated parameters within each two interval levels, instead of using one fixed coefficient on one variable, all these statistically significant tendencies of main effects of geometric factors on stresses are summarized in Table 6-6, in which "+" stands for positive relation, "–" means negative relation, "-/+" and "+/-" represent the significantly inconsistent tendency.

Table 6-6 indicates that decreasing RRPM height can mitigate the stresses in RRPM body, but also may increase failure extent at RRPM bottom. Thus, the RRPM height should be neither too large nor too small. Under the condition that good lens reflectivity performance is retained, bottom width shall be narrow. Lower ratios of top width and bottom width can reduce the stresses generated at RRPM bottom. Since the effects of bottom length is equivocal, it can be determined based on decision makers' other criteria.

Table 6-6 Trends of Stress Magnitudes in Terms of Geometric Factors on Type 1 RRPMs

	Stress in RRPM Body				Stress at RRPM Bottom		
	Equivalent stress	Maximum Shear Stress	Maximum Principal Stress	Minimum Principal Stress	Maximum Normal Stress	Minimum Normal Stress	Shear Stress
H	+	+	+		-	-	
BL					+	-	+
BW	+	+	+		-/+	+	+/-
TOB					+	+	+

6.5.2 Analysis Results for Type 2 RRPMs

Since Type 2 RRPMs do not have the disturbance effects from the bottom curve edge part, they are simpler than Type 1 RRPMs. Similarly, the specific statistical results obtained in SPSS are listed in Appendix C. Generally, the following results on Type 2 RRPMs are observed:

- Instead of BW, the main influences of H and TOB are statistically significant on all types of stresses. This result makes intuitive sense. Since the bottom of Type 1 RRPM has curve edges which can generate slopes on non-lens sides, stresses are distributed from top to bottom along this slope. However, the stress distribution from top to bottom is only contributed by TOB in Type 2 RRPMs, as illustrated in Figure 6-26. This situation also can explain why the main effects of BW also seem weakened in Type 2 RRPMs.
- For the stresses in RRPM body, except maximum principal stresses, there are two-way interactions observed between H and BL. However, there is no significant three-way interaction within these four geometric factors on the RRPM body stresses.
- For the stresses at RRPM bottom, BL and BW are not significant for the RRPM bottom stresses, neither for two- or three-way interactions.

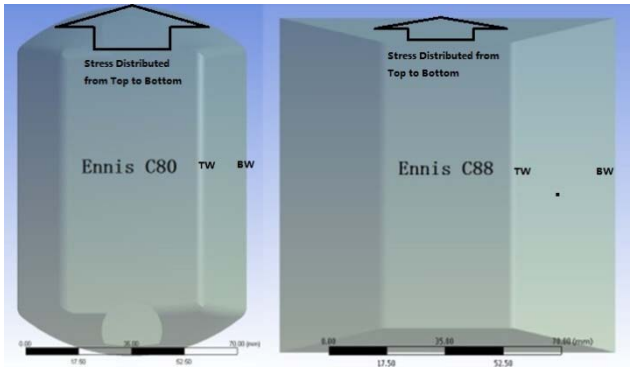

Figure 6-26 Stress Laterally Distributed from Top to Bottom in Two Types of RRPMs

Table 6-7 lists all these significant tendencies of main effects of geometric factors on stresses, in which "+" stands for positive relation, "–" means negative relation, "-/+" and "+/-" represent the significantly inconsistent tendency. For comparison with the results for Type 1 RRPMs, the green areas show the consistent tendencies for Type 1 RRPMs, and the orange areas show the opposite tendencies for Type 1 RRPMs.

Table 6-7 Trends of Stress Magnitudes in Terms of Geometric Factors on Type 2 RRPMs

	Stress in RRPM Body				Stress at RRPM Bottom		
	Equivalent stress	Maximum Shear Stress	Maximum Principal Stress	Minimum Principal Stress	Maximum Normal Stress	Minimum Normal Stress	Shear Stress
H	+	+	+	+	-	-/+	-/+
BL					+	-	-
BW	-				-		
TOB	+	+	+	+	+	+	+

Table 6-7 illustrates that although the RRPM bottom shapes are altered, H, BL, and TOB keep most effects the same, except the main effects of BL for shear stress at RRPM bottom and H for minimum normal stress at RRPM bottom.

Opposite to Type 1 RRPMs, the main effects of BW in Type 2 RRPMs are reduced and even changed significantly from positive to negative, as shown in Table 6-7. Since the shifted bottom shape might cause these opposite effects, these possible effects of bottom shape on BW are checked in the next section.

6.5.3 Effects of Bottom Shape

After individually testing the effects of geometric factors on various stresses in each RRPM type, this section merges these two RRPM types into one, and analyzes their potential connections. Regression analysis was performed to answer the following two questions

- Is there any interaction between BS and BW that can explain the conversion effects of BW from Type 1 RRPM to Type 2 RRPM?
- Which type of RRPM is "statistically" better?

Significant values of all main effects, two-way, three-way, and five-way interactions from SPSS are also listed in Appendix C, which shows two valuable results:

- The effects of BS are statistically significant for ALL stress magnitudes.
- The BS has significant correlation with BW for ALL types of stresses (the least "significant" one for BW*BS is around 90% confidence level). Their interactions directly lead the oscillated effects of BW on stresses. Similarly, the highly significant interactions, such as BL*BS on average shear stress (significance level < 0.001) and H*BS on minimum normal stress (significance level = 0.001), lead the oscillations of H and BL effects.

The estimated marginal means of different stresses in SPSS revealed that bottom with curve edges (Type 1) is generally better than squared bottom (Type 2), except for bottom shear stress and minimum principal stress. These trends are listed in Table 6-8.

Table 6-8 Trends of Stress Magnitudes for Bottom Shape Shift from Type 2 to Type 1

Stress in RRPM Body				Stress at RRPM Bottom		
Equivalent	Maximum Shear	Maximum Principal	Minimum Principal	Maximum Normal	Minimum Normal	Maximum Shear
-	-	-	+	-	-	+

6.5.4 Geometric Effect Conclusion

The conclusions and recommendations for RRPM geometric optimization are listed as follows.

- Increasing RRPM height leads to larger stresses in the RRPM body, which is in accordance with findings from the literature review. Furthermore, the potential failure, found at RRPM bottom, such as detachment or sinking, is mitigated by increasing RRPM height. These opposite effects appear more significantly in Type 1 RRPMs, whose bottom has curve edges. However, if the bottom is squared, the effects of RRPM height on the RRPM bottom failure modes become inconsistent. It is suggested to the decision makers that if the RRPM height is relatively large, the strength of RRPM body should be

improved for sustaining higher internal stresses. As the RRPM height becomes lower, the bond strength of adhesive deserves more attention.

- A larger difference between top width and bottom width can mitigate the potential failure modes at its bottom. If the RRPM bottom is squared, this beneficial effect also significantly exists in the RRPM body. Based on this finding, an ideal RRPM shape is pyramid.
- Since the main effects of RRPM bottom length are insignificant on stresses in the RRPM body and inconsistent on stresses at the RRPM bottom, decision makers can ignore the bottom length in the RRPM geometric design to improve durability.
- RRPM bottom width has high correlation with bottom shape on stress magnitudes. If the RRPM bottom has curve edges, narrow bottom width can contribute less stresses in the RRPM body. However, if the RRPM bottom has squared edges, its effects are altered, and only significant on maximum normal stress at RRPM bottom and equivalent stress in RRPM body.
- For the same sized RRPMs with different bottom edge shapes, the ones with curved bottom edges (Type 1) generally experience lower stresses than the ones with straight bottom edges (Type 2) under the same external scenario, except considering minimum principal stress or bottom shear stress.

6.6 Analysis of RRPM Detachment from Pavements

One of the distresses that tortures the functionality of RRPM is its complete loss, for which it may blame the shear force and perpendicular force between the RRPM and pavement. This section compares both shear and perpendicular forces of the four RRPMs in their base surfaces on rigid and flexible pavements, as plotted in Figure 6-27 through Figure 6-30.

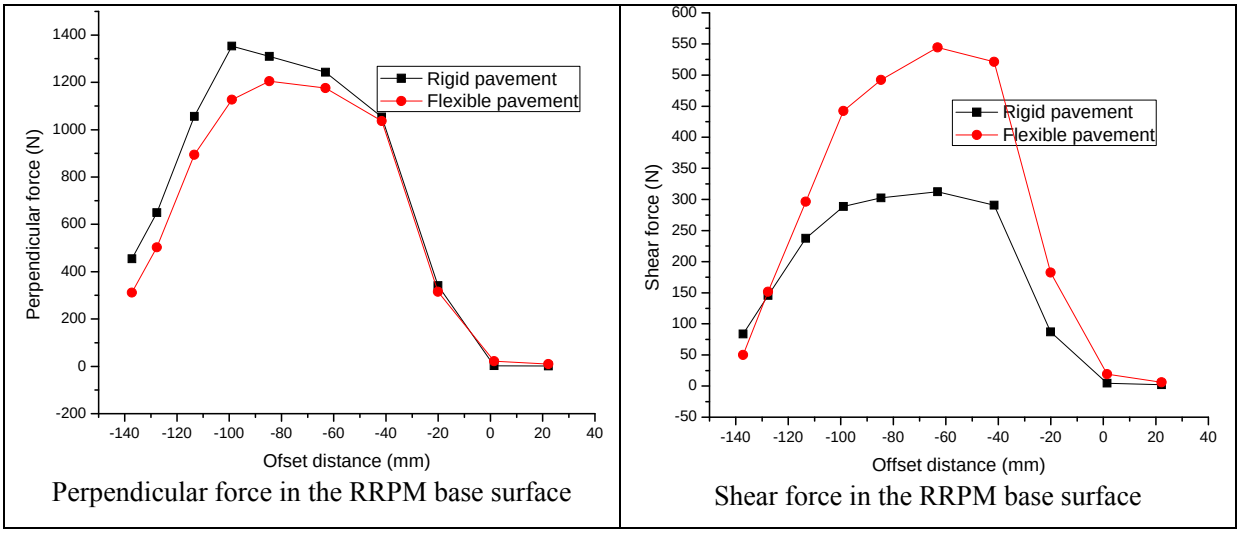

Perpendicular force in the RRPM base surface

Shear force in the RRPM base surface

Figure 6-27 Perpendicular and Shear Forces on 3M 290 Surface

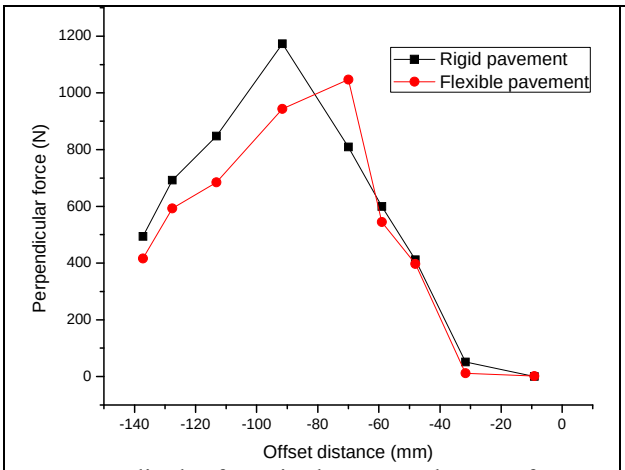

Perpendicular force in the RRPM base surface

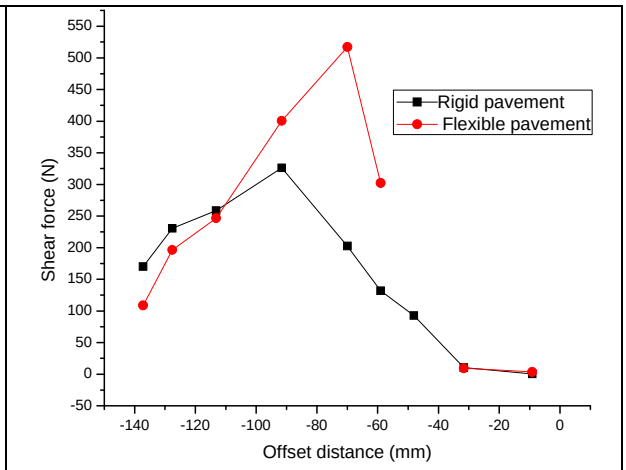

Shear force in the RRPM base surface

Figure 6-28 Perpendicular and Shear Forces on ENNIS C88 Surface

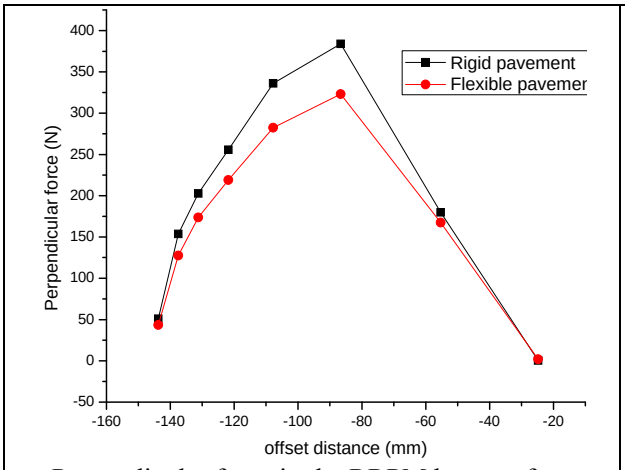

Perpendicular force in the RRPM base surface

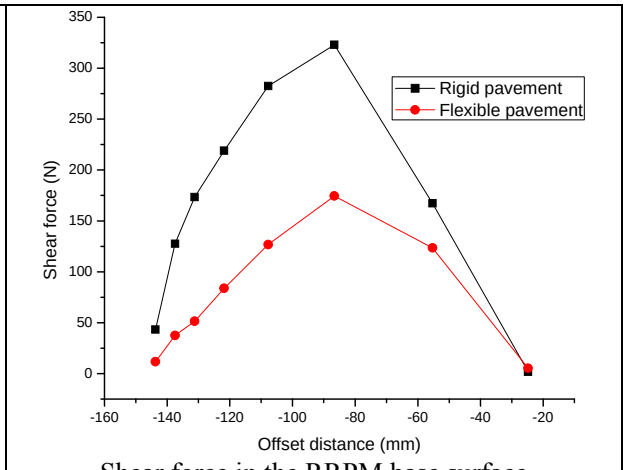

Shear force in the RRPM base surface

Figure 6-29 Perpendicular and Shear Forces on ENNIS C80 Surface

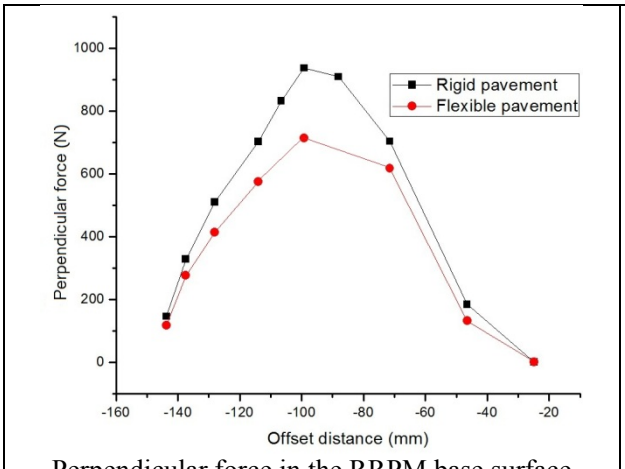

Perpendicular force in the RRPM base surface

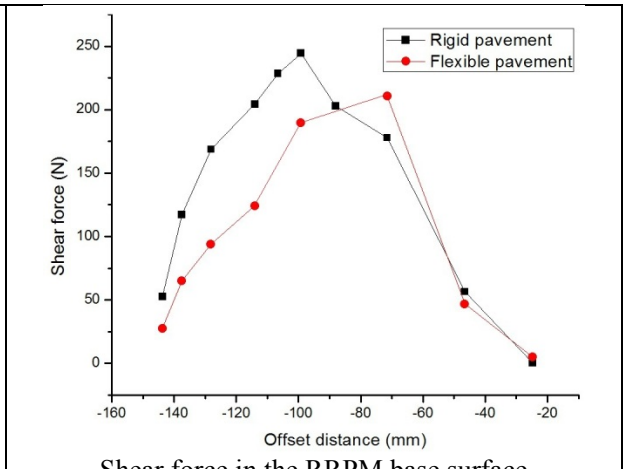

Shear force in the RRPM base surface

Figure 6-30 Perpendicular and Shear Forces on Rayolite RS Surface

Observing from the above figures, several general trends are summarized: first, the perpendicular forces of RRPMs on rigid pavements are larger than those on flexible pavements, with the excess ranging from 10% to 30%; second, there is no consistent rule for the shear forces, some being larger on flexible pavements and some on rigid pavements; third, perpendicular forces are dominating factors compared to shear forces. Considering the three findings, it is reasonable to conclude that retention of RRPMs on rigid pavements experiences more severe loading conditions than those on flexible pavements, which may be one reason to explain the more frequent loss of RRPMs on rigid pavements.

6.7 Material Comparison of RRPMs

Material is another main factor to generate different magnitudes of stresses. Different from geometric factors, the properties (young modulus and Poisson ratios) of materials can be easily changed in the FEM analysis, but the corresponding materials cannot be easily produced in the real word. Thus, in this section, the materials of 3M 290 are replaced by those in Ennis C80, and then used to observe the stress changes, as shown in Figure 6-31. Because the dimensions of 3M 290 are not changed, the stress magnitudes are only affected by materials.

Figure 6-31 shows that, when using the material of Ennis C80, the von Mises stress on 3M 290 drops from 137 MPa to 130 MPa. This 5.1% drop indicates that the material of Ennis C80 seems better than the 3M 290 materials in terms of stress reduction.

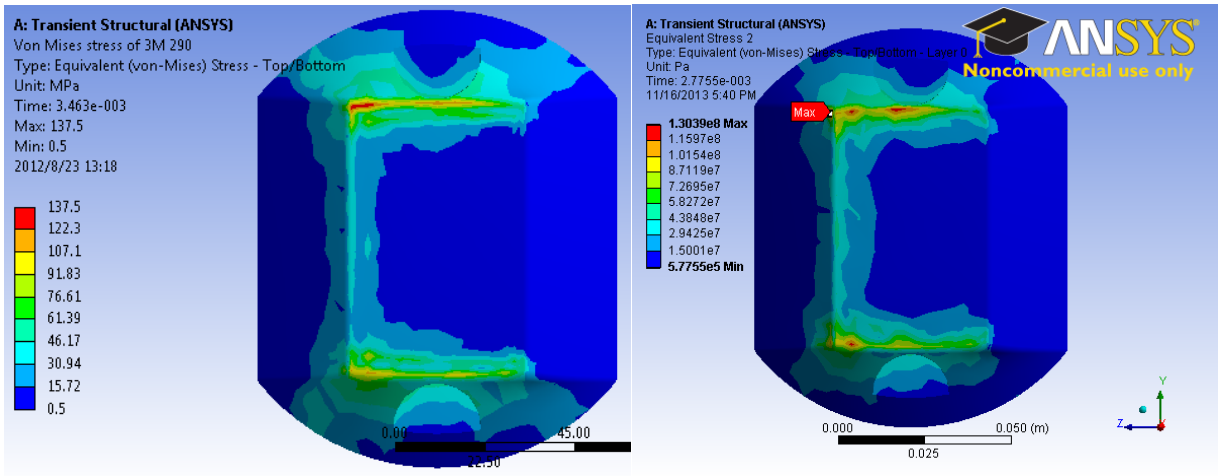

Figure 6-31 3M 290 (Left) and 3M 290 Filled by the Material of Ennis C80 (Right)

CHAPTER 7 FIELD MEASUREMENT OF RRPM STRAINS

The stress analysis of RRPMs in the previous chapter was based on finite element models, which implicitly incorporated a series of assumptions to simply the complex tire/marker/pavement system into manageable mechanistic models. For a direct evaluation of the responses of RRPMs to dynamic wheel loading, a field study was conducted to measure RRPM strains under various wheel loads and speeds.

7.1 Field Measurement Plan

In this field study, strain gauges were attached to both the top and the bottom of markers to measure strain responses under wheel loading. Four types of markers were tested: 3M 290, Ennis 980, Rayolite RS, and Apex 921AR. Ennis 980 has similar geometric features to Ennis C80, while Apex 921AR has similar geometric features to Ennis C88.

Except for Apex 921AR, seven strain gauges were attached to each type of marker: three at the bottom and four at the top, with their positions illustrated in Figure 7-1. Among them, gauge 2 measures a transverse strain (i.e., in a direction perpendicular to vehicle travel direction) while all the other gauges measure longitudinal strains. These gauge locations were selected based on previous FEM analysis as potentially critical locations. Specifically, gauge 4 and gauge 5 aimed to test the unequal critical stresses at two symmetric locations, as mentioned in Section 6.1; gauge 6 was intended to detect high tension, based on the FEM results in Section 6.2; gauge 7 was used to capture critical tension at the second step of tire impact on marker; and gauge 3 was installed at the projection location of top shell corner on RRPM bottom (as illustrated in Figure 7-2), where most bottom critical stresses are located. For Apex 921AR, due to its rough bottom texture, the three bottom strain gauges were not installed, so only four top strains were measured.

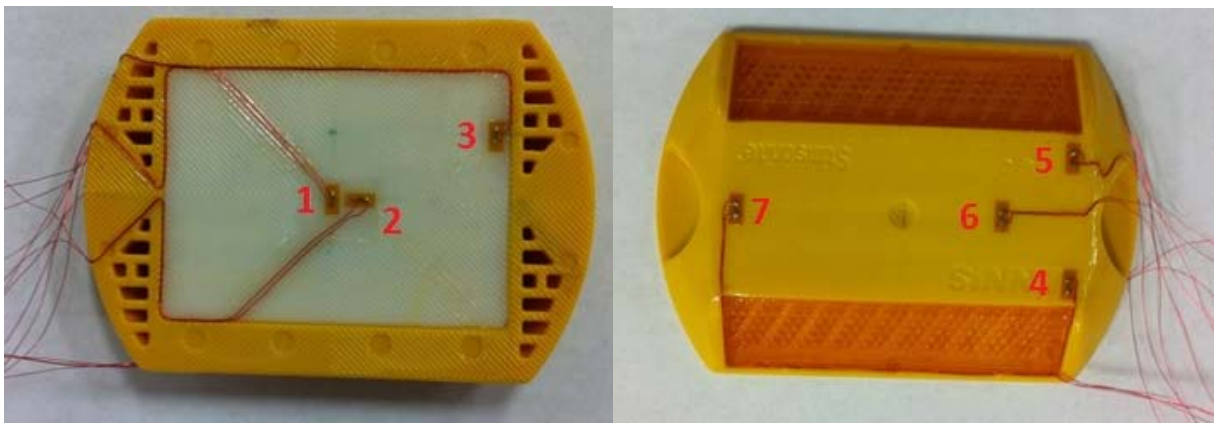

Figure 7-1 Locations of Strain Gauges on RRPM

A trial test was first run on two marker samples (3M 290 and Ennis 980) installed on a driveway with bituminous adhesives. A forklift was used to apply a wheel load of about 1,500 lb to the markers at a slow speed. Breakages of a couple of strain gauges were observed during the test. The strains measured from the other gauges, however, had the same order of magnitude as those calculated from the FEM.

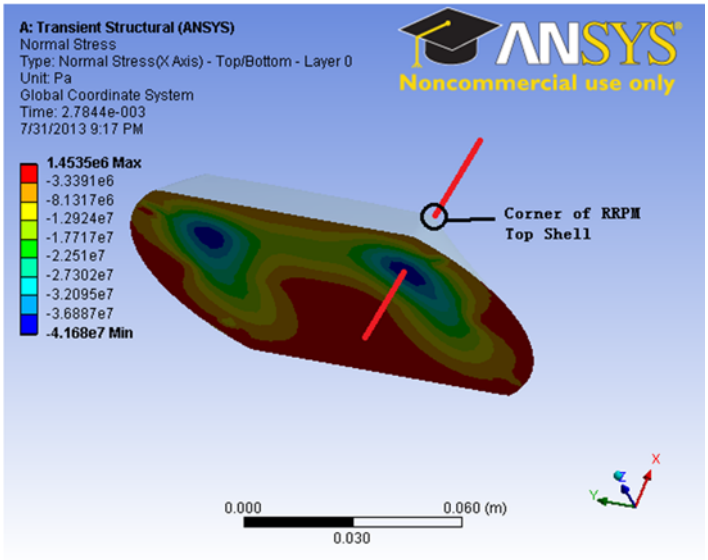

Figure 7-2 Normal Stress on RRPM Bottom

A full-scale field test was then carried out on March 28, 2014 on runways at Texas A and M Flight Test Station Airport in Bryan, Texas. Four markers, one of each type, were installed on the runways with a bituminous adhesive specified in the FDOT standard specifications (FDOT, 2010). The bitumen adhesive was first heated in an oven overnight, transported to the test site, and then heated with a portable oven for 3 to 4 hours to reach a liquid state of an application temperature of 400°F. Figure 7-3 shows the installation of the Rayolite RS marker at the test site.

Figure 7-3 Installation of Rayolite RS Marker at the Test Site

Two vehicles, an F250 pickup and an 18-wheeler tractor, ran over the markers in multiple passes in a sequence of pickup at 20 mph, pickup at 40 mph, pickup at 60 mph, tractor at 20 mph, and tractor at 40 mph. The two vehicles were driven by certified drivers who often drive heavy vehicles for various field tests. Trial runs were conducted to calibrate the lateral positioning in

order to hit the marker in the center of the tire width. During the actual testing, there were a few occasions when the tires hit the marker off-centered, these runs were repeated to ensure the middle of tires hit the marker. The strain response data for those off-centered hits, however, were kept in case that future analysis of RRPM strain response under such off-centered hits is needed. Figure 7-4 presents the testing scenes of the pickup and the tractor running over markers.

Figure 7-4 Testing Scenes of Pickup and Tractor Running Over Marker Specimens

The pickup has two axles, with one wheel at each end of an axle. The tractor has three axles, also with one wheel at each end. The wheel loads of both vehicles are listed in Table 7-1. During the test, the markers were always hit by the center of left wheels with a zero contact angle.

Table 7-1 Wheel Loads of Test Vehicles

Vehicle	Axle	Left Wheel (lb)	Right Wheel (lb)
Pickup	Front	2008	1977
	Rear	1550	1564
Tractor	Front	3820	3670
	Middle	3950	2750
	Rear	2680	3790

7.2 Test Results

A few strain gauges failed during the test. Specifically, gauge 1 on 3M 290 failed during the fifth pass (tractor at 40 mph); gauge 4 on 3M 290 failed in all passes; gauge 5 on 3M 290 failed in the third pass (pickup at 60 mph) and onwards; gauge 6 on Ennis 980 failed in the second pass

(pickup at 40 mph) and onwards; gauge 4 on Rayolite RS failed in all passes; and gauge 5 on Rayolite RS failed in the first pass (pickup at 20 mph).

For other functioning gauges, they recorded the transient strain responses of markers under moving wheel loads. Two examples of the results are shown in Figure 7-5 and Figure 7-6, representing the strain responses of the Ennis 980 marker under the pickup loading at 60 mph and the tractor loading at 40 mph, respectively.

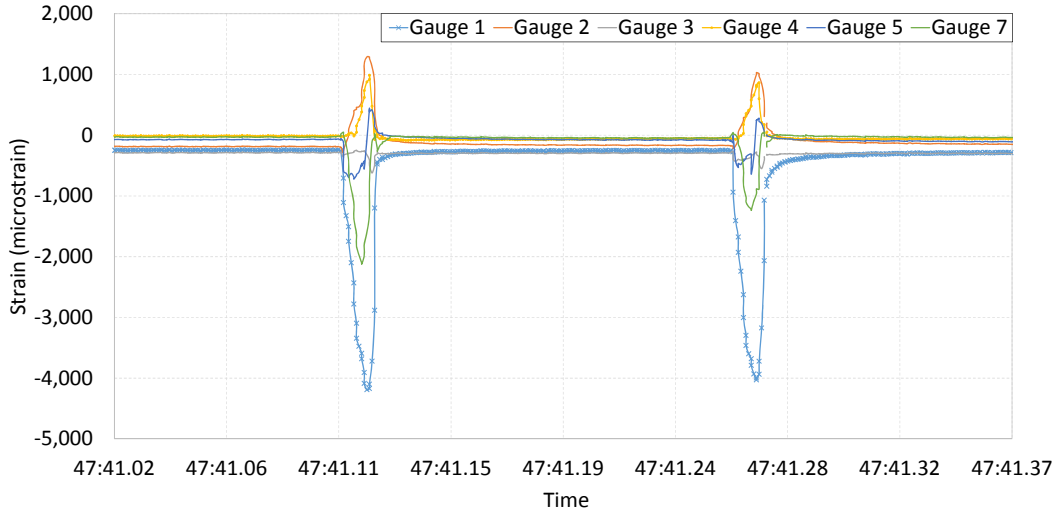

Figure 7-5 Strain Responses in Ennis 980 under Pickup Loading at 60 mph

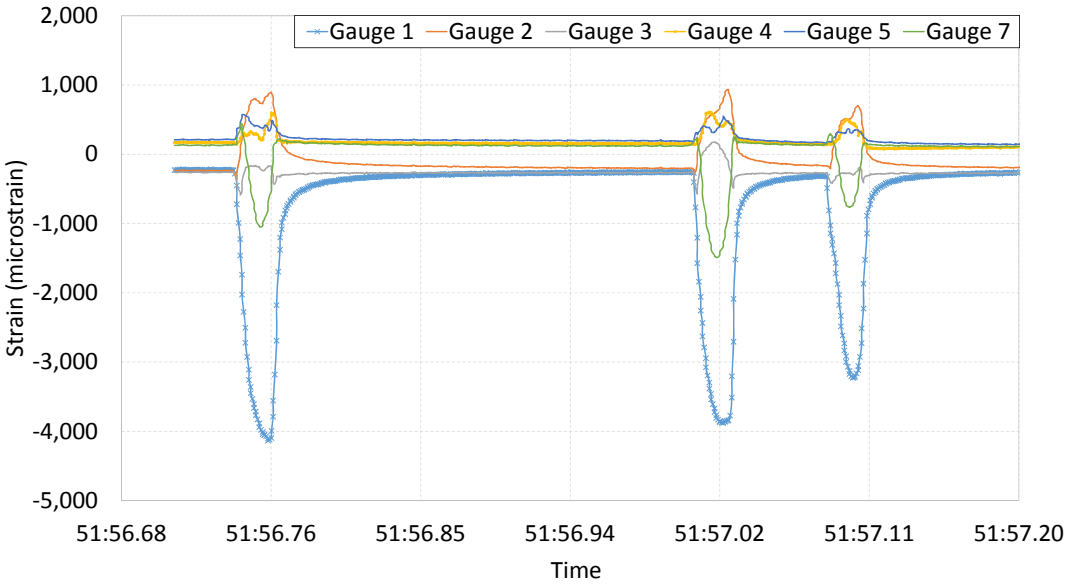

Figure 7-6 Strain Responses in Ennis 980 under Tractor Loading at 40 mph

The positive value in the plots is tensile strain and the negative one is compressive strain. It can be seen from the plots that both tensile and compressive strains may occur at the top and at the bottom of the marker. For example, at the bottom of the Ennis 980 marker, gauge 1 mainly

recorded a compressive strain while gauge 2 mainly measured a tensile strain. This is consistent with the FEM analysis results. Some gauges also recorded a reversal of strain value. For example, in Figure 7-5 the strain measured by gauge 5 was negative (compressive) at first, then became positive (tensile). Figure 7-5 and Figure 7-6 also show that the strain pulses are not symmetric. In general, the strain pulses have longer tails in the unloading stage than in the loading stage, which is more evident in the tractor (heavy) loading scenario. This delayed strain recovery after wheel unloading indicates a viscoelastic behavior of the marker materials. In addition, strains generally returned to their initial (non-loading) values after some period of time after unloading, suggesting that the plastic behavior of the marker materials is insignificant.

The peak values of strain responses measured on each type of marker are plotted in Figure 7-7 through Figure 7-10, respectively. Note that in the plot titles "Max." represents maximum tensile strain, while "Min." represents maximum compressive strain. Also note that the first two points on each curve are the data recorded under the pickup loading, and the rest three points are the data collected under the tractor loading. The following observations can be made from these plots:

- Under pickup loading or under tractor loading, strains generally increased with wheel loads. Strains under pickup loading, however, are not necessarily smaller than strains under tractor loading, although all two pickup wheel loads are smaller than the three tractor wheel loads. One potential reason for this abnormality is that the tractor tires are wider than the pickup tires. A wider tire may distribute more loading to the pavement and less loading to the marker. Therefore, it is possible that the load applied by a tractor tire to the markers may be smaller than the load applied by a pickup tire.
- Vehicle speed has no clear effect on the strain response. This is consistent with the findings from the FEM analysis, as discussed in Section 6.3.
- For 3M 290, the bottom longitudinal tensile strain is larger at the corner (gauge 3 position) than that at the center (gauge 1 position); the top longitudinal tensile strain appears to be larger at the downstream corner (gauge 5 position) that those at other gauge positions. Gauge 2 recorded a transverse compressive strain. Among all the measured strains, the maximum tensile strain is around 4000 με, and the maximum compressive strain is around -3500 με.
- For Ennis 980, gauge 1 recorded a longitudinal compressive strain while gauge 2 recorded a transverse tensile strain. The maximum top longitudinal tensile strain seems to also occur at the downstream corner (gauge 5 position). A compressive strain occurred at gauge 7 position. Among all the measured strains, the maximum tensile strain is around 2500 με, and the maximum compressive strain is around -4000 με.
- For Rayolite RS, compressive strains were primarily measured by gauges 2, 5, and 7, while tensile strains were primarily measured by gauges 1, 3, and 6. Among all the measured strains, the maximum tensile strain is around 1900 με, and the maximum compressive strain is around -3000 με.
- For Apex 921AR, compressive strains were measured by gauges 4, 5, and 6, while tensile strains were measured by gauge 7. Among all the measured strains, the maximum tensile strain is around 1100 με, and the maximum compressive strain is around -5400 με.

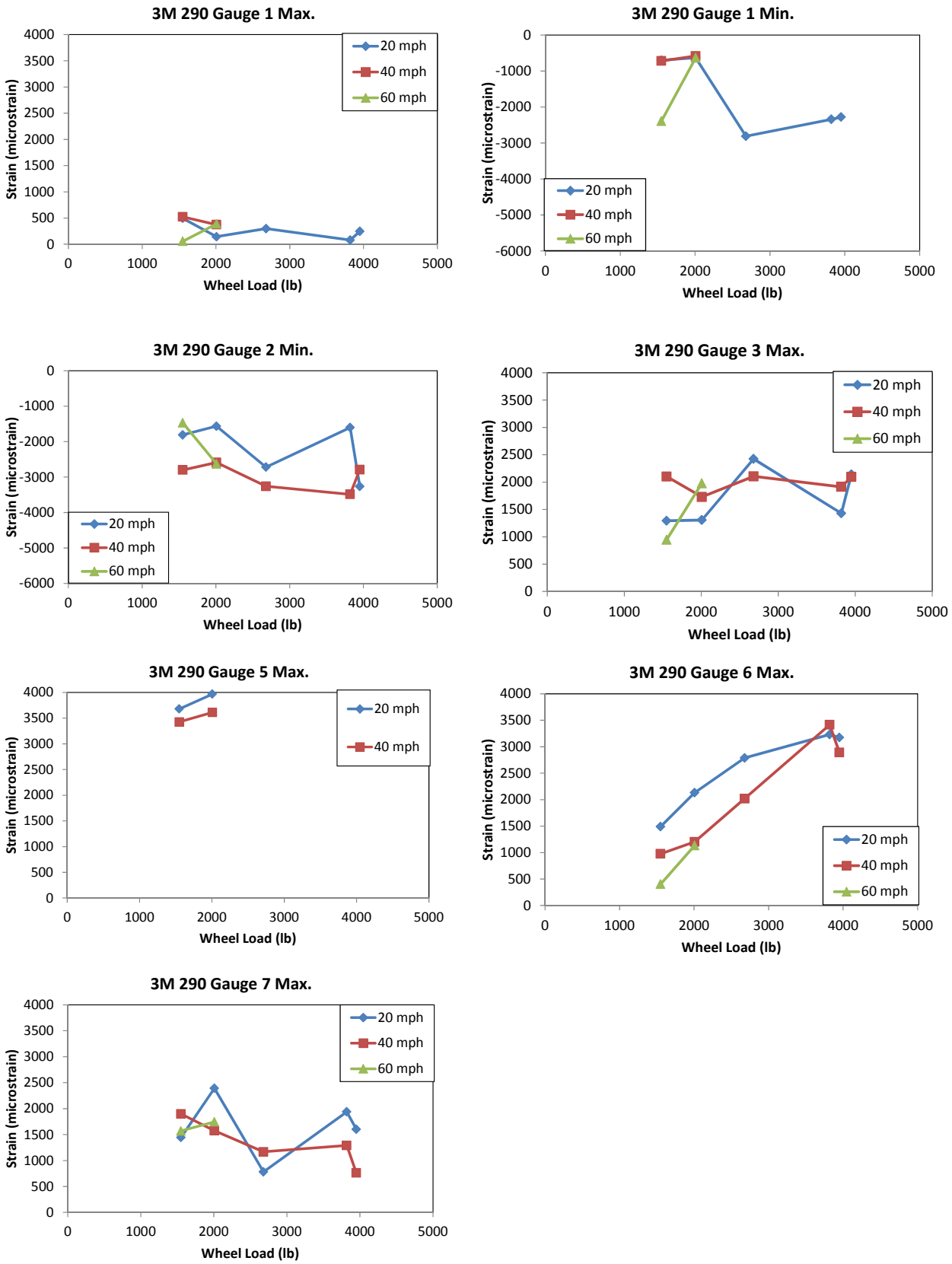

Figure 7-7 Maximum or Minimum Strains Measured by Strain Gauges on 3M 290

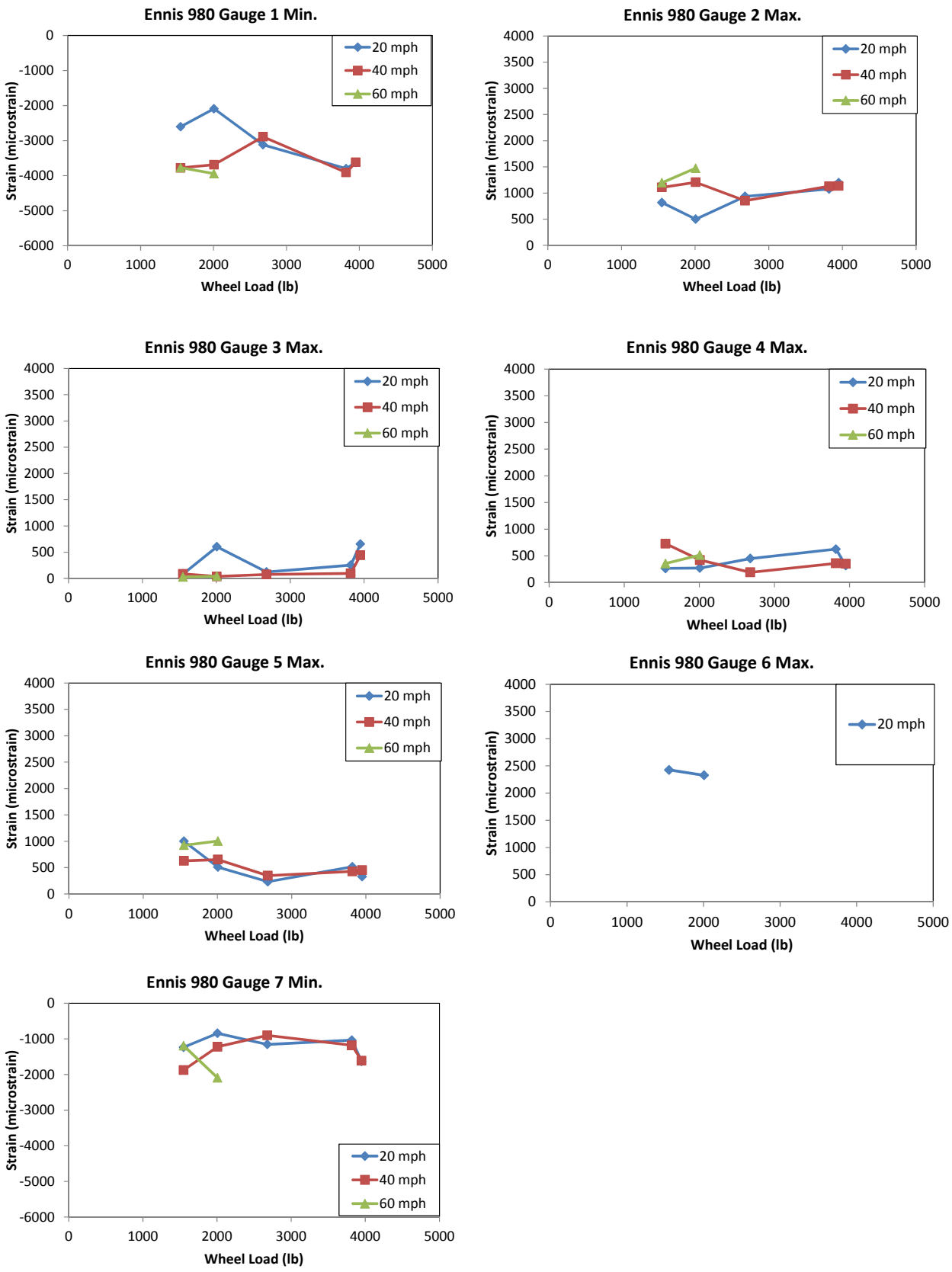

Figure 7-8 Maximum or Minimum Strains Measured by Strain Gauges on Ennis 980

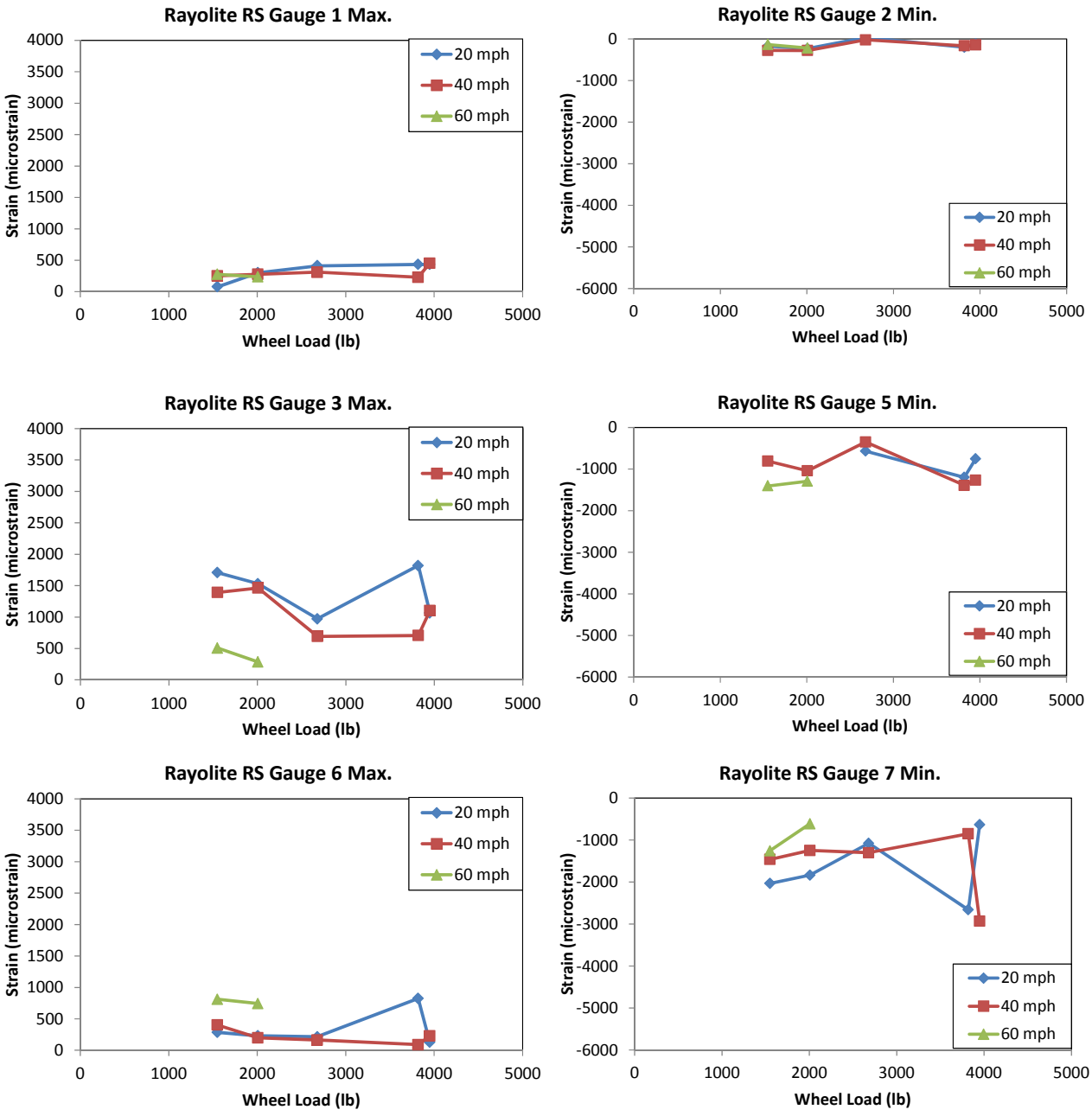

Figure 7-9 Maximum or Minimum Strains Measured by Strain Gauges on Rayolite RS

Figure 7-10 Maximum or Minimum Strains Measured by Strain Gauges on Apex 921AR

- Comparing the strains measured at the same gauge location but on different markers, it can be seen that the signs of the values are generally inconsistent. For example, the strain measured by gauge 5 (top downstream corner) is positive (tensile) on 3M 290 and Ennis 980, but negative (compressive) on Rayolite RS and Apex 921AR. The strain measured by gauge 6 (top center) is positive (tensile) on 3M 290, Ennis 980, and Rayolite RS, but negative (compressive) on Apex 921AR. This inconsistency reflects the differences in the structures and dimensions of various types of RRPM.

7.3 Comparison with FEM Results

A series of stress analysis of field RRPMs were completed in Chapter 6 using FEM. However, the wheel loads and speeds in the previous analysis do not match the values used in the field measurement. Therefore, additional FEM analysis was performed for the four types of RRPM included in the field measurement (3M 290, Ennis 980, Rayolite RS, and Apex 921AR). Due to time constraint, the FEM analysis was only done for the following load and speed combinations: 2008 lb (pickup front axle) at 20, 40, and 60 mph, and 3950 lb (tractor middle axle) at 20 and 40 mph. A total of 20 FEM simulations were run.

In the FEM, strain responses after tire impact were captured using the "probe" tool in ANSYS very conveniently and efficiently. Probes were placed at positions corresponding to the strain gauge locations, and their "result selections" were set along directions corresponding to the measured strains from field tests, as shown in Figure 7-11.

The peak values of strain responses at different strain gauge locations on the four RRPM types were captured and compared with the field measurements, as shown in Figure 7-12 through Figure 7-15.

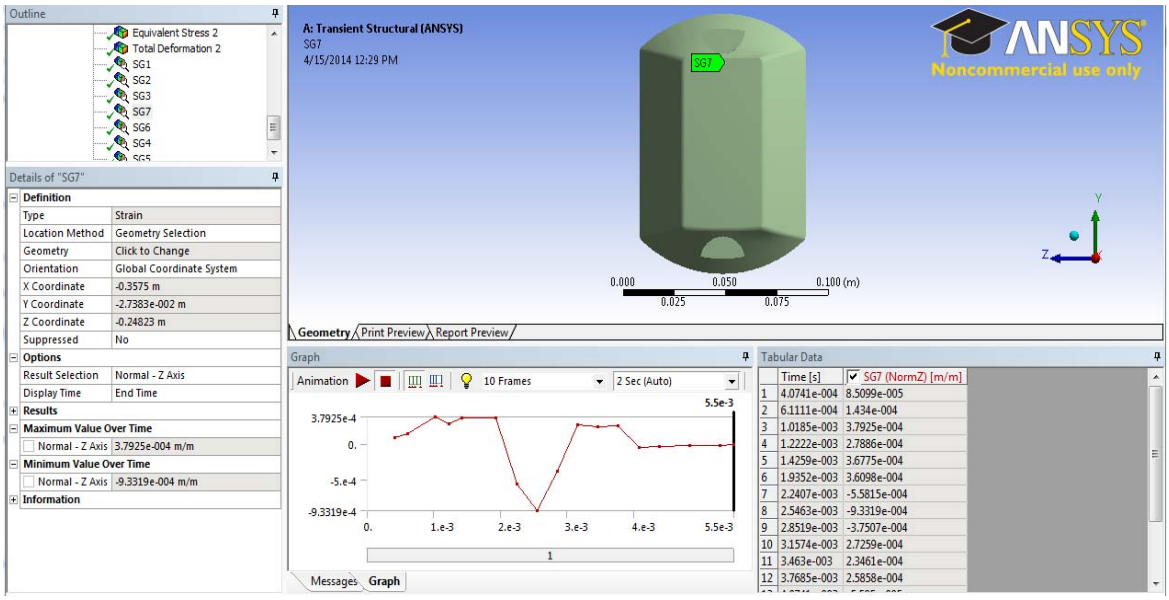

Figure 7-11 Example of Strain Measurement on the Location of Strain Gauge in ANSYS

From Figure 7-12 through Figure 7-15, the following observations can be obtained.

- Most points locate in the first and third quadrants, except for some small strains at gauge 4 on Ennis 980, which means that the strains from field test and FEM simulation are generally of the same sign. In other words, in general FEM predicts correctly the direction of strain (tension or compression).
- The measured strains and the calculated strains are generally of the same order of magnitude for Ennis 980, Rayolite RS, and Apex 921AR markers. The matching between measured and calculated strains is a little worse for 3M 290 markers.
- Strains with relatively large discrepancies between measured and calculated values are mainly on the top shell of 3M 290 and from gauge 2 at RRPM bottom.
- For 3M 290, the strains measured on the top shell are all larger than the FEM simulation results.

The relatively large discrepancies between measured and calculated strains on 3M 290 may be mainly caused by two structural features of this type of marker. First, 3M 290 has a hollow body structure with grid of thin supporting walls. The stress or strain distribution on its top shell is, therefore, very nonuniform. A small change in the strain gauge position may lead to significant change in the measured strain. Second, different from other types of RRPM, 3M 290 has a convex top shell. Such a curved surface might lead gauge to measure a higher strain.

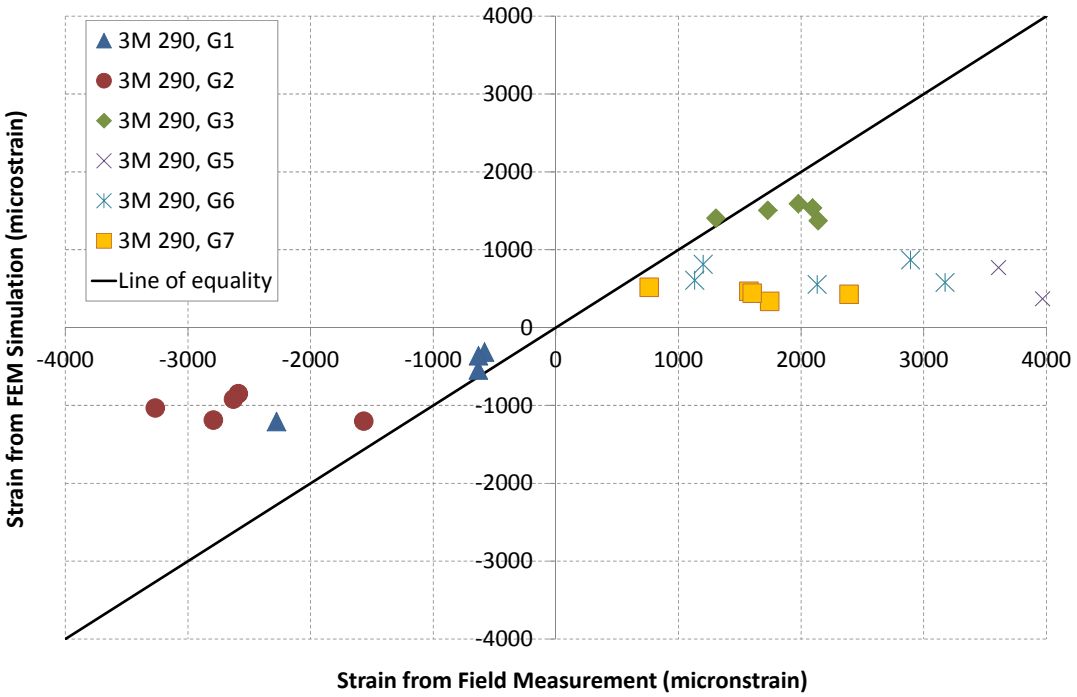

Figure 7-12 Measured Strain versus FEM Simulated Strain for 3M 290

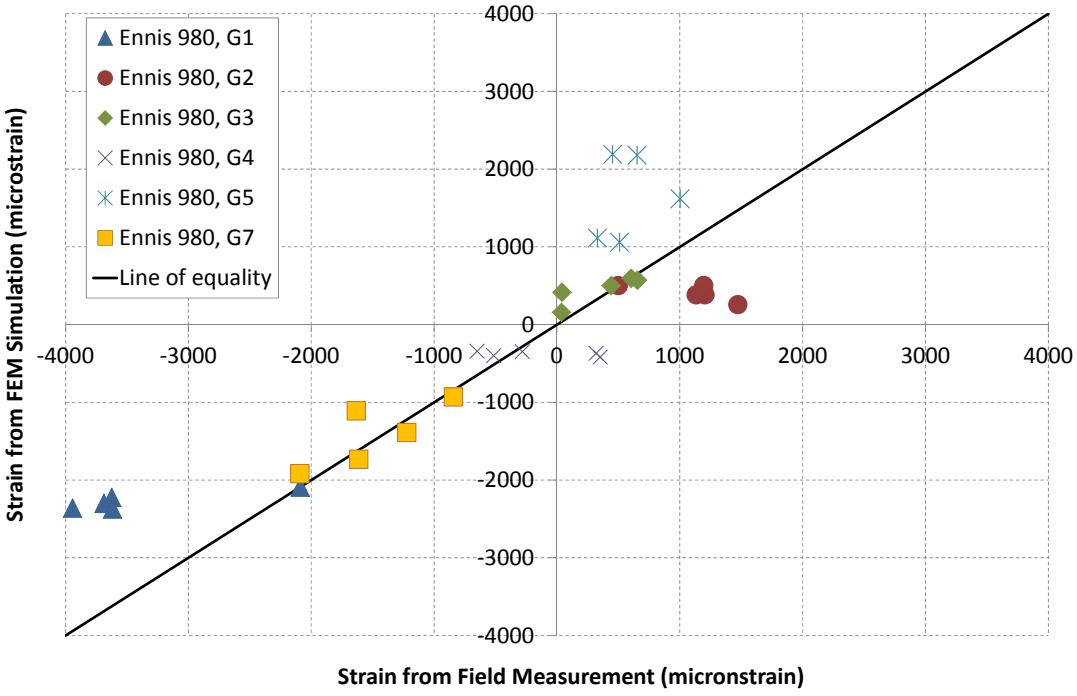

Figure 7-13 Measured Strain versus FEM Simulated Strain for Ennis 980

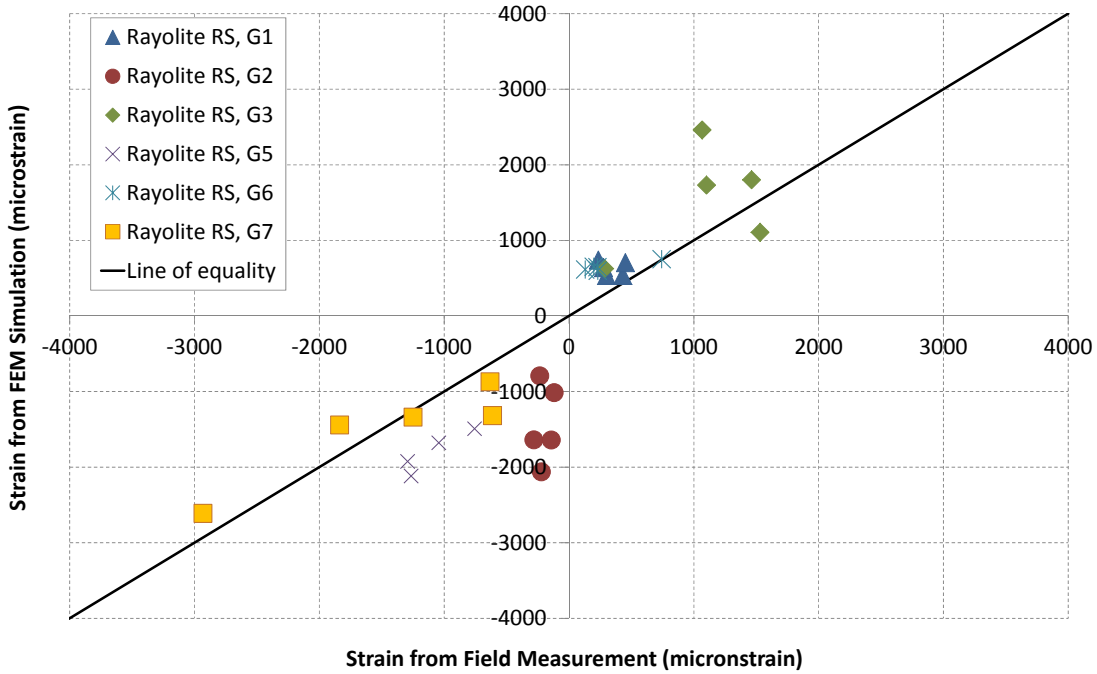

Figure 7-14 Measured Strain versus FEM Simulated Strain for Rayolite RS

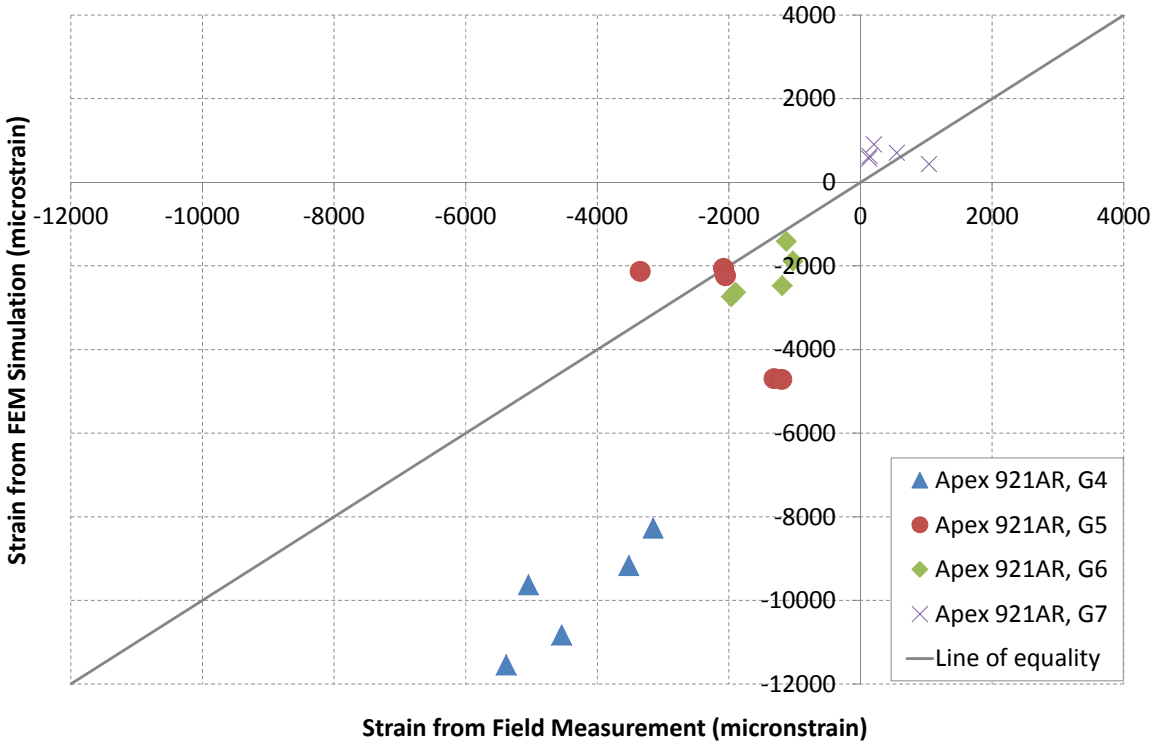

Figure 7-15 Measured Strain versus FEM Simulated Strain for Apex 921AR

There are a number of other factors that may lead to discrepancies between calculated and measured strains. These factors include:

- Difference in the tire tread pattern between test tires and tire model;
- Existence of a bituminous adhesive layer between RRPM and pavement, which is not modeled in the FEM simulation;
- Measurement errors due to variations in contact angle between tire and RRPM, wheel speed, strain gauge accuracy, air temperature, and other factors;
- Differences in the material parameters adopted in the FEM and the actual material properties for pavement, marker, and tire.

Considering the large number of potential sources that may lead to intrinsic differences between measured and calculated strains, the matching results in Figure 7-12 through Figure 7-15 can be treated as acceptable. The stress analysis results based on FEM in the previous chapter, therefore, are deemed valid.

CHAPTER 8 LABORATORY TEST ANALYSIS IN FEM

The tire/marker impact on rigid pavements is selected as benchmark to compare against the laboratory tests. It is desired that these laboratory tests can produce similar kinds of critical stresses in the markers as produced during the tire/marker impact. In other words, the stress distribution pattern (location of critical values) and magnitude shall be approximating. Four stress indices are selected as candidates, including von Mises stress, maximum principal stress, minimum principal stress, and maximum shear strength, to represent the scenarios of possible plastic, tensile, compressive, and shear damage occurring within the structure of RRPMs. The baseline tire/marker case is modeled as the tire rolls over the RRPM perpendicularly at a speed of 31.3 m/s, a tire inflation pressure of 0.7 MPa and a tire load of 22 kN. This chapter mainly includes three parts. First part mainly tests and verifies the current RRPM laboratory tests, including compressive test and flexural test. Second part mainly tests and verifies the proposed RRPM laboratory tests in a previous study, including pendulum impact test (bulleting test), offset test, and reversed longitudinal flexural test. Last part suggests new laboratory tests, such as revised reversed latitude flexure test and offset latitude flexural test. Moreover, the effects of elastomeric pad and on the pendulum impact tests are analyzed in more details.

8.1 Current RRPM Laboratory Tests

The most widely used RRPM laboratory tests for RRPM physical properties are longitudinal flexural test and compressive test, introduced in American Society of Testing and Materials (ASTM) standards D 4280. This section mainly introduces the methods of these two tests and the stress distributions from FEM simulations.

8.1.1 ASTM Compressive Test

The FEM is built to simulate the compressive test described in the ASTM standard D 4280. Per the ASTM standard, the rate of loading is kept at 2.54 mm (0.1 inch) per minute. To simplify the simulation, the elastomeric pad between the marker and steel plate was not included in the FEM. Figure 8-1 depicts the FEM of the test. Figure 8-2 compares the stress distribution of the ASTM compression test and the tire/marker impact, and the stress information is compiled in Table 7-1.

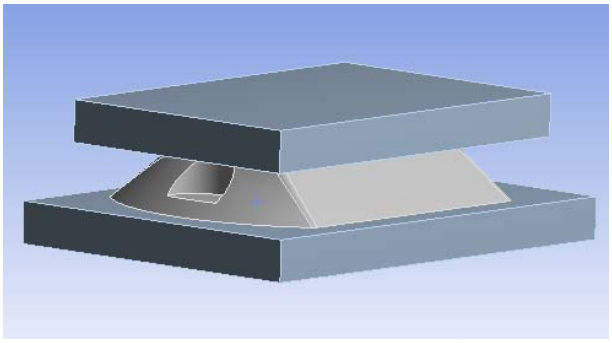

Figure 8-1 FEM of the ASTM Compression Test

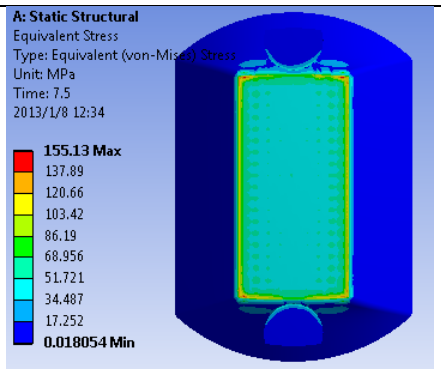

Von Mises stress (compression test)

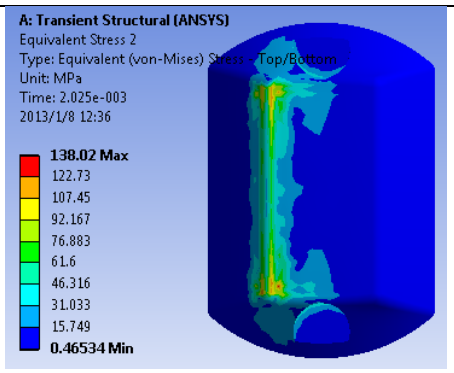

Von Mises stress (tire/marker scenario)

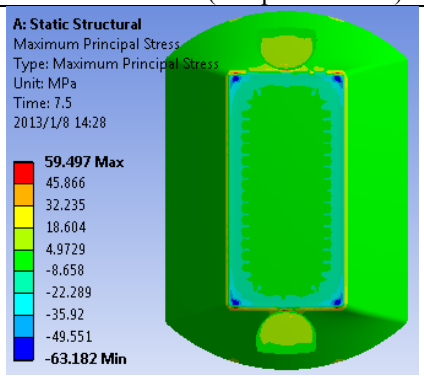

Maximum principal stress (compression test)

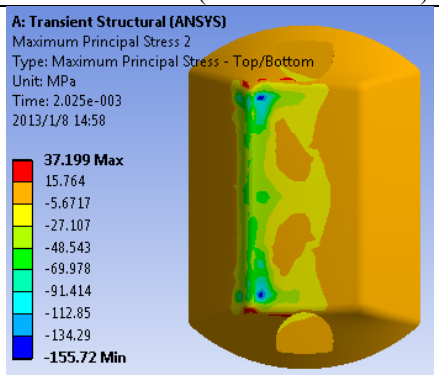

Maximum principal stress (tire/marker scenario)

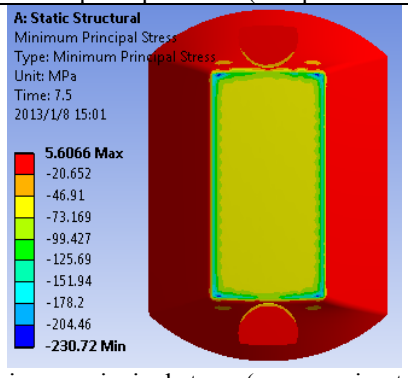

Minimum principal stress (compression test)

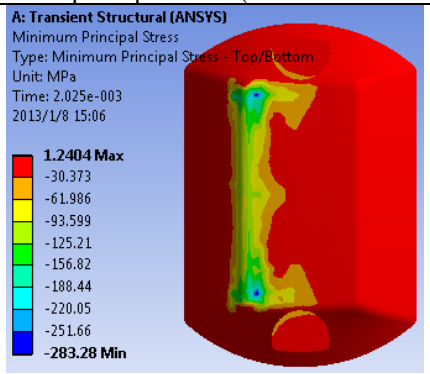

Minimum principal stress (tire/marker scenario)

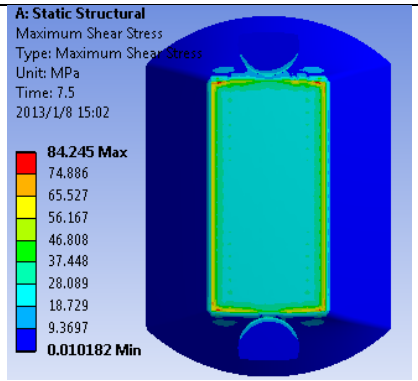

Maximum shear stress (compression test)

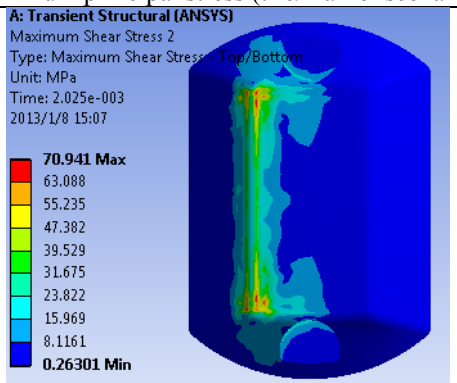

Maximum shear stress (tire/marker scenario)

Figure 8-2 Stress Comparisons of the Two Scenarios

Table 8-1 Result Comparisons of ASTM Compression Test and Tire/Maker Impact

Index	Von Mises Stress (MPa)		Maximum Principal Stress (MPa)		Minimum Principal Stress (MPa)		Maximum Shear Stress (MPa)	
	Critical Value	Location	Critical Value	Location	Critical Value	Location	Critical Value	Location
Compression Test	155	four tips and four rim	84	four tips and four rim	-231*	four tips and four rim	71	four tips and four rim
Tire/Marker Impact	138	Two tips and one rim	71	Two tips and one rim	-283	Surrounding two tips	37	Two tips

*Negative value means compression.

As can be observed from Figure 8-2, the critical stress, despite the type, locates around the two tips and the rim that a tire rolls over. For the ASTM compression test, all four tips and rims bears stress concentration. The marker under tire impact can be deemed as half structure of that under the compression test in terms of critical stress location. However, in a general pattern, the stress grows from the center to the tire contacting rims and tips for the tire/marker scenario while it is uniformly distributed for the ASTM compression test. For the magnitude, the differences between for the two scenarios are 12%, 18%, -18%, and 92% for the four critical stresses in sequence. Considering both the stress distribution and magnitude, it is acceptable to conclude that the ASTM compression test can simulate the tensile and compressive damage on critical parts of RRPMs on pavements.

8.1.2 ASTM Flexural Test

The FEM of the ASTM flexural test on RRPMs was built with a loading rate of 5.08 mm per minute according to the standard of ASTM D 4280. For simplification, no elastomeric pads were inserted between the marker and the steel bars. Figure 8-3 gives the FEM of the ASTM flexural test.

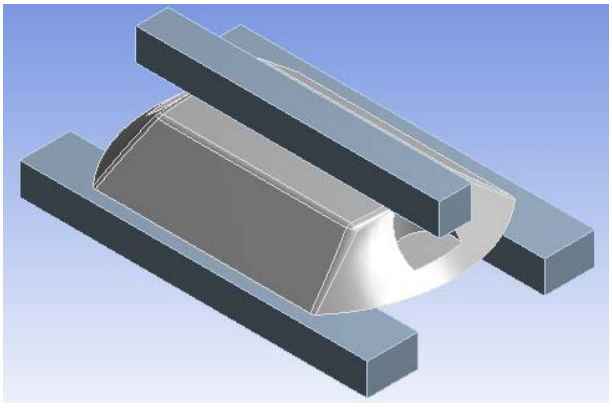

Figure 8-3 FEM of the ASTM Flexural Test

Again the stress information of the ASTM flexural test is compiled in Table 8-2. Figure 8-4 contains the snapshot of stress distribution patterns of the marker in the ASTM flexural test.

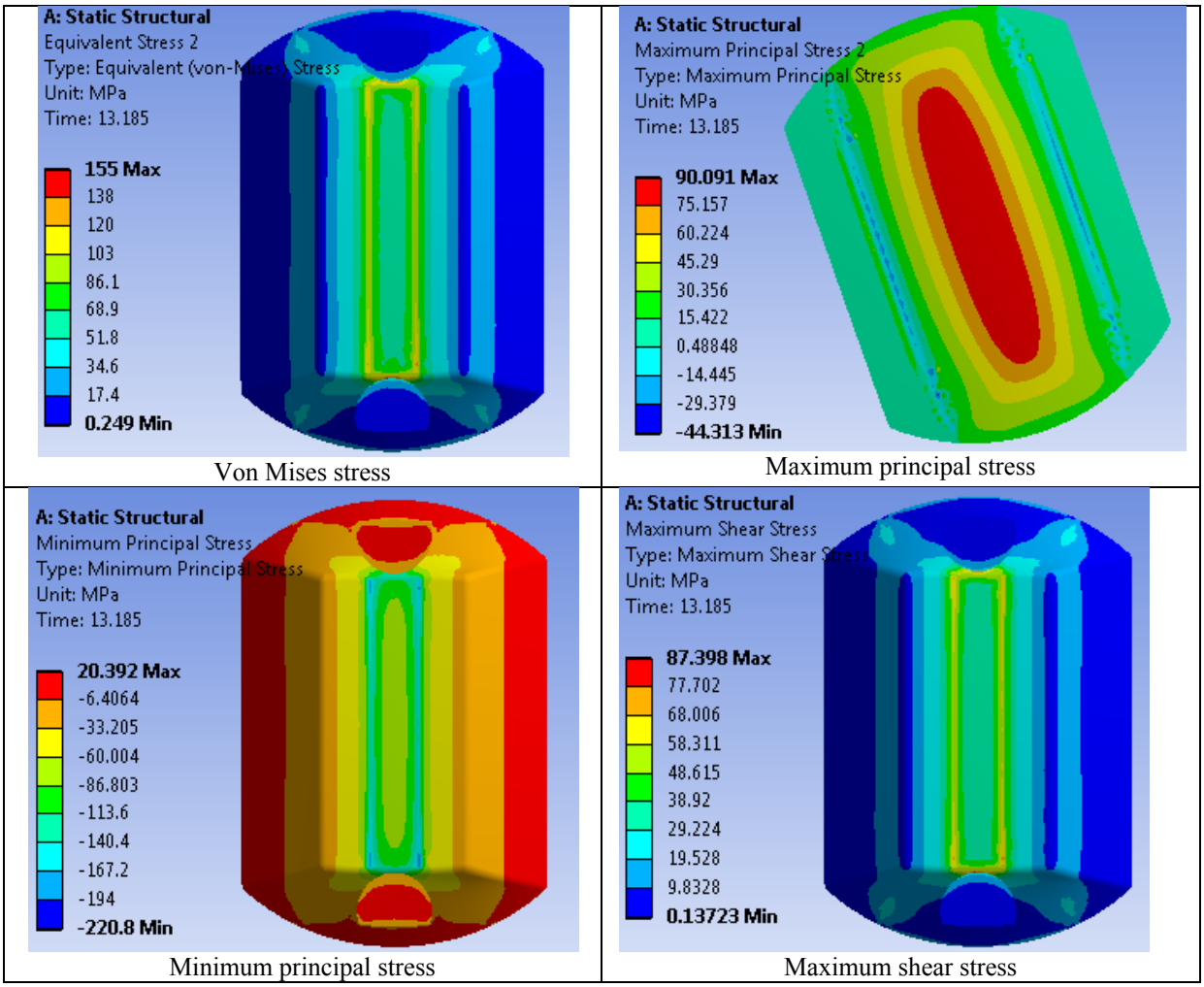

Figure 8-4 Stress Distributions in RRPM in the ASTM Flexural Test

As can be seen in Figure 8-4, the critical values of von Mises stress, minimum principal stress and maximum shear stress locate around the boundary of marker-steel plate contact area while the maximum principal stress focuses around the bottom center of the marker. However, none of these locations has resemblance of those in the tire/marker scenario.

Table 8-2 Results of ASTM Flexural Test

Index	Von Mises stress (MPa)		Maximum Principal Stress (MPa)		Minimum Principal Stress (MPa)		Maximum Shear Stress (MPa)	
	Critical Value	Location	Critical Value	Location	Critical Value	Location	Critical Value	Location
Compression Test	155	Contact boundary	90	Bottom center	-221	Contact boundary	87	Contact boundary

For the magnitude, Table 8-2 shows that the differences between the laboratory test and field conditions are 12%, 27%, -22%, and 135% for the four stress indices in sequence. The first three stress indices are within an acceptable difference range while the maximum shear stress difference is relatively higher.

8.1.3 Elastomeric Pad Effects on Compression Test and Flexural Test

In previous models, the elastomeric pads were not considered. However, elastomeric pads are required in ASTM D 4280. Thus, whether the elastomeric pad affects the stress distribution is necessary to be rechecked.

The specific measurements of plates and elastomeric pads are illustrated in Figure 8-5 and Figure 8-8. Based on these measurements, the FEMs with elastomeric pad are built in ANSYS, as shown in Figure 8-6 and Figure 8-9.

For the compressive test, Figure 8-7 shows the different von Mises stress distributions under these two different scenarios (with and without elastomeric pads). The elastomeric pads make the von Mises stress distribution relatively even, and dramatically mitigate the impact from steel plate under the same loading rate and loading time. As shown in Figure 8-7, comparing the von Mises stress distributions from these two compressive tests and the tire-marker impact field condition, installing elastomeric pad seems unnecessary for compressive tests. The compressive stress, under the pads' effects, will not concentrate on the corner of RRPM top shell, which is opposite to the real scenario.

For the flexural test, Figure 8-10 shows the von Mises stress distributions from this longitudinal flexural test simulation, with and without elastomeric pads. If the longitudinal flexural test is run without elastomeric pads, the critical von Mises stress will concentrates on the edge of contact between the top steel bar and RRPM, which does not match the real tire-marker condition. Thus, on the contrary of compressive test, elastomeric pads are necessary for installing on longitudinal flexural test, and its critical von Mises stress will appear on the middle of non-lens side edges.

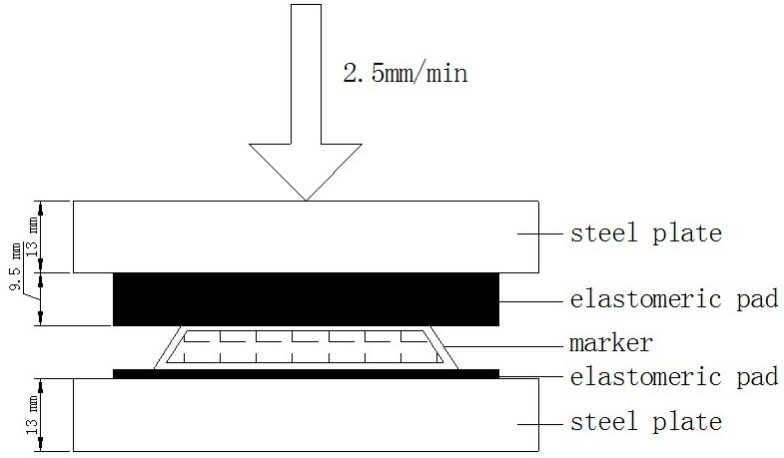

Figure 8-5 ASTM Compressive Test

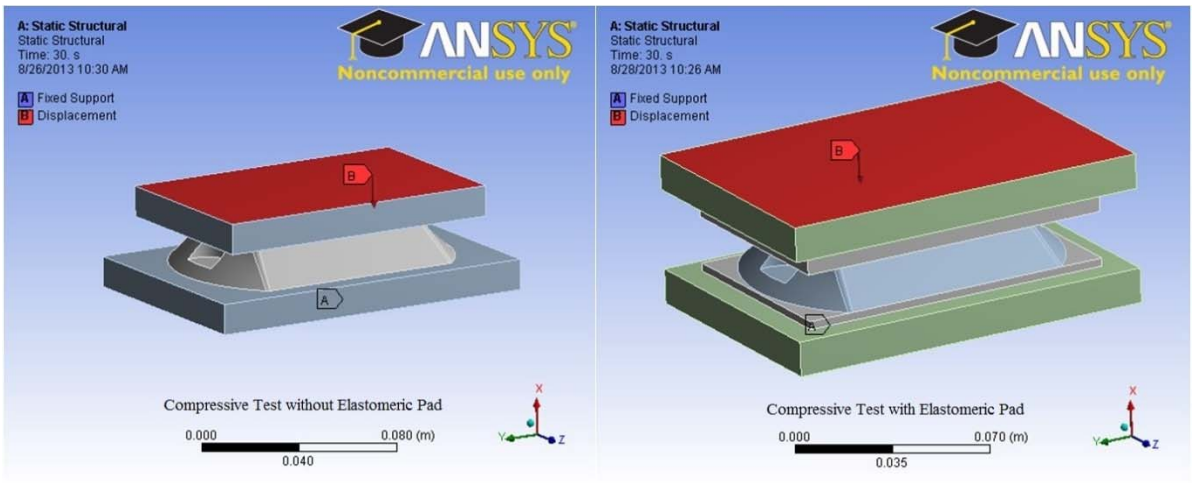

Figure 8-6 Simulated ASTM Compressive Test without and with Elastomeric Pad

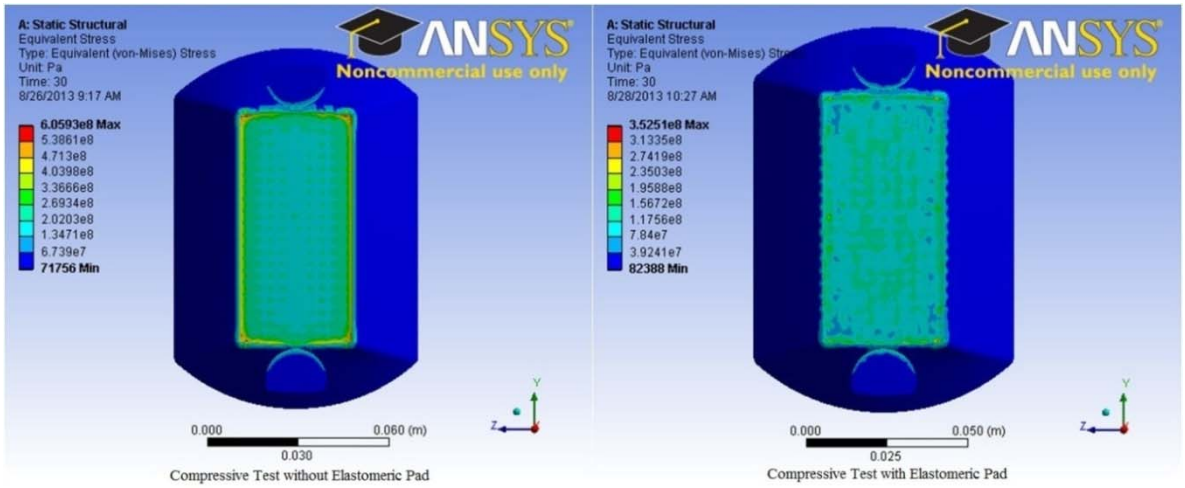

Figure 8-7 Von Mises Stress Distribution in Compressive Test

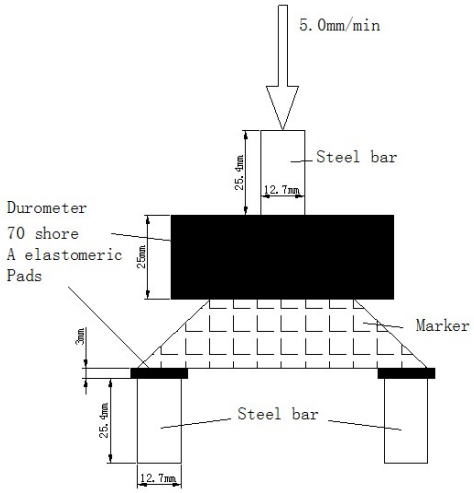

Figure 8-8 ASTM Longitudinal Flexural Test

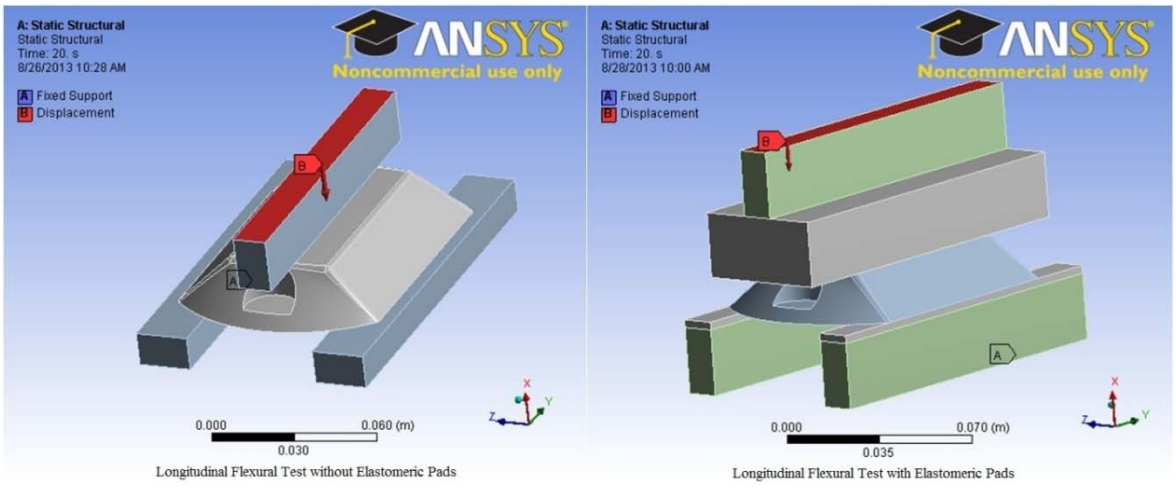

Figure 8-9 Simulated ASTM Longitudinal Flexural Test

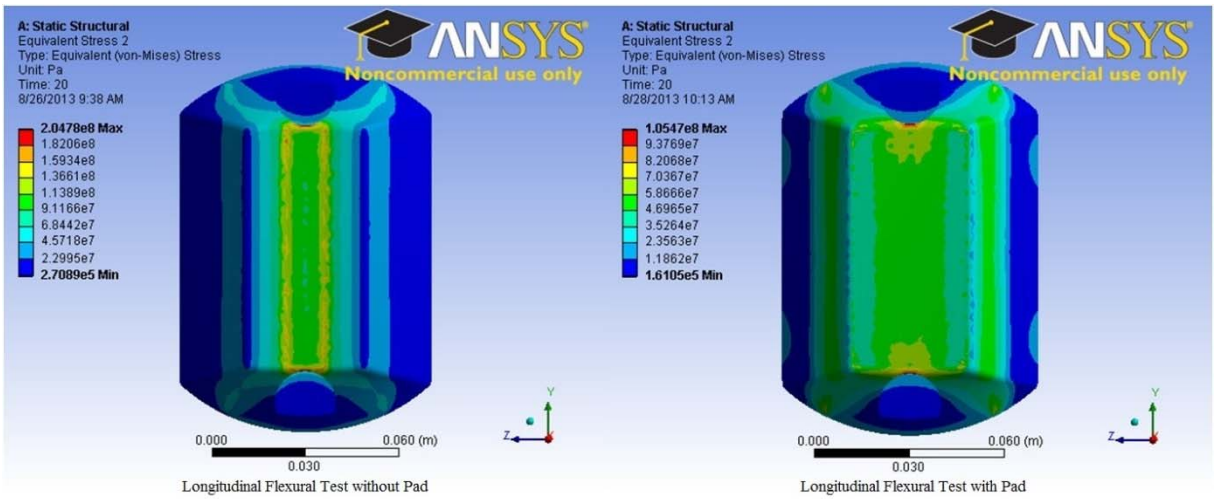

Figure 8-10 Von Mises Stress Distribution by ASTM Longitudinal Flexural Test

8.2 Further RRPM Laboratory Tests

Based on the literature review, some new laboratory tests were previously designed and attempted to simulate the tire-marker impact field condition, such as a cylinder compression test, a bulleting test, an offset test, a reversed longitudinal flexural test, and a pendulum test (Zhang et al., 2009). For clearly explaining the design purposes of these tests, the characteristics of these laboratory tests are summarized in Table 8-3.

8.2.1 Offset Compressive Test

The ASTM compressive test is modified and called “offset compressive test”. The only difference between the ASTM compressive test and the invented test is that a steel bar (12.7 mm or 0.5 inches wide and slightly longer than the marker) is used to replace the steel plate. The steel bar was placed along one of the retroreflective edges of the marker. The rate of loading was kept at 2.54 mm (0.1 inches) per minute as in the ASTM test. Figure 8-11 shows the FEM of the test.

Table 8-3 Further RRPM Laboratory Tests and Their Characteristics

Test	Test Components	Results
Cylindrical Compressive Test	Two cylinders are installed at the top and bottom of the marker, instead of steel plates in the ASTM compressive test.	Large compressive stresses are produced by the top cylinder, and simultaneously, large tensile stresses appear around the bottom cylinder.
Offset Compressive Test	One steel bar is installed along one lens side of RRPM, without steel plate	Major compressive stresses occur under the loading bar, with small tensile stresses in other RRPM parts.
Reversed ASTM Longitudinal Flexural Test	Two steel bars at the RRPM top, and one at the RRPM bottom	Large compressive stresses at the top and major tensile stresses at the center of RRPM top.
Pendulum Test	Similar to the lens impact test in ASTM D 4280, except the impact location can be changed to various location points at the RRPM top.	No previous study built FEM of this test

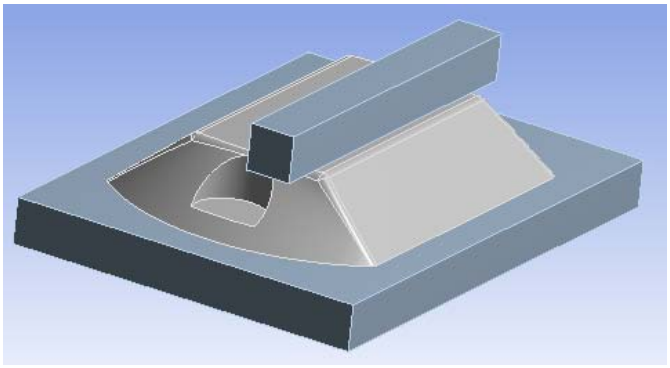

Figure 8-11 FEM of the Offset Compressive Test

Following the convention, the stress values were extracted from the simulation results and the stress distribution pattern are shown in Figure 8-12. Similar to the ASTM compressive test, the stress concentrates around contacting boundary of the steel bar and the marker.

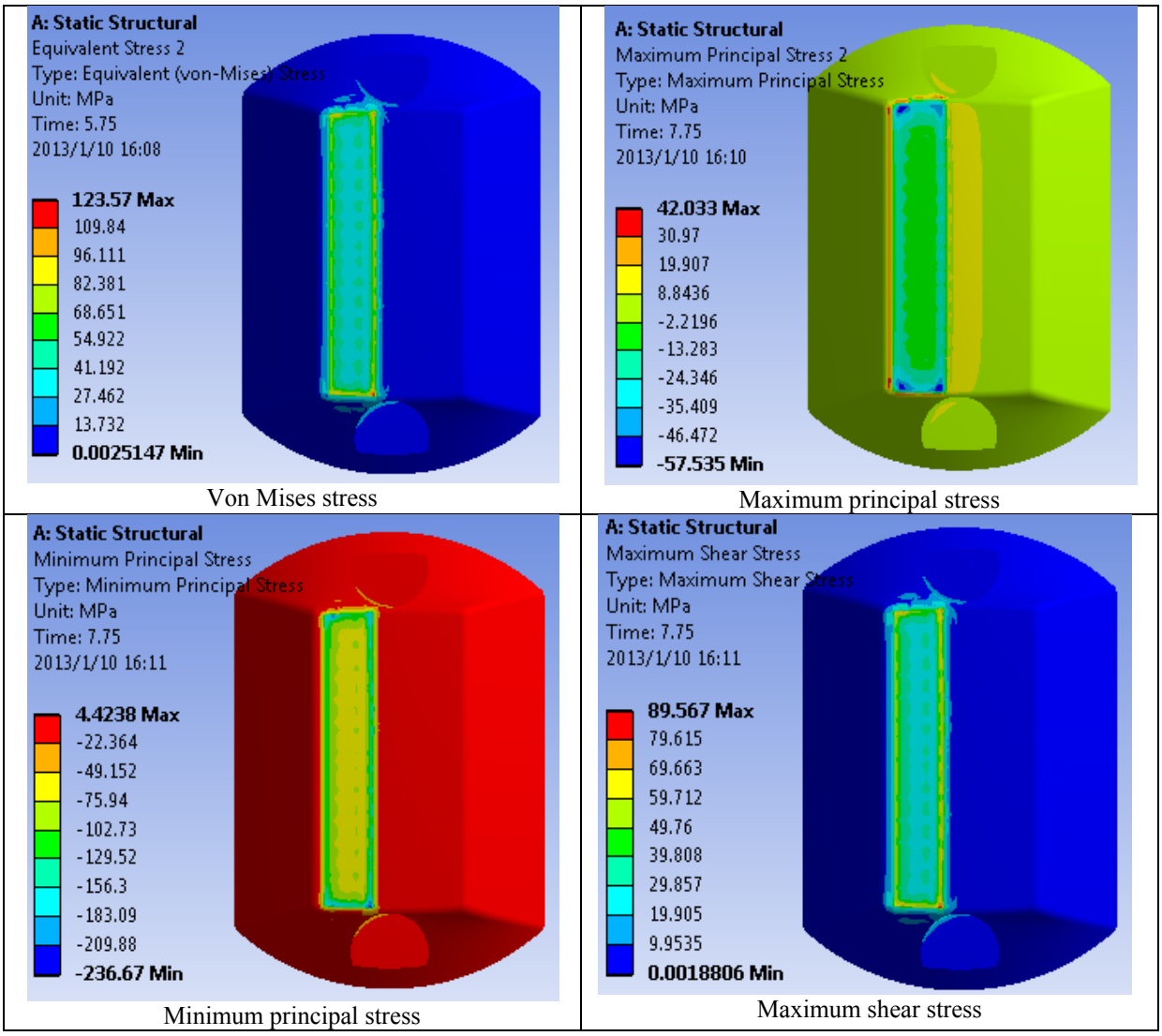

Figure 8-12 Stress Distribution of the Marker under Offset Compressive Test

Table 8-4 Result of the Offset Compressive Test under Offset Compressive Test

Index	Von Mises Stress (MPa)		Maximum Principal Stress (MPa)		Minimum Principal Stress (MPa)		Maximum Shear Stress (MPa)	
	Critical Value	Location	Critical Value	Location	Critical Value	Location	Critical Value	Location
Compressive Test	124	Contact boundary	42	Contact boundary	-237	Contact boundary	90	Contact boundary

For the magnitude, the differences between the laboratory test and the field conditions are -10%, -46%, 19%, and 143% for the four stress indices in sequence. The difference ranges for the offset compressive test are wider than those of the ASTM compressive test. In other words, the original ASTM compressive test is more suitable.

8.2.2 Reversed ASTM Flexural Test

The reversed ASTM flexural test was designed to turn the ASTM flexural test apparatus upside down, as shown in Figure 8-13. The two top steel bars were loaded at a rate of 5.08 mm (0.2 inches) towards to marker structure per minute as done in the ASTM flexural test. Figure 8-14 is the snapshot of the stress distribution of the simulation results and Table 8-5 lists the critical values.

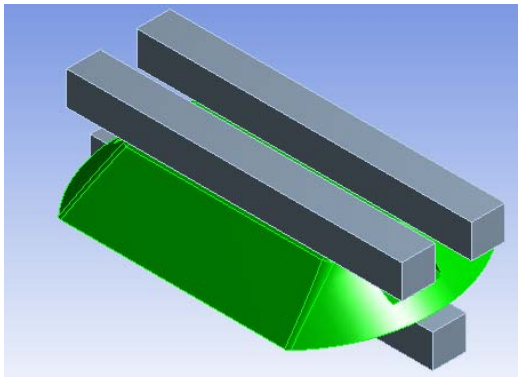

Figure 8-13 FEM of the Reversed ASTM Flexural Test

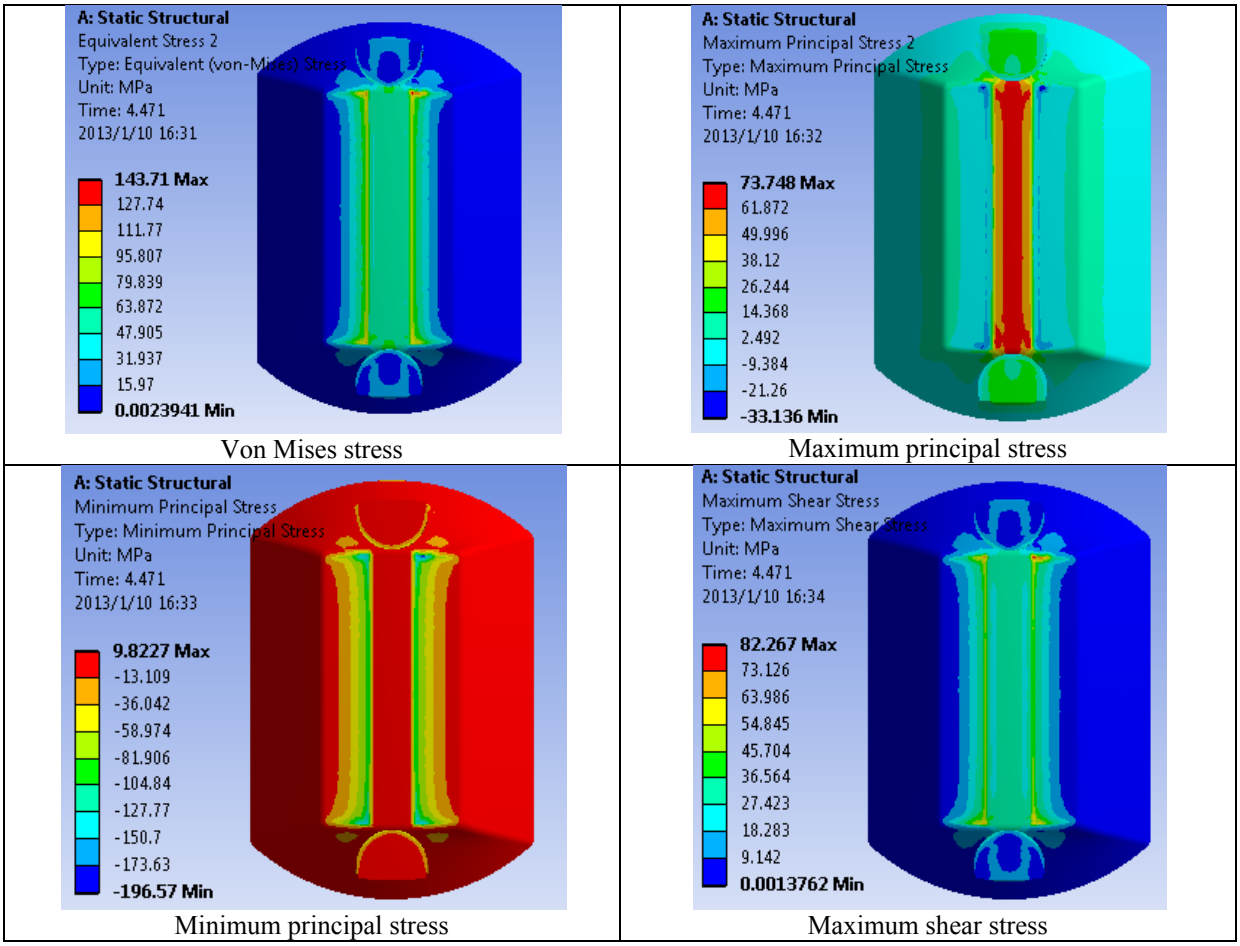

Figure 8-14 Stress Distribution of the Marker in Reversed ASTM Flexural Test

Table 8-5 Result of Reversed ASTM Flexural Test

Index	Von Mises Stress (MPa)		Maximum Principal Stress (MPa)		Minimum Principal Stress (MPa)		Maximum Shear Stress (MPa)	
	Critical Value	Location	Critical Value	Location	Critical Value	Location	Critical Value	Location
Compressive Test	144	Contact boundary	73	Contact area	-196	Contact boundary	82	Contact boundary

For the magnitude, the differences between the laboratory test and field conditions are -4%, -3%, 31%, and 123% for the four stress indices in sequence. The stress concentration area is moved to center for the developed test compared to the tire/marker impact. For the magnitude, the reversed ASTM flexural test produces stresses very approximating to field scenario in terms of von Mises stress and maximum principal stress, similar in terms of minimum principal stress but much larger in terms of maximum shear principal stress. In general, the reversed ATSM flexural test may be used to substitute the original ASTM flexural test.

8.2.3 Pendulum Impact Test

Pendulum test was designed by Texas Transportation Institute (TTI), for emulating dynamic impact from small objects on the RRPM surface in real condition. The principle of this test is also similar to that of the lens impact test in ASTM D 4280. Considering the potential function of the pendulum impact test, this section includes three main parts. First part was to emulate typical pendulum impact test for comparison with real field condition, as other laboratory tests did. Second part was to pick critical impact locations with different stress indicators, through separately analyzing six impact locations with different five impact levels. Third part was to test the effects of weight and velocity on these critical impact locations.

There are two main advantages of the pendulum test: 1) impact location on markers can be adjusted through one adjustable marker support; 2) magnitude of impact on markers can be controlled through adding different weights at the end of the pendulum arm.

8.2.3.1 Typical Pendulum Impact Test Analysis

The failure of RRPMs are frequently found to initiate with the facture of the outer shell, which may be caused by the impact of a hard small object on the surface of the RRPM, such as a stone wedged in the tire tread of the tire. The small-area hard to hard interacting cannot be represented by the currently available test procedure. This pendulum impact test was inspired and modified from the British pendulum friction test.

The developed device is called a RRPM pendulum impact test and is shown in Figure 8-15. The hitting force is delivered to the RRPM by a 1-inch rounded steel rod fixed at the end of a swinging arm. The marker is adjusted to the desired position by a small metal sleeve and a simple metal clip that holds it against an elastomeric pad (0.125-inch, 70 Shore A). The developed devices allowed both horizontal and vertical positioning of the marker relative to the steel rod and its impact point. The adjustable support for the RRPM can be found in Figure 8-16 (Zhang et al., 2009).

Figure 8-15 Overall View of the Pendulum Impact Device

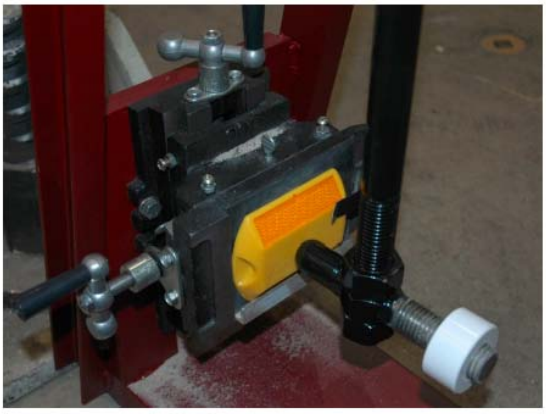

Figure 8-16 View of the Marker Adjustable Support

The device and the impact test were modeled in the FEM. The hitting force can be adjusted by both the weight of the steel ring that is attached to the rod or the speed of the rod hitting the marker which is determined by the height where the rod is released. The swing arm itself weights 8.54 lb.

For simplifying this test in ANSYS, the height of the steel rod is set very close to RRPM, with an initial velocity, which is equivalent to that from free falling from one fixed height. In this section, the initial velocity is set to 4 m/s. The “point mass” function in ANSYS is used to get variation of weights at the end of steel rod, instead of real weight component. The FEM of pendulum test is designed as shown in Figure 8-17. If the impact location is at the RRPM top corner, the stress distributions are shown in Figure 8-18 and the critical values are given in Table 8-6.

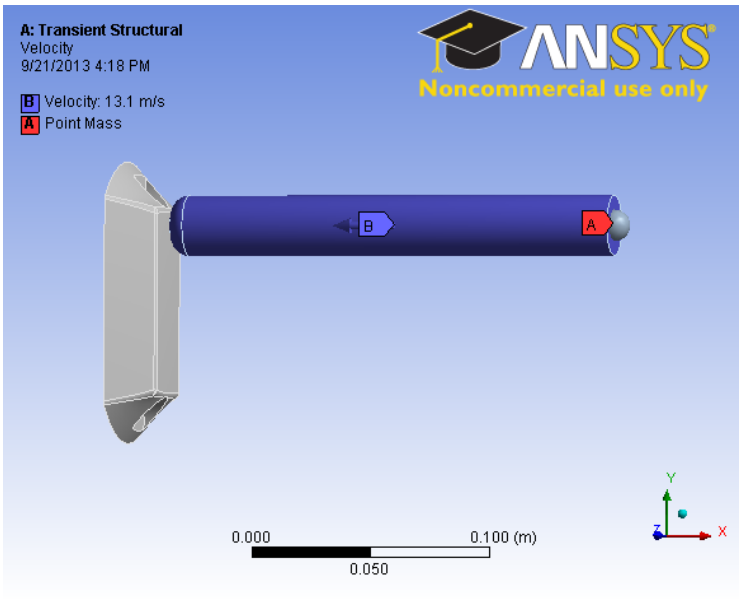

Figure 8-17 Pendulum Test Model in ANSYS

Table 8-6 Result of the Pendulum Impact Test

Index	Von Mises Stress (MPa)		Maximum Principal Stress (MPa)		Minimum Principal Stress (MPa)		Maximum Shear Stress (MPa)	
	Critical Value	Location	Critical Value	Location	Critical Value	Location	Critical Value	Location
Compressive Test	141	Contact boundary	47	Contact boundary	-211	Contact boundary	76	Contact boundary

The FEM deliberately locates the steel rod around the corner of the marker, which produced similar stress concentration area as the tire/marker impact. For the magnitude, the differences between the laboratory test and the field condition are -2%, -37%, 26%, and 105% for the four stress indices in sequence. Both the difference ranges and the critical stress impact locations of the pendulum impact test resemble the field conditions, and therefore this test is recommended as a candidate laboratory test.

8.2.3.2 Pendulum Test with Different Test Parameters

In this section, the same five impact levels for pendulum tests used by TTI were selected, as shown in Table 8-7. Six impact locations were chosen to search for the most potential "fragile" one. Thus, there are a total of $5 \times 6 = 30$ tests. These test IDs are listed as ij, where i represents location ID and j represents weight ID.

The purpose of this section is to locate the most potential "fragile" part on the RRPM. Under the same impact condition, different impact locations contribute to various magnitudes of stresses. Higher stress magnitude indicates more damage risk.

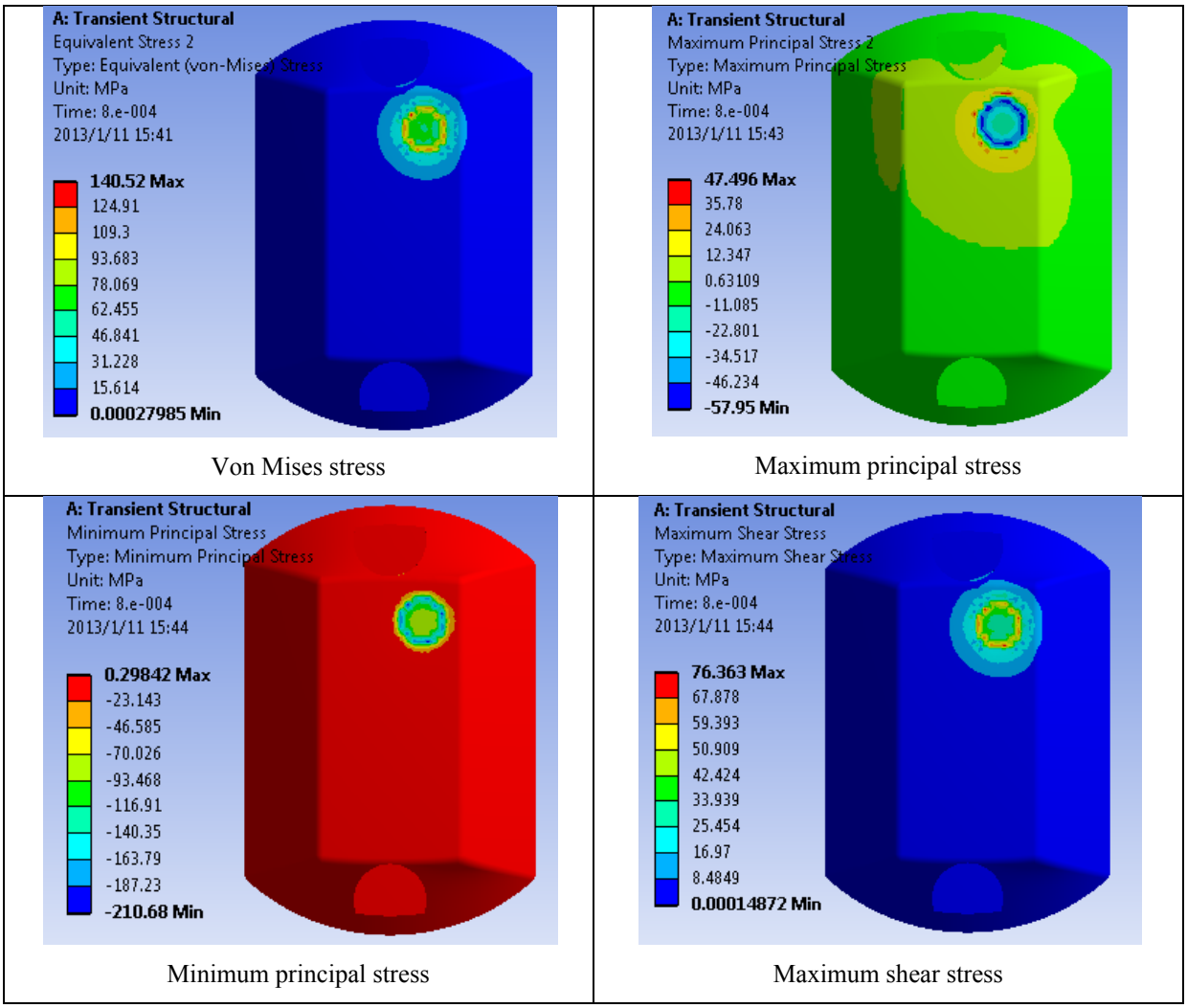

Figure 8-18 Stress Distributions of the Marker under Pendulum Impact Test

Table 8-7 Pendulum Impact Device Weight

Weight ID	Weight (kg)
1	0.16
2	0.31
3	0.62
4	0.78
5	0.93

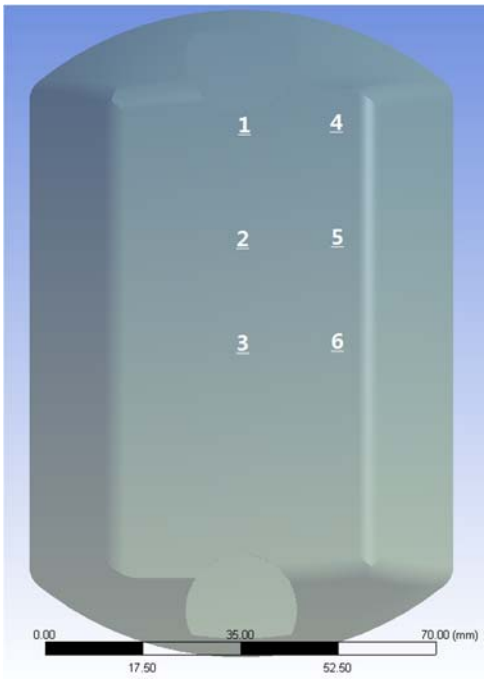

Figure 8-19 RRPM Impact Location ID for Pendulum Test

The stresses, produced by impacts on different RRPM locations with different magnitudes, are obtained with ANSYS and listed in Table 8-8. For clearly observing the stress magnitudes in different scenarios, one line is plotted for each impact location, as shown in Figure 8-20 through Figure 8-22.

Table 8-8 Results from FEMs of Pendulum Tests

Test ID	Von Mises Stress (MPa)	Maximum Principal Stress (MPa)	Minimum Principal Stress (MPa)
11	102.61	38.69	-153.45
12	114.24	42.28	-166.95
13	134.00	48.52	-195.06
14	142.66	51.25	-207.22
15	153.69	54.09	-222.99
21	99.38	26.52	-148.16
22	109.12	29.82	-160.89
23	125.85	35.50	-182.65
24	133.11	38.40	-192.08
25	139.17	42.69	-200.04
31	99.93	24.62	-143.86
32	107.90	27.37	-154.05
33	121.85	32.28	-176.25
34	127.48	34.43	-187.43
35	133.22	36.31	-196.97
41	120.75	25.34	-172.21

Table 8-8 Results from FEMs of Pendulum Tests (Continued)

Test ID	Von Mises Stress (MPa)	Maximum Principal Stress (MPa)	Minimum Principal Stress (MPa)
42	132.76	28.30	-187.30
43	153.65	33.57	-213.44
44	162.77	35.93	-224.83
45	176.14	39.83	-240.29
51	111.96	24.35	-165.56
52	121.70	26.91	-179.80
53	138.75	31.55	-205.74
54	146.32	33.53	-218.53
55	153.17	35.42	-230.30
61	118.71	26.09	-173.36
62	129.25	27.98	-188.71
63	147.55	31.75	-215.47
64	155.57	33.98	-227.21
65	162.83	35.96	-238.04

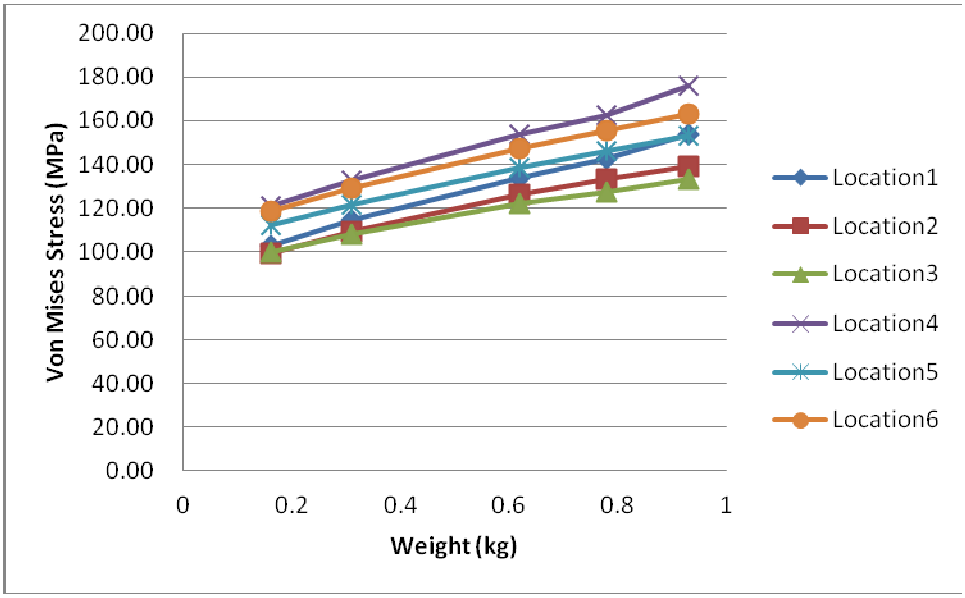

Figure 8-20 Von Mises Stresses vs. Weights and Locations

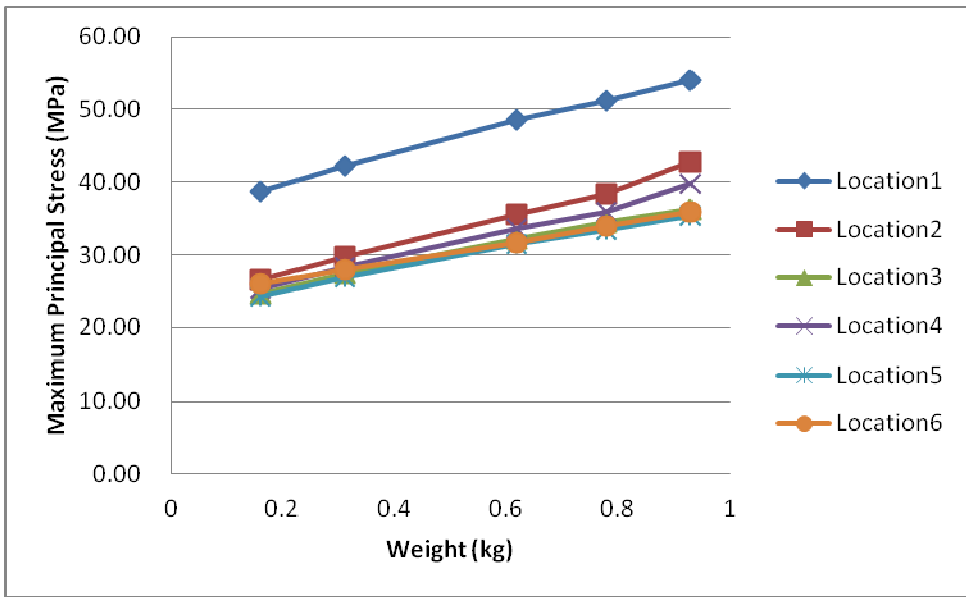

Figure 8-21 Maximum Principal Stresses vs. Weights and Locations

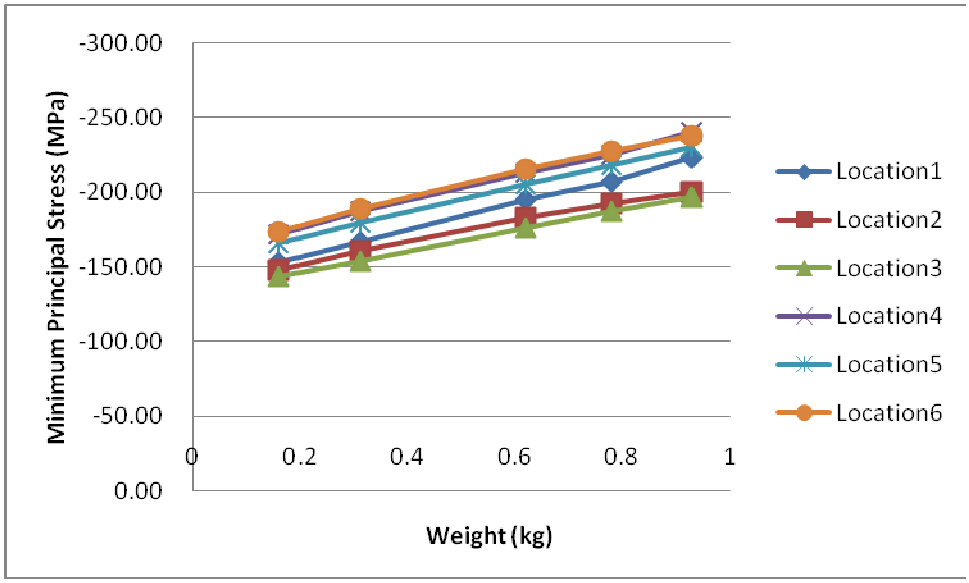

Figure 8-22 Minimum Principal Stresses vs. Weights and Locations

Based on Figure 8-20 through Figure 8-22, the following findings are obtained:

- The order of location ID's by von Mises stress magnitudes is: $2 < 3 < 1 < 5 < 6 < 4$. It means, under the same impact condition, impact on the corner of top shell (location 4) will produce the most critical von Mises stresses and the highest damage risk. The impact location 4 also is the critical stress location under the field loading condition.
- Moreover, compared to other points, except corner or side, the center point has relatively higher risk for failure. These results can explain the observation from field survey: most cracks started from RRPM corners and/or middle of edges.

- Generally, the impact on the lens edge can generate higher von Mises stresses. Furthermore, when the weight is very low (0.16 kg), the von Mises stresses at locations on the same longitude are very close, such as locations 1, 2, and 3. However, when the weight increases, the von Mises stresses are proportionally increased if the locations are on the same latitude, such as locations 1 and 4, locations 2 and 5, and locations 3 and 6. In other words, statistically, the latitude of impact location and weight have no interaction on stress magnitude.
- In this case, Figure 8-20 shows that the von Mises stress from impact location 1 increases to be very close to that at location 5. Figure 8-22 also shows that, based on the trends, impact on location 4 also keep producing the highest von Mises stresses, no matter how much the weight increases.
- Based on the maximum principle stress distribution, the critical stress occurs on the edge of contact area between steel rod and markers, which is very close to impact location. When the weight is 0.16 kg, the order of location ID by maximum principle stress magnitudes is: $5 < 3 < 4 < 6 < 2 < 1$. However, when the weight increases to 0.93 kg, this order is altered to be: $5 < 6 < 3 < 4 < 2 < 1$. Based on this variation, location 6 reveals its lowest sensitivity on weight impact. Moreover, these orders show that impact on the middle of non-lens edge, where the finger grips exist, always can generate much higher tensile stresses than that on all other locations. In other words, this result indicates that the cracks from finger grips are more probably caused by tensile stress. Because the tensile stress generated by impact on point 2 is also high, the crack will have high risk to extend from point 1 to point 2. Moreover, based on the stress magnitudes generated by impact on point 4 and point 5, it is safe to say that the edge and corner are not key factors to produce high tensile stresses, although their von Mises stresses are relatively high.
- The order of location IDs by minimum principle stress magnitudes is: $2 < 3 < 1 < 5 < 6 \approx 4$, which have similar order with von Mises stress. This order illustrates that, without considering the disturbance from the tensile stresses, the compressive stresses generated by impact on locations 6 and 4 are very close. In the field loading condition, because of the tire deformation and its contact points on RRPM, there is almost no chance that locations 6 and 4 have the same impact situation, unless some stones wedged in the middle of vehicle's tire tread. Thus, location 4 still has the highest risk of compressive failure compared to other locations.

8.2.3.3 Critical Impact Location Analysis

Based on the findings in section 7.2.3.2, location 4 is the critical impact location for compressive failure, and location 1 is the critical one for tensile failure. Both locations are in accordance with the field loading condition. Because pendulum impact test is to simulate the instant heavy impact from field condition, in this section, the pendulum tests are analyzed to compare with the field conditions especially under heavy truck scenarios.

Figure 8-23 shows the maximum principal stress distributions generated by impact on location 1 in the pendulum test (left plot) and in the field scenario under heavy truck impact (right plot). Figure 8-24 shows the minimum principal stress distributions generated by impact on location 4 in the pendulum test (left plot) and in the field scenario under heavy truck impact (right plot). Figure 8-23 and Figure 8-24 illustrate that the stress distributions produced by the pendulum test are concentrated on the edge of contact area between steel rod and marker. Thus, differing from

other tests, pendulum test is a better way to impact the markers' critical stress locations, but not to simulate the overall stress distribution. In other words, pendulum test can more easily change and control the critical stress location than other tests.

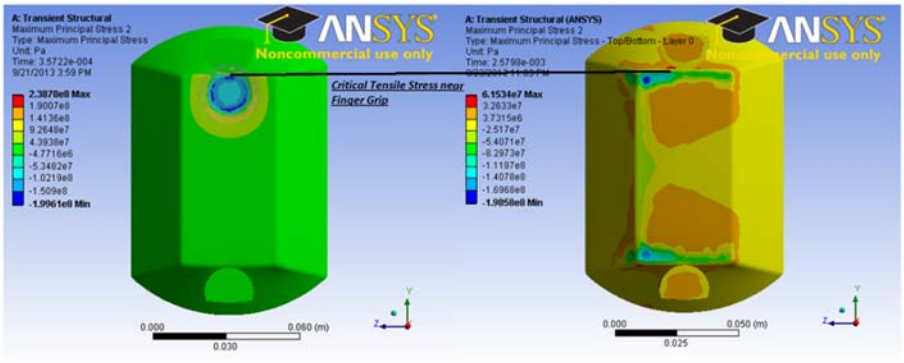

Figure 8-23 Maximum Principal Stress Distributions at Location 1

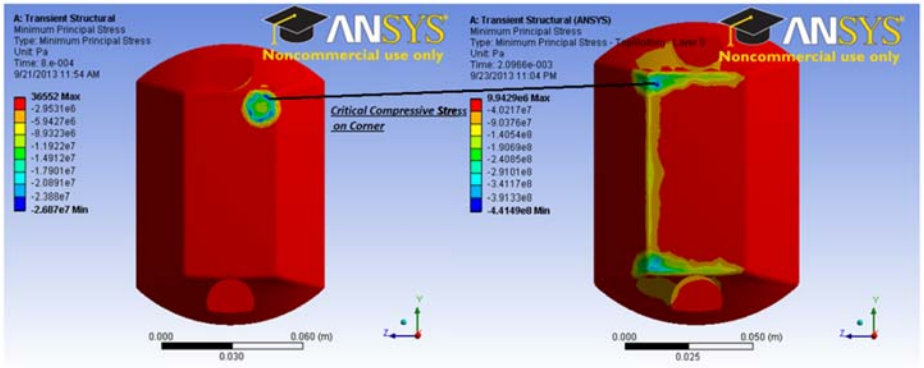

Figure 8-24 Minimum Principal Stress Distributions at Location 4

8.2.3.3.1 Weight Effect on Pendulum Test

In this section, the impact weights were increased to observe the trends of stress increase, and it was found that the critical stresses generated by impact on location 4 and location 1 increase proportionally, as shown in Figure 8-25 and Figure 8-26. Based on Table 8-8, at locations 1 and 4, the slopes of stress between all weight intervals and their variances can be calculated and shown in Table 8-9.

Thus, based on Figure 8-25 and Figure 8-26, if the velocity of steel rod is fixed as 3 m/s, the minimum principal stress and maximum principal stress generated by impact on locations 4 and 1 can be roughly estimated by the following two equations:

Minimum principal stress at location 1 and 4:

$$\sigma_1 \approx \sigma + (m - m_1) \times (-89.2)$$

Maximum principal stress at location 1 and 4:

$$\sigma_3 \approx \sigma + (m - m_1) \times 19.68$$

where,

m is the mass of designed weight;

m_i is the known mass of weight;
σ is the stress generated by the weight with known weight.

Table 8-9 Slopes of Stress Increase with Weight Interval

Location ID	Interval ID	Slope (MPa/kg)	
	(Weight ID to Weight ID)	Maximum Principal Stress	Minimum Principal Stress
1	1 to 2	23.28	-87.54
1	1 to 3	21.46	-90.83
1	1 to 4	20.07	-85.90
1	1 to 5	19.85	-89.65
4	1 to 2	19.19	-97.85
4	1 to 3	17.96	-90.00
4	1 to 4	16.92	-84.06
4	1 to 5	18.68	-87.77
	Standard Error	2.00	4.15
	Average Slope	19.68	-89.20

Based on these two equations, if impact is applied on location 4, with a 3 m/s initial velocity of steel rod, the weight should be 3.4 kg to reach its critical compressive stress (-441.5 MPa). For getting critical tensile stress (61.5 MPa) at location 1, 1.3 kg weight with 3 m/s initial velocity of steel rod should be used to impact location 1.

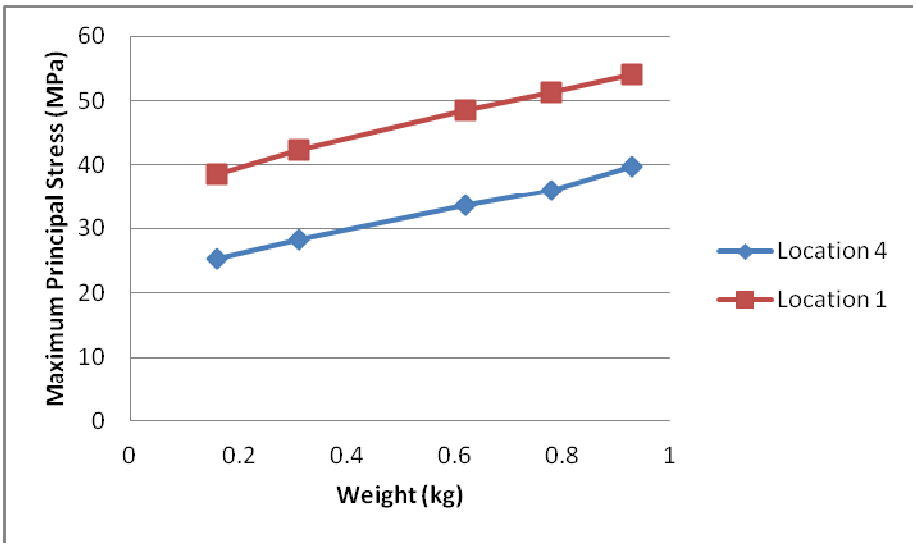

Figure 8-25 Maximum Principal Stresses vs. Weights at Locations 1 and 4

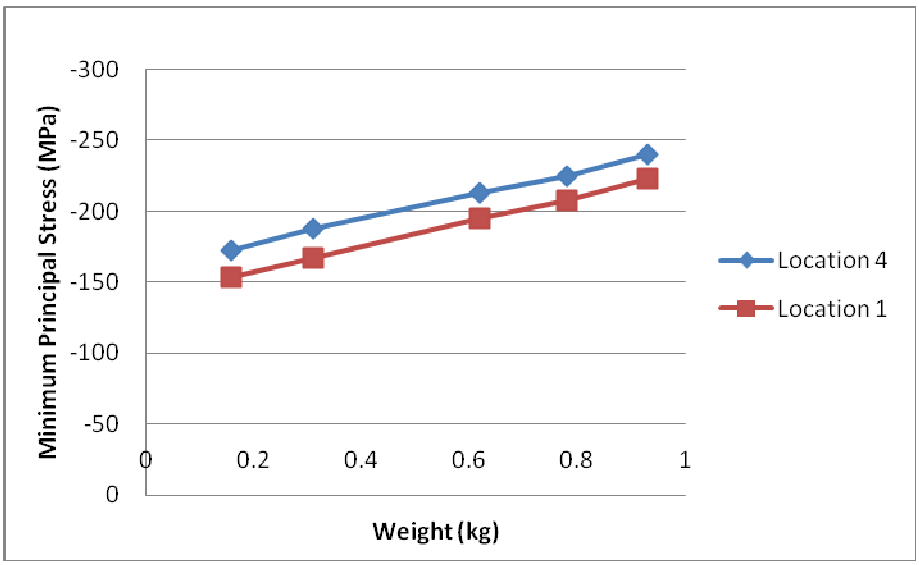

Figure 8-26 Minimum Principal Stresses vs. Weights at Locations 1 and 4

8.2.3.3.2 Steel Rod Velocity Effect on Pendulum Test

In this section, the impact weight is fixed at 0.16 kg, and the initial speed of steel rod is changed to test the stress variation. The results are shown in Table 8-10.

Figure 8-27 and Figure 8-28 verify these two critical stress locations: compressive stresses generated by impact on location 1 remain higher than those at location 4, and on the contrary, tensile stresses generated by impact on location 4 keep higher than those at location 1. However, differing from the influence of weight variation, the difference between the compressive stresses generated by impact on these two locations is enlarged with increased initial velocity of steel rod. For the difference of tensile stresses generated by impact on these two locations, the velocity of steel rod has relatively slight influence.

Table 8-10 Initial Velocity of Steel Rod vs. Stresses at Locations 1 and 4

Velocity (m/s)	Pendulum Fallen Height (m)	Location	Von Mises Stress (MPa)	Maximum Principal Stress (MPa)	Minimum Principal Stress (MPa)	Location	Von Mises Stress (MPa)	Maximum Principal Stress (MPa)	Minimum Principal Stress (MPa)
3	0.46	4	120.75	25.34	-172.21	1	102.61	38.69	-153.45
4.45	1.01	4	169.02	39.768	-234.58	1	147.86	53.161	-214.76
5.9	1.78	4	347.35	60.587	-447.82	1	297.43	102.23	-415.27
7.34	2.75	4	387.11	67.984	-507.08	1	330.67	118.84	-457.53
8.79	3.94	4	482.10	94.62	-617.22	1	389.30	145.69	-531.69
10.23	5.33	4	600.47	144.45	-773.19	1	463.66	184.36	-631.03
11.66	6.94	4	627.65	157.44	-820.51	1	487.35	201.86	-666.34
13.1	8.76	4	700.00	180.93	-921.93	1	528.95	219.10	-719.87

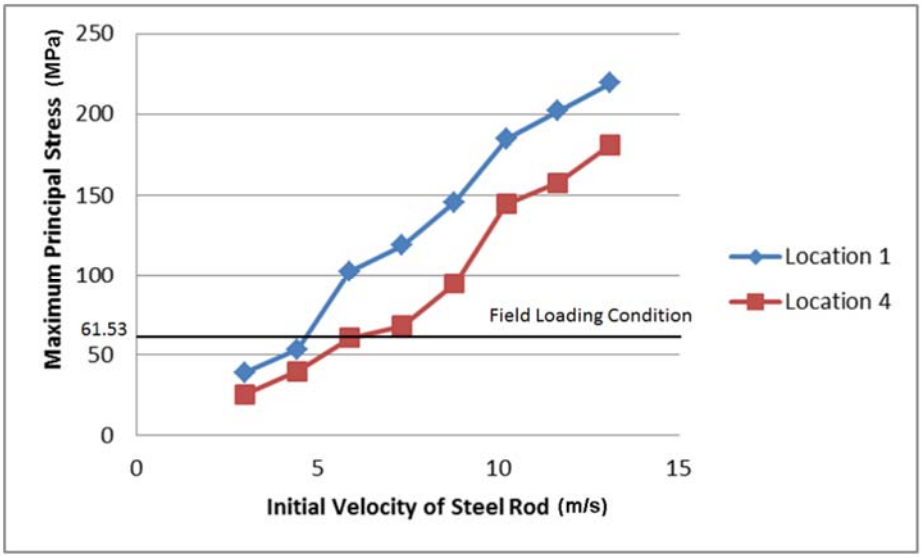

Figure 8-27 Initial Velocity of Steel Rod vs. Maximum Principal Stress at Locations 1 and 4

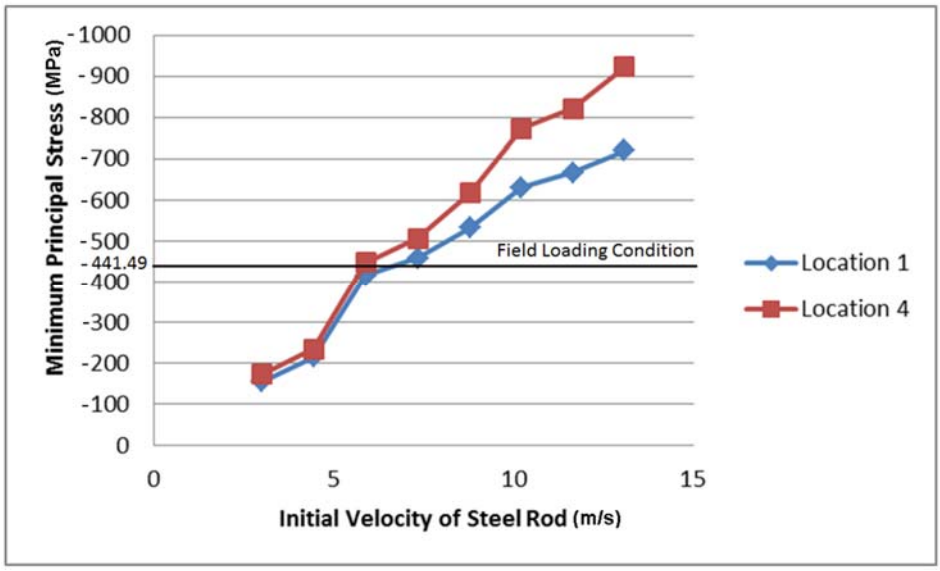

Figure 8-28 Initial Velocity of Steel Rod vs. Minimum Principal Stress at Locations 1 and 4

Figure 8-27 also shows that, compared to field loading condition, through interpolation based on Table 8-10, the critical tensile stress (61.53 MPa) at location 1 can be reached through pendulum test on location 1 with 4.7 m/s initial velocity of steel rod and 0.16 kg weight.

Similarly, Figure 8-28 illustrates that the critical compressive stress (-441.5 MPa) at location 4 under field loading condition are equivalent to that from pendulum test with 5.86 m/s initial velocity of steel rod and 0.16 kg weight on location 4.

8.3 Developed RRPM Laboratory Tests

Given more similar stress distributions between those from laboratory tests and those from tire-marker impact field condition, more laboratory tests were designed and analyzed in this study,

such as reversed latitude flexural test, revised reversed latitude flexure test, and offset latitude flexural test.

8.3.1 Reversed Latitude Flexural Test

Through simulating the tire-marker impact process, as shown in Figure 8-29, the deformation of tire is convex in shape, which lets the tire surface contact with the marker on the no-lens sides of marker's top shell. This finding is in accordance with the von Mises stress distribution, which concentrates on the no-lens sides of marker's top shell. Based on this finding, however, there is no test which produces critical compressive stress on both the non-lens sides of marker's top shell simultaneously. The most similar test is reversed longitudinal flexural test. But this reversed longitudinal flexural test produces the critical compressive stress on the lens sides, not non-lens sides. That is why the reversed latitude flexural test was developed, as shown in Figure 8-30. In this test, both non-lens sides of marker's top shell can be impacted by tire simultaneously. This pair of compressive stresses also can much more easily generate the tensile stress in the middle of marker's shell. Figure 8-31 shows the von Mises stress distribution from this reversed latitude flexural test.

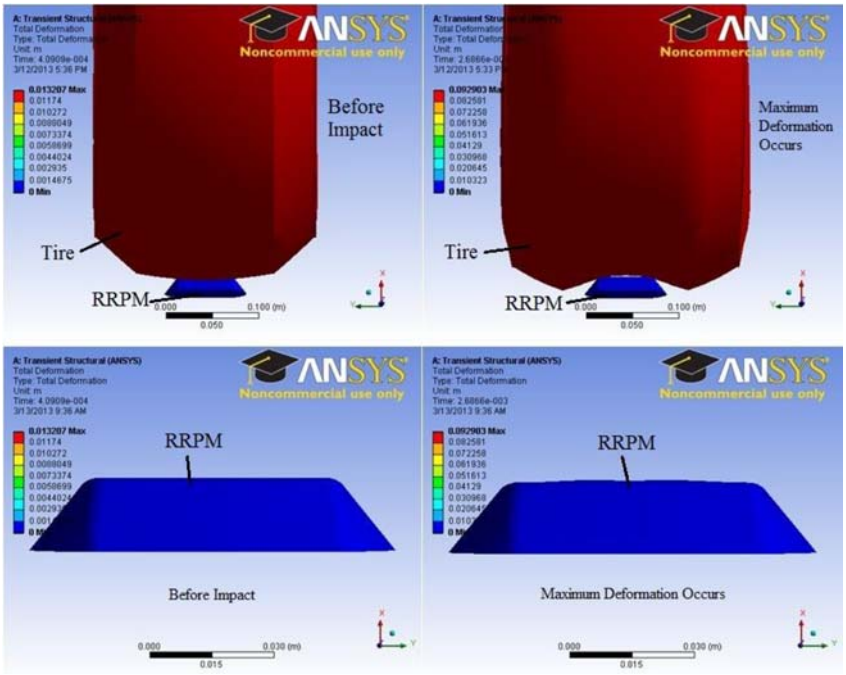

Figure 8-29 Deformation of Tire and RRPM

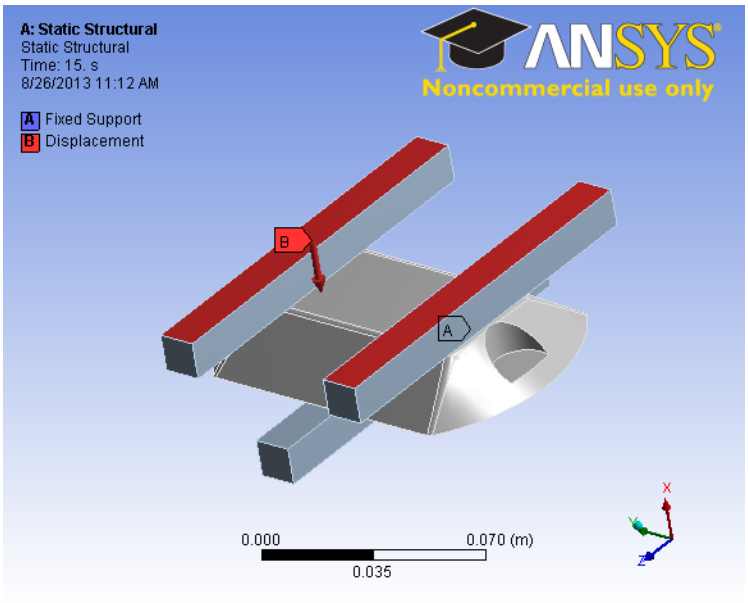

Figure 8-30 Reversed Latitude Flexural Test

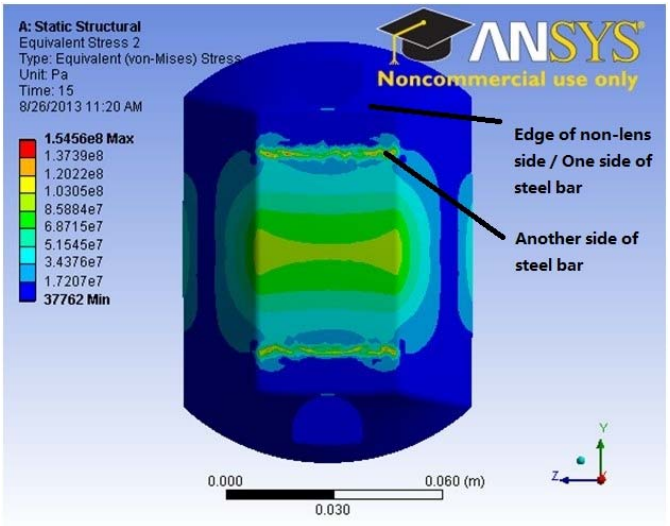

Figure 8-31 Von Mises Stress Distribution in Reversed Latitude Flexural Test

However, Figure 8-31 shows that the Von Mises stress Distribution from this test is not in accordance with that from field condition. The critical von Mises stress is not on the edge of non-lens sides, but on the other side of the steel bar. Figure 8-31 hints that this mismatched von Mises stress distribution might be caused by the steel bar under RRPM. Thus, one revised reversed latitude flexural test was designed.

8.3.2 Revised Reversed Latitude Flexural Test

Based on the von Mises stress distribution by reversed latitude flexural test, for obtaining a stress distribution better matched the tire-impact real condition, two steel bars are installed on non-lens

sides under RRPM bottom, instead of one steel bar in the middle. This test also can produce high shear stresses on the edges of non-lens sides.

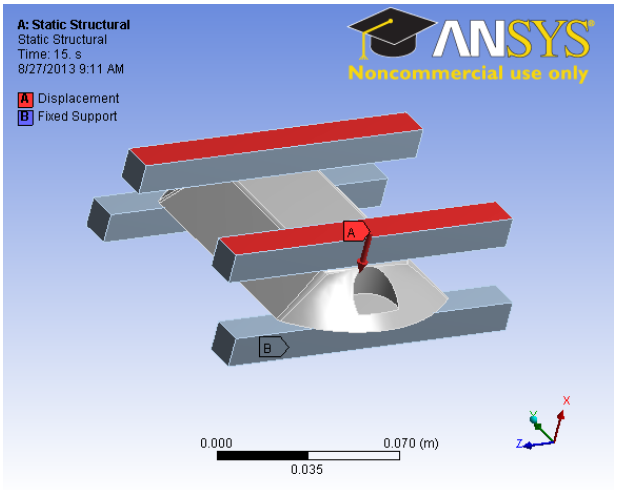

Figure 8-32 Revised Reversed Latitude Flexural Test

The von Mises stress distribution from this test is shown in Figure 8-33. As expected, this revised reversed latitude flexural test can produce higher stress concentration on the RRPM top edge of non-lens sides. In other words, based on the Von Mises stress distribution, compared to the simple reversed latitude flexural test, this revised reversed latitude flexural test matches the tire-marker impact real condition better, as shown in Figure 8-33. Both critical von Mises stresses concentrate on the corner of RRPM top shell, and gradually decrease along the non-lens sides till the middle.

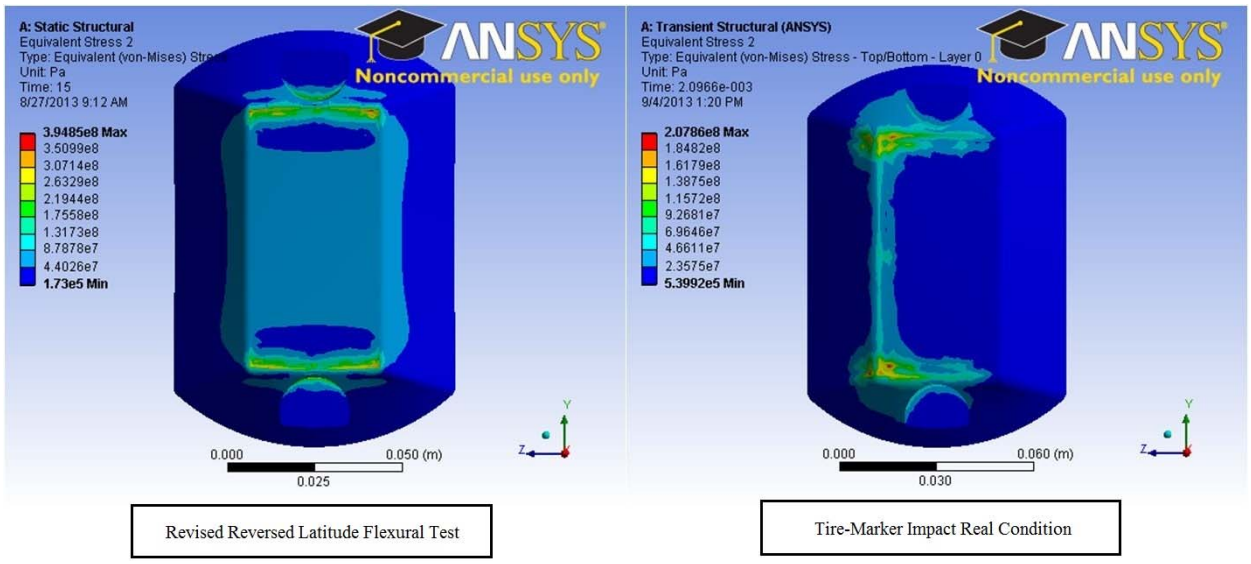

Figure 8-33 Comparison of Von Mises Stress Distributions between Revised Reversed Latitude Flexural Test and Real Condition

8.3.3 Offset Latitude Flexural Test

Similar to the offset test in ASTM D 4280, offset latitude flexural test tries to create large compressive stresses under the half-side steel plate, with small tensile stresses in other RRPM areas. Figure 8-34 shows that, compared to revised reversed latitude flexural test, the magnitude of von Mises stresses, under the same loading rate, changes slightly from offset latitude flexural test.

Moreover, compared to the original offset test, shown in Figure 7-35, the uneven longitudinal stress distribution along lens side from offset latitude flexural test is also more close to the real condition.

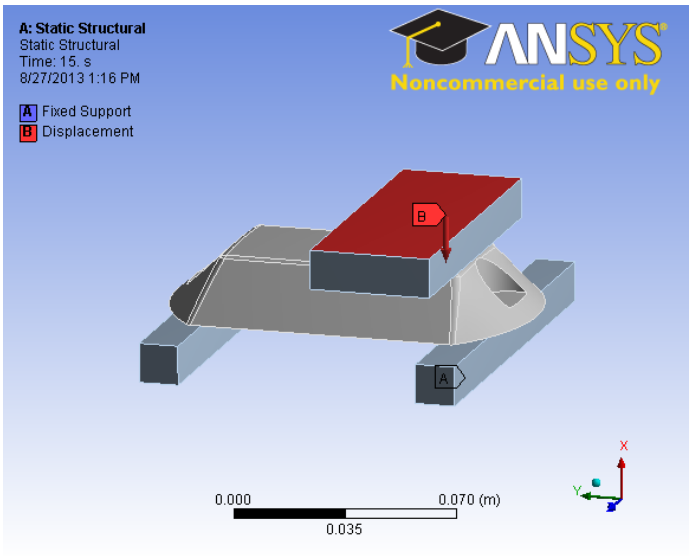

Figure 8-34 Offset Latitude Flexural Test

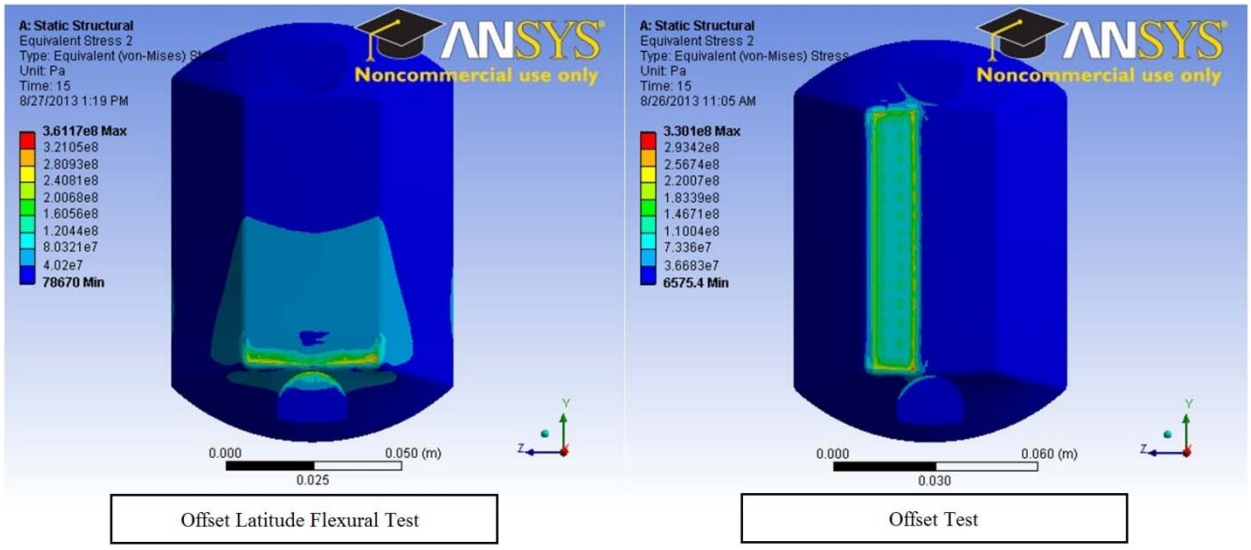

Figure 8-35 Comparison of Von Mises Stress Distribution Between Offset Latitude Flexural Test and Offset Test

8.4 Conclusions of Laboratory Test Analysis

The above analysis and reasoning show that, the ASTM compressive test, the reversed ASTM flexural test, and the pendulum impact test can be candidate laboratory tests to evaluate the field performance of RRPM. Moreover, two new laboratory tests, which can better simulate the real tire-marker condition, are suggested in this study: revised reversed latitude flexural test and offset latitude flexural test. These tests will be conducted and compared in the laboratory on a set of RRPM models that are commonly used on Florida highways.

CHAPTER 9 LABORATORY TEST VERIFICATION

This chapter describes the efforts of laboratory tests of selected RRPM models to provide performance evaluation of the RRPMs according to ASTM standards D 4280 and three new tests identified in the previous chapter. The baseline ASTM tests include a compressive test and a flexural test. In the previous chapter, the reversed ASTM flexural test was suggested to replace the original ASTM flexural test. Due to the difficulty in placing two loading bars on top of markers, however, the reserved flexural test was abandoned. The original ASTM flexural test was conducted instead. Moreover, a variation of the baseline test, called offset flexural test, was also conducted. The three new tests conducted include the pendulum impact test, the revised reversed latitude flexural test, and the offset latitude flexural test. The RRPM performance under these tests was recorded and ranked.

9.1 Standard ASTM Laboratory Tests

Based on ASTM D 4280, two baseline tests (compressive test and flexural test) were conducted on six types of RRPM, i.e., 3M 290 Series, 3M 290 PSA Series, Ennis Model 980, Ennis Model C80, Rayolite Round Shoulder ARC FH, and Apex 921AR.

Before tests, six types of RRPM were labeled as shown in Table 9-1. The quantities used for each test were determined by the total number of markers, as shown in Table 9-2. The two tests are first shown respectively, and then combined to reach a rank of six types of RRPM.

Table 9-1 Labels of Six Types of RRPM

Label	RRPM Type	Simplified RRPM Designation
1	3M 290 Series	3M 290
2	3M 290 PSA Series	3M 290 PSA
3	Ennis Model 980	Ennis 980
4	Ennis Model C80	Ennis C80
5	Rayolite Round Shoulder ARC FH	Rayolite RS
6	Apex 921AR	Apex 921AR

Table 9-2 Quantity of Markers Used in Compressive Test and Flexural Test

RRPM Type	Quantity for Each Test
1 (3M 290)	18
2 (3M 290 PSA)	9
3 (Ennis 980)	18
4 (Ennis C80)	18
5 (Rayolite RS)	18
6 (Apex 921AR)	18

9.1.1 Compressive Test

The compressive test, as described in ASTM D 4280, measures the failure potential of RRPM under a compressive load. Under a load of 6,000 lb, the deformation of marker shall be less than 3.3 mm, and without breakage. A typical view of compressive test is shown in Figure 9-1. Note that the machine in the test was set to stop automatically when the load reached 6,000 lb. However, there were eight cases among 99 in total that reached 6,010 lb. Also note that two

cases (one from type 5 [Rayolite RS] and the other from type 6 [Apex 921AR]) resulted in breakage, as shown in Figure 9-2 and Figure 9-3, and these two cases were considered as failure.

Figure 9-1 Typical View of Compressive Test

Figure 9-2 Edge Breakage of Marker 5-16 in Compressive Test

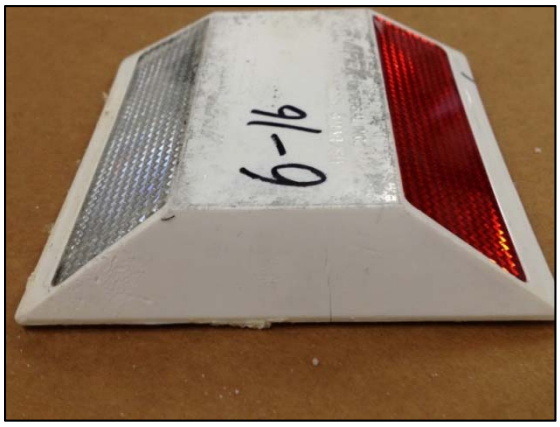

Figure 9-3 Center Breakage of Marker 6-16 in Compressive Test

As can be seen in Table 9-3, the average deformation of each marker is far less than 3.3 mm, which indicates that they meet the baseline of ASTM D 4280. Furthermore, a rank of compressive performance can be expressed as: 1 = 3 = 4 > 5 > 6. Specifically, the performance ranking from the compressive test is: 3M 290 = Ennis 980 = Ennis C80 > Rayolite RS > Apex 921AR. The 3M 290 PSA marker is not included in the ranking list because the existence of an adhesive layer at its bottom significantly increased the measured deformation, which does not represent the marker's structural capacity. Based on the compressive stress analysis under field condition using FEM as described in Section 6.2, the maximum compressive stresses generated in 3M 290, Ennis C80 and Rayolite RS are 134 MPa, 163 MPa, and 324 MPa, respectively. Assuming a low compressive stress or a low deformation corresponds to a low failure potential, the FEM analysis results are in accordance with the above obtained performance ranking from compressive test. The performance trends of RRPMs observed around the City of Tampa area (Section 4.2.3) indicate that performance deterioration over time is less for 3M 290 and Ennis C80 markers than for Rayolite RS markers. This is also consistent with the compressive test results.

Table 9-3 Deformation of Six Types of RRPM

RRPM Type	Average Deformation (mm)	Standard Deviation (mm)
1 (3M 290)	0.062	0.033
2 (3M 290 PSA)	0.280[a]	0.195
3 (Ennis 980)	0.061	0.031
4 (Ennis C80)	0.057	0.043
5 (Rayolite RS)	0.090	0.072
6 (Apex 921AR)	0.189	0.099

[a] The large value is mainly due to the deformation in the pressure sensitive adhesive.

9.1.2 Flexural Test

Based on ASTM D 4280, in the flexural test a compressive load is applied through a top steel bar at a rate of 5.2 mm (0.2 inch) per minute until the marker breaks. The load at breakage should be higher than 8,914 N (2,000 lb). A typical view of flexural test is shown in Figure 9-4.

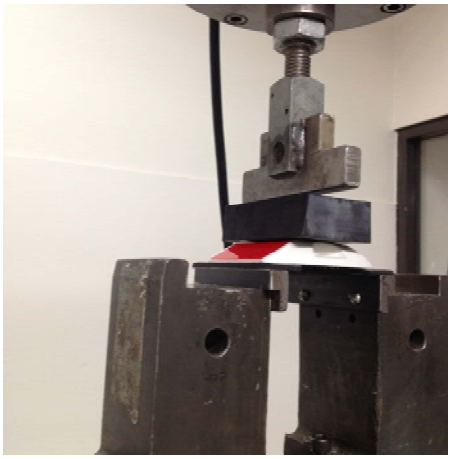

Figure 9-4 Typical View of Flexural Test

Note that for Type 2 (3M 290 PSA) RRPM, the setup of flexural test was different from others in that the rubber coating already on the reflector of Type 2 RRPM acts as the pad. Therefore, two 1/8-inch pads for Type 2 are removed.

Another concern when setting up is spacing of bars. Spacing of bars shall depend on length of marker base, being as great as possible without bars protruding beyond the extreme lengthwise points of the marker base. Note that the spacing of bars was measured for Type 3 (Ennis 980) RRPM and calculated for other 5 types, as shown in Table 9-4.

Table 9-4 Calculation of Spacing of Bars for Flexural Test

RRPM Type	Reflector Length (inch)	Lower Points Outer Width (inch)
1 (3M 290)	3.52	3.614
2 (3M 290 PSA)	3.49	3.583
3 (Ennis 980)	3.18	3.265
4 (Ennis C80)	3.18	3.265
5 (Rayolite RS)	3.92	4.025
6 (Apex 921AR)	3.83	3.932

Basically, there were two types of breakage, edge breakage and center breakage, as shown in Figure 9-5 and Figure 9-6. These two breakage locations are both observed in field conditions. The center breakage can be explained by Figure 8-10, which indicates that the maximum von Mises stress concentrates on the middle of non-lens sides. For the edge breakage, its breakage line is along the edges of internal radiate hollows, which means marker internal structure probably causes this type of breakage.

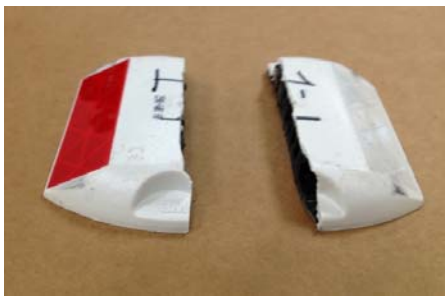

Figure 9-5 Typical Center Breakage in Flexural Test

Figure 9-6 Typical Edge Breakage in Flexural Test

As can be seen in Table 9-5, the average breakage load of six types of RRPM is greater than 2,000 lb, indicating that they all meet ASTM D 4280 baseline. Moreover, a rank of flexural performance is: 3 > 4 > 2 > 1 > 6 > 5. Specifically, the performance ranking from the flexural test is: Ennis 980 > Ennis C80 > 3M 290 PSA > 3M 290 > Apex 921AR > Rayolite RS. This is also consistent with the performance trends of RRPMs observed around the City of Tampa area (Section 4.2.3), i.e., 3M 290 and Ennis C80 markers have better durability than Rayolite RS markers.

Table 9-5 Breakage Load of Six Types of RRPM

RRPM Type	Average Breakage Load (kip)	Standard Deviation (kip)
1 (3M 290)	2.77	0.25
2 (3M 290 PSA)	2.83	0.28
3 (Ennis 980)	4.18	0.42
4 (Ennis C80)	3.99	0.56
5 (Rayolite RS)	2.04	0.45
6 (Apex 921AR)	2.33	0.26

9.2 Variations of the Baseline Laboratory Tests

In order to investigate the effect of different loading position on testing results, two offset flexural tests were developed. The process of this offset flexural test is the same as original flexural test, except that the loading position changes with two variations, i.e. 1/3 offset and 1/4 offset, as can be seen in Figure 9-7. It should be noted that the location of 1/4 offset is the edge of the top bar and that of 1/3 offset is in the middle between original test and 1/4 offset. 1/3 and 1/4 offset do not mean they are at 1/3 or 1/4 position of the marker, but represent approximate position of the offset.

Figure 9-7 View of Offset Flexural Test

Note that for Type 2 (3M 290 PSA) RRPM, the setup of flexural test was different from others in that the rubber coating already on the reflector of Type 2 RRPM acts as the pad. Therefore, only two 1/8-inch pads for Type 2 are removed.

9.2.1 1/3 Offset Flexural Test

For 1/3 offset test, 10 replicates of each marker were tested. A typical view of the test is shown in Figure 9-8. For this test, edge breakage occurred more often than center breakage. Typical views of edge breakage and center breakage are shown in Figure 9-9 and Figure 9-10, respectively. Compared to the breakages generated by standard flexural test, the edge breakage of 1/3 flexural test is much more straight than that from standard flexural test. These two types of breakage can be explained by the stress distributions shown in Figure 8-12.

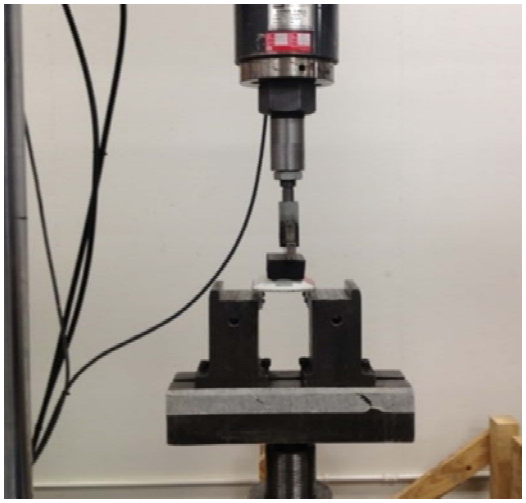

Figure 9-8 Typical View of 1/3 Offset Flexural Test

Figure 9-9 Edge Breakage of Marker 1-1 in 1/3 Flexural Test

Figure 9-10 Center Breakage of Marker 2-5 in 1/3 Flexural Test

9.2.2 1/4 Offset Flexural Test

For Type 1 (3M 290) and Type 2 (3M 290 PSA) markers, the setup of flexural test is the same as that for the 1/3 offset, except loading position, as can be seen from Figure 9-11. However, for Type 3 (Ennis 980) markers, slip occurred too often with the setup in Figure 9-11. Then some modifications of the setup were made by adding a rubber in the left groove, as can be seen in Figure 9-12. However, the situation of slip still occurred even with the additional rubber.

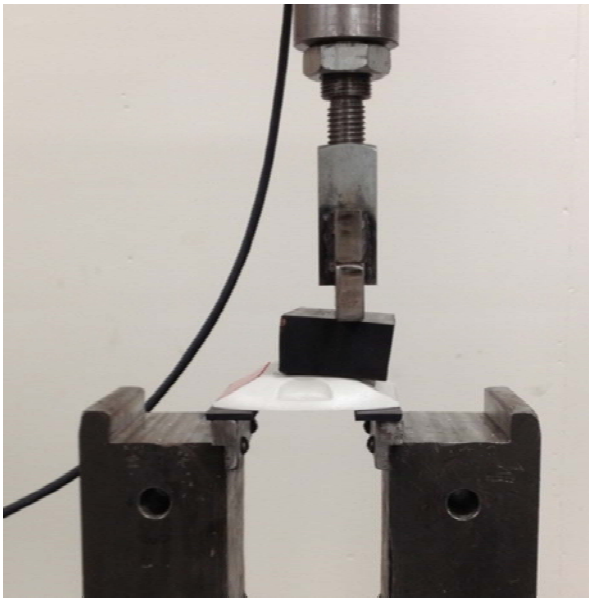

Figure 9-11 Setup of 1/4 Offset Test for Types 1 and 2 Markers

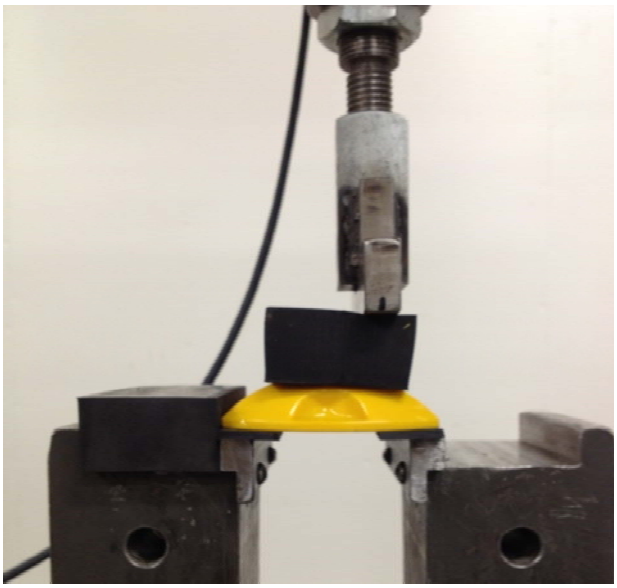

Figure 9-12 Setup of 1/4 Offset Test for Type 3 Marker

In addition, compressive testing with loading with the same two offsets was also conducted. Based on ASTM D 4280, the compressive load was applied through a top steel bar at a rate of 5.2 mm (0.2 inch) per minute until the marker breaks. Thus, the performance ranking from the revised tests with offset loading can be expressed as follows:

- Compressive Test: 3M 290 = Ennis 980 = Ennis C80 > Rayolite RS > Apex 921AR > 3M 290 PSA.
- Flexural Test: Ennis 980 > Ennis C80 > 3M 290 PSA > 3M 290 > Apex 921AR > Rayolite RS.

These performance rankings from revised tests with offset loading are identical to those from standard ASTM laboratory tests. This result also indirectly shows that offset flexural tests have no significant different results from standard ASTM laboratory tests.

9.3 Revised Pendulum Impact Test

One of the failure mechanisms of RRPMs in the field is the damage from impact on RRPMs from vehicle tire hits. A pendulum impact test was initially developed by TTI (Zhang et al., 2009). The original device could only apply one single impact load to RRPM specimens. However, it is rare that RRPMs installed in the field would failure under just one single load. Generally RRPM damages develop from micro cracks or flaws to stages manifested as observable failures, under repeated tire impact loading. Therefore, a modification was made to the original pendulum test device to enable it to apply load impacts repeatedly, using a power motor that lifts the impact arm in cycles. An RRPM can be tested for a given number of impacts, or be tested until it fails with the number of impacts recorded.

In the device, the impact force is delivered to the RRPM by the end of a 1-inch rounded steel rod at the end of a swinging arm, as shown in Figure 8-13. The RRPM under testing is adjustable, allowing both horizontal and vertical positioning relative to the steel rod and its impact point.

The use of the adjustable marker mount allows for a variation of impact locations on the marker. With this setup, impact tests can be done to any impact point on the surface of the marker. In addition, different weights can be added to the end of the pendulum arm to increase the force exerted on the marker at impact.

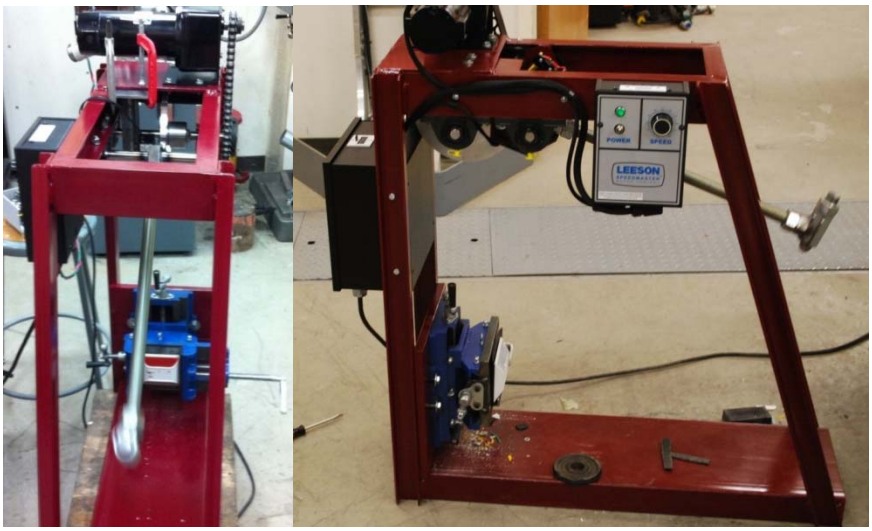

Figure 9-13 Revised Pendulum Impact Device

All the six RRPM models tested in the compressive and flexural tests were tested by the revised pendulum impact device. Six locations, as shown in Figure 8-19, were tested for each type of marker. The effects of speed and load were examined in the tests. The speed at which the hammer hit the marker was adjusted with a knob on the machine itself, and the load was adjusted by adding a 1.25 lb weight on the hammer. In the tests conducted the load has two levels: low (L) and high (H). The speed also has two levels: slow (S) and fast (F). Each combination of location, load, and speed was repeated with 3 markers. Hence there are 6*2*2*3=72 tests for each marker type, and 432 for all six markers.

The marker was placed vertically, with its top facing the hammer. It can be adjusted horizontally or vertically, to meet the requirement on the hitting location. A clipper was used to prevent the marker from moving. The machine also has a counter to record the number of hits on the marker. After starting the machine, the hammer hit the marker at the desired location at a desired speed level, and the machine stopped after breakage occurred. The number on the counter was then recorded.

To save time, the tests were conducted from the heaviest and fastest combination. If no breakage occurs at this combination, it is reasonable to believe that the markers tend not to break at lighter weights or lower speeds. For each marker, the test was stopped after 50 hits. If breakage occurred in 50 hits, the lighter weight and slower speed combination was tested. Three tests were conducted for each combination, and their mean and standard deviation are listed in Table 9-6.

The numbers in Table 9-6 are the number of hits before the marker breaks. A number 50 in the table indicates that the marker still did not break after 50 hits. In the Load/Speed column, an L

represents a lower load and an H represents a higher load. An S represents a slower hitting speed and an F represents a faster hitting speed. The cells in yellow are the combinations where the tests were not actually done, since the markers did not break at the fastest and heaviest combination at this location.

Table 9-6 Results of Revised Pendulum Impact Test (Number of Hits)

Marker Type	Load /Speed	Location					
		1	2	3	4	5	6
3M 290	LS	50 (0)	50 (0)	50 (0)	50 (0)	50 (0)	50 (0)
	LF	38 (5.3)	50 (0)	50 (0)	50 (0)	50 (0)	50 (0)
	HS	14.7 (4.2)	50 (0)	50 (0)	50 (0)	26.7 (9.5)	40.3 (2.5)
	HF	12.7 (4.2)	50 (0)	50 (0)	50 (0)	28 (2)	38
3M 290 PSA	LS	50 (0)	50 (0)	50 (0)	50 (0)	50 (0)	50 (0)
	LF	50 (0)	50 (0)	50 (0)	50 (0)	50 (0)	50 (0)
	HS	21 (2.6)	50 (0)	50 (0)	50 (0)	41.7 (1.5)	50 (0)
	HF	16.3 (1.5)	50 (0)	50 (0)	50 (0)	30 (9.2)	34.7 (6.8)
Ennis 980	LS	50 (0)	50 (0)	50 (0)	50 (0)	50 (0)	50 (0)
	LF	50 (0)	50 (0)	50 (0)	50 (0)	50 (0)	50 (0)
	HS	50 (0)	50 (0)	50 (0)	50 (0)	50 (0)	50 (0)
	HF	50 (0)	50 (0)	50 (0)	50 (0)	50 (0)	50 (0)
Ennis C80	LS	50 (0)	50 (0)	50 (0)	50 (0)	50 (0)	50 (0)
	LF	50 (0)	50 (0)	50 (0)	50 (0)	50 (0)	50 (0)
	HS	50 (0)	50 (0)	50 (0)	50 (0)	50 (0)	50 (0)
	HF	50 (0)	50 (0)	50 (0)	50 (0)	50 (0)	50 (0)
Rayolite RS	LS	25 (21.7)	19 (7.5)	27.3 (5.1)	50 (0)	50 (0)	50 (0)
	LF	13 (5)	11.7 (1.5)	17 (3.6)	23.3 (9.9)	50 (0)	35.3 (13.1)
	HS	2 (1)	2.3 (0.6)	2 (1)	5.3 (0.6)	4.7 (2.3)	2.3 (0.6)
	HF	1.7 (0.6)	2 (1)	1 (0)	4.3 (0.6)	4.7 (0.6)	1 (0)
Apex 921AR	LS	2.7 (0.6)	9 (6.6)	4.7 (1.5)	2.7 (0.6)	50 (0)	50 (0)
	LF	2.7 (0.6)	50 (0)	8.3 (2.9)	50 (0)	44.3 (9.8)	50 (0)
	HS	1.3 (0.6)	1.7 (0.6)	2 (0)	1.3 (0.6)	5 (3.6)	2 (0)
	HF	1 (0)	1.7 (1.2)	2 (1.7)	1 (0)	1 (0)	1.3 (0.6)

Note: the numbers in each cell represent “mean (standard deviation)”.

Based on the results of pendulum impact tests, the performance of the six RPM models are ranked as Ennis series > 3M 290 series > Rayolite RS > Apex 921AR. This rank is similar to that from the ASTM standard flexural test, except that Rayolite RS performed better than Apex 921AR in the pendulum impact test.

The average results for 3M series (3M 290 and 3M 290 PSA), Rayolite RS, and Apex 921AR are also plotted in Figure 9-14, from which it can be seen that generally higher impact load or speed leads to earlier failure of RRPM in the pendulum impact test. This is consistent with the FEM results presented in Section 8.2.

Figure 9-15 plots the results averaged for impact location. It can be seen that for 3M series, Location 1 is the weakest spot among the six impact locations, and for Rayolite RS and Apex 921AR, Locations 1, 2, 3 are weaker than Locations 4, 5, 6. These are generally consistent with the rank based on the maximum principle stress distribution calculated from FEM, as discussed in Section 8.2.

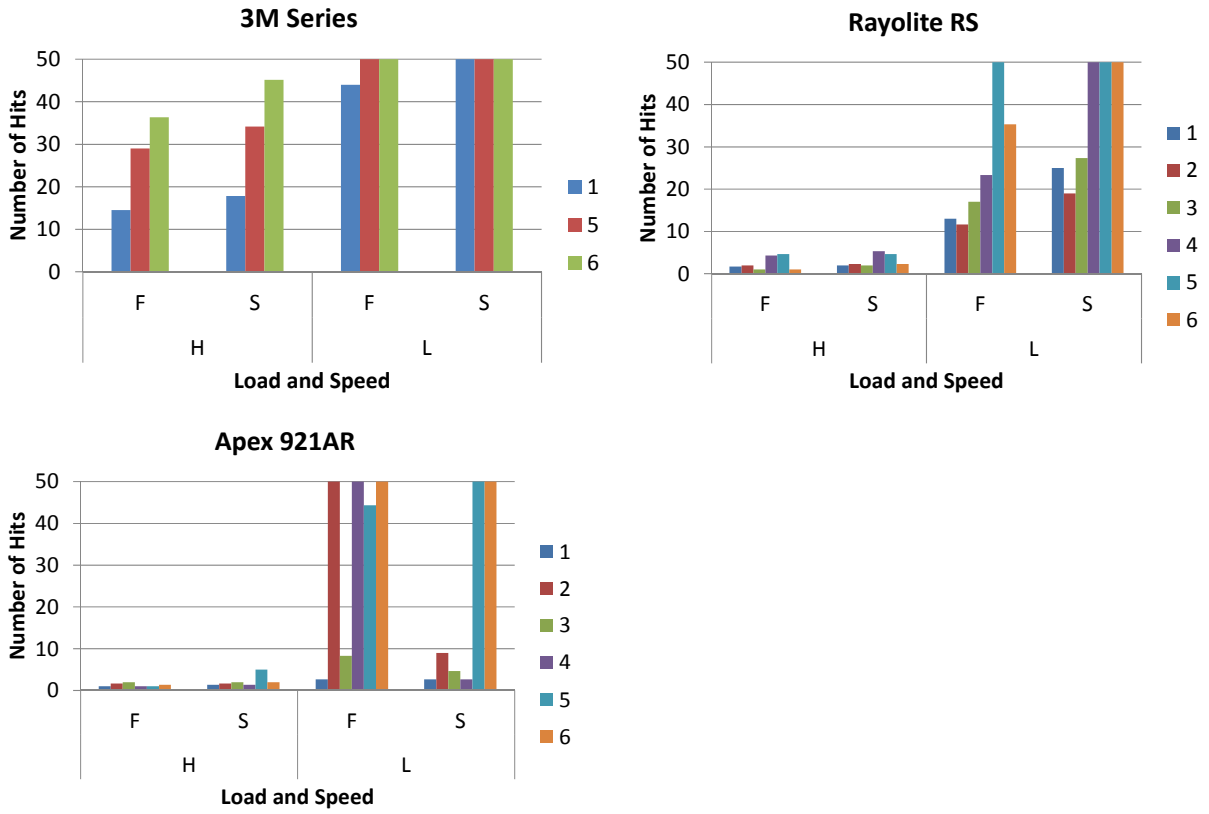

Figure 9-14 Average Results of Revised Pendulum Impact Test

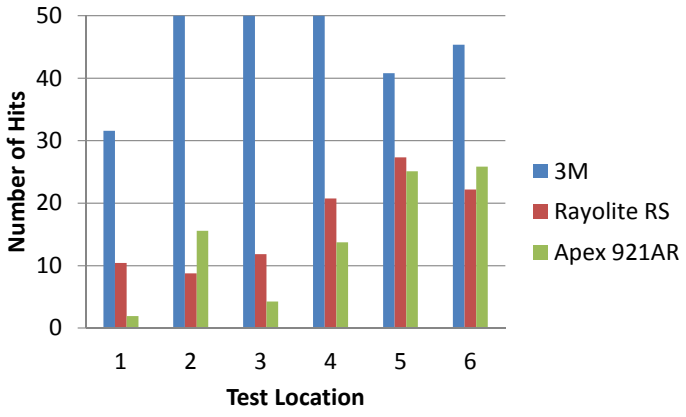

Figure 9-15 Revised Pendulum Impact Test Results Averaged by Location

9.4 Latitude Flexural Tests

Two latitude flexural tests were also conducted on the six types of markers: the revised reversed latitude flexural test (RRLFT) and the offset latitude flexural test (OLFT). Since both tests are flexural tests, the loading rate is 0.2 inches per minute. For each test, twelve markers of each type were tested.

9.4.1 Revised Reversed Latitude Flexural Test

In the revised reversed latitude flexural test (RRLFT), two steel loading bars are applied laterally on two edges of markers, as shown in Figure 9-16. Thus, new loading heads had to be fabricated. Since the distances between the edges of the top shell for markers 1 and 2 are the same, and the distances are also the same for markers 3 and 4, four loading heads with four different distances were made for marker types 1 and 2, 3 and 4, 5, and 6 respectively. Elastomeric pads were placed on top of the markers. The test results are listed in Table 9-7 and the typical failure modes are shown in Figure 9-17 through Figure 9-21.

Figure 9-16 Revised Reversed Latitude Flexural Test

Figure 9-17 Typical 3M 290 Failure in the RRLFT

Figure 9-18 Typical Ennis 980 Failure in the RRLFT

Figure 9-19 Typical Ennis C80 Failure in the RRLFT

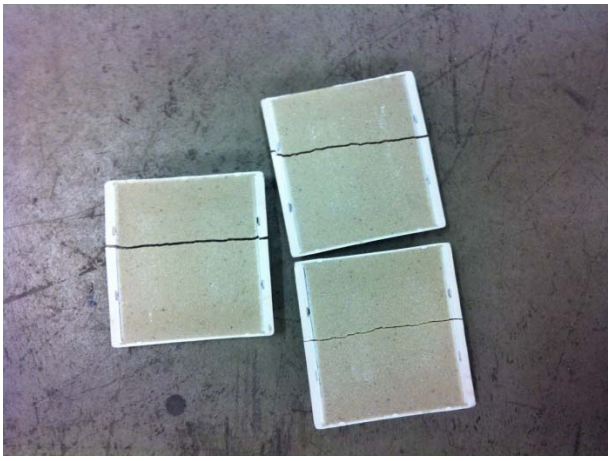

Figure 9-20 Typical Rayolite RS Failure in the RRLFT

Figure 9-21 Typical Apex 921AR Failure in the RRLFT

Table 9-7 Breakage Load of Each RRPM Type in the RRLFT

Marker Type	Marker No.	Force to Break (kip)	Marker Type	Marker No.	Force to Break (kip)	Marker Type	Marker No.	Force to Break (kip)
3M 290	1	5.96	3M 290 PSA	1	5.12	Rayolite RS	1	4.14
	2	4.90		2	5.11		2	3.88
	3	5.83		3	5.26		3	4.34
	4	5.33		4	4.86		4	3.46
	5	5.65		5	4.95		5	3.36
	6	4.92		6	4.68		6	4.12
	7	5.91		7	4.80		7	3.91
	8	5.46		8	5.02		8	4.03
	9	5.52		9	5.44		9	4.30
	10	5.29		10	5.26		10	4.61
	11	5.39		11	4.99		11	4.69
	12	6.08		12	5.22		12	4.06
Ennis 980	1	7.17	Ennis C80	1	6.73	Apex 921AR	1	3.78
	2	8.30		2	7.24		2	4.67
	3	8.87		3	5.22		3	4.96
	4	7.76		4	7.24		4	4.71
	5	7.92		5	7.93		5	4.90
	6	8.70		6	7.61		6	4.71
	7	8.93		7	6.34		7	4.36
	8	8.31		8	9.25		8	4.72
	9	8.23		9	8.07		9	4.66
	10	6.50		10	6.92		10	4.43
	11	8.91		11	7.37		11	4.97
	12	8.84		12	5.13		12	4.14

Based on the typical failure modes shown in Figure 9-17 through Figure 9-21, the locations of cracks observed in Ennis C80 are most diversified: on non-lens side, at the loading location, or at the center of top shell. For 3M 290 and Ennis 980, all cracks only occurred on non-lens side. For Rayolite RS, all cracks were close to the middle part of the markers. For Apex 921AR, most cracks were either near the edge or at the center.

9.4.2 Offset Latitude Flexural Test

In the offset latitude flexural test (OLFT), two rubber bands were placed on the steel bars that acted as the support of the markers, as shown in Figure 9-22. The rubber bands were about the same width as the steel bars. The RRPMs were then placed on the rubber bands. A piece of elastomeric pad was placed on one side of the markers. One piece of steel bar was then placed on top of the elastomeric pad for loading at the edge of the markers. To prevent sliding, a piece of metal is placed on the left side, as shown in Figure 9-22. These offset latitude flexural tests were terminated after markers were broken. The test results are listed in Table 9-8 and the typical failure modes are shown in Figure 9-23 through Figure 9-26.

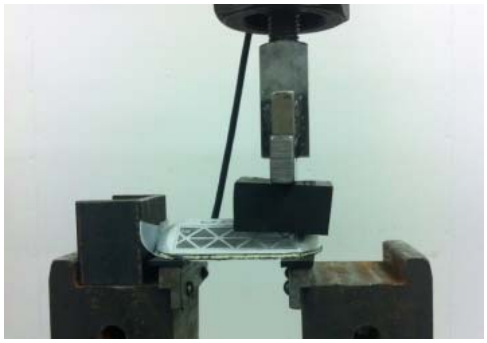

Figure 9-22 Offset Latitude Flexural Test

Figure 9-23 Two Types of 3M 290 Failure in the OLFT

Based on Table 9-8, it is safe to say that Ennis 980 and C80 can take the largest force. They are also the most consistent types of markers. Apex 921AR has the lowest strength, with significant variations between markers. 3M 290 and 3M 290 PSA series seem to fail suddenly, mostly with a cracking sound. A few markers of the 3M 290 series did not have a sound when they failed. Most Ennis 980 and Ennis C90 markers had some initial cracks before the final failure, with cracking sound. For Rayolite RS, some initial cracking sound was observed, while others just broke suddenly. APEX 921AR seems to be the stiffest and the most brittle marker type. Its deformation at breakage is relatively smaller than the other markers, mostly with sudden breakage.

Table 9-8 Breakage Load of Each RRPM Type in the OLFT

Marker Type	Marker No.	Force to Break (kip)	Marker Type	Marker No.	Force to Break (kip)	Marker Type	Marker No.	Force to Break (kip)
3M 290	1	4.97	3M 290 PSA	1	5.35	Rayolite RS	1	6.25
	2	4.98		2	4.39		2	6.80
	3	4.38		3	4.90		3	6.39
	4	4.75		4	5.09		4	6.05
	5	4.60		5	4.57		5	6.26
	6	5.24		6	4.72		6	5.55
	7	4.28		7	4.40		7	5.76
	8	4.53		8	4.39		8	5.39
	9	3.83		9	4.53		9	5.82
	10	4.80		10	5.35		10	5.89
	11	4.39		11	5.18		11	5.73
	12	4.49		12	4.20		12	6.37
Ennis 980	1	7.80	Ennis C80	1	6.95	Apex 921AR	1	2.71
	2	7.46		2	7.03		2	5.41
	3	7.50		3	7.27		3	3.72
	4	7.41		4	6.87		4	4.62
	5	8.05		5	6.79		5	2.73
	6	7.53		6	7.07		6	2.82
	7	8.08		7	7.06		7	3.06
	8	7.59		8	7.12		8	4.12
	9	7.87		9	6.96		9	4.53
	10	7.44		10	7.46		10	3.57
	11	8.02		11	6.78		11	4.00
	12	7.47		12	6.79		12	4.45

Figure 9-24 Typical Ennis 980 and Ennis C80 Failure in the OLFT

Figure 9-25 Typical Rayolite RS Failure in the OLFT

Figure 9-26 Typical Apex 921AR Failure in the OLFT

Based on the information presented in Table 9-7 and Table 9-8, statistics of the results of the two latitude flexural tests are summarized in Table 9-9 and Table 9-10. Thus, the performance ranking from these two developed tests can be expressed as follows:

- Revised Reversed Latitude Flexural Test: Ennis 980 > Ennis C80 > 3M 290 > 3M 290 PSA > Apex 921AR > Rayolite RS.
- Offset Latitude Flexural Test: Ennis 980 > Ennis C80 > Rayolite RS > 3M 290 PSA > 3M290 > Apex 921AR-C.

Table 9-9 Summary of Breakage Load in the RRLFT

Marker Type	Mean (kip)	Median (kip)	Standard Deviation (kip)
3M 290	5.520	5.490	0.384
3M 290 PSA	5.059	5.065	0.219
Ennis 980	8.203	8.305	0.762
Ennis C80	7.088	7.240	1.159
Rayolite RS	4.075	4.090	0.399
Apex 921AR	4.584	4.690	0.353

Table 9-10 Summary of Breakage Load in the OLFT

Marker Type	Mean (kip)	Median (kip)	Standard Deviation (kip)
3M 290	4.603	4.565	0.376
3M 290 PSA	4.756	4.645	0.405
Ennis 980	7.685	7.560	0.261
Ennis C80	7.013	6.995	0.205
Rayolite RS	6.022	5.970	0.405
Apex 921AR	3.812	3.860	0.867

The marker performance ranking from the revised reversed latitude flexural test (RRLFT) is the same as that from the ASTM standard flexural test. However, compared to the standard flexural test, since the stress distribution in markers in the RRLFT is much closer to that under the field condition, the typical failure modes generated in the RRLFT are more diversified and closer to the failure modes under field observation. For the offset latitude flexural test, its performance ranking seems to overestimate the performance of Rayolite RS.

CHAPTER 10 ECONOMIC ANALYSIS ON PROPOSED IMPROVEMENTS

Based on the stress analysis using FEM under different RRPM external and internal conditions, improved RRPM designs are proposed for service life extension. The expected benefits of the RRPM improvements are quantified by potential relationships between reduced stress, extended life expectancy, and associated costs. This chapter discusses in three steps the economic benefits of the proposed RRPM design improvements. In the first step, the new RRPM design is proposed based on the findings in Chapter 5. Stress magnitudes in the new RRPM design are then quantified and verified in ANSYS. Based on comparison of RRPMs with current designs and with proposed designs, the RRPM design improvement is quantified by percentage changes of stress magnitudes. In the second step, the relationship between RRPM ratings collected from field survey and those based on RRPMs' stress magnitudes are determined. Based on this relationship, the RRPM service life can be estimated from RRPM stress magnitudes. In the final step, the economic benefits of RRPM improvement are estimated using the life cycle cost analysis method. It has to be noted that the concept of service life used in this study is mainly based on the structural integrity of a marker. In practice, the service life of an RRPM is determined by its retroreflectivity since that is the main function an RRPM is intended to provide. For the purpose of simplified analysis, this study assumed that a structurally sound marker can maintain good retroreflectivity while a marker with good retroreflectivity also has little structural damage. These assumptions may not be true in some occasions. Measurement and evaluation of RRPM retroreflectivity, however, are out of the scope of this study.

10.1 Proposed RRPM Designs

Because 3M 290 is most widely used in Florida with its cheap price, it was selected as the base for proposed RRPM design.

Based on the geometric effects revealed in Section 6.5.4, RRPMs with small bottom width and small height are suggested. Through searching the dimensions of all current RRPMs, 3M 290 has the narrowest width which is already small and so shall be kept. Then, the height of 3M 290 is modified from 15.7 mm to 12 mm, and the body material of 3M 290 is replaced with the material of Ennis C80, which can decrease the von Mises stresses. Moreover, according to the effects of hollows observed in Section 6.4, these hollows are filled to make RRPMs solid.

Then, after these modifications (height changed to 12 mm; body material use the Ennis C80 material; and hollows are filled), the new RRPM is generated and verified by FEM analysis. Compared to original 3M 290, based on the information from Section 6.1, the obtained von Mises stresses are dropped from 173.5 MPa to 108.51 MPa, which is a 37.5% reduction. Compared to Ennis C80, Ennis C88, and Rayolite RS, the von Mises stresses are also decreased by 17.5%, 5.7%, and 54.4%, respectively.

10.2 Relationship between Stress Magnitudes and Corresponding Life Estimation

According to the stress magnitudes on different RRPMs calculated in Section 6.1 and the observed ratings of some of these RRPMs from field surveys, the proper estimated relationship between ratings and stress magnitudes can be selected. Because 3M 290 and Rayolite RS are the only two types of RRPMs both having sufficient and relatively reliable information from FEM

analysis and from field survey in this study, these two RRPMs were selected as samples. The specific information on these two RRPMs is listed in Table 10-1.

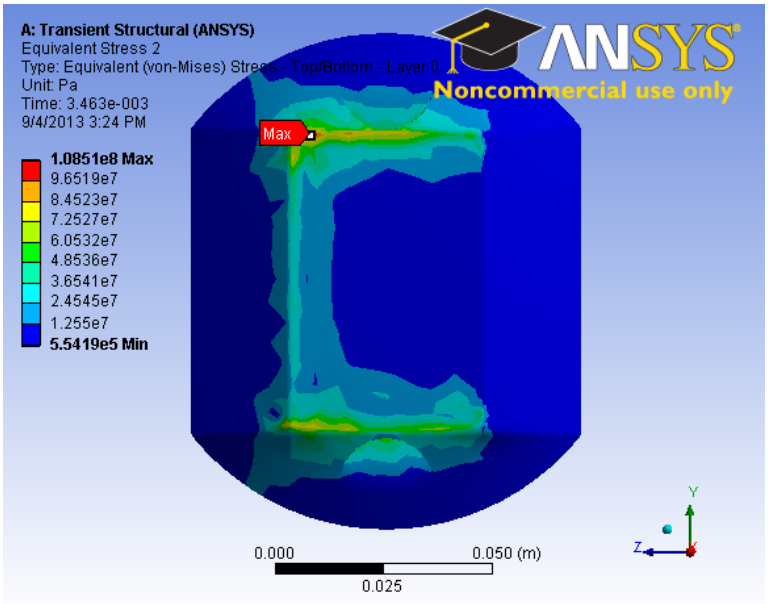

Figure 10-1 Von Mises Stress Plot of Proposed RRPM Model

Table 10-1 Stress and Truck AADT Information for 3M 290 and Rayolite RS at Two Sites

RRPM Type	Von Mises Stress	One Year Rating Difference at One Low Truck AADT Site	Truck AADT of Selected Site
3M 290	173.5	0.2	1152
Rayolite RS	238.2	0.7	1513

As Section 4.2.3 mentioned, the reason for that "one year rating difference at one low truck AADT site" was picked as the comparison rating is these typical rating changes (RC) under low truck volume seem more "fair" to RRPM comparison. Moreover, because Section 4.2.5 shows that the truck AADT has nonlinear effects on RC (best fit by cubic regression model), the revised RCs from current RCs divided by the cubic ratio of truck AADTs were calculated at two sites. It was found that the ratios of von Mises stress over revised RC in these two RRPM types are very close, as shown below:

$$\text{For 3M 290: } \frac{Stress}{Revised\ RC} = \frac{173.5}{0.2 \times (1513/1152)^3} = 382.9$$

$$\text{For Rayolite RS: } \frac{Stress}{Rating\ RC} = \frac{238.2}{0.7 \times (1513/1513)^2} = 340.3$$

Thus, it is assumed that the von Mises stress magnitude is positively linearly proportional to RRPM rating change.

Based on the definition of RRPM rating in NTPEP, the rating of new RRPM is 5 and the rating of marginally functional RRPM is set to 2. Thus, the life length of RRPM can be defined as the

time through RRPM rating drops from 5 to 2. Based on this definition, it is safe to say that the RRPM rating change is inversely linearly proportional to RRPM life length. Thus, the von Mises stress shall be also inversely linearly proportional to RRPM life length.

To estimate the service life extension by the proposed RRPM design, it was assumed that the yearly average rating changes of 3M 290 is 1.0/year, which means that it takes 3 years to drop rating from 5 (new) to 2 (marginally functional). Based on the linear relationship between rating change and von Mises stress, the proposed RRPM can slow the rate of rating drop to 0.6/year, which extends RRPM service life to 5 years. Thus, within an analysis period of 15 years, the number of times of RRPM replacement is decreased from five to at most three.

10.3 Life Cycle Cost Analysis

The total RRPM costs are determined and compared using the life cycle cost analysis (LCCA) approach. The analysis period was selected to be 15 years. Based on one discounting approach by Weitzman, since the service life of current RRPMs and proposed RRPMs both are less than or around five years, a discount rate of 4 percent was selected (Weitzman, 1998). After selecting the proper discount rate, the present values of RRPMs before and after improvement were estimated.

For current 3M 290, the present value, which is converted from the accumulation of future RRPM replacement costs at a three-year interval, is:

$$PV_1 = P_{01} + \frac{P_{01}}{(1+4\%)^3} + \frac{P_{01}}{(1+4\%)^6} + \frac{P_{01}}{(1+4\%)^9} + \frac{P_{01}}{(1+4\%)^{12}} + \frac{P_{01}}{(1+4\%)^{15}} = 4.56P_{01}$$

where P_{01} is the current cost of 3M 290 and PV_1 is the present value of total 3M 290 costs during the analysis period.

Similarly, for the proposed RRPM design, its present value is:

$$PV_2 = P_{02} + \frac{P_{02}}{(1+4\%)^5} + \frac{P_{02}}{(1+4\%)^{10}} + \frac{P_{02}}{(1+4\%)^{15}} = 3.05P_{02}$$

where P_{02} is the current cost of proposed RRPM and PV_2 is the present value of total costs of the proposed RRPM design during the analysis period.

From RRPM manufactures it is known that the price of 3M 290 is around $1.20 and the price of Ennis C80 is around $0.90. Since the materials in the proposed RRPM use those of Ennis C80 and the hollows are filled, the price of new proposed RRPM should be around 1$. Thus, the current costs of 3M 290 and the proposed new RRPM should be also changed very slightly. Thus, using this proposed new RRPM to replace 3M 290 can approximately save about $\frac{4.56P_{01} - 3.05P_{02}}{4.56P_{01}} = 44.3\%$ costs in a period of 15 years at sites where 3M 290s are installed.

CHAPTER 11 CONCLUSIONS AND RECOMMENDATIONS

This study investigated the main failure modes of retroreflective raised pavement markers (RRPMs) on Florida's roadways and the contributing stresses induced by live traffic in RRPMs. Appropriate laboratory tests to evaluate and rank RRPMs were analyzed and developed, and areas of improvement in RRPM design were identified and recommended.

Field survey on selected roadways around Tampa, Florida revealed various failure modes of RRPMs, including lens cracking and loss, body cracking and breakage, detachment, sinking, and contamination, were captured. The RRPM ratings characterized from the field survey indicated that heavy traffic load may significantly lead to more RRPM damages. Moreover, tire/RRPM contact angle is another significant factor that influences the critical stress in RRPMs. It was also observed that RRPMs have higher risk of detachment on rigid pavements than on flexible pavements, especially in areas like intersections. High precipitation and high temperature may accelerate RRPM failures.

Finite element model (FEM) analysis revealed that maximum von Mises stress, compressive maximum principal stress, and shear stress all concentrate on the corner and edges of RRPM's top shell. Tensile stress scatters on the top shell and the bottom edges of RRPM. 3M 290, Ennis C80, and Ennis C88 RRPMs exhibit similar stress responses while the Rayolite RS has much higher ones. RRPMs suffer from a large compressive stress and relatively smaller shear and tensile stresses, which indicate that RRPMs are more prone to be damaged by compression or shear rather than tension. Moreover, RRPMs on rigid pavements suffer more compressive and shear impacts than on flexible pavements.

Based on the FEM analysis of the effects of RRPM geometric factors on critical stresses, it is suggested that for RRPMs with larger height, the strength of RRPM body should be improved to sustain higher internal stresses, while for RRPMs with lower height, the bond strength of adhesive at the interface of RRPM and pavement deserves more attention. Besides height, a larger difference between top width and bottom width can mitigate potential failures at RRPM bottom. For the same sized RRPMs with different bottom edge shapes, the ones with curved bottom edges (Type 1) generally experience lower stresses than the ones with straight bottom edges (Type 2) under the same external conditions, except considering minimum principal stress or bottom shear stress. Moreover, the internal hollow structure of RRPM can accelerate the failure on RRPM body. Considering the RRPM materials, the material in Ennis C80 is better than that in 3M 290 in terms of producing lower stresses under the same structure and loading conditions.

Field measurements of strains in RRPMs under various wheel loads, tire types, and speeds showed a trend of strain increase with wheel load, but no clear relationship between strain and vehicle speed. Moreover, tire type may confound the relationship between strain and wheel load. Marker materials showed slight viscoelastic behavior but no discernible plastic behavior under wheel loading. Under the same loading conditions, the highest tensile strain was measured on 3M 290 and the highest compressive strain was measured on Apex 921AR among four marker types (3M 290, Ennis 980, Rayolite RS, and Apex 921AR).

Strains calculated from FEMs are in general consistent with the field measured strains. Discrepancies exist for some model type (i.e., 3M 290) or for some gauge locations, likely due to the complex RRPM structure features that were not completely captured in the FEM.

For current RRPM laboratory tests, based on FEM analysis of stress distribution in RRPMs in both the laboratory and field conditions, it is acceptable to conclude that the ASTM compressive test can better simulate the tensile and compressive damage in critical parts of RRPMs, than the ASTM flexural test. Moreover, elastomeric pads are necessary to be used in the longitudinal flexural test, but not necessary for the compressive test.

Through FEM analysis, it was determined that the pendulum impact test, originally developed by TTI, can generate proper stresses on "fragile" RRPM points (i.e., the corner and the middle of non-lens edge of RRPM top shell) to test RRPM qualities. The critical stresses generated by impact on these locations can be adjusted by changing the weight of the impact steel rod. FEM analysis also suggested two new laboratory tests to be further evaluated: revised reversed latitude flexural test and offset latitude flexural test. These two new laboratory tests can better simulate the real tire-marker condition in terms of critical stress distribution match.

In the laboratory test evaluation, the compressive and flexural tests specified in ASTM standards D 4280, an offset flexural test (a variation of the ASTM flexural test), and three new tests (a revised pendulum impact test, a revised reversed latitude flexural test [RRLFT], and an offset latitude flexural test [OLFT]) were conducted to evaluate the performance of several RRPM models. The rank of marker performance based on the ASTM compressive or flexural test results is generally consistent with FEM results and observed marker field performance. The marker performance ranking from the offset flexural test or the RRLFT is the same as that from the ASTM standard flexural test. However, the typical marker failure modes generated in the RRLFT are more diversified and closer to the failure modes observed in the field. The OLFT provides no significant advantage over the RRLFT. The pendulum impact test was revised from its original design by incorporating a repetitive impact load whose magnitude and speed can be adjusted. Results of this test are consistent with the FEM results and observed field performance. The revised pendulum impact test, however, is portable, versatile, and easy to operate. It is recommended that the revised pendulum impact test should receive further evaluation, development, and standardization.

For the RRPM design improvement, one new RRPM design is recommended based on the original 3M 290 design, by reducing the 3M 290 height to 12 mm, replacing the original materials in 3M 290 with those in Ennis C80, and filling the hollows of 3M 290 body with solid. Based on the assumption that the service life of an RRPM can be defined by its structural integrity, a preliminary life cycle cost analysis estimated that this proposed new RRPM design may extend the average RRPM service life from 3 years to 5 years, and save about 44% cost in an analysis period of 15 years.

REFERENCES

ADOT. 2008. *Standard Specifications for Road and Bridge Construction.* Arizona Department of Transportation, pp. 628-633.

ADOT. 2011. *Approved Products List.* Arizona Department of Transportation, pp. 99-100.

AHTD. 2003. *Standard Specification for Highway Construction*. Arkansas State Highway and Transportation Department, pp. 611-615.

AHTD. 2012. *Qualified Products List 721.02*. Arkansas State Highway and Transportation Department, pp. 1-2.

ALDOT. 2010. *List V-2: Permanent Pavement Markers, Temporary Pavement Markers, Markers, Marker Adhesives, Delineators and Hazard Markers.* Alabama Department of Transportation, pp. 1.

ALDOT. 2012. *Standard Specifications for Highway Construction.* Alabama Department of Transportation, pp. 668.

ANSYS. 2012. *ANSYS Mechanical APDL Contact Technology Guide*. ANSYS, Inc., pp. 42-62.

ASTM. 2001. *Standard E 1845-01 Standard Practice for Calculating Pavement Macrotexture Mean Profile Depth*. ASTM, International, West Conshohocken, PA.

ASTM. 2006. *Standard E 274-06 Standard Test Method for Skid Resistance of Paved Surfaces Using a Full-Scale Tire*. ASTM International, West Conshohocken, PA.

ASTM. 2008. *Standard Specification for Extended Life Type, Nonplowable, Raised Retroreflective Pavement Markers*. ASTM International, West Conshohocken, PA.

Caltrans. 2006. *Test Method for Non-reflective and Retro-reflective Pavement Markers.* California Department of Transportation, pp. 1-6.

Caltrans. 2010. *Standard Specifications.* California Department of Transportation, pp. 889-890.

Cole Farms. 2012. *Raised Pavement Markers.* The Pavement Marking Store, www.pavementmarkingtape.com/Adhesive-Pads-for-Road-Markers_c6.htm. Accessed July 8, 2012.

De Beer, M., and C. Fisher. 2002. *Tire Contact Stress Measurements with the Stress-In-Motion (SIM) Mk 1V System for the Texas Transportation Institute (TTI)*. Report CR-2002/82. Division of Road and Transportation Technology, Council for Scientific and Industrial Research, Pretoria, South Africa.

De Beer, M., C. Fisher, and F. J. Jooste. 1997. *Determination of Pneumatic Tire/Pavement Interface Contact Stresses under Moving Loads and Some Effects on Pavements with Thin Asphalt Surfacing Layers.* Proceedings of 8th International Conference on Asphalt Pavements

(Volume I), Seattle, Washington, pp. 179-227.

DOTD. 2006. *Standard Specifications for Roads and Bridges*. State of Louisiana Department of Transportation and Development, pp. 840.

DOTD. 2012. *Qualified Products List 59*. State of Louisiana Department of Transportation and Development, pp. 1-2.

Ennis. 2014. *Surface Mounted Raised Pavement Markers (Non-plowable)*. Ennis-Flint, www.ennisflint.com/Products/Raised-Pavement-Markers/Sun-Surface-Markers. Accessed February 12, 2014.

FDOT. 2000. *Florida Method of Test for Raised Pavement Markers Laboratory and Field Test, Designation: FM 5-566*. Florida Department of Transportation, pp. 1-5.

FDOT. 2010. *Standard Specifications for Road and Bridge Construction.* Florida Department of Transportation, pp. 791-792.

FDOT. 2012. *Qualified Product List S706.* Florida Department of Transportation, pp. 1.

FHWA. 2003. *Manual on Uniform Traffic Control Devices for Streets and Highways.* Federal Highway Administration, U.S. Department of Transportation, mutcd.fhwa.dot.gov/htm/2003r1/part3/part3b1.htm. Accessed August 10, 2012.

Fwa, T.F., and G. P. Ong. 2008. Wet-pavement hydroplaning risk and skid-resistance: Analysis, *ASCE Journal of Transportation Engineering*, 134(5), pp. 182-190.

GDOT. 2012. *Specifications: Section 919-Raised Pavement Markers.* Georgia Department of Transportation, pp.1-6.

HDOT. 2005. *Standard Specifications: Section 755- Pavement Marking Materials.* Hawaii Department of Transportation, pp. 8-9.

Hedayat, A. S., N. J. A. Sloane, and J. Stufken. 1999. *Orthogonal Arrays*: *Theory and Applications*, New York: Springer.

Hill, T., and P. Lewicki. 2006. *Statistics: Methods and Applications*. StatSoft, ISBN 1-884233-59-7.

Hofmann, K. L., and M. Dunning. 1995. *Evaluation of Raised and Recessed Pavement Markers Final Report.* Oregon Department of Transportation, OD-RD-96-06, pp. 3.

Kosgolla, J. V. 2012. *Numerical Simulation of Sliding Friction and Wet Traction Force on A Smooth Tire Sliding on A Random Rough Pavement*. Dissertation, Civil and Environmental Engineering, University of South Florida.

KYTC. 2012. *List of Approved Materials.* Kentucky Transportation Cabinet Department of Highways, pp. 68.

Matbase. 2012. www.matbase.com/index.php. Accessed November 15, 2012.

Matthias, J. S. 1988. *Spacing of Raised Reflective Pavement Markers.* Arizona Department of Transportation, FHWA-AZ88-836.

MDOT. 2004. *Standard Specifications for Road and Bridge Construction.* Mississippi Department of Transportation, pp. 731.

MDOT. 2012. *Approved Product Report.* Mississippi Department of Transportation, pp. 1.

NCDOT. 2002. *Standard Specifications: Division 10 Materials.* State of North Carolina Department of Transportation, pp. 178.

NDOT. 2001. *Standard Specifications for Road and Bridge Construction.* State of Nevada Department of Transportation, pp. 633.

NDOT. 2012. *Qualified Products List.* State of Nevada Department of Transportation, pp. 35.

NMDOT. 2007. *Standard Specifications for Highway and Bridge Construction.* New Mexico State Department of Transportation, pp. 504-508.

NTPEP. 2010. *Laboratory and Field Evaluations of Bituminous Pavement Marker Adhesive Georgia Test Deck Two Year Evaluation*. AASHTO's National Transportation Product Evaluation Program NTPEP Report 5009.1, Washington D.C..

NTPEP. 2011. *Laboratory and Field Evaluations of Permanent Non-Plowable Raised Pavement Markers Georgia Test Deck Two Year Evaluation*. AASHTO's National Transportation Product Evaluation Program, NTPEP Report 4013.1, Washington D.C..

ODOT. 2009. *Transportation Commission*. Oklahoma Department of Transportation, pp. 684.

ORDOT. 2000. *Standard Guidelines for Product Review Pavement Markers, Type 1; Section 02840.60.* Oregon Department of Transportation, pp. 1-2.

ORDOT. 2008. *Oregon Standard Specifications for Construction.* Oregon Department of Transportation, pp. 558.

ORDOT. 2012. *Qualified Products list.* Oregon Department of Transportation, pp. 93.

Plastics International. 2012. www.plasticsintl.com/sortable_materials.php?display=mechanical. Accessed November 15, 2012.

SCDOT. 2006. *Laboratory Procedures Manual.* South Carolina Department of Transportation, pp. 11-13.

SCDOT. 2007. *Standard Specifications for Highway Construction.* South Carolina Department of Transportation, pp. 440-444.

Smithers Rapra. 2012. www.rapra.net/consultancy/failure-analysis-trouble-shooting-why-plastic-products-fail.asp. Access November 5, 2012.

TDOT. 2006. *Standard Specifications for Road and Bridge Construction.* Tennessee Department of Transportation, pp. 638-639.

TDOT. 2012. *Qualified Products List and Evaluation Procedures*. Tennessee Department of Transportation, pp. 12-31.

TxDOT. 2010. *Department Materials Specification-4200*. Texas Department of Transportation, pp. 1-7.

Ullman, G.L. 1994. *Retroreflective Raised Pavement Markers: A Two-year Field Evaluation in Texas.* Texas Transportation Institute, pp. 18.

VDOT. 2007. *Road and Bridge Specifications*. Virginia Department of Transportation, pp. 223.

Weitzman, M. 1998. *Why the Far-distant Future Should Be Discounted at Its Lowest Possible Rate.* Journal of Environmental Economics and Management, 36(3), pp. 201-208.

Wikipedia. 2013. *Von Mises Yield Criterion.* The Free Encyclopedia. en.wikipedia.org/wiki/Von_Mises_yield_criterion. Accessed January 27, 2013.

WSDOT. 2012a. *Standard Specifications for Road, Bridge, and Municipal Construction.* Washington State Department of Transportation, M41-10, American Public Works Association, Washington State Chapter.

WSDOT. 2012b. *Qualified Products List: Standard Specification: 9-02.1(8).* Washington State Department of Transportation, www.wsdot.wa.gov/biz/mats/QPL/QPL_Search.cfm. Accessed July 17, 2012.

Zador, P. L., P. H. Wright, and R. S. Karpf. 1982. *Effect of Pavement Markers on Nighttime Crashes in Georgia.* Insurance Institute for Highway Safety.

Zhang, Y., J. Tong, P. Carlson, G. Hawkins, and P. Keating. 2009. *Development of Measures to Improve Field Performance of Retroreflective Raised Pavement Markers.* Texas Transportation Institute, Project 0-5089, Technical Report 0-5089-1.

APPENDIX A OTHER LABORATORY TESTS FOR RRPMS

A.1 Optical Test

The optical test can be divided into two categories: lens color test and coefficient of luminous intensity test.

A.1.1 Lens Color Test

In ASTM D 4280, lens color test uses CIE Standard Source A and one receptor. The source positions at the 0 entrance angle, and the receptor is at 0.2 observation angle. Their angular apertures are 6 min. of arc each. The specific position is shown in Figure A-1 (ASTM, 2008). When the retro-reflector is illuminated by CIE Standard Source A and observed through receiver, the color of the retro-reflected light shall fall within the color gamut given by the following corner points and shown in Figure A-2.

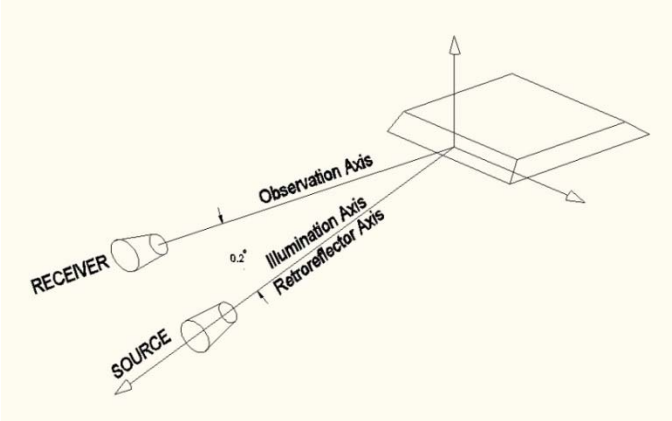

Figure A-1 Placement of Marker, Receiver, and Source

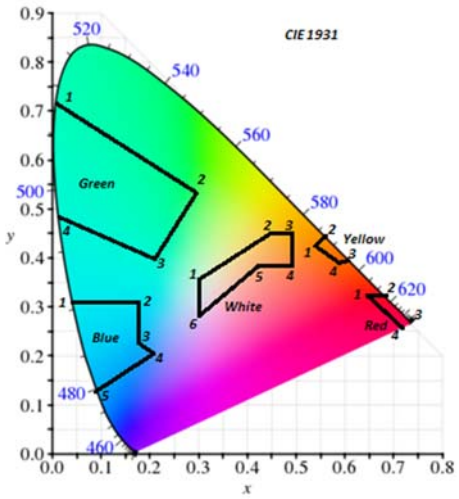

Figure A-2 Color Gamut

Three replicates are tested, and more than one failure of them will cause the rejection of the entire lot (ASTM, 2008).

The lens color tests in Florida, Alabama, Arkansas, Louisiana, and Tennessee are all in accordance with ASTM D 4280. NTPEP does not require this test in laboratory evaluations. California conducts the color test only about yellow one and the procedure is similar to that in ASTM D 4280. However, the range in CIE 1931 (four pairs of chromaticity coordinates) differs from ASTM, as shown in Table A-1.

Table A-1 Standard Color Gamut in California

x	y
0.451	0.458
0.481	0.429
0.545	0.464
0.495	0.500

Hawaii, Nevada, and Arizona use white light from sealed-beam automobile headlight to illuminate the colorful retroreflectors (yellow, red, or blue). Their specifications mention that the off-color reflection shall constitute grounds for rejection, and the daylight color of marker body shall be compatible with the color of primary lens and acceptance by the Engineer.

Mississippi uses FHWA Highway Color Tolerance Chart PR Color #l to select the markers' color. The color must be within the range of the chart (MDOT, 2004).

New Mexico and Georgia just mention the markers shall be not off-color reflection, without details of color tests (NMDOT, 2007; GDOT, 2012).

A.1.2 Coefficient of Luminous Intensity Test

Luminous intensity directly expresses the reflecting ability of lens, and makes the optical standard more specific and accurate. Tests of this property are not only for new RRPMs, but also for old ones. Moreover, such tests are often conducted after the abrasion test.

A.1.2.1 Coefficient of Luminous Intensity for New RRPMs Test

In ASTM D 4280, the specific placement of apparatus is similar to that of the color test, except having more dimensional requirements, as shown in Table A-2.

Table A-2 Apparatus Dimensions in Luminous Intensity Test

	Source	Receiver	Retroreflective element
Angular aperture (deg.)	0.1	0.1	0.02
Diameter (mm)	25.4	25.4	≤5.3

ASTM D 4280 also suggests that test dimensions can be 15.2 mm. The marker shall subtend no more than 1° at the source. The distance from the light source exit pupil to the center of the retroreflective face of the marker is measured. The tolerance on entrance angle is ±0.5°. Markers are conditioned and tested in a laboratory environment at 23±2°, and 50±25%RH. Before photometry, the lens are gently wiped by a soft damp towel, and dried with a soft towel for keeping clear (ASTM, 2008).

Based on the reflected illuminance and normal illuminance measured by a photometer, the coefficient of luminous intensity test is calculated as

$$R_I = m_1' d^2 / m_2$$

where,

d = observation distance, in meters,

m_1' = meter reading (minus stray light) used to measure reflected illuminance at observation position, relative units, and

m_2 = meter reading used to measure normal illuminance, relative units.

The calculated coefficient of luminous intensity shall be no less than the values in Table A-3.

Table A-3 Minimum Coefficient of Luminous Intensity in ASTM

Entrance Angle Component $\beta 2$	Observation Angle α	Minimum Value R_I, mcd/lx (cd/fc)				
		White	Yellow	Red	Green	Blue
0°	0.2°	279(3.0)	167(1.8)	70(0.75)	93(1.0)	26(0.28)
+20° / –20°	0.2°	112(1.2)	67(0.72)	28(0.30)	37(0.4)	10(0.11)

For coefficient of luminous intensity, the entire specimens shall be tested. Failure shall be less than 10 % of the reflective faces, or the entire lot will be rejected (ASTM, 2008). This test is used so widely that almost every state conducts it to measure the lens' optical quality. NTPEP, North Carolina, South Carolina, Kentucky, Alabama, Louisiana, Florida, Mississippi and Tennessee all use the same procedure as in ASTM D 4280. Nevada, Arizona, Texas, Arkansas, New Mexico, Oregon, Virginia, Georgia, California and Washington provide their acceptable coefficient of luminous intensity, as shown in Table A-4. The former eight states do not provide the testing procedure in DOT specifications, but the latter two states mention it. California also provides more details about using optical apparatus in California Test 669.

Table A-4 Minimum Coefficient of Luminous Intensity in States' Specifications

	Incidence angle		Clear	Yellow	Red
Nevada/New Mexico/ Georgia/Hawaii	0		3	1.5	0.75
	20		1.2	0.6	0.3
Arizona/Virginia/ Washington/ASTM	0		3	1.8	0.75
	20		1.2	0.72	0.3
Texas	0		3	2	0.75
	20		1.5	1	0.3
Arkansas	0		3	1.8	0.75
	20		1.2	0.72	0.3
	After one year	0	0.301	0.1806	0.07525
		20	0.129	0.0774	0.03225
Oregon	0		3	1.5	/
	20		1.2	0.6	/
California	0		3	1.5	0.75
	20		1.2	0.60	0.3
	After one year	0	0.30	0.15	0.08

Table A-4 shows that:

- States specifications only request the coefficients of luminous intensity in clear, yellow and red color, not green and blue ones which are mentioned in ASTM D 4280.
- In all specifications, the coefficients of luminous intensity in clear lens are the same: 3 candelas/foot-candle in 0 degree incident angle. Difference exists in other colors. Some states use 60% coefficient for yellow lens and 25% coefficient for red lens, but some states use 50% coefficient for yellow lens, instead. Moreover, only Texas uses 1.8 candelas/foot-candle in 0 degree incident angle for yellow lens.
- Only Oregon does not request the standard about red color.

It needs to be noted that Hawaii and Florida also request steel wool abrasion prior to the optical test.

Georgia and Washington apply the same principle, but different measurements from ASTM D 4280. The distance from a uniform light source to the center of the reflecting lens is 5 ft (1.5 m). The effective diameter of light source is 0.2 inch and the photocell receptor is 0.5 in. (13 mm) wide. The center of the light source aperture is placed 0.2 in. (5 mm) from the center of the photocell, for eliminating stray light. If a test distance other than 5 ft (1.5 m) is used, the source and receptor is modified to keep in the same proportion as the test distance.

A.1.2.2 Coefficient of Luminous Intensity for Aged RRPMs Test

This test requests that the 1-year aged markers are removed from the pavement to undergo coefficient of luminous intensity test. Because ASTM D 4280 does not request tests on aged RRPMs, this test is not widely used in states.

NTPEP observes aged RRPMs in 6, 12, 18, and 24 months, and analyzes the tendency of the coefficient of luminous intensity changing with time.

California, Texas, Hawaii, and Arkansas also specify criteria of coefficient of luminous intensity for aged RRPMs, as shown in Table A-5.

Table A-5 Coefficient of Luminous Intensity for RRPMs Aged after 12 Months

	Incidence angle	Clear	Yellow	Red
Arkansas	0	0.301	0.1806	0.07525
	20	0.129	0.0774	0.03225
California/Hawaii	0	0.30	0.15	0.08
Texas	0	1	0.7	0.2

A.2 Resistance to Temperature Cycling Test

ASTM D 4280 includes a resistance to temperature cycling test to check the influence of thermal expansion and contraction on markers. In this test, specimens are conditioned for 3 cycles of four hours at 60°C (140°F) followed by four hours at −7°C (20°F). After the cycling conditioning, no cracking or delamination shall be observed in specimens. Failure of more than one of ten specimens in either test will cause rejection of the entire lot (ASTM 2008).

NTPEP, Florida, Arizona, Alabama, North Carolina, Arkansas, Kentucky, Louisiana, Mississippi, Tennessee, and Georgia all include the same test following ASTM D 4280.

Texas conducts the similar test method called heat resistance test, but only requests that the marker shall be heated at 140°F and the SI of the pavement marker must not be less than 80% of its initial value after being subjected to the heat test (TxDOT, 2010).

A.3 Abrasion Resistance for Lens Surface Test

In ASTM D 4280, abrasion resistance test uses particular sand to fall onto the front of a marker for abrading the lens surface, and then measures the coefficient of luminous intensity at 0° entrance angle. The result shall at least meet the criteria in the SI standard table multiplied by 0.5 in ASTM D 4280.

NTPEP, Florida, Alabama, North Carolina, South Carolina, Kentucky, Louisiana, and Tennessee all include the same procedure as that in ASTM D 4280. However, Arizona and California follow a steel wool abrasion procedure, summarized as follows. A one-inch diameter flat pad is formed using No. 3 coarse steel wool in accordance with Federal Specification FF-W1825. The steel wool pad is placed on the reflector lens face, and then a force of 50 pounds is applied to rub the entire lens surface for 100 times. After the lens surface has been abraded, the specific intensity of each clear and yellow reflective surface shall be no less than that required for the original specific intensity. On two color units, the red lens may not be abrasion resistant and if so they should not be abraded.

A.4 Water Soak Resistance Test

California and Nevada use water soak resistance test to check the influence of water on markers. The test procedure is simple: immerse pavement markers in the water bath, maintained at (35° ± 3°C) for 48 hours, and then remove it from water to examine for any delamination or other deleterious effects. Measure the retro-reflectance and any significant loss of reflectance will cause rejection (Caltrans, 2006).

This test is not mentioned in ASTM D 4280 and not widely used in other states.

A.5 Adhesive Bond Strength Test

ASMT D 4280 does not provide a practical laboratory procedure to obtain complete, reliable, and predictive information on adhesive bond strength, but recommends field tests instead. However, California and Oregon provide a bond strength test for RRPMs as following. Before testing, apparatus, markers and adhesive are conditioned at 23 ± 2ºC for a minimum of four hours. Then, a small amount of epoxy adhesive is spread on the center of the bottom surface of the marker, with a diameter of approximately 2 inches. A thin layer of adhesive is placed on the sandblasted surface of the plug and pressed to fix the sandblasted surface on the center of the bottom surface of the marker through slight rotation. A tongue depressor with a squared end is used to carefully remove any adhesive that extrudes from under the plug. The assembly is then cured for 48 hours at 25ºC (Caltrans, 2006). At the end of the 48-hour curing period, the test plugs are tensile loaded at a rate of 2200 kg/min to failure through a tensile testing machine (ORDOT, 2000).

Hawaii, Nevada, Arkansas, Oregon apply the similar method in accordance with California Test 669, and require that the bond strength shall be larger than 500 psi (3.4 MPa).

APPENDIX B CURRENT RRPM INSTALLATION TECHNIQUES

Knowledge in RRPM installation can be separated into two aspects: surface preparation and adhesive requirement. A general guideline is that marker placement shall comply with DOT Standard Plans for proper positions on roadways; road surface shall be kept clean and at proper temperatures before RRPM installation for good bonding with the adhesive; and the adhesive shall be selected from a DOT qualified product list (QPL), for achieving good retention on pavements. Following are a summary of specific standards and methods.

B.1 Surface Preparation

Before adhesives are applied, the pavement surface shall keep free of dirt, curing compound, grease, oil, moisture, paint, and any other material that would adversely influence the bond of adhesive (AHTD, 2003). Arizona also requests sweeping and the use of high-pressure air spray. Especially, sandblasting shall be applied to clean the Portland cement concrete pavement and old asphaltic concrete pavements (ADOT, 2008). California does not require abrasive blasting clean for new hot mix asphalt (HMA) and seal coat surface (Caltrans, 2010).

B.2 Adhesive Requirement

Currently, adhesives can be mainly divided into two categories: bituminous and epoxy. Bituminous adhesives are hot melt during application. Epoxy adhesives are prepared by hand mixing, which is named Standard Set Type adhesive, or by automatic mixing and extrusion apparatus, which is named Rapid Set Type adhesive. Furthermore, many states also use adhesive pad instead, such as double butyl pads and thermoplastic melt down adhesive pads.

B.2.1 Bituminous Adhesive

Bituminous adhesive is applied to the bonding surface (pavement), not the markers. It is applied uniformly to an area large enough to cover 100% of the bonding area of a marker, without any voids. Sufficient amount is applied to ensure, that when the marker is pressed downward into the adhesive, adhesive will flow about the periphery of the marker (FDOT, 2010). Arkansas also requests that excess adhesive which flows about the periphery of the marker shall not exceed 1½" (38 mm) (AHTD, 2003), and this excess part shall be immediately removed by solvent. Oregon and Washington DOT request that excess adhesive shall be a small bead approximately 1/8 inch thick forming around all edges and corners. Tennessee DOT mentions that the adhesive shall be smeared in a puddle approximately 2/3 to 3/4 of the diameter of the marker. Markers shall be attached to the adhesive within 10 seconds to assure bonding (TDOT, 2006). Only soft rags moistened with mineral spirits meeting Federal Specifications TT-T-291 and kerosene are accepted (FDOT, 2010). In FDOT, bituminous adhesive is the only approved adhesive for RRPMs.

In Arkansas, application of bituminous adhesives requires the use of melting apparatus, before and during installation, to keep homogeneity. For keeping a proper working temperature (from 400° F to 450° F), diffuse heat distortion (diffuse plate) and a dispensing nozzle are utilized. The bituminous adhesive is not used when either the pavement or air temperature is less than 0°C (32°F) (AHTD, 2003). Arizona tolerates a 4.4°C (40° F) minimum temperature if the relative humidity is 80 percent or higher (ADOT, 2008).

Tennessee and Florida also introduce thermostatically controlled double boiler type units (utilizing heat transfer oil) and thermostatically controlled electric heating pots to melt and heat adhesives. Direct flame melting units are forbidden. The application temperature is maintained between 190 and 220°C (375 and 425°F), because lower temperatures may cause decreased adhesion while higher temperatures may damage the adhesive (TDOT, 2006).

South Carolina also points out that bituminous adhesives are suitable for bonding ceramic and plastic markers to portland cement concrete, asphalt concrete, and chip-seal road surfaces and are applicable for a road surface temperature in the approximate range of 4.4°C to 71°C (40ºF to 160ºF). When either air or oil-jacketed melters are used, the adhesive shall retain its properties when heated to and applied at temperatures up to 218°C (425ºF) (SCDOT, 2007).

In California, bituminous adhesive is termed as flexible bituminous adhesive, which is distinguished from adhesive pad. Bituminous adhesive can be applied in pavement recesses, where the adhesive pad cannot attach RRPMs completely (Caltrans, 2010).

B.2.2 Epoxy Adhesive

The methods of using epoxy adhesives and bituminous adhesives are similar: both methods require pressing markers to achieve firm contact with the pavement, and the excess adhesives be immediately removed. However, due to different material properties, epoxy adhesives require that the mixing operation and placing procedure be more rapid and proper. Therefore, automatic proportioning and mixing machines are often used for producing epoxy adhesive. As mentioned previously, rapid-set epoxy adhesives are commonly prepared by automatic apparatus, while standard-set epoxy adhesives are prepared through hand mixing, sometimes also by automatic apparatus.

B.2.2.1 Standard Set Type Adhesive

When mixed by hand, the volume of epoxy adhesive shall be controlled to be less than 1 liter (1 quart) for each batch, and the temperature shall be lower than 10°C (50°F). Markers shall be aligned and pressed into place within 5 minutes since the beginning of mixing. The mixed adhesive shall not be too viscous to be readily extruded from bottom of the marker under slight pressure (AHTD, 2003). When polymerization has caused stiffening and reduced workability, the adhesive shall be discarded (WSDOT, 2012b).

Opposite of Florida, New Mexico only approves standard-set epoxy adhesives to cement markers to the pavement, unless a project manager requests to use rapid-set epoxy adhesive for substitution (NMDOT, 2007).

B.2.2.2 Rapid Set Type Adhesive

Markers may be placed with a rapid-set epoxy adhesive by an automatic machine. During the mixing of the rapid-set epoxy adhesive by automatic apparatus (e.g., positive displacement pumps), time control is required at every step:

- After the adhesive is pumped into the mixing head, the adhesive shall be placed on the pavement within 90 seconds and no further movement is allowed;
- After the adhesive has been mixed and extruded, markers shall be placed within 60 seconds and no further movement is allowed;

- The mixed adhesive shall not remain in the mixing head for more than 45 seconds.

To avoid black or white streaks in the mixed material, volumes of the two components (A and B) of epoxy adhesive shall be properly measured in a specified ratio, with a toleration range of ±5%. This ratio shall be checked by disconnecting the mixing heads, or using suitable bypass valves, and filling 2 suitable containers with the unmixed components. Moreover, neither the pavement nor the air temperature shall be less than -1°C **(**30°F) (AHTD, 2003).

B.3 Adhesive Pads

Adhesive pads are not included in state DOT specifications. However, due to their convenience feature, they are gaining more popularity. Product details are available in manufacturers' product specifications and manuals.

B.3.1 Thermoplastic Melt-down Adhesive Pads

Thermoplastic melt-down adhesive pad is one popular adhesive pad on RRPM installation. The procedure of applying this product is simple: cleaning the area, heating the asphalt pavement, laying the pad down, continuing to heat until the pad melts, and placing the marker and pressing it in.

B.3.2 Double Butyl Pads

Another popular type of adhesive pad is double butyl pad. The application procedure is also simple: cleaning the area, peeling off the wax paper from one side of the pad, pressing the pad onto the surface, peeling the other piece of wax paper off, and placing the marker and pressing it under a vehicle tire (Cole Farms, 2012).

B.4 Brands of Adhesives

Based on the state DOT QPLs, the main approved brands of adhesives are summarized in Table B-1 and

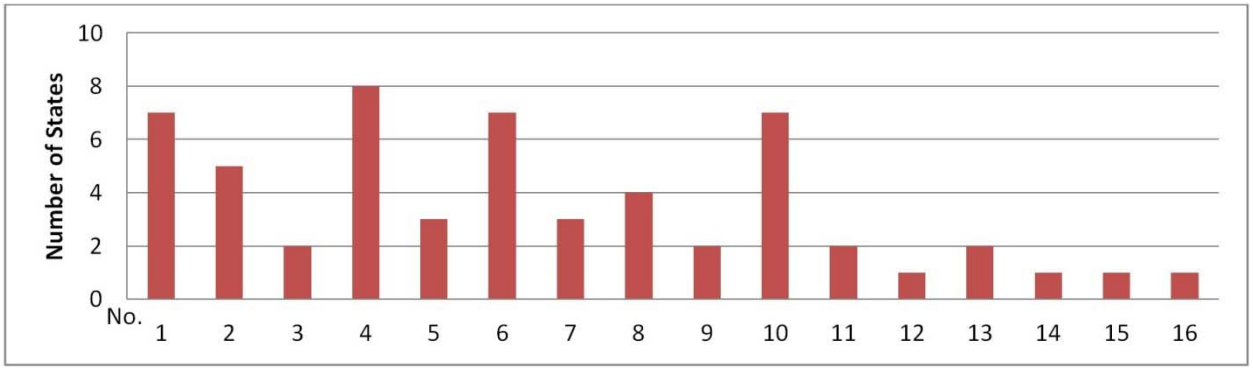

Figure **B-1**.

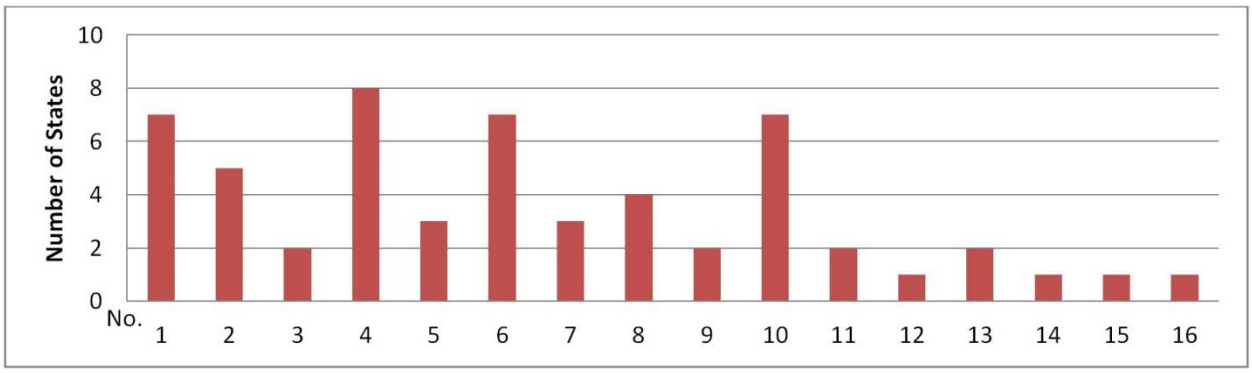

Figure B-1 Number of States Using Various Adhesives (the codes of adhesive brands on the x axis are shown in Table B-1)

Table B-1 and

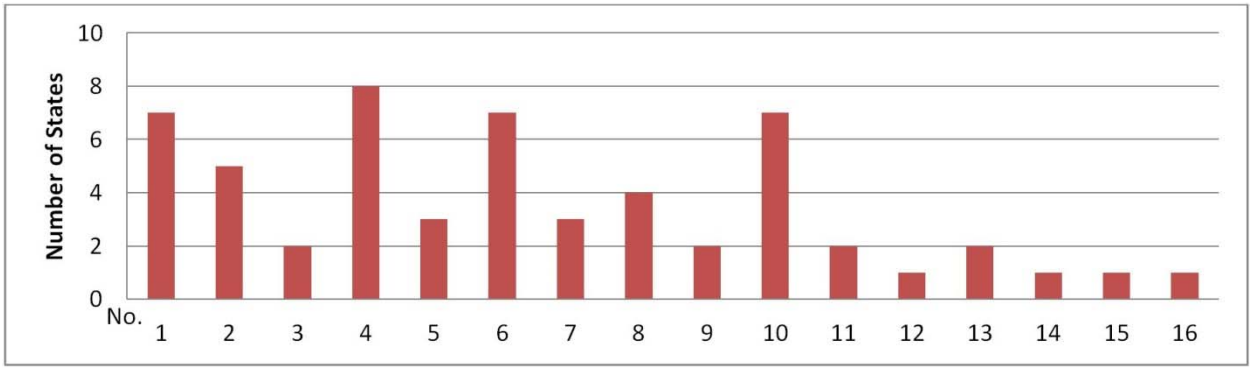

Figure **B-1** show that CRAFCO (34270 and 34269) is the most popular adhesive brand for RRPMs in the U.S. Martin Asphalt Company EverGrip Adhesive and HE193 DOT Stick are the second popular brands. Moreover, the bituminous adhesive has more brand options than the epoxy and melt-in-place thermoplastic adhesives. In some QPLs, the bituminous adhesives are divided into flexible and rigid categories. However, most QPLs do not clearly distinguish these two categories.

Table B-1 Brands of Adhesives Approved in Different U.S. States

Type	Brand	No.	AL	AZ	AR	FL	LA	MS	TN	NV	OR	WA
Bituminous	Crafco Flexible Hot-applied Marker Adhesive (34270)	1	✓	✓				✓	✓	✓	✓	✓
	Stimsonite Bituminous Adhesive (2202031/836098)	2	✓	✓				✓	✓	✓		
	Pave-mark Standard Bituminous Adhesive	3	✓						✓			
	CRAFCO (34269)	4	✓	✓	✓	✓	✓	✓	✓		✓	

	EAGLE	5	✓		✓			✓				
	HE193 DOT Stick	6	✓	✓		✓	✓	✓		✓	✓	
	Golf-seal standard adhesive	7		✓	✓			✓				
	HE184 Flexible Dot Stick	8		✓			✓	✓			✓	
	3M BT-69	9			✓			✓				
	Martin Asphalt Company EverGrip Adhesive	10	✓		✓	✓	✓		✓	✓	✓	
	MarkerGrip	11					✓	✓				
	DURA-fill MA	12							✓			
Melt-In-Place Thermoplastic	Flint Trading Bundy	13		✓						✓		
Epoxy	Structurbond Resin with 550 Hardener	14		✓								
	E-Bond 1240/1241	15			✓							
	Poly Carb Mark 29/ 29.9	16									✓	

APPENDIX C STATISTICAL RESULTS FROM FULL FACTORIAL DESIGN ON RRPM GEOMETRIC OPTIMIZATION

This appendix provides all statistic results of regression models on full factorial analysis for RRPM geometric factors' effects.

Table C-1 Statistical Analysis Results of Full Factorial Design for Type 1 RRPMs

Bottom Shape 1 (curve edge)									
Stress in RRPM Body									
Variables		F	Sig.	F	Sig.	F	Sig.	F	Sig.
Name	Type	Equivalent Stress		Maximum Shear Stress		Maximum Principal Stress		Minimum Principal Stress	
Intercept		3347.83	0	3198.726	0	1505.099	0	4616.069	0
BL	Main Effect	0.807	0.464	0.939	0.412	0.231	0.796	2.749	0.094
BW		4.086	0.037	4.892	0.022	3.64	0.05	3.513	0.054
H		7.046	0.006	8.888	0.003	4.822	0.023	2.296	0.133
TOB		0.134	0.876	0.04	0.961	2.354	0.127	0.118	0.889
BL*TOB	2-Way Interaction	3.235	0.04	2.88	0.057	0.578	0.683	8.16	0.001
BW*TOB		2.103	0.128	2.009	0.142	0.899	0.488	4.063	0.018
H*TOB		2.042	0.137	2.234	0.111	1.036	0.419	1.936	0.153
BL*BW		0.715	0.594	0.616	0.657	0.237	0.913	0.651	0.634
BL*H		1.003	0.435	1.272	0.322	0.759	0.567	1.707	0.198
BW*H		1.528	0.241	1.271	0.322	1.012	0.431	1.792	0.18
BL*BW*TOB	3-Way Interaction	2.411	0.064	1.947	0.122	1.136	0.392	2.599	0.049
BL*H*TOB		1.576	0.209	1.448	0.251	0.901	0.538	4.442	0.005
BW*H*TOB		0.635	0.738	0.674	0.708	0.748	0.651	1.047	0.443
BL*BW*H		1.441	0.254	1.284	0.318	0.849	0.575	0.836	0.585
Adjusted R Squared		0.39		0.838		0.062		0.551	
Stress at RRPM Bottom									
Name	Type	Maximum Normal Stress		Minimum Normal Stress		Average Shear Stress			
Intercept		111.86	0	84904.782	0	2100.751	0		
BL	Main Effect	10.436	0.001	110.457	0	98.852	0		
BW		4.603	0.026	32.491	0	25.086	0		
H		8.703	0.003	116.137	0	1.185	0.331		
TOB		4.679	0.025	65.987	0	17.962	0		
BL*TOB	2-Way Interaction	2.659	0.071	4.277	0.015	2.125	0.125		
BW*TOB		0.602	0.666	15.819	0	1.108	0.387		
H*TOB		1.612	0.22	3.17	0.043	1.638	0.213		
BL*BW		6.307	0.003	1.45	0.263	26.344	0		
BL*H		1.877	0.164	5.747	0.005	2.237	0.111		
BW*H		0.291	0.88	2.388	0.094	0.244	0.909		
BL*BW*TOB	3-Way Interaction	1.638	0.191	2.75	0.041	3.299	0.02		
BL*H*TOB		1.439	0.254	1.426	0.259	1.541	0.22		
BW*H*TOB		0.735	0.661	1.385	0.275	1.197	0.36		
BL*BW*H		1.071	0.429	2.277	0.077	1.234	0.342		
Adjusted R Squared		0.516		0.907		0.838			

Note: All statistically significant effects are marked by gray areas in Table C-1.

Table C-2 Statistical Analysis Results of Full Factorial Design for Type 2 RRPMs

Bottom Shape 2 (squared bottom)									
Stress in RRPM Body									
Variables		Coefficients							
		F	Sig.	F	Sig.	F	Sig.	F	Sig
Name	Type	Equivalent Stress		Maximum Shear Stress		Maximum Principal Stress		Minimum Principal Stress	
Intercept		27594.502	0	25644.996	0	8039.026	0	24860.227	0
BL	Main Effect	2.049	0.172	2.297	0.143	0.407	0.674	2.56	0.119
BW		4.028	0.046	1.435	0.276	0.471	0.635	0.918	0.425
H		118.689	0	112.827	0	56.619	0	88.383	0
TOB		230.071	0	231.88	0	15	0	37.702	0
BL*TOB	2-Way Interaction	1.794	0.183	1.391	0.294	1.537	0.248	1.677	0.21
BW*TOB		1.747	0.211	1.488	0.268	4.266	0.029	2.156	0.146
H*TOB		1.069	0.432	0.908	0.521	2.607	0.074	0.545	0.765
BL*BW		0.793	0.552	0.412	0.797	1.308	0.322	0.226	0.918
BL*H		9.291	0.001	8.783	0.001	0.88	0.505	10.55	0.001
BW*H		1.307	0.322	0.811	0.542	2.012	0.157	0.874	0.507
BL*BW*TOB	3-Way Interaction	0.387	0.873	0.239	0.955	0.37	0.884	0.217	0.964
BL*H*TOB		1.854	0.149	1.5	0.247	2.127	0.103	2.431	0.069
BW*H*TOB		1.972	0.149	1.136	0.399	2.824	0.059	1.019	0.458
BL*BW*H		0.888	0.554	0.502	0.833	1.622	0.217	0.921	0.532
Adjusted R Squared		0.925		0.923		0.73		0.814	
Stress at RRPM Bottom									
Name	Type	Maximum Normal Stress		Minimum Normal Stress		Average Shear Stress			
Intercept		9240.502	0	48296.128	0	5144.069	0		
BL	Main Effect	573.49	0	47.02	0	3.918	0.049		
BW		8.767	0.004	1.484	0.265	3.258	0.074		
H		128.56	0	4.589	0.033	8.314	0.005		
TOB		188.074	0	1706.357	0	133.438	0		
BL*TOB	2-Way Interaction	1.978	0.148	3.106	0.045	1.321	0.32		
BW*TOB		6.724	0.007	1.916	0.181	2.768	0.088		
H*TOB		10.484	0	4.002	0.02	5.134	0.008		
BL*BW		1.156	0.378	2.104	0.143	1.173	0.371		
BL*H		9.412	0.001	9.193	0.001	2.57	0.092		
BW*H		2.663	0.084	5.836	0.008	4.594	0.018		
BL*BW*TOB	3-Way Interaction	0.772	0.607	1.393	0.294	0.814	0.579		
BL*H*TOB		1.353	0.304	3.123	0.03	1.507	0.244		
BW*H*TOB		1.412	0.287	4.848	0.01	2.804	0.061		
BL*BW*H		1.292	0.332	1.98	0.138	1.311	0.324		
Adjusted R Squared		0.965		0.907		0.864			

Note: All effects which are same as those for type 1 RRPM are marked in green areas, and all other statistically significant effects which only exist in type 2 RRPMs are marked in gray areas.

Table C-3 Statistical Analysis Results of Full Factorial Design for Both RRPMs

Variables		Sig.						
		Stress in RRPM Body				Stress at RRPM Bottom		
Name	Type	Equiv.	Max. Shear	Max. Principal	Min. Principal	Max. Normal	Min. Normal	Ave. Shear
Intercept		0	0	0	0	0	0	0
BL	Main Effect	0.964	0.914	0.821	0.452	0	0	0
BW		0.073	0.034	0.107	0.031	0.063	0.256	0
H		0	0	0	0	0	0	0.06
BS		0.001	0	0	0	0.033	0	0
TOB		0	0	0.002	0.011	0	0	0
BL*BS	2-Way Interaction	0.157	0.126	0.86	0.01	0.471	0.02	0
BL*BW		0.665	0.809	0.636	0.604	0.003	0.592	0
BL*H		0.24	0.196	0.436	0.05	0.067	0	0.02
BL*TOB		0.079	0.125	0.682	0.001	0.073	0.045	0.202
BW*BS		0.066	0.062	0.105	0.068	0.007	0.003	0
H*BS		0.259	0.339	0.026	0.015	0.035	0.001	0.915
BS*TOB		0	0	0.076	0.008	0.994	0	0.21
BW*H		0.627	0.602	0.562	0.169	0.653	0.078	0.883
BW*TOB		0.337	0.405	0.219	0.076	0.547	0.706	0.717
H * TOB		0.338	0.349	0.669	0.186	0.475	0.012	0.054
BL*BW*BS	3-Way Interaction	0.644	0.641	0.972	0.595	0.002	0.359	0
BL*H*BS		0.201	0.138	0.683	0.05	0.219	0.003	0.579
BL*BS*TOB		0.052	0.065	0.425	0	0.053	0.101	0.116
BL*BW*H		0.456	0.479	0.828	0.544	0.411	0.803	0.471
BL*BW*TOB		0.148	0.267	0.505	0.051	0.178	0.446	0.056
BL*H*TOB		0.235	0.29	0.296	0.002	0.24	0.031	0.097
BW*H*BS		0.116	0.223	0.299	0.1	0.964	0.023	0.612
BW*BS*TOB		0.032	0.043	0.178	0.001	0.634	0.008	0.204
H*BS*TOB		0.118	0.098	0.097	0.092	0.05	0.141	0.486
BW*H*TOB		0.839	0.917	0.507	0.387	0.591	0.117	0.348
BL*BW*H*BS	4-Way Interaction	0.28	0.417	0.406	0.406	0.356	0.15	0.35
BL*BW*BS*TOB		0.112	0.198	0.54	0.032	0.149	0.344	0.023
BL*H*BS*TOB		0.327	0.38	0.604	0.006	0.203	0.126	0.632
BL*BW*H*TOB		0.643	0.657	0.468	0.23	0.407	0.944	0.621
BW*H*BS*TOB		0.589	0.515	0.341	0.315	0.648	0.034	0.345

Note: All significant effects related to bottom shape are marked in grey areas in Table C-3.